Colour 85

CRANFIELD INSTITUTE OF TECHNOLOGY

SCHOOL OF INDUSTRIAL SCIENCE

Ph.D. THESIS

NABIL ABDUL-JALIL AL-HADITHY

FRACTURE TOUGHNESS TESTING OF A WELDABLE STEEL

SUPERVISOR: Professor P. HANCOCK

AUGUST 1981

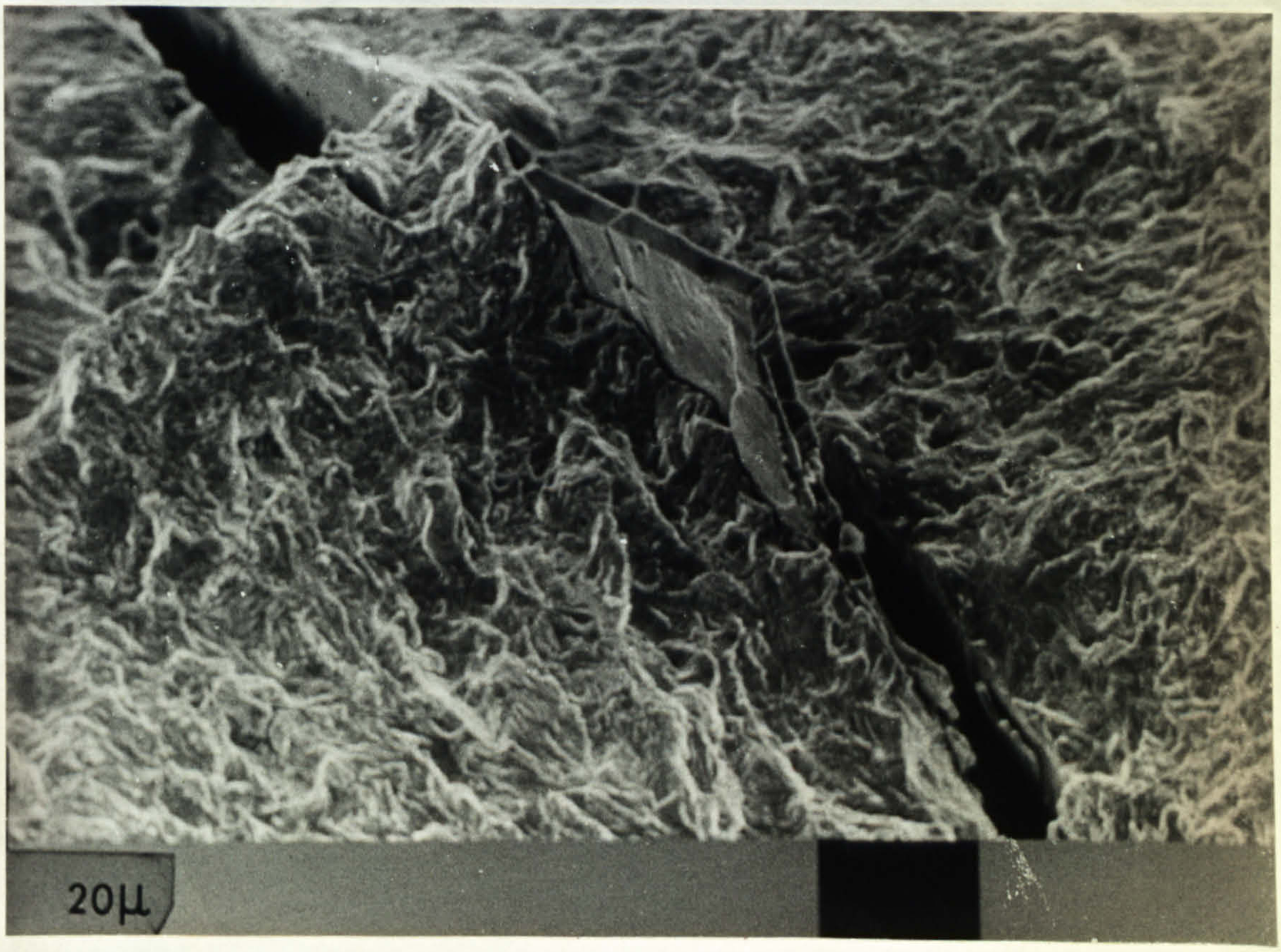

Mn S inclusion on fatigue surface

To my family

ABSTRACT

The mechanical anisotropies of two varieties of BS 4360 50D steel were demonstrated for tensile, Charpy V impact and COD testing. The detrimental effect of sulphide inclusions for through thickness behaviour was related to the total inclusion length per unit area and the interaction of inclusions within the plastic zone.

Sulphide inclusions in the through thickness orientation were found to increase crack tip constraints, reduce the plastic zone size and the post-yield load bearing capacity of the specimen ligament. This was achieved by the ease of movement of the growing crack tip to various planes containing suitable clusters of inclusions.

COD at maximum load was shown to decrease exponentially with increasing inclusion content. For acceptable through thickness toughness it was shown necessary to limit the inclusion density to 1 to 1.5mm/mm^2, according to the constraints in its application. For plate or pipe material made from highly rolled steel, low sulphur steel melts must be used. Even rare-earth-modified steels will show unacceptable inclusion densities after high rolling strains in the mill. The inclusion density would increase both in the ZR and ZT through thickness directions. Notches along the rolling plane gave lower toughness levels due to inclusion interactions out-of-plane facilitated by the added length of the inclusion caused by hot rolling.

A computer program was included which uses a polynomial fitting technique relating COD to inclusion density to predict through thickness toughness for any given inclusion content.

A method was devised for through thickness testing of thin plate materials. Valid maximum load COD values were obtained by friction welding of extensions to undersized specimens. The effect of free surfaces that interacted with the plastic zone at the crack tip were found to be beneficial to crack tip deformations. For these reasons thin plates were shown to be unsusceptible to through thickness failures, such as, lamellar tearing, unless the effects

of the free surface were removed by welding attachments to the surface.

At upper shelf temperatures for ductile structural materials, it was shown that the measured toughness was related to the size of the plastic zone and, hence, to specimen geometry. The measured toughness related more to the absolute length of uncracked ligament rather than to crack length or crack length to width ratio. To achieve geometry independence, the ligament length was required to be greater than the characteristic plastic zone size for the specimen thickness and testing temperature.

The extensive plastic zone and the small highly strained zone sizes were shown to be dependent on temperature. At high temperatures the crack tip strains increased which resulted in crack blunting and stress dissipation. The work hardened material ahead of the crack tip showed evidence of small crack fissuring which led to stable crack growth. At low temperatures, where brittle fracture occurred, the highly strained region and extensive plastic zone were much smaller in size. Crack blunting was greatly reduced which allowed brittle fracture stresses to be achieved at the crack tip. At intermediate temperatures the crack tip blunting was extensive and it was shown that the amount of ductile cracking required to increase the constraint necessary to achieve brittle fracture decreased with decreasing temperature.

Large specimen sizes resulted in high stored energy which, at transition temperatures, drove the ductile crack to catastrophic failures. This resulted in narrower transition regions which effectively shifted the transition to higher temperatures.

The transition from ductile to brittle behaviour was considered, from the experimental evidence supplied, not to represent a shift in the state of stress. The through-thickness strain decrease associated with this transition was a result of the associated decrease in COD. As the COD was shown to vary with specimen geometry independently of specimen thickness and, hence, independently of the state of stress, then the associated change in through

thickness strains were also not indicative of a change in the state of stress. A shift in the state of stress was considered to occur only when the through thickness strains varied with respect to COD.

The method of load application was shown to have a significant effect on the measured toughness. Generally yielded specimens were shown to be under greater crack tip constraints when the specimen was loaded in bending rather then in tension.

ACKNOWLEDGEMENTS

The author is indebted to Professor P. Hancock whose guidance and encouragement have been invaluable.

The author would also like to express his gratitude to Dr. J. Spurrier for his help during the experimental part of the research.

Thanks are due to my brother, Mr. A.A.J. Al-Hadithy for his help in the programming.

Special thanks are due to Messrs R. Hardwicke, D. Timpson and K. Nelson and their staff for their help in solving the numerous practical problems.

Finally, to the Rank Xerox, 860 IPS word processor without which this thesis would have been typed in less than half the time!

CONTENTS

LIST OF FIGURES

FIGURE

FIGURE

FIGURE

LIST OF PLATES

LIST OF TABLES

LIST OF NOTATIONS

A	area
a	half crack length of centre crack or depth of surface crack
a*	$(a + r_p)$
a_c	critical (a)
B	thickness of component
C, M, m	constants
E	Youngs modulus in plane stress
E'	Youngs modulus in plane strain
f	flexibility or compliance of a body
e	engineering strain
e_x, e_y, e_z	strain in x, y, z directions
e_Y	yield strain
G	crack extension force
G_c	critical crack extension force
H	centre of rotation of bending specimen
J	the J contour integral
J_i	J at initiation of ductile cracking
J_{Ic}	critical plane strain J
K	elastic stress intensity factor
K_c	critical stress intensity factor
K_{Ic}	critical plane strain K
K_{Jc}	K at J_c
K_Q	K measured at 5% offset secant
L	longitudinal orientations

n	strain hardening exponent
P	load
P_f	fracture load
P_m	maximum load
P_Q	load at 5% offset secant
q	displacement
R	resistance to crack growth
r	radial distance measured from crack tip
r_p	radial distance measured from crack tip, that corresponds to the plastic zone
r_c^*	maximum attainable r_p for a given thickness and temperature
r_Y	radial distance measured from the crack tip at the point of general yielding
s	plastic zone size in Dugdale model
t	surface traction
T	shear stress
u, v, w	displacements in the x,y,z directions
V	crack mouth opening displacements
Vg	clip gauge crack mouth opening displacement
Vi, Vc, Vm, Vu	values of V at initiation, critical event, maximum load and critical event with ductile cracking, respectively
W	specimen width
$(W - a)_c$	characteristic (W - a), equivalent to r_c^*
x,y,z	Cartesian co-ordinates
Y	stress intensity coefficient
z	knife edge height
γ	surface energy
γ_e	elastic components of γ

γ_p	plastic components of γ
π	path contour for J integral
Δ	linear displacement
δ	COD
δ_c, δ_i & δ_m & δ_u	COD at critical value, initiation and maximum load and at critical value with ductile cracking, respectively
θ	angular displacement
μ	shear modulus
ν	Poisson's ratio
σ	stress
σ_f, σ_Y & σ_{UTS}	fracture stress, yield stress and ultimate tensile stress respectively
ε	true strain
$\Sigma l/A$	total inclusion length in unit area
ASM	American Society for Metals
ASME	American Society of Mechanical Engineers
ASTM	American Society for Testing and Materials
BSC	British Steel Corporation
BS, BSI	British Standard Institution
CC	Centre Cracked Specimen
CERL	Central Electricity Research Laboratories (Central Electricity Generating Board)
COD	Crack Opening Displacement
CT, CTS	Compact Tension Specimen
CV, CVN	Charpy V Notch
EBW	Electron Beam Welding
EPFM	Elastic Plastic Fracture Mechanics
FW	Friction Welding

GYFM	General Yielding Fracture Mechanics
HAZ	Heat Affected Zone
HSLA	High Strength Low Alloy
IME	Institute of Mechanical Engineers
JISI	Journal of the Iron and Steel Institute
LSD	Longitudinal Specimen, Surface Notch, Steel D
LSS	Longitudinal Specimen, Surface Notch, Steel S.
LEFM	Linear Elastic Fracture Mechanics
OECD/NEA	Organisation for Economic Cooperation and Development-Nuclear Energy Authority
PVT	Pressure Vessel Technology
SCF	Stress Concentration Factor
SENTfg	Single Edge Notch Tension, fixed grips
SENB	Single Edge Notch Bend
STP	Standard Technical Publication
SZW	Stretch Zone Width
UKAEA	United Kingdom Atomic Energy Authority
ZRD	Through Thickness Direction, Notch Perpendicular to the Rolling Plane, Steel D.
ZRS	Through Thickness Direction, Notch Perpendicular to the Rolling Plane, Steel S.
ZTD	Through Thickness Direction, Notch in Rolling Plane, Steel D
ZTS	Through Thickness Direction, Notch in Rolling Plane, Steel S

CHAPTER 1

INTRODUCTION

Today, Britain and the industrialised Western nations in general cannot compete with some developing nations, such as the OPEC group, in the production of low technology steels. This is due to the availability of cheap fuels, relatively cheap labour and heavy subsidies to protect the nationalised industries. For many such countries industry has political rather than economic significance.

The next decade in Britain should see a change from scattered, small steel making enterprises to large, modern, specialised founderies offering the highly technical advancements available to Britain's western competitors. This would involve greater social and economic upheavals and hardships but the alternative would inevitably lead to greater dependence on state aid to subsidise production costs.

The pressure vessel and aerospace industries are involved in the use of heavy sections and high strength steels respectively. Such materials exhibit limited plasticity and have benefited from the application of, essentially, linear elastic fracture mechanics design codes since the sixties.

Recently, the development in fracture mechanics has tended towards general engineering applications that show higher degrees of plasticity. The importance of the arrival of general yielding fracture mechanics was that it had a potential for greater practical application. The seventies had seen a great expansion of the science, leading to design curves for defect assessment. However, no widely accepted approach exists for fracture characterisation in the general yielding mode of deformation. A major drawback of general yielding fracture mechanics is in the empiricial nature of the experimental techniques developed and in general use.

Much interest was given to obtaining valid toughness characteristics from small and, hence, cheaper laboratory specimens. However, the general yielding regime of fracture with associated high tough-

nesses led to the measurement of geometry dependent toughness values. These are of limited use outside their accepted role as comparative tools.

The use of cheap, high sulphur fuels has led to the increase of the incidence of lamellar tearing since the sixties. This problem has proved to be costly, both for rewelding the damaged structures and the long delays thereby imposed on major construction projects. This problem has been attacked from two approaches, by desulphurisation techniques and by inclusion shape control.

The central objective of this research program has been to study the effects of sulphide inclusions in steels and to find a suitable technique for through thickness toughness measurements of medium to low thickness plates. As a result, a close examination of the geometry dependence of laboratory specimens that exhibit extensive plasticity was undertaken. The work led to a greater understanding of the deformation processes and their interactions with specimen boundaries. In view of this, previous work was questioned and re-examined.

CHAPTER 2

FRACTURE MECHANICS

Materials seldom show their theoretical fracture capacity because most materials are imperfect crystalline structures that fail by an accumulation of an irreversible strain at much lower stress levels. Engineering materials contain numerous defects such as pores, slag particles, inclusions and a variety of manufacturing flaws which may act as concentrators for the stresses built up in a body.

Recent developments in the North Sea oil search have led to construction of very heavy steel structures, mainly built of a low alloy steel specified by BS 4360. Of this steel, the 50D variety was specifically made for nodal constructions to avoid failure in through thickness directions by lamellar tearing. Two varieties of BS 4360 50D steel were available for this research programme for a study of the effects of inclusions on the mechanical properties of small sized laboratory specimens. Fracture mechanics techniques were used to study the effect of stresses at the tip of a sharp crack in a variety of crack orientations, specimen size and type and loading actions.

The development of fracture mechanics is discussed through the linear elastic and the general yielding approaches. Laboratory studies of fracture involve scaled down versions of the real problem and these geometric restraints are examined in later sections. There have been many material characteristics and testing variables examined that have been shown to affect the toughness characteristics and some of these have been reviewed in the latter part of this chapter.

2.1. LINEAR ELASTIC FRACTURE MECHANICS (LEFM)

In 1913 Professor Inglis (1) introduced the idea of stress concentration. His calculations showed that the stress at the tip of an elliptical hole through the thickness of a thin plate was concentrated such that:

$$\sigma^* = \sigma \left(1 + 2\sqrt{\frac{a}{\rho}}\right) \qquad \ldots.2.1$$

where σ^* is the stress concentration factor

a is the crack length, and

ρ is the root radius.

2.1.1. ENERGY BALANCE APPROACH

Griffith (2) devised the energy balance approach to fracture of cracked bodies. He offered evidence from his experiments on glass rods containing defects of various lengths, pertaining to the premise that unstable crack propagation takes place if an incremental growth of a crack results in more stored energy being released than is absorbed by the creation of new crack surfaces. This statement is appealing, since it conforms to elementary ideas about the requirements for an unstable process, and also, because it enables the treatment of the fracture situation in terms of the change in energy remote from the immediate environment of the crack tip. Practically, however, detailed evaluations of these energy terms prove very difficult, the theory does not account for any non-linear effect prior to fracture, which rather limits any engineering situations to be analysed.

From Griffith's thermodynamic treatment for a sharp crack in an infinite plate stressed uniaxially, an expression for the fracture stress at the threshold of an instability can be defined as:

$$\sigma_c = \sqrt{\frac{2E\gamma}{\pi a}} \qquad \ldots.2.2$$

in plane stress.

$$\sigma_c = \sqrt{\frac{2E\gamma}{\pi a\ (1 - \nu^2)}} \qquad \ldots.2.3$$

in plane strain

where σ_c is the critical stress at instability
γ is the surface energy term, and
ν is Poission's ratio.
This is shown graphically in Figure (3).

It must be stated that Griffith realised the limitations of his theory and observed that his value was out by two orders of magnitude.

Almost thirty years later Irwin (3) and Orowan (4) suggested that the surface energy term (γ) should be altered to include a plastic energy term (γ_p); the term ($\gamma + \gamma_p$) thus represented the energy of plastic distortion absorbed by the fracture process. Orowan (5) noticed that this plastic energy term in ductile engineering materials was two orders of magnitude larger than the surface energy term and proposed that the latter term be ignored as a consequence of this.

The redefinition of the energy term according to Irwin (6), could only be accepted if the deformation taking place occurred within a zone sufficiently small with respect to the crack itself and to the remaining segment of plate thickness. If these two stipulations are satisfied then their assumptions are true and, hence, the linear elastic approach may be followed. In this view, the modified theory consisted of evaluating the strain energy release rate at the point of fracture. This energy release rate would reach a critical value at the event of fracture and may be regarded as a material property if the fracture process was essentially similar for different loadings and specimen size.

The advantage of the energy approach is that it does not rely on the uncertainty of stresses at the crack tip. If G is to be found it must be done so experimentally, otherwise it would be necessary to integrate over the entire volume and surface to determine the energy released by crack extension. This is very difficult as it may not be easy to obtain an analytical expression for the stresses.

Irwin and Kies (6) proposed a means for determining the value of the energy release rate for different loading conditions and geometries through the expression:

$$f = v/P \qquad \ldots.2.4$$

where f = the flexibility or compliance of the body
P = the characterising load, and
v = the displacement.
This is illustrated in Fig.(2).

The strain energy of the plate is equal to half the load multiplied by the distance moved:

$$U = \tfrac{1}{2} P v \qquad \ldots.2.5$$

by substituting for v,

$$U = \tfrac{1}{2} f P^2 \qquad \ldots.2.6$$

For this expression, the strain energy release rate, G, with respect to an incremental crack growth, ∂a, is:

$$\partial U/\partial a = \tfrac{1}{2} P^2 \ (\partial f/\partial a) \qquad \ldots.2.7$$

By measuring the compliance, f, of a material with various edge cracks, $\partial f/\partial a$ can easily be measured for the chosen geometric shape (7). The fracture test could then be interpreted by evaluating $\partial U/\partial a$ at fracture by measuring P and v at various values of (a). The compliance of various specimen shapes were determined on this basis (8,9).

Irwin (10,11) proposed that the strain energy release rate be denoted as G and that it be defined as an irreversible energy loss per unit area of newly created surface. This material fracture toughness parameter became critical at the point of crack instability, G_c . G had the advantage of being independent of the machine hardness characteristics.

Thus, the energy approach avoids the uncertainty of the stress state at a crack tip. G must, however, be determined experimentally,

otherwise it is necessary to integrate over the entire volume and surface to determine the energy released by crack extension, not withstanding the difficulty in analysing the stresses.

2.1.2. STRESS INTENSITY FRACTURE APPROACH

An alternative approach to the study of fracture is to consider the highly stressed region immediately surrounding the crack tip. Irwin (10,11) used the analyses due to Westergaard (12), which treated the stress field in the vicinity of an elliptical internal void or notch using functions of a complex variable to define the stress intensity factor K. The value of the constant depends upon the fracture mode. There are three basic types.

The crack opening mode, Mode I, is associated with a local displacement in which the crack surfaces move directly apart; in the shearing mode, Mode II, the crack surface moves normally to the crack front and remains in the crack plane and finally anti-plane shear mode, Mode III, where the crack surfaces move parallel to the crack front and remain in the crack plane, see Figure (3).

Thus we obtain for Mode I the following stresses and displacement fields for the case of a rectilinear crack lying in the x - z plane,

$$\begin{bmatrix} \sigma_x \\ \sigma_y \\ T_{xy} \end{bmatrix} = \frac{K_I \cos(\theta/2)}{\sqrt{2\pi r}} \begin{bmatrix} 1 - \sin\frac{\theta}{2}\sin\frac{3\theta}{2} \\ 1 + \sin\frac{\theta}{2}\sin\frac{3\theta}{2} \\ \sin\frac{\theta}{2}\cos\frac{3\theta}{2} \end{bmatrix} \quad \ldots.2.8$$

$$\sigma_z = \nu(\sigma_x + \sigma_y)$$

$$T_{xz} = T_{yz} = 0 \quad \ldots.2.9$$

$$u = \frac{K_I}{E} (r/(2\pi))^{\frac{1}{2}} [\cos(\theta/2) (1 - 2\nu + \sin^2 (\theta/2))]$$

$$v = \frac{K_I}{E} (r/(2\pi))^{\frac{1}{2}} [\sin(\theta/2) (2 - 2\nu - \cos^2 (\theta/2))]$$

$$w = 0 \qquad \ldots.2.10$$

Equation [2.8] applies for plane stress and plain strain, Equation [2.10] applies for plane stress with slight alteration may be expressed for plain strain.

The value of σ_z depends on whether the stress state is plane strain ($\epsilon_z = 0$) or plane stress ($\sigma_z = 0$).

The stress intensity factor K_I is not dependent on θ and r, hence it controls the intensity but not the distribution of the stress field for different crack configurations.

K_I is defined here as:

$$K_I = \sigma\sqrt{\pi a} \qquad \ldots.2.11$$

more generally

$$K_I = Y\ \sigma\sqrt{\pi a} \qquad \ldots.2.11a$$

where Y is a geometric factor and takes into account boundary conditions such as surfaces, crack shape and distribution of load.

Hence, K can be physically interpreted as the parameter which reflects the redistribution of crack tip stresses.

For edge sliding mode or shearing mode, Mode II, we obtain:

$$\begin{bmatrix} \sigma_x \\ \sigma_y \\ \tau_{xy} \end{bmatrix} = \frac{K_{II} \sin(\theta/2)}{\sqrt{2\pi r}} \begin{bmatrix} 2 + \cos\frac{\theta}{2}\sin\frac{3\theta}{2} \\ \cos\frac{\theta}{2}\sin\frac{3\theta}{2} \\ \cos\frac{\theta}{2}\sin\frac{3\theta}{2} \end{bmatrix} \qquad \ldots.2.12$$

again σ_z depends whether plane stress or plane strain applies.

For plane strain:

$$\sigma_z = \nu\ (\sigma_x + \sigma_y)$$

$$T_{xz} = T_{zy} = 0 \qquad \ldots.2.13$$

$$u = \frac{K_{II}}{E}\ (r/(2\pi))^{\frac{1}{2}}\ [\sin(\theta/2)\ (2 - 2\ \nu + \cos^2\ (\theta/2))]$$

$$v = \frac{K_{II}}{E}\ (r/(2\pi))^{\frac{1}{2}}\ [\cos(\theta/2)\ (-1 + 2\ \nu + \sin^2\ (\theta/2))]$$

$$w = 0 \qquad \ldots.2.14$$

For Mode III

$$T_{xy} = -\ \frac{K_{III}}{\sqrt{2\pi r}}\ \sin\ (\theta/2)$$

$$T_{yz} = \frac{K_{III}}{\sqrt{2\pi r}}\ \cos\ (\theta/2) \qquad \ldots.2.15$$

$$\sigma_x = \sigma_y = \sigma_z = T_{xy} = 0 \qquad \ldots.2.16$$

$$w = \frac{K_{III}}{E}\ (2\ r/\pi)^{\frac{1}{2}}\ \sin\ (\theta/2)$$

$$u = v = 0$$

A few points must be made here; since the above solution is developed from a linear elastic analysis, provided that only one mode is present, the stress intensity factors, due to different loadings, can be superimposed by algebraic additions and if more than one mode is present the individual stress components and displacements can be similarly superimposed. A compendium of solutions is given by Paris and Sih (13).

These equations have been obtained by neglecting higher orders of r and hence they can be regarded as good approximations where r is small. Hence, the value of K will become more inaccurate the further away from the crack tip, Figure (4).

This analysis will also fail when relating to the immediate vicinity of the crack tip that is, where r = 0 we have σ_x being at infinity.

An important feature of the above equations is that the distribution of stresses around any crack in a structure is similar and is dependent only on r and θ. The difference in different crack components relies upon the magnitude of the stress field parameter K, Figure (5).

In this thesis, Mode I will be used solely and no further reference will be made to the other modes since the three point bending tests of the COD techniques involves, roughly, a Mode I opening.

2.1.3. CORRELATION OF G AND K

Irwin was able to correlate G, the strain energy release rate, to the stress intensity factor, K.

$$G = K^2/E \qquad \text{for plane stress} \qquad ....2.18$$

$$G = K^2/E\ (1 - \nu^2) \qquad \text{for plane strain} \qquad ....2.19$$

This proof is of fundamental importance since it links the fracture toughness parameters of the stress approach to that of the energy approach.

Consider the work done in closing a crack of half length a + Δ a to (a), under a fixed grips and plane strain:

work done in closing crack = G Δ a

$$G\ \Delta\ a = \tfrac{1}{2} \int_0^{\Delta a} \sigma_y\ u_y\ dx \qquad ....2.20$$

from Westergaard:

$$\sigma_y = \frac{K}{\sqrt{2\pi r}} \cos(\theta/2) \left[1 + \sin(\theta/2)\sin(3\theta/2)\right] \quad ....2.21$$

so at $r = x$ and $\theta = 0$,

$$\sigma_y = \frac{K}{\sqrt{2\pi x}} \quad ....2.22$$

Similarly the displacement u_y from Westergaard:

$$u_y = \frac{2K(1+\nu)}{E} \sqrt{r/(2\pi)} \sin(\theta/2) \left[2 - 2\nu - 2\cos^2(\theta/2)\right]$$

and at $r = \Delta a - x$ and $\theta = \pi$

$$u_y = \frac{2K(1-\nu^2)}{E} \left[(\Delta a - x)/(2\pi)\right]^{\frac{1}{2}}$$

$$G\,\Delta a = \frac{K^2(1-\nu^2)}{2\pi E} \int_0^{\Delta a} \left[(\Delta a - x)/x\right]^{\frac{1}{2}} dx \quad ....2.23$$

using $x = \Delta a \sin^2 \omega$

$$G = \left[K^2(1-\nu^2)\right]/E \quad ....2.24$$

2.1.4. PLASTIC ZONE SIZE

As mentioned before, the highly stressed region at the tip of a crack is a region of plastic flow and this region may be estimated by substituting a yield criterion into the stress field equation when $\theta = 0$, this leads to:

$$r_Y = 1/(2\pi) \left(K_I/\sigma_Y\right)^2 \quad ....2.25$$

for plane stress conditions. Hence, our crack lengths must be considered to be:

$$2\ (a + r_Y)$$

or $$2\ [a + 1/(2\pi)\ (K_I/\sigma_Y)^2] \qquad \ldots.2.26$$

For the plane strain, where the strain $\epsilon_z = 0$, one can derive the expression for σ_z from:

$$\epsilon_z = 0 = 1/E\ [\sigma_z - \nu\ (\sigma_x + \sigma_y)] \qquad \ldots.2.27$$

Along OX $\sigma_x = \sigma_y$, hence, $\sigma_z = 0.6\ \sigma_x$, given that Poissons ratio, ν, is equal to 0.3.

Given that the Mises Flow Rule is:

$$\bar{\sigma} = \sqrt{\tfrac{1}{2}\ [(\sigma_x - \sigma_y)^2 + (\sigma_y - \sigma_z)^2 + (\sigma_z - \sigma_x)^2} \qquad \ldots.2.28$$

with $\sigma_x = \sigma_y$ and $0.6\ \sigma_x = \sigma_z$

$$\bar{\sigma} = 0.4\ \sigma_x \qquad \ldots.2.29$$

where $\bar{\sigma}$ is the mean stress.

From Westergaard's analysis, the yield strength along OX is:

$$\bar{\sigma} = 0.4\ \sigma_x = (0.4\ \sigma\ \sqrt{\pi a})/(\sqrt{2\pi r}) \qquad \ldots.2.30$$

$$r = (0.16\ \sigma^2\ a)/(2\bar{\sigma}^2) \qquad \ldots.2.31$$

or

$$r = (0.16/2\pi)\ (K_I/\bar{\sigma})^2 \qquad \ldots.2.31a$$

Where $\bar{\sigma}$, the mean stress, is equal to σ_Y in uniaxial tensile tests. Hence, the plastic zone size in plane stress is much larger than that in plane strain. A more general way of describing r_Y is by:

$$r_Y = [1/(2\pi)][K_I/m\ \sigma_Y]^2$$

where m is the constraint factor and is equal to 1 in plane stress and 3 in plane strain.

Two points to be made about r_Y; first, that it depends on the position along the crack front, being largest at the two free surfaces and smallest at the midplane. It also varies with angle θ and in terms of r and θ it is,

$$r_Y = [1/(2\pi)] \ (K_I/\sigma_Y)^2 \cos^2(\theta/2)(1 + 3 \sin^2 \theta/2) \qquad ....2.32$$

in plane stress. The zone assumes a dog-bone shape. This has been proven by etching techniques. Secondly, that this expression of r_Y itself depends on the value of K which, in linear elasticity, does not account for effects of work hardening or large strains, Figure (6).

2.1.5. EFFECT OF MATERIAL THICKNESS ON K_C AND G_C

The larger plastic zone associated with conditions of plane stress implies a larger G and K than for plane strain because of the work expenditure involved in the flow mechanisms. This explains the fear associated with the handling of thick materials for heavy constructions such as the case of the off-shore industry.

The plot of K_{Ic} and G_C against thickness (14 - 16) is shown in Figure (7) and is discussed in detail in the table below. The graph plotted out shows that a large variation in toughness is produced for thicknesses used in practically all engineering practices. This casts doubts on the possibility of measuring a single parameter to gauge the fracture toughness in such a way as to be applicable in general practice.

Region A: In this region, one is concerned with thin specimens where the mode of fracture is by sliding at 45^o to the crack plane. Specimens show increase in toughness with thickness. It is a region of plane stress where any stresses generated in the z direction are relieved by yielding. Yielding occurs at uniaxial

yield stress. K_I values measured here tend to scatter a lot.

Region C: Here one is concerned with thick specimens,

$$B \geq 2.5 \ (K_{Ic}/\sigma_Y)^2 \qquad \ldots.2.33$$

The fracture is observed to follow a flat face with only a small region of shear lips at the edges. This is a region of plane strain. A stress triaxiality is created within the body because of its thickness increase and its ability to transmit a force through it. The shear lips, which can be looked at as a plastic zone area, are limited to the surfaces of the specimens. This region will give valid K_{Ic}.

Region B: This is the intermediate region where neither pure plane stress nor plane strain reign. A cracked specimen falling within this region of thicknesses will initially fail with a flat surface at σ_p, Figure (7), within the centre of thickness of test piece. Catastrophic failure is evaded due to the load carrying role of the side ligaments which comprise a fair proportion of the total thickness. If the square fracture tunnels ahead rapidly, a 'pop-in' will occur and is recorded by a sudden extension for constant or decreasing load. With increasing load, the plastic zone increases in size and hence more relaxation of σ_z occurs which inhibits the plane strain fracture, ending eventually with slanting fracture. Since a longer crack is involved, the fracture load is lower than for thin specimens.

Assuming a value of K_c of around 135 $MNm^{-3/2}$, one is left with a problem of testing steel specimens with a width in excess of 0.5 metres. Such large specimens involve considerable expense and effort in testing. Furthermore, most engineering structures are built of plates normally much less than 50mm in thickness.

For such thicknesses the specimen is in a plane stress regime and K will vary rapidly with slight alterations in the thickness. It is, therefore, necessary to find an alternative to this approach that is less sensitive to slight thickness variations in a plane stress regime.

2.2. GENERAL YIELDING FRACTURE MECHANICS (GYFM)

Aided by LEFM, one may find a measure of stresses and strains at the crack tip. The accuracy of the test decreases with decreasing specimen size and, for a structural steel, the plane strain dimensions are normally prohibitively large, expensive or both. The effect of the state of stress on strain was first shown experimentally by Bridgman (17), showing the increased strain to failure under reduced mean-stresses brought about by carrying out the experiment under high pressure.

The reason for the development of greater strains with plane stress lies in the development of a comparatively large plastic zone. Yielding spreads under shear stress components and for a given amount of opening at the crack tip, the Tresca criterion for yielding predicts that the shear modulus, T, will be greater for plane stress than plane strain since:

for plane stress $\sigma_z = 0$, $\sigma_y = \sigma_x$

therefore $T = (\sigma_y - \sigma_x)/2$

for plane strain $\sigma_y > \sigma_z > \sigma_x$

hence $T = (\sigma_y - \sigma_x)/2$ 2.34

This was first shown by Ludwig (18) who realised that to keep material flowing in plane strain, the maximum principal stress needs to be much greater than when only one principal stress was non-zero.

The formation of large plastic zones requires the flow of a large amount of material, plastically. This is seen on a load-displacement trace as non-linearity and is associated with the loss of triaxiality by the formation of a comparatively large strain in

the thickness, or z-direction. The occurrence of the plane stress regime with large ε_z deformations in engineering structures is very common-place; in fact, plane strain exists only in special cases of ultra high yeild strength materials, restrictive geometries such as welded T junctions and at temperatures that represent the lower energy shelf of the material.

A plane strain situation, with all its constraints, forms a very high stress gradient at the crack tip and hence, concentrates the strains, this enhances the initiation mechanisms for fracture. Since σ_z is zero at the specimen surface, it is reasonable to assume it is at a maximum in the centre, thus, suggesting maximum constraint and it is here that fracture initiates in a thumbnail type of crack. This stable cracking is allowed to reach a critical stage in stress concentration and catastrophic failure sets in. Figure (7) shows that in region C, in every thick specimen, this type of behaviour will occur.

Plane strain deformation increases with thickness of specimen and is likely to occur when a certain thickness is exceeded. The standard publication suggests that this thickness is achieved when:

$$B, a \geq m \, (K_{Ic}/\sigma_Y)^2 \qquad \ldots.2.35$$

The ASTM publication (19) suggests that m be taken as equal to 2.5 and the BS 5447:1977 publication (20) equates m to a more restrictive 4. Thus the ASTM requires B as 50 times the plastic zone size and the BS requires it to be 80 times greater.

2.2.1. THE CHARPY TEST

Thickness requirements, to meet plane strain fracture, are rarely met in engineering structures and it was apparent that a new approach to elastic plastic fracture was needed. Up until recently, it was necessary to use a non-fracture mechanics technique to predict the quality of metals and, in particular, welds; this was the Charpy V notch (CVN) impact test. CVN lacked applications in a quantitative way even though many authors tried to relate Charpy

impact energies to fracture parameters like K_{Ic} for example, the authors listed (21 - 27). This permitted a quantitative assessment of critical flaw size and allowable stress levels. These correlations are empirical in nature for the following reasons:

(i) Charpy V notches are blunt and this may lead to totally unrealistic characterisations of the toughness of the materials. In some cases it was shown that CVN gives erroneous toughness characterisations (28).

(ii) Impact conditions are not comparable to static testing.

(iii) In tough materials, the CV notches are too shallow to prevent gross sectional yielding from the top surface of the test piece.

(iv) Fracture parameters normally distinguish between initiation and propagation. K_{Ic} allows for very limited thumb-nail cracks, Charpy allows for complete rupture and, in ductile materials, over two thirds of the energy is expended in propagating the crack.

(v) z-direction strains are large in Charpy V specimens while they are restricted in K_{Ic}.

Therefore, what the Charpy parameter represents, is energy absorbed by the deforming material ahead of a crack, whilst for K_{Ic} it is the critical values of stresses at instability.

It is also apparent from recent developments that, at best, the CVN test is dependable only as a quality assurance test, and again, it would be improved if sharp cracks were used. Any correlation between CVN energy and K_{Ic} is purely empirical and only realistic in very brittle materials that, as a consequence, show little energy absorption for crack propagation.

2.2.2. DEVELOPMENT OF GYFM APPROACH

Having realised the problems of Charpy testing and the need

for a parameter that can be applied in terms of critical defect assessment in structures, there appeared a multitude of approximating parameters in the past twenty years. Some have been applicable and are discussed below. The past decade has brought about another problem and that is cost effectiveness as a result of world economic recession. This has played an important role on the volume of publications attempting to establish cheaper methods of relating to these newly developed elastic-plastic fracture parameters and in turn relating to critical crack assessment or to linear elastic parameters. To complicate issues further, the economics of metal fabrications has shifted to lighter structures with higher strength metals and smaller factors of safety. This has led to the tolerance of cracks only a fraction of the size tolerated in more ductile materials that had lower proportionate loads to carry. As a consequence, the non-destructive testing for flaws is becoming more difficult as allowable flaw sizes shrink.

It is important to note here the necessity of assessing the criticality of a defect. Present methods of testing the safety of pressure vessels is to proof load to a pressure in excess of their service requirements, any failures of the system are repaired and the vessel is shipped out for active service. That the excessive loading may have caused growth is accepted as a necessary evil. Another method, is to repair all defects picked up by non-destructive examination; that the repair operation would introduce welding stresses and cause further embrittling of the materials by the grain coarsening and grain boundary embrittlement is, sometimes ignored.

The fact that most work is conducted on welds leads to the conclusion that welds are the weakest point in a welded structure and this, in general, is true. The welds deposited are generally more brittle and have inherent defects associated with the welding process. Only when working at high design stresses and very low temperatures does the plate material come under the critical eye and in particular when through thickness ductilities are required.

Having established that the stresses applied to a system cannot be used to evaluate the local stresses and strains at a crack tip,

Cottrell (29) and Wells (30) were the first to attempt to characterise the fracture toughness of a tough material, in the presence of a sharp crack, on the basis of opening displacements at the crack tip where the extent of plasticity had rendered LEFM analyses inapplicable.

2.2.3. CRACK OPENING DISPLACEMENTS

Allowable stresses in a body rapidly approach a limiting value upon general yielding. With a progressively rising stress, the plastic zone associated with the crack tip must simply grow in size until, at a given temperature, a critical crack tip displacement is reached at which fracture occurs. The mode of failure is also dependent on specimen geometry. It was seen above, that the calculations of the plastic zone size was necessary to adjust K for crack tip plasticity by the following relationship:

$$K^* = \sigma \sqrt{(\pi\ a^*)} \qquad \ldots.2.36$$

where $a^* = a + r_Y$

Unfortunately, r_Y, the plastic zone, becomes more difficult to calculate as it grows in size, thus incorporating a limit to how much K can be adjusted for plasticity. This leads to an understanding of the advantages of studying the behaviour of the strains in this region, that is, the crack tip displacements.

A theoretical rationalization of the COD concept is outlined below, the theoretical validity is subject to argument (31). Ductile engineering materials exhibit crack tip blunting in the upper energy shelf prior to the onset of crack extension. Small plastic zones of the size $r_Y \leq 10^{-2}a$, which occur in situations of limited yielding can be dealt with as mentioned above by the Irwin r_Y correction factor which, in effect, increases the crack length and hence, the elastic stress intensity factor. This situation of limited yielding is of limited use to the present work where extensive plasticity occurs at the design temperatures.

With this and Westergaard's equations for a through crack in an infinite plate, Wells produced, for plane stress:

$$2v = (4\ \sigma/E)\ [\sqrt{(a^2 - x^2)}] \qquad x < a \qquad ....2.37$$

since $x = a - r$

$$2v = (4\ \sigma/E)\ [\sqrt{r(2a - r)}] \qquad ....2.38$$

When the crack length, a, is much greater than the plastic zone size, it is simplified to:

$$2v = (4\ \sigma/E\ (\sqrt{2ar}) \qquad ....2.39$$

which gives

$$2v = (4K/E)\ (\sqrt{2r/\pi}) \qquad ....2.40$$

from

$$K = \sigma\sqrt{(\pi a)}$$

assuming that under yielding r is equal to r_Y which, in turn, is given by Westergaard's analysis, then substituting gives:

$$2v = (4K_I^2)/(E\ \pi\ \sigma_Y) \qquad .....2.41$$

ans since 2v is assumed to be δ, the crack opening displacement, this can be re-written as:

$$\delta = (4K_I^2)/(E\ \pi\ \sigma_Y) = 4G/(\pi\ \sigma_Y) \qquad ....2.42$$

correct for plane stress and for plane strain the numerator is multiplied by $(1 - \nu^2)$.

The above equation can be represented for general situations incorporating a geometrical constraint parameter m.

$$\delta = (K_I^2)/(m\ \sigma_Y E) = G/(m\ \sigma_Y) \qquad ....2.43$$

where limited constraint in plane stress allows m to equal 1 and in plane strain m to equal 3, due to greater constraints.

Dugdale (32) and Barenblatt (33) provided an improved model for the extent of the plastic zone in the crack plane ahead of the crack tip. Figure (8) represents this idea. Dugdale considered a crack of length 2a in an infinite plate subject to a remotely applied uniform stress, σ. The length of the crack is increased from 2a to 2a* by the addition of notional plastic zones of length s. The faces of the crack over the distance s from both ends are partially restricted from opening by a restraining force t, acting directly on the 'crack' faces. The opening of the crack walls at the distance $x = \pm a$ corresponds to the COD at the ends of the original crack.

One of the assumptions of the Dugdale model is that yielding occurs in the form of narrow bands of thickness comparable to the dimensions of the slit opening and lying along the plane of the cut with a length of s, such that there are no stress singularities at the end of the slits. This seems unlikely but has been observed in very thin sheet materials (32).

The strip yield model was interpreted in terms of fracture by Wells (34,35). He observed that under plastic deformations the tip of the crack tended to blunt with a near square end contour. This opening was termed the Crack Opening Displacement (COD).

In early applications of this model (36) t, the restraining force, was equated to the uniaxial yield stress:

$$a/a^* = \cos [(\pi \sigma)/(2 \sigma_Y)] \quad ....2.44$$

Burdekin and Stone (36) pursued this experimentally and theoretically for plane stress Mode I crack tip displacements, producing:

$$\delta = 2 r = [(8 \sigma_Y a)/(\pi E)] \ln \sec [(\pi \sigma)/(2 \sigma_Y)] \quad ....2.45$$

which by expanding produces:

$$\delta = [(\pi\ \sigma^2\ a)/(E\ \sigma_Y)]\ [1 + (\pi^2/24)(\sigma/\sigma_Y)^2 + \ldots] \qquad \ldots.2.46$$

ignoring all higher powered terms, this approximates to:

$$\delta = \frac{\pi\ \sigma^2\ a}{E\ \sigma_Y} \qquad \ldots.2.47$$

that is:

$$\delta = \frac{K^2}{E\ \sigma_Y} = \frac{G}{\sigma_Y} \qquad \ldots.2.48$$

This derivation of COD has been experimentally validated for low applied stresses when plastic flow at the crack tip is limited.

COD becomes critical when it reaches a critical value, δ_c, this is similar to the LEFM concept where $K < K_{Ic}$. COD thus bridges the elastic and plastic conditions since δ may be computed for conditions of plane stress and plane strain. However, there are many complications that prohibit a simple correlation between δ and δ_c.

One drawback for the strip yield model is the limitation in geometry for which solutions are available. For the strip yield itself, computational methods are available (37,38), using finite element analyses for elastic-plastic studies. COD will be inherent in the elastic formulation but in the plastic form the difficulty lay in the inability to identify, precisely, the point in the crack tip region for which COD should be calculated.

2.2.3.1. EXPERIMENTAL COD

COD is literally the amount of opening the crack will undergo when subject to opening stresses. When the amount of opening is well into the plastic regime, i.e. $\sigma/\sigma_y > 1$ and into general yielding, then the measured opening is subject to much controversy. More relevant to this section are experimental difficulties associated with measurements of such small displacements and also

the difficulties in relating experimental and theoretical analyses.

COD may be measured on a variety of specimen and notch geometries. The former are usually limited to square cross-sectioned bar of 4 to 1 span to width ratio, or a 2 to 1 cross-sectional area as dictated by DD19 (39) and later by the British Standards (40). COD has also been observed for totally different specimen geometries. The notch may vary from machined notches (41-43) to fine fatigue cracks, grown under specified loads (39), single and double notches (44,45) straight and angled notches.

Dawes (46) suggested that the opening at the crack tip be defined as that opening which occurs at the original crack tip, to avoid ambiguity of previous COD definitions which sometimes involved the stretch zone width (defined as the yielded and sheared area at crack tip), other crack tip profiles and finally the elastic plastic interface on the flanks of the crack.

The crack tip deformation behaviour will depend on the stress state, temperature, strain rate and, of course, the material properties at the crack tip. The properties that are of interest are grain size, hardness, inclusion content, yield strength, anisotropies of fabrication history and others. The crack front may take on a variety of profiles and these are documented by Dawes (46).

2.2.3.2. MODES OF FAILURE IN THE COD TEST

Figure (9) categorises three general types of instability during fracture toughness testing. The figure represents a transition of COD with temperature from tough upper shelf, at high temperatures, to brittle lower shelf, at cold temperatures. This is usually separated by a steeply inclined transition region. This type of behaviour is found for any one specimen size in COD; the transition temperature will depend on a variety of factors such as specimen size and rate of straining.

The transition curve is also apparent to CVN testing and K_{Ic}, all varying with temperature.

Region I is characterised by low toughness, showing very limited plastic strain and fracture tends to be fast or catastrophic, in the form of brittle cleavage fracture that occurs prior to yielding of the material.

Region II is the transition region; in this region there appears to be some ductility beyond general yielding before the brittle fracture sets in. Knott (44) suggests that the reason for this is due to the inability of the material to increase its constraint, to reach a sufficient stress intensity necessary to cause brittle fracture, without prior strain hardening below the notch which will have the effect of increasing the flow stress.

Region III exhibits high toughness and for structural materials, the failure mechanism is fully plastic and occurs when sufficient plastic strain has developed across the remaining ligament to cause instability. The crack tip blunts at general yielding and may continue to do so up to instability but as more often the case, the crack tip begins to grow in a stable and ductile manner before maximum load is reached. Small specimens tend to fracture after general yield and large specimens favour fracture before general yield.

2.2.3.3. MEASUREMENT OF COD

Initially, the opening of the crack tip could be studied by an ingenious device, referred to as the rotating paddle (24,58). This could be done because the crack profile was square and could accommodate the paddle but, since then, fatigue cracks have become a requirement. At the UKAEA Conference (47), it was finally decided to abandon the paddle-technique. Note, however, that this technique could be used on-load. The technique was found to show unacceptable scatter in results and care should be taken when reference is made to its use.

Measurements later involved surface replicas (48,49) strain measurement techniques such as moire fringes (50,51) and measurement of through or z-strains at the crack tip (52,53). Camera techniques

have been developed (36,54) to compare on-load and off-load openings, clip gauges at the crack mouth and double clip gauges (55). Post-mortem measurements on broken samples have been made (56,57) and on the notch root contraction on or off-load. The most precise representation of COD is the silica gel replica technique suggested by Robinson and Tetelman (58) for on-load studies. It is apparent, however, that this technique is too time consuming and delicate for practical applications, even if better catalysts are developed to speed up hardening.

There has been a considerable amount of work relating COD to other parameters, such as stretch zone with (59-61) but this involved considerable errors since the zone is not of constant width along the crack front. COD has also been associated with cross head displacements (62), angle of bend (47,58), notch root contraction, on-load and off-load (47,58,63-65) and notch mouth opening displacement (47,58,66-68). The notch mouth opening by clip gauge calibration is the accepted method for measuring displacements, according to DD19 (39) and BS 5762 (40).

In DD19, two calculations for relating crack mouth opening, Vg, to COD have been suggested. The Wells formula (41) relates well with LEFM while the Ingham formula (42) is recommended for thicknesses below 50mm and is accurate up to a crack tip opening of about 0.5 mm; this method is based upon a trigonometric calculation, assuming that there is plastic rotation of a hinge mechanism about a point located a third of the distance of the remaining uncracked ligament, below the notch:

Calibration of COD versus position of measuring from a clip gauge to the crack tip, have been established to determine the relationship between Vg and δ. This was done by marking datum points on the crack faces and the calibration of which revealed that, except for a region near the crack tip, the two faces of the notch remained planar during the test and open apart like a hinge. The apparent centre of rotation remains constant for a considerable part of the test range and even tolerates some crack growth. This

leads to the simple geometric relation between V and δ. Furthermore, measurement of δ at the original crack tip takes account of the shifting centre of rotation.

The most recent publication, BS 5762:1979 differs in that now, the crack mouth opening (Vg) is divided such that it separates the elastic and plastic components of the opening. The elastic component is related to the LEFM at the maximum load of interest and, as such, is temperature related. The plastic component is converted into crack opening by a modified rotational constant version. For plastic materials that show considerable ductilities, the elastic component of crack opening becomes vanishingly small. The new BSI guidelines suggest that the crack length be averaged and not that of the maximum extent. It restricts loading by three point bending and although it still allows the use of W = B and W = 2B specimen geometries, it shows preference for the latter, more restrictive geometry.

Whereas, previously, three COD values were identified: at crack instability (δ_c), crack initiation (δ_i) and at maximum load (δ_m), there now exist four categories of values calculated from the following plastic components of crack mouth openings V:

Vc plastic components of opening at either of the following where no ductile crack growth has occurred.
   a) unstable fracture
   b) onset of arrested brittle fracture (pop in) - gives δ_c.

Vi crack opening at onset of slow crack growth - gives δ_i.

Vm at first attainment of maximum load - gives δ_m.

Vu opening at either
   a) unstable fracture
   b) onset of arrest of brittle crack (pop in), where in both cases ductile crack growth has occurred - gives δ_u.

2.2.3.4. DETECTION OF THE POINT OF CRACK INITIATION

There have been many methods devised to determine the point of

crack initiation from a gradually increasing load against displacement plot for COD and J Integral testing. BS 5762 recommends some publications for a variety of techniques. Clark (69) has made a recent study of these techniques and it is best to clarify this point here, for tests on ductile steels.

(i) Acoustic emission techniques are only successful on high strength steels. Low strength ductile steels tend to be 'too noisy' to be able to distinguish between different emissions.

(ii) Potential difference techniques are not sensitive enough to define initiation.

(iii) Values of δ_i at low temperatures that just fail to show fibrous thumbnail cracking, yield conservative estimates of δ_i.

(iv) Off-load δ_i are conservative.

(v) δ_i measured at the surface of the specimen are unconservative, due to crack bowing and prior initiation of ductile cracking in the centre of the specimen.

(vi) Replica techniques are inapplicable for fast strain rates.

2.2.3.5. COD AT INITIATION OF DUCTILE CRACK GROWTH

Burdekin (70) suggested that crack opening becomes critical at the first instant of ductile tearing, to be calculated at the original crack tip. The term for initiation becomes δ_i. Any COD measurement that involved tearing was not considered critical to the fracture process. Two such values were thus classified as non-critical; one at maximum load, δ_m, characteristic of tough materials that show a maximum load plateau after general yielding and before plastic collapse, and the second is δ_u, that according to BS 5762 occurs at sudden load instability and which should occur after some ductile cracking.

Ductile materials tend not to show a pop-in or fail at first occurrence of ductile tearing. The smoothly increasing load

against crack opening trace, normally involves considerable crack growth before maximum load. Stresses, being more triaxial in the centre of the specimen than at the surfaces, tend to cause cracking at the centre, giving a tunnelling effect and making it difficult to determine crack initiation. The methods of detecting crack initiation have been reviewed above. In conclusion, it must be said that at best, the accuracy is dependent on: the accuracy of the technique, complications of both SZW and fatigue crack front and also the subjective view of the experimenter.

The reason for excluding any value of crack opening that involves crack growth is due to the understanding that the amount of opening up to initiation can be considered as a materials parameter whilst that beyond it is subject to dependencies on specimen geometry and the stiffness of the testing system (71-73). Green and Knott (74) have shown that a value of a crack opening beyond initiation, if held with fixed loads, may lead to crack growth, hence the necessity for working with δ_i.

Recently, however, as testing techniques became more precise, it has been found that δ_i is not as constant as once thought. It appears that it is dependent on a/W ratios at temperatures above the lower half of the transition curve, as recently shown by Chipperfield and de Castro (75,76). The crack length to specimen width ratio (a/W) dependence of δ_i is due to the stress state at the crack tip, such that longer cracks appear to provide a more highly restraining regime at the crack tip than do short cracks. δ_i therefore decreases with increasing a/W as a consequence of the stress state. It is foreseen that as more work is conducted in the plane stress regime it will become apparent that δ_i tends to be size dependent.

2.2.3.6. COD AT MAXIMUM LOAD

δ_m is the measure of crack opening at the first attainment of maximum load on an autographic plot of load versus clip gauge opening and as such, is easily recognisable. However, it was apparent that δ_m for structural steels, in the plane stress mode

of deformation, is a measure of opening involving considerable amounts of ductile crack growth. Smith (77) represented δ_m as:

$$\delta_m = \delta_i + C \qquad \ldots.2.49$$

where C was found to be about 0.17 mm for mild steel for his particular geometry. The above equation was, naturally, empirical and was considered of little value outside its context. The limitation is due to the geometrical dependence of the failure load and, hence, of the quantity C.

Crack propagation is dependent on geometry in plane stress because of the formation of shear lips, which are the surface manifestations of the plastic zone. Shear lips form at free surfaces where σ_z is negligible and high plastic strains involve much utilization of energy in the flow of material. The shear lips size of test piece thickness decreases for increasing specimen thickness. In plane stress, this ratio is considerable but for a sufficiently large specimen size it becomes comparatively small in terms of energy absorbed during deformation; such conditions prevail in plane strain. For this reason it was assumed that the quantity C is of little value, especially since it could be related to the stiffness of the testing system and geometrical restrictions. Recent developments in COD have been an attempt to reduce the value C by inducing stress triaxialities in small specimens, through geometrical restrictions.

δ_i was considered to be very conservative for calculating maximum tolerable defect sizes in structures from COD design curves (45,78-82). Dawes and Kamath (45) recommended the use of either δ_m or δ_i in their COD design curve approach. Barr et al (82) reflect the strongest and most critical view to δ_i, quote 'that it is difficult to see ... how the δ_i values can have a bearing on the final fracture of a structure which is controlled by tensile instability' for situations of small crack sizes. They suggested the use of δ_m or better still plastic collapse calculations.

In conclusion, the value of δ_m exceedes δ_i by the constant C,

which has been shown to be very dependent on many parameters. It is easy to see situations of extreme compliance where the value C would tend to zero, yet by ignoring it, conservative design results. It appears that the value C should be included in the design subject to geometrical, environmental and strain rate considerations. That is, the constant C appears to be a function of the amount of ductile crack growth. By increasing the specimen thickness or increasing the compliance of the system the amount of ductile crack growth is reduced before unstable fracture takes place, this leads to a reduction of the value of C.

2.2.4. RESISTANCE CURVES

Where ductile materials show considerable crack growth at maximum load for J Integral or COD measurements, the use of such parameters can be justified only as a representation of a lower bound to unstable fracture by cleavage (84). The curves describe the behaviour of a ductile tear as it extends through the material. A simple plot would be a linearly rising fracture toughness value against ductile crack extension. The slope of the curve represents the energy increase required to grow the crack.

The R curve is normally viewed in an energy balance form, such that the rate of energy absorbed for growing crack, which also involves dissipative energies such as plastic zone and shear lip formation, is equal to the strain energy release rate for the cracked material, that is:

$$R = G$$

or

$$dW/da = dV/da \qquad \ldots.2.50$$

at instability, the energy absorbed is equal to the energy released and for unstable propagation the energy released is in excess of that absorbed, that is,

$$dG/da > dR/da \qquad \ldots.2.51$$

There is much controversy over the geometric dependence of R curves and the state of the art is summarised by the ASTM STP 527 publication (85) and more recently by Kamath (84). Again the specimen size is recommended to be of similar thickness as the structure. Furthermore, it is recognised that displacement controlled testing (which is the characteristic of screw driven machines) enables maximum stable crack growth and the attainment of a plateau toughness level.

Garwood (86,87), regarded that R curves did not represent purely a measure of the extension of the shear lips but it also characterised the advancing crack tip. However, he then suggested that a new parameter which reaches equilibrium just after initial crack growth, represented a constant for the growing crack tip and defines it as δ_a, which is some constant fraction of δ_i. Fields and Miller (59), also suggested that crack resistance does play some importance in design and that δ_i may not bear any relation to the resistance of crack propagation of the material. A different view was reached in the conclusion of the conference (88), where it was stated that the resistance curve as seen in J_{Ic} did not represent an intrinsic material toughness increase with crack extension and that redundant plastic work (as discussed earlier) was responsible for the rise in the resistance curve. Hence, design was based on δ_i measurements and any stable crack growth was considered to be a bonus or an extra factor of safety.

Chipperfield (75) found that the crack growth resistance curve was related to the initiation of fracture value. Working with prestrained material, he found that a good value of δ_i was associated with a steep $d\delta/da$ or δ_R curve. This is probably true for a plate steel that is ductile and isotropic but may not be for welds or anisotropic materials. Thaulow (89) gave δ_m and δ_i values for welds, good δ_i values do not, in all cases, imply a good δ_m. This view was supported by Fields and Miller (59). Design based on a δ_i value which, apparently good, may not have good crack growth resistance, will lead to danger catastrophic failures. Further evidence against δ_i was offered by Berry and Brook (83), who found

that δ_i was insensitive to temper embrittlement, hence, of little use without some indication of the material resistance to crack growth. McCabe (90) and Fearnehough (80) concluded that resistance to growth information was very necessary where slow stable crack growth was expected before failure.

2.2.4.1. USE OF R CURVES

From the review of R curves, it is possible to establish that, as yet, little agreement is found for geometrical dependence, standardization of testing techniques or even the measuring of an R curve. It is necessary, however, to note that the alternatives to R curve analyses in the general yielding regime are either δ_i or δ_m values or both values, and R curves do lead to a clearer understanding of the two. It is generally accepted that initiation values are conservative and that maximum load values are geometry dependent. δ_m does give a more complete picture of the resistance of the material to failure by incorporating a measure of crack growth in the overall value. It is for this reason that maximum load values must be of the same thickness as the component if relevant information is to be expected. It must also be borne in mind that strain rate is known to affect the fracture behaviour and this must be experimentally determined for the relevant situation.

A further use of resistance curves is in the estimation of the initiation values by extrapolating from the linear part back to zero ductile crack length. This method is the most accurate for determining initiation values.

R curves have been used successfully to interpret various experimental restrictions. A very interesting paper by Server (91) showing resistance curves for both impact and slow bend tests plotted as energy against crack extension, three points from his work are referred to. First that for all materials tested, the point of initiation under a variety of strain rates did not coincide with maximum load. Second, that the energy for initiation was higher under impact conditions (due probably to the corresponding

increase of σ_Y) when measuring the so called macroinitiation (defined as the point of intersection of the lines of crack blunting and crack extension). Finally, he found that there was little change in initiation value with strain rate for the higher yield strength materials.

It was therefore decided that R curves would reveal more information for post-initiation behaviour of the materials under investigation. In particular the effect of inclusions on crack propagation and as a method of calculating the δ_i values. However, as maximum load values were shown to be geometry dependent, so the resistance curves will appear to be dependent on specimen width and crack length.

2.5.5. EQUIVALENT ENERGY

This work was developed by Witt (92) and later developed and applied on both sides of the Atlantic (93-95). The approach is empiricial and is based on a universal load-displacement curve constructed for geometrically similar specimens. The analysis assumes that the proportions of linear dimensions for geometrically similar specimens are similar to the proportions of the energy requirements for failure. The assumption has been extended from LEFM to GYFM if the plane strain conditions are met (44). The work has been modified for undersized specimens by the CERL (95). For impact conditions they suggest that the equivalent energy is comparable to initiation toughness values.

2.2.6. J INTEGRAL

The crack tip plasticity was characterised by the COD theory as seen above. This was done because of the difficulties in analysing the stresses in elastic-plastic materials. It was observed that many difficulties arose when experimentally determing COD, partially due to the inhomogenieties of the plastic zone in the immediate vicinity of the crack tip and the consequences of crack tip deformations. There is merit, therefore, in finding a parameter that covers a wider zone that smoothes out local irregularities, in a similar way that LEFM deals with finite zones

to represent the unknown stresses. Such studies are the path-independent line integrals which may be used to find approximate descriptions of the crack tip environments prior to fracture. Rice's integral (96, 97) was accepted because of its association with contemporary stress-strain solutions for a non-elastic crack tip model. J is defined as a line integral on any path τ surrounding a crack tip. For a crack lying in the x-direction of unit thickness problem (i.e. two dimensional):

$$J = \int_{\tau} (\omega dy - t_i \frac{\partial u_i}{\partial x} ds) \qquad \ldots.2.52$$

where τ is any contour anticlockwise around the crack from the lower crack face to the upper,

ω is the strain energy density,

t_i is the fraction vector normal to the line which moves through displacement vector u_i,

hence,

$t_i \partial u_i$ are work terms,

S is the path length along this contour,

J is, therefore; concerned with the difference between the strain energy in the direction of crack opening, within the boundary and the work done in crack opening.

Rice et al (98-100) interpreted equation [2.52] as the potential energy difference between two identically loaded bodies having slightly different crack lengths, such that the potential energy release rate is equal to J_I in the elastic conditions:

$$J = - (1/B) (\partial U/\partial a) \qquad \ldots.2.53$$

where U is the potential energy,

and,

1/B is the thickness dependency.

It does not hold true very close to the crack tip or where extensive plasticity occurs, since much energy is lost in plastic

deformations rather than crack growth and, hence, J loses its physical meaning (101-103). Therefore, equation [2.53] represents the rate, with respect to crack length, of elastic and plastic work done. In GYFM this equation is not dependent on energy balance but on path independence and the degree to which the value of J is related to a singularity of stress or strain in the crack tip region.

J values may be estimated from areas under single load versus displacement diagrams that either directly relate to the work done, such as the total energy under the experimental load versus load point displacement record, or indirectly related to the work done as in crack mouth opening displacement (104); most work relates to the load point displacement technique.

For three point single-edge notch bend specimens with a/W values greater than 0.45 and less than 0.65, one obtains:

$$J = \frac{2(U_E + U_p)}{B(W - a)} = \frac{2U}{B(W - a)} \qquad \ldots.2.54$$

where U is the energy in the form of area under the curve,

U_E is the elastic component of this energy,

and

U_p is the plastic component of this energy.

2.2.6.1. EXPERIMENTAL J INTEGRAL

There are several problems associated with the experimental and theoretical J integral. Experimentally, the difficulties lie in separating the purely loading point displacements from the displacements of the testing system. The plastic zone associated with J must be contained within the uncracked ligament which restricts the situation to limited ductilities. The path dependence will also break down when the crack starts to run because the deformation field changes markedly due to work hardening effects (105) and the energy flow in the elastic region will then differ from that in the plastic (106).

The simplest method of estimating J is shown in Figure (10) which represents the loading curves of specimens with different crack lengths, (a) and a + Δa, under displacement controlled conditions such that the loads and displacements are taken at loading points.

Since structural steels are shown to tolerate considerable amounts of ductile crack growth it has become necessary to study J versus Δa or J_i curves to determine the point of crack initiation of J_{Ic}.

2.2.6.2. USE OF J

J_{Ic} has been used in the USA for determining K_{Ic} from subsized specimens and, hence, the saving of considerable expense by using the equation (107,108):

$$K_{Ic} = (J_{Ic}E')^{\frac{1}{2}} \quad \text{....2.55}$$

where $E' = E(1 - \nu^2)$.

This method of obtaining K_{Ic} results may lead to considerable misunderstandings and two points are noted below to show this:

(i) K_{Ic} determined in plane strain represents a higher triaxiality state than for small J_{Ic} specimens, this will lead to the shift of transition points to higher temperatures with increased triaxiality, hence K_{Jc} or K values determine from J_{Ic}, will overestimate the K values considerably at transition temperatures.

(ii) If both K_{Ic} and K_{Jc} lie in the ductile range, it is possible that K_{Jc} will show conservative values since J_{Ic} is measured at initiation of ductile crack growth whereas K_{Ic} is associated with a 2% ductile crack growth in the form of a thumbnail crack, as recommended by ASTM E 399-74 guidelines. This has been observed by Smith (109) working with A533B pressure vessel steel and by Schwalbe (110).

Hence, it must be understood that K_{Jc} values are prone to be misunderstood if the above points are not considered. It was therefore suggested that J_{Ic} values be studied on specimens of similar size to the structure so as to negate possibilities of geometry dependence.

The problems of J are, therefore, similar to those of COD, in that initiation values must be measured to give meaningful values. This leads to the same problem of determining the point of initiation in a ductile steel at upper shelf temperatures. J has little meaning in the post initiation regime whereas δ_m is purely an opening at the original crack tip related to the specimen geometry. It has been practise to use J measurements in situations of limited ductilities and since BS 4360 steel tolerates much crack growth at highly plastic deformations, it was considered better to use COD in the present research programme. Nevertheless, COD and J have been directly correlated and this is investigated further below.

2.2.7. CORRELATION OF COD AND CVN

It was shown in Section 2.2.1. that CVN energies did not relate well with K_{Ic} unless the material tested was brittle. In a situation of low ductility, the majority of the energy absorbed is associated with crack initiation in a Charpy specimen which is the case in the K_{Ic} test.

The correlation of CVN to COD has yielded a more diverse set of observations. Cotton (111) favours a limited correlation in homogeneous structures where a good CVN results in good COD values but the reverse was not always true. Garland (112) similarly found that good COD for welded, full thickness test, did not necessarily mean a good CVN energy. Garland (112) and Hicks (113) agree that CVN tests result in conservative values, CVN never exceeding COD criteria. Cotton (111) showed very large scatter where CVN was shown to fall either side of the COD criterion. In general, however, it is accepted that the relationship is subjective and empiricial, with scatter too large to accept (113). In conclusion, therefore, the CVN test must remain unrelated to

COD and used only in limited qualitative tests.

Another important point to remember is that high strain rates associated with CV testing shifts the transition to higher temperatures. This creates a very significant difference in toughness characterisation over the range of temperature affected.

2.2.8. RELATIONSHIP BETWEEN COD AND J INTEGRAL

For small scale yielding the estimate of COD was:

$$\delta = \frac{G}{m\,\sigma_Y} = \frac{K^2}{m\,\sigma_Y E} \qquad \ldots.2.56$$

and for J in similar small scale yielding was defined as:

$$J = G = K^2/E' \qquad \ldots.2.57$$

Thus,

$$J = m\,\sigma_Y\,\delta \qquad \ldots.2.58$$

A review by Dawes (45) gave the majority of values of m to be between 1.0 to 2.0 but there are discrepancies between experimental details and definitions and to the value of σ_Y taken. Turner (114) has found more varying values, up to m = 2.6 and concluded that a J - δ relationship is still unproven and may depend on geometry and material property. The value m was noted to decrease with increasing σ_Y brought about by lowering temperatures (46,76).

2.3. FACTORS AFFECTING NOTCH TIP DUCTILITIES

2.3.1. INCLUSION CONTENT AND SPECIMEN GEOMETRY

The factors that are of most interest in affecting the notch tip ductilities and hence COD, are the presence of inclusions and the effect of specimen geometry. These two variables have been extensively investigated in the past. Section 2.1.5 reviewed the effect of thickness on K_c and G_c, specimen geometry is further investigated in Section 2.3.5.2 and in the Chapter 5, with particular reference to the recent research on a/W ratios.

Inclusions are reviewed more comprehensively in Chapters 3 and 4.

2.3.2. TEMPERATURE

K_{Ic}, J and COD are usually represented as a function of temperature for a particular strain rate. Structural materials usually show upper and lower energy shelves separated by a narrow transition region.

The upper shelf occurs at higher temperatures, the actual toughness value depends both on the material and the geometry and is always characterised by ductile rupture. The lower shelf, giving lower toughness values, is less geometry dependent and is characterised by a brittle, cleavage failure. Both shelves are represented as straight lines where the value taken is usually a lower bound trace of the scatter obtained. The transition region is associated with the greatest scatter since small changes in temperature are normally associated with large variations in toughness. The lower shelf appears to yield the most predictable and accurate results since plastic yielding is very limited.

The toughness values at any temperature will depend on material properties, such as microstructure, alloying, inhomogeities and texture as well as non-material parameters such as temperature, strain rate, geometry etc. A few relevant parameters are discussed below. Initiation values of COD and J were considered to be "material parameters" and should not be affected by such geometric variations as crack length and specimen width. The fact that δ_i and J_i do depend on such variations leads one to seek a better understanding of the mechanisms of geometry related toughness measurements.

2.3.3. STRAIN RATE

It becomes increasingly difficult to determine toughness as it is understood by COD or J integral techniques as strain rate increases. The point of initiation of cracking on a smooth and continuous load-extension trace becomes difficult to distinguish.

One is faced with the difficulty of measuring a relevant fracture criterion under high impact rates. What is normally taken as a function of toughness is the total energy to failure or a fixed percentage of the total energy, obtained from tests such as Charpy V, or more sophisticated techniques which give a load versus time graphical display of energy absorbed from an instrument impact specimen in three point bending (115,116). The load control is normally in the form of output from a calibrated strain gauge, stuck on to the specimen or the tup that hits the specimen. Again, the toughness is the measure of the energy absorbed, calculated by some means, from the plot. The equivalent energy method is one such tool for calculating the energy (see Section 2.2.5). The problem here, as with COD testing, is that maximum load is geometry and strain rate dependent for ductile specimens and would not represent the true value of the initiation. Furthermore, taking a value mid-way between general yield and maximum load would also not be a true representation of fracture load.

Knott (117) and Radon and Turner (118) surmise that upper shelf energy values decrease with increasing strain rates due to the increase of yield strength and the decrease of work hardening. Barsom and Rolfe (119) show that the transition temperature shift between slow bend and impact Charpy V tests is greatest for low yield strength steels and negligible for very high strength materials. This was also verified for plane strain fracture toughness samples. However, they also found that upper shelf energies increase with strain rate and this shift has also been referred to by Hertzberg (120).

There appears to be a disturbing lack of published evidence of strain rate sensitivity in the ductile mode of tearing, although a considerable amount of work has been done on transition temperature shifts in Charpy, K_{Ic} and other testing techniques (117, 119,121).

A rare example of strain rate sensitivity has been offered by Ostensson (122) working with pressure vessel steel, ASTM A533B, where he showed that between 80°C to 350°C higher strain rates of

50 mm/sec gave substantially higher K_J values (K values calculated from J Integral measurements) than at 0.005 mm/sec. Although the temperature range did suggest some dynamic strain ageing process existing, it is very difficult to explain why this phenomenon is completely reversed by the extrapolation of Ostensson's values to ambient temperatures, Figure (11), and may be a result of scatter.

2.3.4. STRAIN HARDENING 'n'

Initially, n must be defined from the following relationship:

$$\sigma = M \varepsilon^n \qquad \ldots.2.59$$

where M is a constant.

For true stress and true strain at maximum load conditions,

$$\frac{d\sigma}{d\varepsilon} = \sigma \qquad \ldots.2.60$$

From [2.59].

$$\frac{d\sigma}{d\varepsilon} = nM\varepsilon^{n-1} \qquad \ldots.2.61$$

therefore,

$$M\varepsilon^n = nM\varepsilon^{n-1} \qquad \ldots.2.62$$

$$n\varepsilon^{-1} = 0 \qquad \ldots.2.63$$

$$\varepsilon = n \qquad \ldots.2.64$$

Kraft (123), in the early sixties, associated n from simple tensile tests in uniaxial tension to K_{IC} by the following equation:

$$K_{Ic} = E\, n \sqrt{2\pi\, d_T} \qquad \ldots.2.65$$

which is similar to $K = \sigma\sqrt{\pi a}$ but the σ is equal to E_ε and at maximum load $\varepsilon = n$, d_T is a tensile ligament distance over which ε is greater than n; this distance is characteristic of the material

and Kraft termed it the Process Zone. Although Kraft realised the importance of the process zone he had not quantified it and thus suggested that within d_T lies a smaller zone, d_f, which might correspond to the diameter of an aquiaxed microvoid. No specific relationship was offered between d_T and d_f. However, Kraft found that K_{Ic} increases with increasing microvoid size which is very important in relating to non metallic inclusions.

Yoder (124) agree with this suggestion but Barsom (125) and Hahn (126) comment on the inability of uniaxial values to predict plane strain behaviour of a K_{Ic} test. Weiss (127) showed that fracture strain ε_f decreases markedly in plane strain by a factor of four to five.

Hahn (126) produced the expression:

$$K_{Ic} \simeq n \sqrt{2E\ \sigma_Y\ (\varepsilon_f/3)} \qquad \ldots.2.66$$

where $\varepsilon_f/3$ represented a compromised plane strain manifestation of a plane stress σ_f. The equation proved to be 30% accurate for a variety of materials.

Garrett (128) observed that there is a good correlation between n and δ_i for aluminium copper alloys and close correlation between n^2 and δ_i for pure aluminium. Fields and Miller (129) also found that n is in general related to fracture toughness. Chipperfield (130) working with stainless steel found that changes in n^2 did not follow fracture toughness changes closely enough to enable him to accept it. Clark (69) showed that n fails to predict fracture when localized shear occurs at the crack tip, otherwise n is related in general to fracture toughness.

The association of n with crack tip ductilities is expected since strain hardening is the ability of the material to deform under given conditions. An easy way to view the relationship between n and crack tip ductility was given by Kim (131) who explained that for mode II deformation, a material with high n value will have a smaller plastic zone than a material with low

n value for the same stress applied, hence the material with high n value has a greater reserve of plastic deformation than a low n value material.

n was also associated with second phase particles, where the relationship is inversely proportional (117). The value n has long been included in calculations of the damage rate of a material due to void coalescence by McClintock (132) where the rate of damage is enhanced by small values of n.

The strain at maximum load, ε_u, although related directly to n, has been less accepted in general due to the difficulties associated with its evaluation from a uniaxial tensile test, because maximum load is normally a large plateau region for structural materials.

The strain at fracture (ε_f) has also been used extensively, such as by Hahn in equation [2.66], where K_{IC} was directly related to root ($\varepsilon_f/3$) where ε_f is the plane stress fracture strain and $\varepsilon_f/3$ is the approximate biaxial strain. Broek (133) has found that ε_f was inversely proportional to the volume fraction of second phase particles. Since δ_i is related in a similar manner to the second phase particles, it was only time that separated Chipperfield and Knott (134) from finding the following relationship:

$$\delta_i = \varepsilon_f \, l \qquad \ldots.2.67$$

where l was related to the inclusion spacing and was associated with Kraft's process zone. Fields and Miller agreed with this principle and suggested that ε_f be accepted as an inexpensive guide to fracture prior to embarking on expensive COD testing.

2.3.5. NOTCH CHARACTERISTICS

2.3.5.1. NOTCH ACUITY

It was established (135) that sharp notches would greatly reduce the energy to fracture in brittle tensile specimens but only slightly decrease the value for ductile steels. The requirement for a sharp notch brought about an ingenious method of

introducing the crack. It was considered that a crack may be introduced in a Charpy specimen from a notch, by bending the specimen at -196°C with the notch in compression. On releasing the specimen, the residual stresses resulting from the local plastic compression which occurred during loading would cause a crack to run in the embrittled material. Another method was to hit a Charpy specimen on the reverse side of the notch at -196°C to introduce a crack.

Orner and Hartbower (136) suggested that fatiguing a Charpy specimen would lead to a sharp crack that can be controlled with greater accuracy than by embrittling the material. They showed that Charpy energy was greatly reduced with increasing sharpness of crack.

Notch acuity has been studied recently by Chipperfield and Knott (134) who have found that δ_i decreases with notch acuity until a certain minimum size is reached. This minimum size has been related to inclusion spacing such that the width of the notch does not exceed the inter-inclusion spacing. This enables the δ_i value to be independent of notch width. Fields and Miller (129) gave similar conclusions.

A slightly different view put by Lereim (137) who noted that δ_i, although still sensitive to notch acuity in high strength low alloy steels (HSLA), the relationship to inter-inclusion spacing was less clear. The complication was seen to be the formation of delaminations ahead of the crack tip in longitudinal specimens.

Surprisingly, Ritchie (138), working on ultra-high strength steels, showed the most usual dependence of fracture on notch acuity. He showed that blunt notches gave a decrease of energy to fracture with austenitizing temperature where sharp cracks showed an increase of energy for both impact and slow bend tests.

Wilkowski (39), working on drop wight tear tests, again showed a dependence on notch acuity; he found that sharp cracks reduce the upper shelf values and shifted the transition to higher temperatures than did conventional blunt cracks.

2.3.5.2. NOTCH LENGTH

As fracture toughness techniques were perfected, it became apparent that crack tip ductilities measured by K, J or COD do depend on the crack size to specimen width or a/W ratio. Chell (72), Chipperfield (75) and de Castro (76) all show this for various materials. It was concluded, by de Castro, that this dependence was more relevant to higher temperatures than to the lower energy shelf.

Knott (117) suggested that the critical ratio of a/W required to produce constrained general net-section yielding before gross yielding was 0.3. Crack length to width ratios, at present, are usually recommended at 0.3 or 0.5.

2.3.6. EFFECTS OF WELDS ON DUCTILE PLATES

Burdekin and Stone (36) proposed a design curve based on COD. This took into account the relationship between a non-dimensional value of COD and normalised strain, e/e_Y, on a gauge across a crack in an infinite plate subject to tension. Dawes (140) modified the relationship for a realistic design situation where the design stress ratio σ_1/σ_Y is less than 1 and where the a/W ratio is less than 0.1:

$$a_{max} = \frac{\delta_c E \sigma_Y}{2 \sigma_1^2} \quad \text{for} \quad \frac{\sigma_1}{\sigma_Y} \leq 0.5 \qquad \ldots.2.68$$

and

$$a_{max} = \frac{\delta_c E}{2 (\sigma_1 - 0.25 \sigma_Y)} \quad \text{for} \quad \frac{\sigma_1}{\sigma_Y} \geq 0.5 \qquad \ldots.2.69$$

Since welded joints represent the weakest points of a structure, the value of σ_1 was related to problems associated with welds. Four categories were defined as:

(i) σ_1 adjacent to a stress concentrator in a welded joint is equal to (SCF. σ) + σ_Y.

(ii) σ_1 adjacent to a stress concentrator that has been relieved by PWHT is equal to (SCF. σ).

(iii) σ_1 remote from stress concentrator in a welded joint is equal to $\sigma + \sigma_Y$.

(iv) σ_1 remote from a stress concentrator in a stress relieved joint is equal to σ.

where σ is the design stress, σ_Y is the yield stress and SCF is the stress concentrator factor.

Hence, the magnitude of the residual stresses are additive and are generalised in all situations to equal σ_Y. This may lead to conservative estimates of a_{max}. On the other hand, BS 1515 suggests that PWHT temperature 480 - 620^{o}C for an hour per 25mm of thickness to relieve the built up stresses, and there is evidence that under conditions of very high heat input this is not always sufficient to completely relieve the stresses. Hence, a_{max} can be over-estimated. In cases (i) and (iii) above σ_1 is greater than σ_Y which implies that there is general uncontained yielding and with very short cracks the plastic zone may spread to the upper surface making it a plastic collapse situation.

There is another effect that a weld may introduce which cannot be dealt with by this method. Should the conditions be favourable that a brittle zone be introduced into the plate by the weld, it is possible that the weld itself may act as a crack. The energy release from the embrittled area may be great enough to cause the crack to propagate into the ductile material in a brittle manner. Spurrier et al (216) have shown that with this condition, the transition temperature for brittle/ductile fracture may shift to considerably higher temperatures. This point is of considerable interest and will be discussed in more detail.

CHAPTER 3
INCLUSION TYPE, BEHAVIOUR AND EFFECTS ON STEELS

INTRODUCTION

The inclusions in steel are of many varied forms and compositions, sulphides being by far the most common but silicates, aluminates, oxides and combinations of these are well known.

Because of the dominance of the sulphide inclusions in steel, the vast majority of the research has been carried out on sulphides. The classification of most forms is straight forward but for that of the sulphide family and for this reason a section has been dedicated to reviewing this family.

Those inclusions that are studied in the billet are not those found in the end product nor are they responsible for the lamellar tearing of heavy welded joints. It is only after the billet has been rolled out to form plates that the harmful elongated and flat shapes are produced. For this reason the deformation behaviour of inclusions is discussed in some detail.

The mechanisms of ductile fracture have been discussed and compared in a comprehensive manner, the analyses of deformation processes are not discussed in depth but adequate references are included and several reviews on this subject are available.

Naturally, many investigators have studied the effect of inclusions on the mechanical properties of steels and Section 3.4 reviews some of these publications. The best known failure mode caused by inclusions is the lamellar tearing phenomenon; for this reason a separate section reviews this problem and the method used to study its effects. Finally, methods of achieving better properties by controlling or removing the inclusions are discussed.

The reader is reminded of the relevance of this section since one of the two varieties of 50D steel used in this research

programme has a high inclusion content and may, therefore, be susceptible to lamellar tearing. Furthermore, the deformation behaviour of sulphide inclusions is of interest where hot rolling is used as a technique to elongate existing inclusions, as was found necessary during this research programme.

3.1. SULPHIDE INCLUSIONS IN STEEL

When one discusses the subject of sulphide inclusions in steels, one is not concerned with manganese sulphide inclusions alone but a whole host of inclusion compositions. Sulphide inclusions consist of sulphides of iron, chromium, titanium, zirconium and manganese. The transition elements are taken up by the manganese sulphide in varying amounts, substituting with manganese atoms (142). Iron and chromium may replace half the manganese sites with little distortion of the crystal lattice. Non-transition metals may also be found in substitutional solid solution form (143), of these the most important are oxygen, selenium (144) and tellurium (145).

It is the manganese sulphides, the light grey appearing inclusions in reflected light or green when internally reflected, that most metallurgists are familiar with and are, by far, the most common. They have the simple cubic form of common salt and are isostructural with common oxides like periclase and calcium oxide.

Sims (146) originally classified these sulphides into their three distinct morphological and also evolutionary classes. These classes are controlled by oxygen content and the composition of the steel (146, 147).

Type I Manganese sulphide occurs when oxygen concentration in the melt is in excess of 0.01%. These inclusions are pear-drop shaped with a random distribution in relation to the steel structure. This arises because the inclusions are precipitated from the solidifying steel as globules of liquid, rich in sulphur and oxygen, by a monotectic reaction (148). They will be observed in a variety of sizes and clustering is common. This reflects

their formation over a large temperature range. The largest naturally forming first and since they will have the highest oxygen content they occur as duplex inclusions, the manganese sulphide being associated with large proportions of an MnO - MnS eutectic phase. The smallest inclusions being last to form will have the least oxygen content, are wholly MnS (147).

.Type II MnS of type II replaces type I when oxygen decreases. This type is interdendritic, rod-like sulphide growing parallel as they are constrained to grow between parallel dendrites (149). Traditionally, type II MnS were thought to be formed simply as a eutectic between iron and manganese sulphide. However, it has been suggested that they are a cooperative monotectic due to the melting point of the sulphide being depressed by the presence of iron and other elements in solution (150). These sulphides are, hence, observed in fully killed steels.

Type III MnS of type III are found in the presence of a high concentration of carbon, aluminium, silicon and phosporous. This phase appears as irregular and angular inclusions on polished surfaces (146) and on cracked surfaces appear as perfect octahedrons. Type III MnS are formed by a divorced eutectic reaction, the high concentration of alloying elements brings about a depression in the freezing point of the steel to such an extent that it becomes less than that of the MnS.

3.1.1. DEFORMATION OF INCLUSIONS

The major deformations that inclusions undergo occur mainly during the hot working stage where a billet is hot rolled repeatedly in the manufacture of sheet or plate steel. In this way, initially globular and harmless Type I and Type III manganese sulphide and silicate inclusions will deform to produce elongated or elliptical geometries. Where the initial inclusion geometries are more complex such as in colonies or clusters of aluminosilicate

inclusions or Type II sulphides, the effect is that the deforming steel matrix will reorientate such colonies into the rolling plane and subsequently elongate them. The effects of hot rolling are deleterious to the mechanical properties and produce anisotropy. it is for this reason that one must look into this subject in more detail.

The rolling ratios and hot working temperatures have a dominating role on inclusion deformation. An increase in the parameter will effectively increase the inclusion length. It is well established now that inclusions will deform differently according to rolling temperatures (151-153).

The extent of inclusion deformation relates to the flow stress of the inclusions to that of the matrix. This ratio is itself a function of temperature and composition of the two phases. Interfacial energy and mechanical constraint also exert some influence on deformation, especially where large reductions are involved.

It has been shown that for most isotropic materials, hardness is directly related to the flow stress at low strains (154). Baker et al (155) used this relationship to study the inclusion and matrix hardness in situ, at elevated temperatures. From available data (156) and by determining the relative elasticities (α, which is the ratio of inclusion true strain to overall matrix true strain) the following relationship was obtained:

$$\alpha \simeq 2 - h_i/h_m \qquad \ldots.3.1$$

$$(0 \leq \alpha \leq 2)$$

where h_i is the inclusion hardness and h_m is the matrix hardness. This has further support from Goodier (157) who found the matrix stress acting on a rigid, spherical inclusion to be twice the uniaxial stress applied to the matrix, again neglecting the effects of strain hardening.

Visco-elastic theoretical analyses in relating to elastic inclusions and matrix taking into account the effect of strain hardening have been published in a few papers, for example (158, 159).

The deformability of manganese sulphide inclusions increases gradually from Type I to Type III. The temperature dependence of their deformability is subject to disagreement. Bernard et al (160) believe that sulphides deform less than the matrix at temperatures greater than 900^{o}C whilst above 1200^{o}C they do not deform, the critical temperature being 900^{o}C where the matrix and inclusion deform equally. Bernard et al suggest that the relative plasticities, as defined in equation [3.1] above, of type I and III go up with rolling temperature. The opposing view is held by other authors like Baker et al. Deformation of type II sulphides have proved difficult to study.

Theories of the deformation behaviour of these steel inclusions are concerned with the differences in the work hardening rates between the inclusions and the matrices which would be temperature dependent, thus making the effect more complicated.

Other theories involve the inclusion shape and its interaction with the flow of the matrix past it; yet another theory involves the formation of work hardened shell around the inclusion which protects it from deforming (156).

The deformability of the silicates may be considered to increase with temperature, becoming partly fluid above 1100^{o}C and with slight pressures tend to stringers of very long dimensions which may leave two unwelded surfaces coated by a thin layer of silicate.

To avoid these harmful elongated shapes, deformation should be kept to a minimum at the rolling mill. This can be done by correct use of temperature control. This unfortunately, is not always possible since modern techniques require high deformations at around 800^{o}C which may explain the common occurrence of lamellar tearing in

modern steels.

Cross rolling has been suggested as being a method of controlling or even reducing the anisotropies of steels, this technique cannot, however, reduce anisotrophy in the through thickness direction; it can only equalise the longitudinal and long transverse properties.

Baker and Charles (147) have also suggested that the material's properties improve with a reduction in inclusion size, however, it was suggested not to reduce the inclusion size too much since this would necessarily reduce the inter-inclusion spacing.

On considering the effect of inclusion shape on a material's property, one must first establish which direction is being highly stressed and in danger of failing if sufficiently large second phase particles exist. Having done so, the objective is then to reduce the particle lengths in that direction by the choice of the right material or correct orientation of the available material. If, however, the through thickness direction is at danger then there is no better choice than an inclusion free material. This is because the through thickness direction is particularly vulnerable to elongated inclusions. The next section will consider the reasoning behind this on a micromechanics scale.

3.2. MECHANISMS OF DUCTILE FRACTURE

The four categories of crack growth are transgranular cleavage, intergranular cleavage, ductile rupture and fatigue crack growth. Environmentally assisted mechanisms may also aid in crack propagation. Crack growth usually tends to be a combination of these micromechanisms.

For brittle fracture, a critical stress (σ_f) will be reached ahead of the crack tip that leads to cleavage. This stress is not reached in ductile materials and a mechanistically more energetic, ductile fracture process will occur at a critical strain.

It will be seen that the two steels of interest are ductile to very low temperatures. Since North Sea temperatures in the British sector seldom reach -10°C and those of the Norwegian sector do not usually drop below -30°C and even Arctic temperatures do not drop much below -50°C, it became apparent that for the BS 4360 steel the likely failure mode would be in a ductile manner unless embrittled by weld deposits, or geometric constraints.

Void formation is known to occur with ductile failure and the first to associate void formation with ductility was Puttick (161). Since then, the theories of ductile failure have attached much significance to the sequential events of void initiation, void growth and final void coalescence associated with second phase particles. The following review of the subject will serve to introduce the readers to the salient points of the subject and especially to shed light on the agreements and disagreements among the many authors on this subject. For the reader who requires an in-depth understanding of the subject, a large number of references have been included and for those who require a more mathematical detail to the models are referred to the work by Knott (117) and the review by Rosenfield (162).

There is general agreement that second phase particles nucleate voids and that these voids may grow plastically under various combinations of shear stresses and negative pressure until they coalesce by the shearing of the separating ligaments. Analyses of homogeneous plastic cavitation by McClintock (163), Rice and Tracy (164) and others have elucidated the importance of negative pressures in the flow field in hardening void expansion processes. Experiments have shown that smaller plastic strains are required for local ductile fracture due to the localization of dilational deformation into zones (165), followed by formation and propagation of cracks where the whole expansion process is sharply confined into portions of the highly strained region at the crack tip (166, 167), see Figure (12).

3.2.1. VOID INITIATION

Conflicting reports of void initiation from inclusions are reported, ranging from debonding of the interface at very low strains, to immediate initiation upon yielding, to the initiation only after very large plastic strains. The literature suggests that there are three models of cavity nucleation. That voids are already present due to the effect of the differences in thermal expansion in hot rolling, by interface decohesion or by particle cracking (168,169). The actual mode depending on the intrinsic properties of the matrix, partice and matrix-particle interface. On the other hand, semi-quantitative theoretical studies have been made, based on release of stored elastic energy (170,171), production of high stresses by impingement of dislocation pile-up of plastic accommodation loops initiated by punching from the interface (172). More phenomenological models have also been proposed where high local shear strains are associated with particle-matrix interfaces (173).

There is much discrepancy as to the role taken by inclusion size on initiation mechanisms. In the experimental work of Edelson and Baldwin (174) and the theoretical formulations of Garland and Plateau (170) and of Galdman (175), particle size is not considered as being of importance. On the other hand, Baker (149) has suggested that the effects of inclusion volume fraction, shape and size on ductility can be uniquely expressed in terms of the projected length of inclusions. Later, Baker et al (177) found the parameter P which is the total projected length of inclusions per unit area. The advantages of this parameter was considered to be its inclusion of many of the inclusion variables and the relative ease of measurement automatically.

The work of Ashby (178) and of Palmer and Smith (168) indicate that the smaller particles do not initiate voids and hence are preferable from a ductility point of view, while the findings of Broek and Brown and also of Stobbs (179) suggest that fine particles are detrimental to the steel. Roesch (180) with his studies on alumina inclusions in steel showed no adverse effect of

second phase particles on steel behaviour when the size of such particles varied from 0.5 μm to 40 μm.

Argon et al (181) suggest that a critical local elastic energy condition is necessary but not sufficient in all cases to produce cavity formation since there is a need to take into account the inclusion-matrix interfacial strengths. They suggest that for inclusions above 100 A the stored elastic energy is found to be insufficient to cause spontaneous debonding but that possible interactions of the plastic zones of these smaller inclusions with each other in such a way that interfacial stress concentration met the required levels for cavity formation. Thus, suggesting no small-inclusion size effect for small volume fractions of inclusions but a definite size dependency for larger volume fractions which allow the necessary condition of plastic zone interaction.

The matrix-particle interface is therefore considered by some authors to play an important role in ductile failure, however, as yet there is disagreement in-so-far as the strength of the bond is concerned. This is probably due to the difficulties of testing the interface mechanically and in observing its deformation in situ. It is known that the smaller particles, such as carbides and nitrites, are well bonded to the matrix. The larger inclusions, that is, the non-metallic inclusions, may be well bonded or free of the matrix.

During the quenching of a steel from a high rolling temperature, fairly high stresses are likely to be set up at the interface. These stresses are caused by the differences of the two coefficients of thermal expansions of the matrix and inclusion. These stresses are termed tessellated stresses and are generally referred to in the following form:

$$\pm \phi \left[(\beta_2 - \beta_1)\ \Delta T\right] \qquad \ldots.3.2$$

where ϕ is a function of the elastic moduli of the inclusion and matrix and of the inclusion shape, size and distribution, β_2 and β_1 are the coefficients of thermal expansion of the matrix and

inclusion respectively, while ΔT is the temperature change.

Tessellated stresses can be quite high and as a consequence, the inclusion-matrix interface normally contains tight packed loops if dislocations, except in places where cracking has occurred. The critical stress for nucleating a crack is dependent on the local dislocation density, methods of reducing the dislocation density prior to stressing the steel could be advantageous.

The shape and orientation of inclusions are generally accepted as being of importance and were briefly mentioned above. Their importance lies not only in their effect on initiation but also on void growth and coalescence. It is verified by experimental evidence that large and elongated inclusions tend to undergo internal fracturing whilst equiaxed inclusions nucleate holes by interfacial separation. Gladman et al (182) show that disc shaped sulphide inclusions are more detrimental to ductility (and hence void formation and coalesence) when oriented perpendicular to the stress axes, than sulphides lying parallel to the tensile axis. Spheroidal carbides require very large true strains to initiate voids and are hence, an improvement to the material properties.

3.2.2. VOID GROWTH AND COALESCENCE

Voids will grow laterally only after necking has set in, as seen in uniaxial tensile tearing. It was also noted that void formation will decrease the plasticity of a material by allowing void growth. With large compressive hydrostatic pressure, abnormally high failure strains may be found (183), indeed superplasticity is achieved by the absence of void growth.

McClintock (173) modelled a matrix with cylindrical holes of initial radius r and space s, equivalent strain to fracture is given as:

$$\bar{\varepsilon}_f = \frac{(1 - n\,(\ln (s/2r)}{\mathrm{sh}\,[(1 - n)\,(\sigma_1 - \sigma_2)\,\sqrt{3/2}\,\bar{\sigma}]} \qquad \ldots.3.3$$

where n is the work hardening exponent and $\bar{\sigma}$ is the equivalent stress. The expression shows strong dependence on stress

triaxiality and a dependence on the volume fraction of inclusions. The expression has been shown to overestimate $\bar{\varepsilon}_f$ by assuming two small a dependence on the volume fraction of inclusions.

Edelson and Baldwin (174) compared existing theories to their experimental results. They showed that the strain to fracture depends on volume fraction of second phase particles and not on the interface strength, type or size of particle.

Void coalescence implies relatively rapid lateral expansion of the voids so that lateral coalescence occurs by a shearing of the inter-void ligament upon the attainment of a critical strain. This gives rise to a macroscopic crack having the characteristic dimple features of a ductile crack. If failure results from a single slip band system, that is, a dominant shear band, then the cusps or dimples have a characteristically elongated form. Theories of ductile failure have postulated a critical void length to lateral void spacing ratio which permits the development of localised bands between neighbouring voids (168, 170, 182).

Attention must be drawn to the geometric distribution of the particles since these particles may be grouped into clusters or arrays by the effect of hot working or sulphide segregation in the billets (184). This segregation will affect the inclusion spacing and, hence, the criterion for the onset of void coalescence and ductile rupture. Chipperfield and Knott (134) found that for a pseudo-randomly distributed inclusion population, the mean separation of inclusion arrays in the direction of the principal stress is the important parameter in ductile fracture. The effect of the occasional large inclusion is determing the path of the rupture by affecting the crack tip strain field has been substantiated by their observations and by those of Clayton (185). Leighton and Easterling found that local fluctuations in inclusion densities are more important in determining the fracture process than is the total volume fraction of voids. DeArdo and Hamburg (186) found that replacing elongated inclusions by clusters of small inclusions does not improve the properties of steel.

3.3. EFFECT OF INCLUSIONS ON MECHANICAL PROPERTIES

The effects of inclusions on mechanical anisotropies have been shown for a variety of tests from simple tensile tests to COD and J Integral testing.

The effects of inclusions on the reduction of area (% RA) are well documented (160). The correlation between % RA and sulphur content is a poor one but suggests a definite trend, as shown in Figure (13). It was later found that the projected inclusion length per unit area, P, gave better correlation to % RA, Figure (17). The behaviour was similar to that by Gladman et al (182) when camparing various inclusion shapes.

The inclusion orientation is known to introduce an anisotropic influence on properties; where inclusions lie parallel to the major tensile stress axis it affects the material least and where they lie perpendicular to this direction, a maximum effect on the deterioration of the mechanical properties is observed. This is to say, moving from longitudinal to long-transverse to short-transverse directions shows a gradual deterioration in properties. This was directly related to inclusion shape.

Charpy impact tests on elongated inclusion-bearing steels also shows anisotropy. Charpy toughness is associated with crack propagation through the material. This implies that the fewer the inclusions the crack cuts across in its path, the higher the energy required to propagate the crack.

Initially, the effect of inclusions on the Charpy ductile to brittle transition was thought to have been small (187) or may have gone a complex variation (188). More systematic analyses of the problem has not fully solved the relationship between inclusions and transition temperatures.

In low to medium strength steels the effect of inclusions on the fracture appearance transition temperature, FATT, anistropy is generally small. Higher strength steels show a definite variation of the absolute value of FATT with sulphur content , see

Figure (15). In Figure (16) where the effect of cross-rolling is shown, FATT undergoes a similar change to that of the shelf energy. Figure (17) shows the correlation between FATT and shelf energy, both of which are affected by sulphur contents. Region I of this figure shows an improvement of FATT with increasing shelf energy. Region II where shelf energy increases independently of FATT and Region III where FATT is lowered with decreasing energy.

Bernard et al attempted to use the P parameter to predict the Charpy V anisotropy ratio, Figure (18). It can be seen that when compared to Figure (19) the P parameter, although showing less scatter than a plot against purely sulphur content, is nevertheless, not successful. Bernard et al went on to give two explanations of the reason for the inability to correlate Charpy anisotrophy with P. First, P reflects both inclusion content and geometry and therefore, inter-inclusion spacing which controls the mode of failure in through thickness ductile tearing, hence, it is capable of predicting ductile rupture mechanisms such as %RA. Charpy impact specimens fail mechanistically by shearing along the inclusion-matrix interface and the physical relevance of P is not understood. Secondly, it has been found (160) that impact energy integrates contributions from many of the steel characteristics upon failure. It was shown that the longitudinal impact shelf energy was related to steel tensile characteristics thus:

$$K_v = A + B \log (1/(1 - z) + C (\sigma_{UTS}/\sigma_Y) \qquad ....3.4$$

z = Reduction of area

σ_Y = Yield strength

σ_{UTS} = Ultimate tensile strength

A, B and C are constants

This equation serves to show that the longitudinal transverse energy ratio does not negate the existence of matrix characteristics which the parameter P does not consider. Furthermore, the matrix will obviously have a sensitivity to fracture initiation which is, to an extent, brought out by Charpy testing. Therefore,

impact failure will involve complex mechanistic interactions of both inclusion geometry and matrix properties.

Shape change of inclusions is expected to affect the properties in a similar manner in which the orientation of inclusions affects the fracture. In low and medium strength steels, a change from elongated to globular or rectangular shape will improve properties. However, Brownrigg et al (189) reported this for rare-earth modified (REM) steels, Heisterkamic et al for zircomium modified steel (190) and also reported a deterioration of FATT with shape control. In high strength steels the situation is different and an improvement of FATT and a decrease in anisotropy was observed. This seems to verify what Bernard et al found about the influence of the matrix properties.

The inclusion effect on COD is seen in Figure (20). A study by Farrar and Dolby on projected inclusion length against crack opening displacement confirms the general trend of low COD values with increasing inclusion lengths. Chipperfield and Knott (134) show that inclusion spacing is the important parameter and not the length of the larger inclusions, this conclusion was supported by Broek (133) working on aluminium and by Errikson (191) and Lentinen (192). Smith and Knott (73) found that the spacing also accounted for the dependence of COD on orientation of inclusions.

3.4. LAMELLAR TEARING

In 1965 the term 'lamellar tearing' was proposed by Nicholls at Cranfield (193) to through thickness failure that appeared as step like tearing in susceptible rolled steel plate. Associated with the planes at the tear surface were elongated inclusions, mainly of manganese sulphide composition. It was not until the advent of scanning electron microscopy that the mechanism of tearing became more clearly understood.

Lamellar tearing was first studied in the laboratory by replicating or simulating the actual design situation. One such test was the Cranfield Test (193) and the Welding Institute's Window

Test (194). These tests were time consuming, costly and gave no more information than the probability of tearing to occur under the conditions of the test. They in no way assess the tearing quantitatively. The slice bend is also used (194, 195) where a through thickness slice is bent until a tear of 3.175 mm (1/8 inch) is produced on the tension face of the dent. The maximum deflection is the measure of resistance to lamellar tearing. The best this test achieves is to inform whether the test piece will crack in bending or not. This amount of knowledge may be concluded beforehand by a simple metallographical examination for elongated inclusions.

It later became apparent that a simple tensile test obviated the likelihood of lamellar cracking such that low through thickness ductility and high inclusion content would, if associated with a highly restraining welded joint or joints, lead to the occurrence of lamellar tearing. The most common occurrence of lamellar tears is in hot rolled plate where the fusion boundary plan of a weld is in the plane of rolling. Delamination is unknown with through thickness ductilities of 20% or more (196).

Cotton (196) shows that steels with less than 0.007% sulphur are generally of higher resistance to delamination. It is clearly shown in metallographic examination that elongated sulphides are the cause of lamellar tearing. It is also shown that sulphides are elongated during hot or controlled rolling operations in steel plate manufacture, in Section 3.1.1.

Lamellar tearing is a costly business; Cotton (196) noted that it is the costliest of deficiencies of a modern steel. It is particularly harmful in armour plating where a sharp impact of a projectile may lead to a 'scab' detaching from the opposite side to the point of impact, causing much damage. Where a plate is known to be susceptible to tearing, the welders have resorted to either hacking or gouging out the plate, where the join is to occur, and filling it with weld metal deposit, hoping that it is improved, or where possible to 'butter' the surface of the metal with a low

yielding material (usually of very low carbon content). Alternatively, they may try to avoid laying a weld fusion boundary plane parallel to the rolling plane.

The practice of depositing weld metal can lead to serious embrittlement of the parent plate in the heat affected zone. Some experiments were performed to show the effect of laying bad welds on ductile plate in reducing the crack arrest properties of such plates.

In hind-sight, it is understandable why so much time was lost and expenses suffered by industry for a problem that is easily solved by restricting the use of steel to a minimum through thickness reduction in area of 20%.

3.5. IMPROVING STEEL CLEANLINESS

Having established the marked reduction in properties of steels containing inclusions and especially those of sulphur, one is left wondering of the possibilities of either removing or changing these inclusions into less destructive forms.

Selection of charge materials for the blast furnace in the hope of having hot metal sulphur levels below 0.01% S is practically impossible. A further problem is the increase in premium low sulphur oil prices which has tended to dictate the use of higher sulphur oil and coke to fuel the furnaces (197).

The problem of steel cleanliness is achieved by the following practices:

(1) Vacuum melting, rather than air melting. This enables the entrapped gases in the melt to escape, also reduces the oxide formation.

(2) Vacuum arc remelting.

(3) Electroslag remelting of the original melt. Here the molten electrode droplets pass through a filter before

reaching the metal pool. The slag may selectively remove chemicals from the droplets.

(4) Reduction in carbon. Carbon reduction in solid solution is found to be beneficial since it reduces the number of sites for nucleation of cracks from carbides. Inter-metallic compounds may be used for precipitation hardening, McMahon (208).

(5) Rare Earth Modification (REM). Since the alternative methods involve considerable expenses in the use of higher lime contents, higher temperatures, more steps in the production of the steel and dearer fuels, the REM has proved to be very useful. It involves the plunging or injection of reactive metals (RE, Ca and Mg) under the slag after deoxidation.

There are many advantages in the last process. First, there is no need to agitate the mixture to produce intimate contact between reactants. Second, the residual sulphur content is tied up as globular, refractory Type I sulphides and oxysulphides which are continuously formed during cooling and solidification of the steel (199). This is advantageous since rare-earth-free steel melts tend to precipitate the oxysulphides and/or sulphides of manganese only at the last stages of solidification, along the solute-enriched interdendritic cell boundaries which is the main reason for the formation of streaks and stringers upon hot working of steels. Lastly, the rare earths have a deoxidizing effect on the steel which enhances the ladle desulphurization by lime or low iron oxide slags.

The metals used in desulphurization, namely magnesium, calcium and the lanthanides or rare-earths all show one characteristic in common and that is that their reactivity with carbon and nitrogen at elevated temperatures is, unlike Zr and Ti, advantageously limited, allowing no inteference with the complicated thermo-mechanical strengthening and grain refinement processes of H.S.L.A. steels (200). A fourth element that should

become a contender in the future is Uranium 238 (U^{238}) in spite of its stable nitride UN (201). An added advantage of the rare-earths is their significant hydrogen 'occlusion' properties which have been known for a few decades.

The rare-earth metal industry is a relatively new one and has come to play a vary important role in steel making. However, it must be remembered that even before the days of rare earth additions, very low levels of sulphur in steels were achieved by simple processes, like double deslagging.

The need for very low sulphur steels is limited today but no doubt, the future will bring an increasing demand. For the present day automobile and construction industries, what is required of the steel is 360^{o} formability, good weldability without lamellar tearing, reasonable impact properties at temperatures down to $-30^{o}C$ and reasonable crack arrest properties. This may be achieved by a simple process of oxysulphide inclusion shape control. For the heavier constructions and especially those created for hiemal environments, such as the Arctic pipelines and the North Sea oil rigs, would probably require inclusion free steels.

CHAPTER 4
TOUGHNESS CHARACTERISATION OF A WELDABLE STEEL

In this section the mechanical and fracture toughness properties of two steels were studied. The effects of inclusion contents were related to the tensile properties, Charpy impact, COD and plastic zone size.

Temperature effects on the material behaviour were considered with respect to tensile strength, plastic zone size, COD and its interaction with the effects of inclusions on the measured toughness.

In some cases, it was necessary to relate the effects of inclusions and temperature on toughness to specimen geometry. In such cases, the reader was referred to Chapter 5, which deals specifically with the effects of specimen geometry on the fracture toughness characterisation.

A technique was detailed for the measurement of toughness of thin plates in the critical through thickness direction. The effects of free surfaces adjacent to crack tips in thin plates was studied by simulation techniques.

Finally, the effect of rolling operations on toughness was considered and recommendations for the amount of hot-reduction tolerated in steel plates were specified.

4.1. EFFECT OF INCLUSIONS ON STEEL PROPERTIES

Inclusion varieties were considered in Chapter 3 and their effects on mechanical properties were reviewed. The recent developments in fracture toughness testing of materials in the general yielding regime led to widespread acceptance of the COD and J Integral techniques for solving industrial problems (202) and this has led to the publication of a British Standard (40) on COD testing.

The work presented below studies the effects of inclusions on mechanical anisotropies of two, widely differing, varieties of BS 4360 50D steel. The study investigates the relationship between COD and inclusions from a mechanistic and quantitative view.

The COD at the point of ductile crack initiation was discussed in section 2.2.3. The literature initially found δ_i to be material constant. With more accurate techniques of measuring small displacements, it became clear that δ_i was dependent on specimen geometry. Hence, the difficulties associated with measurement of small crack tip displacements, the difficulties of determining the point of ductile crack initiation and the added costs of using multiple specimens for accurate identification of δ_i, were not considered to be outweighed by the usefulness of δ_i. Many researchers utilized general yielding fracture mechanics techniques as tools for comparing the properties of various materials. In such situations, if the testing parameters are not altered, the maximum load COD serves adequately as a comparative tool. The important testing variables that have been considered were specimen geometry and size and the stiffness of the testing system. To overcome the δ_m problems, only one machine was used and the geometry was limited, on the whole, to 10 x 10mm specimens with an a/W ratio of 0.3 ± 0.05.

The use of one specimen geometry and the same loading compliance, has entitled the experimenter to refer to equation [2.49] to argue the validity of δ_m as good indicator of the initiation value, δ_i. This is because at upper shelf temperatures, the use of

a single specimen geometry and size will validate the constant C of the above mentioned equation.

4.1.1. METALLOGRAPHIC EXAMINATION OF THE STEELS

Two varieties were chosen of the BS 4360 50D steel to show greatest variation in inclusion content. Both steels were control-rolled plate materials and came in a fine grained, banded structure, Plates (1,2).

Steel D variety came as 104mm thick plate with a chemical composition of Table (1). It should be noted that the sulphur level is below 0.005%. Metallographic examination showed equiaxed grains with a 30% elongation in the direction of the rolling. The mid-section of the plate showed a 10% grain enlargement due to slow cooling differentials.

Traces of elongated inclusions were present, well dispersed and of average length to thickness aspect ratio of 5. X-ray micro-probe analyses of these inclusions showed them to be complex clusters of alumino-silicates, see Figure (21). Occasional manganese sulphide inclusions of higher aspect ratio were found.

Steel S variety came as 50mm thick plate with a chemical composition shown in Table (1). The sulphur level is 0.016%. Metallographic examinations showed equiaxed grains with a 20% elongation in the direction of rolling. The grain structure was finer than for steel D. No mid-section coarsening was observed.

Elongated sulphide inclusions were found with aspect ratios of up to 50, with maximum inclusion length under 2mm. Table (2) shows the distribution of inclusion size through the thickness of the steel. It was noted that inclusions became larger and less numerous to the mid-thickness of the plate. There was some suggestion of inclusion banding as a result of the rolling operations. Figure (22) shows the X-ray micro-probe analysis of the inclusions.

4.1.2. EXPERIMENTAL

4.1.2.1. TENSILE TESTING

Hounsfield 14 specimens loaded in tension on a screw driven machine of 45 KN capacity. Tests conducted at cryogenic temperatures required immersing the specimen in an alcohol bath with liquid nitrogen as coolant. Temperatures were monitored by thermometer and a thermocouple, spot welded to the specimen.

Two directions of each steel were tested, longitudinal (L) and through thickness (Z). Various areas of the plates were tested to show consistency of results.

4.1.2.2. CHARPY V IMPACT TESTING

10 x 10 x 55mm Charpy specimens were machined, where possible, in the orientations noted in Figure (23).

Through thickness S steel specimens could only be made in 10 x 10 x 50mm due to thickness of plate.

Cooling was again conducted in liquid nitrogen cooled alcohol in a Dewar flask. Temperature was monitored by thermocouple and thermometer readings. At the required temperature the specimen was broken within five seconds of leaving the bath.

4.1.2.3. COD TESTING

In this section of the thesis, two specimen geometries were used, 10 x 10mm and 18 x 18 mm with span to width ratios of 4. In later sections other geometries were considered. Crack length to width ratios were limited to 0.3 $\pm$ 0.05.

The orientations tested were LS, ZT and ZR as are described by Figure (23). The notches were machined slots 0.15mm wide and less than 1.2mm deep. Fatigue precracking was carried out with K_m less than 22 MN $m^{-3/2}$ with the minimum load just above zero to ensure specimen position in the three point fatigue rig.

Cooling was again achieved by liquid nitrogen cooled alcohol bath, with thermocouple spot welded by electrical discharge adjacent to the crack tip. The bath liquid was constantly agitated by electrical stirers. Specimen heating was conducted by immersion in preheated, low density oil. The bath was again agitated and monitored by thermocouple readings.

A screw-driven Instron testing machine was used with cross-head speed of 1.27mm/minute. It was determined prior to commencing the tests that cross-head speeds up to 127/minute constitute static loading conditions.

Crack mouth opening was monitored through a double-cantilever clip gauge located between knife edges. These knife edges were either screwed-on or glued, with contact adhesive, into position. The clip gauges were of various sizes to cope with a variety of specimen geometries. The clip gauges were pre-calibrated before every test program at ambient temperatures and before and after each test at cryogenic temperatures. The calibrations were carried out on a micrometer jig.

Clip gauge opening was autographically plotted against load on an x-y recorder. The value of crack opening at first attainment of maximuum load was used to calculate δ_m.

The COD-resistance curves were used to define the COD at crack initiation. This was conducted on 10 x 10mm specimens using up to eight specimens loaded to various values of clip gauge opening and unloaded. The specimens were heat tinted at 350^{o}C for 30 minutes and broken in a brittle manner in liquid nitrogen, thereby determining the average extent of ductile crack extension.

The magnitude of the crack extension was measured by a travelling optical microscope readings of an average of five points along the crack front. Throughout the study, the stretch zone width was not added to the crack length.

4.1.3. RESULTS

Yield and ultimate tensile stresses of the two materials in longitudinal and through thickness orientations (L and Z respectively) are shown as a function of testing temperature in Tables (3 to 6) and Figures (24, 25). Reduction of area (%RA) was also measured for some tests. Very low %RA values for through thickness specimens of steel S were noted.

Charpy V impact temperature transition curves are presented in Tables (7, 8) and Figures (26, 27). The curves lay fairly close together except that for through thickness specimens of steel S (noted as ZTS). The ZTS curve registered very low Charpy impact toughnesses and this corresponded to the low %RA found for simple uniaxial tensile testing.

Fracture toughness testing using the COD concept was conducted according to regulations specified in BS 5762:1979. The COD was calculated at first attainment of maximum load for δ_m calculations or at the specific load required for COD-resistance curves.

Two calculations were employed to determine δ_m, that described in DD19 by Ingham based on the hinge rotation model:

$$\delta = V_g / [1 + r \quad ((a+z)/(W-a))] \qquad \ldots.4.1$$

where V_g is the clip gauge measurement, z is the knife edge height and r is the rotational constant, used here as 1/3.

The other method used, was first recommended as the draft for public comment 78/71533 DC. This was based on elastic and plastic components to the value of COD.

$$\delta = (K^2 \ (1 - \nu^2))/(2 \ \sigma_Y \ E) + (0.4 \ (W-a) \ V_p)/(0.4 \ W + 0.6 \ a + z)$$

$$\ldots.4.2$$

and $K = Y \ P/B \ W^{\frac{1}{2}}$ where P and V_p are load and plastic component of

the clip gauge opening respectively and Y is the stress intensity factor coefficient.

The COD results of the three orientations for the two steels and of the two sizes are given in Tables (9 to 16) and Figures (28 to 30). Note, all 18 x 18mm specimen size results are given in the form of equation [4.1] since comparisons were made with de Castro (203) who only presented results in this manner. The 10 x 10mm specimen COD values were calculated using equation [4.2].

It will be noticed that δ_m is given with the range of δ values for a 0.5% load variation. This gives a measure of the size of the plateau region which can be very considerable for ductile materials.

What was shown by these graphs was the high levels of ductility for all orientations of the two steels except the through thickness results of the high sulphur steel, that is, ZRS and ZTS specimens. It was also noticed that δ_m increased with specimen size, as noted before, and that the transition temperature shifted to the right with size increase. Figure (31) from Kamath et al (141) shows a wide range of results using

$$0.4\ (W - a)\ V_g\ /\ (0.4W + 0.6a + z) \qquad \ldots.4.2a$$

The upper shelf values were not constant but tended to decrease with increasing temperature. Since this was first noted, there have been other observations of this behaviour and these will be discussed in greater detail.

COD-resistance curves are plotted in Figures (32 to 35) and Table (17). The resistance curves were calculated using equation [4.2] using fatigue crack length, a_f, and also fatigue crack length plus ductile crack length $a_f + \Delta a$. The tables also include notch root contractions (NRC) measured just beyond the crack tip using a point-micrometer.

The resistance curves (i) showed an increase in COD with Δa beyond maximum load. Curves (ii) of Figures (32 - 35) where $a = a_f + \Delta a$ showed a tendency for COD to level off to a plateau region beyond δ_m. A linear extrapolation was used to determine δ_i, where possible.

4.1.4. DISCUSSION

Through thickness Charpy impact values for steel S could only be obtained from 10 x 10 x 50mm specimens; that is, 5mm shorter than standard specimen size. To test the effect of short specimens, a series of tests on 50mm and 55mm ZTD specimens were conducted. The results are given in Table (18) and it can be seen that no effect was measured.

It should be borne in mind that the clean steel specimens were of much higher toughness and the specimen did not break in two but suffered considerable deformation. As a specimen was forced, by the anvil, through the holding blocks there was considerable friction. This friction would, naturally, be more important in a ZTD specimen, which was forced through intact, than a ZTS specimen, which was broken in two. The exercise proved that no variation in Charpy energy would be noted by the undersized, ZTS, specimens.

The Charpy V impact test results have shown distinctly ductile upper shelf toughness values for ZTD, LSS and LSD specimens, in ascending order of toughness. The transition temperature of these specimens lay between -60°C and -75°C, with the LSD specimens at the lower end. Only ZTS specimens showed an unacceptably low toughness with no visible transition.

This behaviour was repeated for δ_m testing, there were, however, some differences. The transition temperature shifted to lower temperatures, between -80°C to -90°C. This shift was associated with the static loading conditions of COD testing. Both COD and Charpy toughness characterisations reflected the %RA behaviour for tensile testing, Tables (3-6), as was discussed in Chapter 3.

The upper shelf COD was noted to show a decrease with increasing temperature. This decrease was first noticed by Al-Hadithy (204). It was difficult to explain this behaviour in terms of yield strength, since referring to Figures (24, 25), there was no significant uniaxial yield or ultimate strength variation over the wide range of δ_m upper shelf temperatures.

Since it was first reported, there has been new evidence of J Integral and K_Q decreasing with increasing temperatures for upper shelf values.

The upper shelf decrease of toughness with increasing temperature was noted to be greater with the high sulphide bearing steel plate, (S). It was found, from Figures (24, 25), that although the yield strength variation over the temperature range considered was very small, the dirty steel (S) exhibited the greatest change. It was, therefore, likely that the δ_m variation over the upper shelf reflected the small changes in the tensile properties. This view is in agreement with that held by Tobler (205).

The practical implications of such results are significant. Having established that the upper shelf toughness values are not constant, one is no longer tempted to use room-temperature toughness values for design purposes of high temperature applications.

The effect of inclusions on COD behaviour was well documented in Chapter 3. Taking y, x and z to be the longitudinal, transverse and short-transverse axes of an inclusion as in Figure (23) one can more easily discuss inclusion orientation.

The LS specimens have notches that cut across the steel banding and inclusions along the x-direction. As the crack tip approached a sulphide inclusion, the matrix-inclusion interface debonded easily. The electron micrograph at the front of the thesis shows an example of an easily delaminated MnS inclusion in a fatigue fractured surface. The growing crack tip was not affected by the inclusions lying in this direction. The result was that only a minimal effect on the crack tip strains were noted.

By observing the clean (D) and dirty (S) steel behaviour it was found that the longitudinal specimens in both steels showed high toughness values. The δ_m values of LSS specimens when compared to LSD specimens showed a 15% decrease of upper

upper shelf values and a slight shift in transition to higher temperatures. The inclusions present were in an unfavourable orientation that did not facilitate crack growth. The measured reduction could have been due to the ease of void formation around the small inclusions which may have aided ductile crack growth. In certain cases, the debonding along very large inclusions (up to 2mm), caused re-routing of the crack front locally, giving the appearance of lamination and leading to high COD values.

The tensile strength and transition temperatures of the longitudinal direction did not suggest a significant variation in mechanical properties of the two steels. It was also apparent that the grain structure of steel S was more refined than in steel D, this implied improved properties of steel S. Therefore, the variation in COD must be a function more of the sulphide inclusion content than of other inherent property differences between the two steels.

Taking through thickness testing, the ZR and ZT specimens were chosen to examine the effect of inclusion orientation. The ZT crack front ran across the major, x-y, inclusion plane, along the longitudinal y-axis of the inclusion. The ZR crack ran across the x-y plane and along the intermediate, x-axis. Thus, the ZT crack ran along the rolling direction and consequently along the elongated inclusion axis and elongated grains. Hence, the deleterious effects of rolling should be noted more in the ZT rather than ZR orientation if inclusion length is considered to be of importance.

Figure (28) for steel D showed minor upper shelf variations between δ_m for ZRD and ZTD specimens, both lay within the scatter range 0.70mm to 0.95mm with the ZRD falling more to the higher values of this range. The longitudinal specimens showed a scatter band that overlapped that for the through thickness specimens, that is, 0.72mm to 1.00mm. There was no variation for transition temperature for the different orientations. Hence, it must be assumed that grain size variation noted in Table (2), the ferrite

banding and the small amount of inclusions present in steel D, did not adversely affect the measured toughness properties.

The longitudinal δ_m values of steel S were three to four times those of the through thickness directions. Of the through thickness directions, the ZRS specimens gave measurably higher δ_m values than the ZTS. From Table (2) it can be seen that the ZT orientation registered a 20-30% elongation of inclusions. The interaction of inclusions in the ZT direction would have facilitated ductile crack growth and led to the drop in δ_m values. Appendix A (i) and (iii) shows the manner of inclusion interaction and this is discussed below.

The inclusions did not lead to a significant deterioration in LSS specimens when compared to LSD specimens. The LSS inclusions lay perpendicularly to the crack front and did not lead to a stress concentration at the inclusion apices. Their effects could only have been due to the ease of void formation which may have aided ductile crack growth. However, the total inclusion length in the direction of crack growth of an LSS specimen (that is, the z-dimension of the inclusion) would be very small.

It can be seen from Table (2) that the inclusion morphology between plate edges and plate mid-thickness was different. This was due to two factors. First, there was inclusion segregation within the plate during manufacture, and, secondly, the process of controlled rolling caused differential flow in the plate. Even though the rolling operations were essentially under plane strain conditions, there was a measurable excess of flow of the surface materials, in the longitudinal direction. Cumulatively, surface inclusions became slightly elongated and discontinuous, with higher aspect ratios than in the centre. However, the total inclusion length/unit area did not vary significantly between edge and centre of plate as only a small, near surface volume was affected.

It was noted earlier that grain size varied only for steel D, where the mid-section of the plate was 30% larger in size than the

edges. Furthermore, steel S showed finer grain size than steel D, see Plates (1, 2).

The grain size variation and inclusion morphology change would be of interest to investigate since the result would determine the relative importance of the various inclusion parameters and the significance of grain size variations within the plate.

The larger, 18 x 18mm, specimens showed δ_m values higher for the upper shelf and a shift to higher transition temperatures. This was more clearly shown in the Kamath et al results of Figure (31) for various specimen sizes.

The COD resistance curves are given in Figures (32-35) and in Table (17). It can be seen that COD increased with crack extension, Δa. Using fatigue crack length (a_f) and fatigue crack plus ductile crack length ($a_f + \Delta a$) to calculate COD give curves (i) and (ii) respectively. Curve (ii) tended to a plateau region for high values of Δa. ZTS specimens showed a decrease in COD due to the ease of crack growth at high loads where the average Δa was 2mm.

From Figures (32-35) it was seen that δ_i values, extrapolated from $\Delta a = 0$, for clean steel (d) was 0.4mm. Figure (33) shows a comparison of de Castro's results (203) where clean steel initiation COD varied from 0.44 to 1.0 according to the value of a/W. This supports other workers evidence that δ_i is dependent on specimen geometry in situations of extensive plasticity.

4.1.5. CONCLUSIONS

Charpy impact values obtained from undersized specimens of 10 x 10 x 50mm gave impact energies that did not differ from full size ZTD specimens. Undersized ZTS specimens were also tested and the results were considered valid.

Upper shelf Charpy impact energies in the through thickness direction reflected the inclusion content and orientation in the steel specimens. Therefore, rated in ascending order of upper shelf impact toughness gave ZTS/ZRS, ZTD/ZRD, LSS then LSD.

The maximum load COD curves portrayed a trend similar to Charpy impact results, that is, the upper shelf reflected the same order of toughness for the various steels and orientations. Greater sensitivity to inclusion orientation was noted with COD. ZRS specimens gave higher δ_m values than ZTS, Figure (30). This was due to the smaller average inclusion length which led to fewer inclusion interactions.

The Charpy impact test gave higher ductile to brittle transition temperatures than the static COD test. The deleterious effects of inclusions in the through thickness direction was exaggerated by impact testing conditions. Hence, the impact conditions gave a generally more conservative characterisation of toughness than static loading tests.

The ductile to brittle transition of both Charpy and COD testing was less pronounced for through thickness specimens in dirty steel, that is, ZTS and ZRS.

Upper shelf COD values decreased with increasing temperature. This may be due to the very sensitive dependence of maximum load COD on small, temperature related variations of yield strength.

For materials unaffected by inclusions, that is, LSS, LSD, ZTD and ZRD specimens, the COD resistance showed a plateau region at values higher than δ_m. The δ_i values were found to be geometry related, being higher for the larger specimens, Figures (32-34).

COD - Δa curves for 10 x 10mm steel S specimens showed the significant drop of δ_i values in through thickness testing. The resistance to crack growth was greatly reduced in the through thickness direction, Figure (35).

4.2. THE EFFECT OF FREE SURFACES ON CRACK TIP DUCTILITIES

The problem found in Section 4.1 was how to obtain COD values for the through thickness direction near the edge of the steel plates S and D to determine the effects of inclusion morphology and minor grain size variations. Likewise, how does one determine the toughness of thin plates in the critical through-thickness orientation? Two problems are encountered. First, in what manner will the close proximity of free surfaces to the crack tip affect the results? Second, how does one produce a through thickness specimen out of thin plate, too thin for conventional specimens?

Without studying the effect of free surfaces on crack tip ductilities one cannot attempt to explain through thickness toughness values and their relationship to plate thicknesses. The position of a through thickness crack in a plate with respect to the surface is of importance. Other problems arise on welding of attachments to thin pipe or plate since that involves the removal of the effects of the free surface. In such cases there is a serious consideration of through thickness delamination, probably enhanced by stresses caused by weld thermal shock and weld metal shrinkage. The crack will be under a high degree of constraint due to the welded section which removed the effects of the free surface.

4.2.1. EXPERIMENTAL

Because the free surface lies in the y-direction with respect to the through thickness crack or lamination see Figure (5), a simulation in terms of a fracture toughness specimen must include the free surfaces in that direction. A simple change of specimen geometry cannot bring about the desired effect and the exercise should not be categorised with the multitude of publications concerned with changes in specimen geometry.

After much trial and error it was found that the best method of simulation involved the use of prefatigued COD specimens,

10 x 10mm in size with 2.5mm diameter holes drilled through the specimen, one at either side of the crack tip. Two parameters were varied; the depth of the hole from the notched surface and the proximity of the hole to the crack tip. The experiment was conducted at ambient temperatures for the two steels and at various orientations. The exercise was repeated for Charpy V specimens.

COD was measured at first attainment of maximum load. The procedure detailed in Section 4.1 was followed using equation [4.2].

4.2.2. RESULTS AND DISCUSSION

The Charpy V impact results given in Tables (19, 20) for LSS and LSD specimens show an increase in absorbed energy with the presence of holes, when such holes were placed 2mm below the V notch, in the direction of the crack propagation. This increase was most noticeable for LSD specimens where the free surface to notch separation was nearly 3.5mm. The magnitude of the change was a 28% increase in absorbed energy, associated with a deformation of the hole measured at 0.30 strain. However, at 5mm separation, a strain of up to 0.18 of the holes was not shown to have an effect on absorbed energy.

The COD also indicated an increase in measured toughness with proximity of the free surfaces. This was clearly shown in Table (21) and Figure (37). The COD and straining of the holes first appeared in Figure (37) at a separation of 4.2mm see Plates (3A, B). This indicated that COD was more sensitive to material flow than Charpy testing, since no Charpy impact energy increase was noted for hole strains up to 0.19.

These results suggest that the presence of a free surface adjacent to a deforming crack tip was beneficial to the toughness. In the absence of welded attachments adjacent to the through thickness crack there would be little reason to suspect crack growth. Under such situations it would be better to just monitor the crack.

Taking the free surface to crack tip separation at which the holes were first noted to deform as the measure of the plastic zone extension in the y-direction, it can be seen that the 5.5mm for Charpy specimens exceeded the 4.2mm for COD testing. The reason why the COD plastic zone was smaller can be explained in terms of three factors: the presence of a longer crack that was also very sharp and the limited amount of deformation corresponding to maximum load in the COD test.

The Charpy insenstivity to a hole strain of 0.19 was explained in terms of the higher energies absorbed during crack propagation rather than initiation. This implies that the holes would strain early in the deformation history. Thus, the straining of a hole would more likely be influential on the COD testing, where the deformations stopped at maximum load, than on Charpy, which carried on for a considerable extent beyond it and beyond the holes. The COD increased asymptotically with free surface proximity. At 2mm and below, the intense flow of the material separating the crack tip and free surfaces resulted in the shearing of the separating ligament.

It should be noted that the diameter of the plastic zone in the y-direction for COD specimens appeared to be 8.4mm, which was greater than the 7.0mm extent in the same direction measured without the presence of holes, using optical techniques. It, therefore, appears that this increase was a result of the presence of free surfaces which had the effect of reducing crack-tip constraints and increasing e_y. By the same token, the free surface in the y-direction was considered to have increased crack tip flow by reducing σ_y.

The extent of the plastic zone in the y-direction (7.5mm) in a regular specimen was of the size of the unbroken ligament ahead of the crack in the x-direction (7mm). The plastic zone at the crack tip can be considered to be near cylindrical in shape, of diameter roughly equal to the unbroken ligament length. That is, the size of the plastic zone in the y-direction is limited in size to its extent in the x-direction but enlarges in the presence of

free surfaces. The size of the plastic zone appears to affect the measured COD at maximum load.

4.2.3. CONCLUSIONS

The plastic zone developed early in the deformation history of a bending notched bar. The δ_m which depended on the plastic zone size was also shown to be affected by the strain of the holes. The Charpy impact toughness was considered to depend more on crack growth and showed less dependency on hole strain which occurred earlier in the deformation history, Figure (37) and Tables (19-21).

The toughness increase caused by the presence of holes was due to the reduction of the stresses developed at a free surface in the y-direction, namely σ_y. As the stresses reduced with free surface proximity, so the strains increased in that direction.

Measuring valid toughness characteristics of the material of thin plates in through thickness directions should not be conducted in a manner where the effects of a free surface on crack tip strains is interfered with. Situations which involve the welding of a bar perpendicular to a thin plate surface, by means of which a bending moment is applied removes the possibility of strain from one surface and hence, reduces the toughness of the plate.

The presence of a through thickness crack or delamination adjacent to a free surface renders the crack as harmless in the absence of loading through the thickness. Welding of attachments adjacent to the crack should be avoided since the weld would remove the beneficial effect of the stress-free surface and add weld shrinkage stresses through the plate thickness.

4.3. THE EFFECT OF INCLUSIONS ON THIN PLATE STEEL DUCTILITIES

With thin plate or edge samples of thicker plates, the limiting factor is in machining fracture toughness specimens in the through thickness direction of suitable size. Accepted three point bend specimen geometries, are of L = 4W and W = B or W = 2 B dimensions. For through thickness specimens, the plate should be ideally a minimum of 50mm thick, to produce specimen widths of 10mm. A thinner plate would produce specimens too small to allow the growth of conventional fatigue cracks. This minimum thickness is too restrictive for the majority of industrial purposes and thinner plates would not allow the critical through thickness direction to be tested. The problems encountered for edge samples of thicker plates are, obviously, even greater.

The work presented, studies a method of producing through thickness specimens 10 x 10mm in cross section from short, edge samples of thick plates and for thin plate testing. This technique was used in studying the efffects of inclusions in steel plates.

4.3.1. EXPERIMENTAL

Many possibilities were considered for attaching 'dummy' ends to either side of an undersized specimen to bring the overall size to the acceptable specimen dimensions. Welding was finally considered as the best method of attachment and has recently been used for such purposes (129). The effects of two suitable welding processes on the material properties of BS 4360 50D steel were considered. The two processes chosen were, electron beam welding (EBW) and friction welding (FW).

EBW samples were prepared by welding individual specimens cut out to 12 x 12mm cross-section, or by welding larger steel blocks which were then cut up to produce five to ten specimens. The centrally welded pieces were through thickness samples, 12.5mm and 25mm long, machined from the edge and from the centre of the two steel plates, S and D. Weld heat input was kept to a

minimum. For EBW, a single pass was sufficient for individual specimens. For the larger blocks, a pass was necessary from either side to ensure complete penetration.

The FW specimens were constructed by welding cylindrical sections 19mm in diameter by 25mm long at either end of the central sample to be tested. The central samples were 10 x 10mm in section with 12.5mm and 25mm lengths. The welding parameters were controlled to allow a minimum of burn-off and hence small heated affected zones, (HAZ).

The HAZ was measured optically, by etching with 2% Nital solution and mechanically, by Vickers hardness testing using a 10 kg load. The maximum hardness and lateral extent of the HAZ were recorded.

To produce steel samples with varying inclusion content, 50mm thick sections of steel S and D were hot rolled, in stages, to produce elongated inclusion stringers. The hot rolling was carried out in the original rolling direction at temperatures around 1300^{o}C. Final strains of 0.5 and 0.75 were produced, that is, hot reduced down to 25mm and 12.5mm respectively. The resulting plates were then heat treated at 1310^{o}C for one hour and immediately oil quenched. This was followed by tempering at 710^{o}C for 50 minutes. It was found that this heat treatment gave best strength and low temperature ductility.

To be able to compare hot rolled and heat treated plate toughness values with the original, as-rolled, plate it was necessary to similarly heat treat the original plate specimens and obtain a quench and tempered (Q & T) grain structure.

COD was measured at the first attainment of maximum load as noted earlier. Microhardness measurements were used to determine the size of the plastic zone at mid-thickness sections.

4.3.2. RESULTS

Vickers hardness results for the as-welded HAZ produced

during FW and EBW are shown graphically in Figure (38). It shows that the HAZ reached 360 Vickers for friction welds and extended for 0.75mm at either side of weld centre line. With one run, the EBW hardness reached similar values but, due to the higher heat input, the HAZ extended for 1.75mm. The double run EBW showed slightly lower hardnesses of 250 Vickers but extended further to 2.0mm either side of the fusion centre line.

COD results of 12.5mm and 25mm central sections of EBW and FW specimens from centre and edge locations, tested through the thickness at ambient temperatures are given in Table (22). It shows that edge and centre specimens of steel S and D gave no indications of differing δ_m variations were noted for the slight variations in grain size for steel D for the inclusions aspect ratio variations of steel S, noted in Table (2).

The original plate specimens of steel S and D in the longitudinal and through thickness directions that underwent the 1310°C heat treatment followed by quenching in oil and tempering at 710°C gave the results in Tables (23, 24) and Figures (39,40). This shows a slight reduction for upper shelf values and a considerable shift in transition temperature down to -140°C. The structure produced by the heat treatment was a very fine grained matrix characteristic of quenched and tempered steels.

The hot rolled, Q & T, longitudinal and through thickness welded samples of steel D at 0.5 and 0.75 strains showed a similar trend to the as-rolled and heat treated specimens. The through thickness specimens showed slight reductions for upper shelf values as the strain increased, see Table (25) and Figure (41).

Hot rolled, steel S specimens were tested for through thickness and longitudinal directions, the results are given in Table (26) and Figure (42). The longitudinal specimens showed slight δ_m reductions.

4.3.3. DISCUSSION OF THE WELDING TECHNIQUES

The FW technique produced very small heat affected zones due to the tighter control of the welding parameters. By using square 10 x 10mm cross-sections for the central pieces to be welded which fitted into a suitably designed holding chuck, the machining time was considerably reduced. The end cylindrical pieces were cut off a mild steel bar, of the required diameters, which negated the necessity for a turning operation. With clean and rough welding surfaces, the flash or burn-off was reduced to an absolute minimum, thus reducing the heat input.

The EBW technique required machining to tight tolerances. The 12.5mm thick plates required a weld run on either side to give full penetration. The weld HAZ was found to be considerably larger than for the FW technique due to the greater heat input, Figure (38).

The disadvantages of high costs and large HAZ outweighed the advantages of better fusion of EBW. FW, with its lower costs and greater versatility was considered to be more advantageous for welding undersized specimens.

The COD results for as-welded specimens of 12.5mm and 25mm long central sections showed no variations with parent plate results, Table (22), thus, providing the successful application of the welded specimens. The limited heat inputs were not sufficient to alter the material at the crack tip nor to interfere with the plastic deformations in the specimen. This could be accounted for, since only a maximum of 4mm was embrittled in the central piece, with maximum shrinkage of 1.5mm in the weld. Hence, in the smaller sections, 7mm of unaffected material was left. It was shown in section 4.2 that the maximum lateral expansion of the plastic zone (in a 10 x 10mm specimen) in the absence of holes measured 7.0mm in total. For the largest HAZ, found for EBW with two runs, the extremities of the HAZ were only marginally embrittled and would not have affected the plastic zone to any degree of significance. Certainly, even with the interaction of the HAZ with r_p, values of δ_m showed no effects.

If use is made of initiation values of COD (where the associated plasticity is limited), the effects of the HAZ would be even less restrictive.

The limitation of the above technique for through thickness testing of the thin plate materials should be outlined. The technique is valid as test for the plate material alone and not for the effect of free surfaces on through thickness cracks. The effect of the free surfaces should best be studied by the simulation technique, considered in the previous section.

The importance of specimen geometry was reviewed in Chapter 1 and is studied at greater depth in Chapter 5. Although it is possible to weld a specimen of any dimension using a thin plate, the plate thickness, T, will be the limiting factor. The reason for this is the interaction of the crack tip plastic zone with the brittle weld HAZ. Naturally, there can be no specific rule for the specimen geometry limitations as r_p can be very small with respect to the plate thickness, for example, with very brittle materials or at temperature representative of the lower toughness shelf. In general, however, using engineering materials which are relatively tough, at ambient or upper shelf temperatures, the deformations are characteristic of general yielding. Under such conditions the plastic zone will be equivalent in lateral dimensions to the unbroken ligament, (W - a). Hence, for any geometry considered, the specimen dimensions will be limited by:

$$(W - a) \geq T - 3$$

where T is the plate thickness and all measurements are in millimetres. The constant represents a measure of the weld shrinkage plus the HAZ measured for FW. With EBW, a larger constant should be substituted, representative of the HAZ formed under the chosen welding parameters used. Thus, by limiting (W - a) in terms of T one is able to calculate the maximum specimen thickness to be tested for a given plate thickness which depends, naturally, on the geometry desired.

4.3.4. DISCUSSION OF RESULTS

Welded samples from the edge of the clean steel parent plate material, D, showed no variations in δ_m results associated with the slightly finer grain size associated with this position, Table (22). Although there was a maximum grain size variation of 25% from edge to centre of steel D, the welded samples were testing the material at 6mm and 12mm from the edge and, as can be seen from Table (2), these positions corresponded to 18% and 10% smaller grain size respectively. It will be shown below that large grain size variations did not significantly affect δ_m values at the upper shelf but they did play a more significant role on low temperature toughness.

The edge sample of the dirty steel, S, also showed no variations associated with the change in inclusion morphology. However, it was shown in Section 4.1 that the δ_m values were sensitive to changes in specimen orientation from ZR to ZT. That the δ_m values did not show a difference between edge and central sections was, therefore, not due to the insensitivity of δ_m to variations in inclusion content. A count was made of the total inclusion length per unit area, according to Appendix A. It can been seen from Table (22) that the effects of controlled rolling did not significantly increase this value from edge to central positions. It is apparent that the higher concentration of MnS inclusions in the centre is offset by the greater elongation of inclusions at the surface, where the aspect ratios of the inclusions were higher. Furthermore, the welded specimens were not testing the material at the surface but 6mm and 12mm away from it in the 12mm and 25mm welded specimens respectively.

The welded, hot rolled and heat treated clean steel specimens gave δ_m values, Figure (41), only slightly inferior to the heat treated parent plate specimens of zero hot-reduction strain, Table (25) and Figure (39). The through thickness specimens showed a small reduction in δ_m values at upper shelf values with increasing hot rolling. The presence of a few alumino-silicate

inclusions did not lead to a significant increase in inclusion length due to the low relative plasticity of such inclusions, Section 3.1.1.

Table (26) and Figure (42) showed the effect the hot rolling and heat treating on steel S, containing MnS inclusions. The reduction of δ_m in longitudinal specimens was small. The through thickness values showed very considerable deterioration in toughness. Even at a hot rolling strain 0.5 in the ZR orientation, the values of δ_m was 0.08 $\pm$ 0.03mm. Figure (43) shows a load-clip gauge opening sketch for such steels in comparison to the behaviour of a longitudinal specimen. Very small plastic components of opening were noted for the though thickness, steel S specimen. The low toughnesses were, naturally, reflected by the plastic zone sizes. Hence, at maximum load, Plate (4) shows the variation of r_p with inclusion content for the through thickness direction at ambient temperatures.

It was observed from optical and scanning electron microscopy that ductile failure in hot rolled through thickness specimens, when compared to the parent plate ductile cracking, initiated early in the loading history and rapidly grew into suitably aligned inclusions. The crack front took on a jagged appearance with local extensions into inclusions up to a few millimetres length, as seen in Plates (5, 6, 7).

At 0.5 hot rolling strain, the inclusions were very considerably longer, Plate (5). In COD testing, the crack front was affected by such inclusions in ZTS and ZRS specimens. The crack extended locally into the easily debonded inclusions. These extensions reached a length of 3mm locally. These frond-like extensions interdigitated with steel matrix. The unbroken matrix between the extensions suffered a high degree of stress triaxiality, being surrounded by sharp cracks. The effect was that the matrix fractured with visibly less ductility. The consequence of the increased constraints was to enhance the tendency of brittle cleavage fracture. Such a situation can be seen in the scanning

electron micrograph of Plate (6). This fracture appearance differed markedly from parent plate behaviour with its smaller inclusions.

With maximum crack tip stress triaxiality developing at the specimen centre, the possibilities of inclusion delamination and crack growth was maximised in this position. With a localised but large crack extension into an inclusion cluster at the centre, the effect was to increase the constraint and, hence, the stress levels. This led to tunnelling effects of the crack front which added to the constraints. Hence, the effects of large inclusions on through thickness toughness was not only to decrease it by facilitating crack growth into suitably aligned inclusions but also by causing high crack tip constraints.

Weld metal, subjected to fatigue cycling, shows the well known effects of non-uniform crack-front growth. This could be due to the presence of high internal stresses caused by weld metal shrinkages or may be associated with large imhomogeneities such as slag, grain size variations and microcracking. To overcome this problem, the samples were subjected to small compressive strains in the region of the crack tip. This had the effect of evenly distributing the stresses built up in the weld metal and led to more even crack growth.

To artifically induce an even crack front profile was not always possible if the cause was primarily due to microstructural inhomogeneities, such as inclusions. Furthermore, this does not represent the more realistic, uneven crack profiles in service conditions. An artificially induced regular crack would lead to optimistic values of tolerable crack tip strains.

BS 5762 limits the crack front shape to slightly uneven contours. Due to the presence of inclusions, the crack front was very irregular in shape and fell outside the limits laid down in the standard. Since it was impossible to grow a fatigue crack with a more regular front in the through thickness direction of a dirty steel, it would appear that the standard does not distinguish

between irregularly grown fatigue cracks (formed by uneven loading or over-loading) and cracks that appear irregular inherent to the material's microstructural inhomogeneities. Plate (7) shows the shape of the crack front and fracture surface for the through thickness directions of a clean and dirty steel.

It is interesting to note here that inclusions in steel may act in a way to improve ductility, as noted on testing steels in the longitudinal direction with a through thickness crack, i.e. an LT direction of Figure (23). Here, the effect of the inclusions was to shift the ductile to brittle transition to colder temperatures. COD results are available for this direction (206) but no account was given for this shift. It is now possible to account for the mechanisms leading to this behaviour; it seems understandable in terms of the arguments presented above.

In an LT specimen of an inclusion bearing steel, the crack front cuts the xz plane along the x-axis of the inclusion. The effect was to laminate the crack front, as schematically presented in Figure (44). Upon loading the specimen, the inclusion/matrix interface debonded and void growth occurred, as has been observed in other longitudinal specimens. This facilitated crack growth and should have reduced the upper shelf toughness values. The effect of the voids also acted in laminating the crack front and added free surfaces which facilitated flow. A through thickness stress would not develop and the specimen behaved as if of much reduced B dimension. As the experiments with holes adjacent to the crack served in reducing the stress triaxiality at the crack tip in the y-direction, so do these voids act in reducing the stresses developing in the z-direction. The effect was to lower the transition temperature in the same way as the reduction of specimen thickness did. That is, because σ_z had been effectively removed, the maximum attainable stresses at the crack tip approached the uniaxial σ_y. The material at the crack tip would act as a series of small tensile specimens achieving σ_f conditions only at very low temperatures. Results of LT orientations were given by May et al (206) but no explanation was given for the lower

transition temperatures associated with such orientations in dirty steels.

The parent steel plate material, of type S, was control rolled from a billet to 51mm thick. The rolling operations were carried out at temperatures of high relative plasticity of the MnS inclusions with respect to the steel matrix. High inclusion elongations resulted which caused a drastic reduction in through thickness properties. It was shown earlier that the crack would initiate into ductile growth at loads comparable to the general yielding loads for small 10 x 10mm ZTS specimens and these loads were lower than general yield loads for ZTD specimens. Crack growth would continue under increasing load, giving rise to the δ_R curve of Figure (35). When load did not increase with Δa, it resulted in the removal of the safety factor from the system. A running crack would not be arrested and catastrophic failure would occur.

With small 10 x 10mm specimens, the strains through the ZTD specimen thickness were allowed to develop to a significant value. This allowed the large plastic zone formed at the specimen surface to absorb much of the energy of deformation and give rise to considerably larger δ_m values of 0.90mm, whereas the initiation value was less than half the value. The difference between δ_i and δ_m was that the plastic zone size increased with load, until beyond δ_m, crack extension caused specimen collapse.

4.3.5. THE SIGNIFICANCE OF INCLUSION LENGTH

For through thickness testing, the controlled rolling operations on steel S caused the increase of inclusion length. This led to the reduction of the load bearing capacity of the material. The plastic zone could not extend in size significantly and the strains tolerated at the crack tip were reduced. The measure of plasticity in a specimen can be observed from Figure (43) which clearly shows the reduction of past yield load bearing capacity in the though thickness direction with increased inclusion content.

The relationship between COD or %RA and inclusion content cannot be considered to be a linear one. The 20% RA limit set by Cotton (196) for reasonable through thickness ductilities can be used as a guideline for our purposes, in the absence of a universally accepted limit. From this, one may set an equivalent COD limit and, hence, an acceptable inclusion content. First, however, one must lay the rules for measuring the inclusion content in a given direction.

It was considered that when two individual inclusions were separated by less than half the average length of the two inclusions, they be considered as one inclusion, see Appendix A (i). However, inclusions not on the same plane could only have their total lengths and intervening space added if the two planes were separated by less than the average of the sum of the two inclusion thicknesses, see Appendix A (ii). Where inclusions in steels were hot rolled they became highly elongated in the direction of rolling and exceedingly thin. The distance separating two inclusion planes became very small and yet exceeded the average of two inclusion thicknesses, as exemplified in Plates (2, 5). At the deforming crack tip, the directions of maximum shear occurred at 60° to the crack plane. An inclusion placed in that direction became a suitable defect for the crack to grow into. For this reason it was considered that two inclusions in a loaded body would interact and act as a single inclusion if they lay within a segment extended 60° to each other and within a radius of the average of the sum of their lengths, as in Appendix A (iii). The effect of this was to increase the measured total inclusion length for unit area, $\Sigma l/A$.

The interaction of inclusions out-of-plane suggests that the crack front would follow the inclusions out-of-plane. This behaviour was seen to occur when growing the fatigue crack. The typical zig-zag shapes of ductile crack paths can also be explained by this behaviour. As the crack followed suitable inclusions that lay within the plastic zone, a step-like fracture surface was produced. This fracture surface topography is

typical also of lamellar tearing surfaces.

The lack of δ_m variation of the edge and centre positions of steel S was due to the insignificant variation in the inclusion density, $\Sigma l/A$. Furthermore, the $\Sigma l/A$ for ZR and ZT orientations of steel S showed a difference not because of the greater inclusion density in the ZTS specimen but because of the more frequent interactions of the inclusions in the ZT direction as a consequence of their elongation during rolling.

Under the plane strain conditions of rolling a steel billet at the mill, it can be shown that with each hot rolling strain of 0.5 the transverse or ZR direction would register no increase in the actual inclusion length but a doubling of $\Sigma l/A$ due to the reduction in thickness (neglecting the interaction of inclusions as shown in Apppendix A (iii)). Assuming similar flow characteristics of both steel matrix and sulphide inclusions, the inter-inclusion spacing to inclusion length ratio would not alter after the rolling operation in the longitudinal or ZT plane. $\Sigma l/A$ would double due only to the halving of the thickness, as with the ZR orientation. However, with inclusions in the ZT direction now double the length that they are in the ZR direction, the effect of out-of-plane inclusion interaction, as specified in Appendix A (iii), would show a significantly greater $\Sigma l/A$ in the ZT direction than in the ZR direction.

Even with globular, rare-earth-modified inclusions the rolling operations would produce elongated inclusions in the direction of rolling. These results suggest that it was the interaction of inclusions that primarily affected COD and not the length of individual inclusions. For example, in the hot-rolled dirty steels of Figure (42) the ZRS specimens showed a small improvement in COD results over the ZTS specimens. This suggests that the average inclusion length, which was far greater in the ZTS direction, cannot be the significant factor. However, with Appendix A interactions, $\Sigma l/A$ would be only slightly higher in the ZTS direction as a consequence of lateral interaction, and would account for the small COD difference.

To support the view of attaching importance to out of plane inclusion interactions it was necessary to study the mechanisms of through thickness fracture. For localised, out of plane crack tip movements the steel plate would have suffered considerable hot-reduction, bringing the separation of adjacent inclusion planes to a distance equal to the average length of the inclusions. At the same time, the inter-inclusion separation, within one plane was increased, thus, the minimum distance between inclusions would be out of plane. Under such conditions, the straining crack tip would jump, laterally, from one inclusion plane to the next by shearing of the intervening matrix. This would give rise to a step-like fracture surface typical of lamellar tearing. Plate (7) shows the irregular, step-like appearance of the ZT and ZR fracture surfaces of steel S in comparison to the smooth ZT fracture surface of the clean steel. Plates (13, 14) discussed below, show the crack tip jumping out of plane to follow inclusion concentrations that lay within the plastic zone.

Returning to the relationship between δ_m and $\Sigma 1/A$, Figure (45) shows that as the inclusion concentration increased, δ_m was seen to reduce exponentially. On the same figure was plotted %RA against $\Sigma 1/A$. The scale of %RA was chosen such that the two curves were in close proximity. The inclusions affected %RA and δ_m in a very similar way. Only two %RA against $\Sigma 1/A$ points were available but the steepness of curve would have justified even a straight line relationship. However, as %RA and COD were shown to be related in Section 3.3, the two curves were shown to have similar trends. From Figure (45) the 20% RA was equated to an inclusion concentration of $1.25mm^{-1}$. This was equivalent to a δ_m value of 0.4mm. This was double the value of the ZTS and ZRS specimens.

Before discussing the merits of this technique it is necessary to show its limitations. First, as mentioned earlier, the 20% RA was a recommended and not an absolute value. Second, the δ_m curve was shown to be specimen geometry and size related and may shift to the left as size increases. Finally, the curves plotted are incomplete and relevant to this material.

Nevertheless, the figure shows that the steel S variety contained unacceptably high sulphide inclusions of approximately $2mm^{-1}$, nearly double the accepted value. This suggests that the 50mm thick steel S plate would have shown acceptable through thickness toughnesses had the controlled-rolling operations stopped at 100mm of plate thickness. Obviously, this would have halved the inclusion concentration.

It is difficult to suggest a single value of $1.25mm^{-1}$ as the limiting factor because of the limitations listed above. However, more generally, one should use a range of 1.0 to $1.5mm^{-1}$ as the limit which would depend on experimental variables and fitness for purpose. Specific requirements of a steel plate may allow for inclusion concentrations well outside the range quoted. For example, where no z-ductility is required, as in thin plates with no stresses normal to the surface. Alternatively, where very high z-ductilities are required as in nodal joint constructions, a lower $\Sigma l/A$ is necessary.

It is highly unlikely that a steel billet with high sulphide content will be of any use as medium to low thickness plate requiring good through thickness ductilities. The high rolling strains necessary for producing the medium to low thickness plates would create an unacceptably high value of $\Sigma l/A$. It would be produced not only by increasing the average inclusion length in the rolling direction but primarily by the close proximity of adjacent inclusion planes as a result of thinning.

For ductile engineering materials tested at the upper shelf temperature range, the behaviour was that of general yielding and the toughness, measured as δ_m, was found to be equivalent to the unbroken ligament (W - a). It will be shown in Chapter 5 that the toughness is independent of crack length considerations under such conditions. Therefore, it would be of value to correlate the inclusion content of a steel (simply obtained by a metallographic examination) to an equivalent reduction of (W - a) and, hence, COD. Physically, one may view the ligament (W - a) as ductile material capable of sustaining a certain COD. Where inclusions are

introduced, the through thickness orientation will register a COD value equivalent to a smaller (W - a). The difference in the ligament lengths would be directly equivalent to $\Sigma l/A$.

The above was created graphically by plotting δ_m against $\Sigma l/A$ and δ_m against (W - a). The former curve was obtained from Figure (45) and the latter from Chapter 5, Figure (53). Fitting the two graphs together produced Figure (46). It can, thus, be seen that ZTS specimens with $\Sigma l/A$ of approximately $2.5mm^{-1}$ was equivalent to an inclusion-free specimen with (W - a) of 3.2mm (compared to the normal 7mm). That is, introducing $2.5mm^{-1}$ of inclusions into a steel was equivalent, in the through thickness direction, to increasing the crack length from 3.0mm to 6.8mm for a 10 x 10mm specimen.

It should be noted that Figures (45 and 46) suggested that COD decreased exponentially with inclusion content, expressed as $\Sigma l/A$. COD can be plotted against $\Sigma l/A$ for various temperatures, each producing a characteristic curve. If a set of curves thus produced were expressed mathematically, by polynomial fitting techniques, one would be able to predict the COD dependence for any given value of $\Sigma l/A$ for 10mm specimen.

Given that through-thickness testing can be difficult for thin plate, it would be of great benefit to predict the through thickness COD from a given longitudinal COD transition curve. The assumption made here was that the longitudinal direction COD would be equivalent to the COD through the thickness of that steel if no inclusions were present. The COD evidence from Figures (28, 29) for LSD and ZTD specimens of a relatively clean steel showed that this assumption was acceptable.

Using the results obtained it was possible, using a computer model fitting technique, to predict the through thickness COD-temperature transition for 10mm specimens for any given inclusion content. The programme is detailed in Appendix B and also gives a worked example for an inclusion content of $1.65mm/mm^2$.

The computer model is of value since an approximate COD-

temperature transition curve may be constructed for the through thickness direction from a longitudinal curve, given only the inclusion density. This is especially valuable in thin plate materials where it is difficult to obtain through thickness specimens.

The model is limited to small scale specimens and it assumes that the behaviour of COD dependence on $\Sigma l/A$, as portrayed in Figure (45), to be universal.

4.3.6. CONCLUSIONS

Friction welding was chosen as the most suitable technique to use in welding of undersized specimens. It was more versatile than electron beam welding, it produced a smaller heat affected zone and cost less to produce specimens.

The brittle heat affected zone would not interfere with yielding processes in the plastic zone if it lay outside the plastically affected area. For general yielding conditions, this could be satisfied if the specimen geometry is limited by:

$$(W - a) \geq T - 3$$

where T is the plate thickness and all measurements are in millimetres. If general yielding conditions did not apply then (W - a) could exceed T - 3. The constant 3 represented the burn-off plus HAZ and would depend on specimen size and welding variables.

Inclusions in steel led to reductions in through thickness toughness due to the ease of crack growth out of plane to the nearest inclusion within the plastic zone. The sulphide inclusions in steel S delaminated easily at very small loads, the complex alumino-silicates of steel D did not debond as easily and were considered to be less harmful. The presence of inclusions in this direction caused the post-yield, load bearing capacity of the ligament to reduce significantly. This led to smaller plastic zone sizes being developed. Plate (4) and Figure (43). The growth of

the crack front into large inclusions caused an overall increase in constraint created by the tunnelling effects. Further increases in constraint resulted for the matrix separating two large inclusions, Plate (6).

$\Sigma l/A$ accounted for the toughness dependence on inclusion length indirectly, in the increased incidence of interaction of long inclusions out-of-plane, as in Appendix A (iii). The lack of variation of δ_m for near edge and centre specimens was due to the lack of variation in $\Sigma l/A$.

Rolling operations did not bring about very large variations in $\Sigma l/A$ for ZR and ZT directions, even where the inclusions suffered unidirectional elongation. Any variations in measured COD was due to the out-of-plane migration resulting from the interaction of the crack tip with inclusions. This was shown to be the manner in which crack growth occurred in the z-direction of sulphide bearing steels, Plates (7, 13, 14). Hence, it was shown that high rolling deformations would result in unacceptable through thickness toughness even in steels with relatively low sulphide content. As a result, it is the final inclusion density that should be limited, according to fitness for purpose. The inclusion density would depend on the initial sulphide content and the resulting ratio. It was suggested that a value of $\Sigma l/A$ limited to less than $1.25mm/mm^2$ would achieve 0.4mm δ_m values in 10mm specimens. This was equivalent to 20% RA, recommended by Cotton (196) as a value necessary to inhibit lamellar tearing. From this, it was considered that steel S was unacceptable and could suffer through thickness failures.

Small variations in grain size did not affect δ_m values significantly. With large variations in grain size, as produced in the quenched and tempered specimens, the effect was most noticeable in improved cryogenic toughnesses. Upper shelf values were slightly reduced.

For high sulphur, rolled plate or pipes, load bearing attachments should be welded in the ZR orientation, perpindicularly to

the main rolling direction, to take full advantage of the slightly superior properties.

LT specimens with elongated inclusions behave as laminated materials. The inclusion-matrix interfaces debond to form large voids which act as free surfaces. The large number of newly created free surfaces act in such a way as to decrease σ_z. Reducing the stress triaxiality causes a shift in transition to lower temperatures.

BS 5762 should distinguish between irregular cracks fronts caused by crack growth into inclusion stringers and irregular cracks shapes caused by uneven loading actions, Plate (7). Uneven crack fronts formed by favourable inclusion alignment and weld metal inhomogeneities, caused an increase in crack tip constraints and led to more conservative toughness values. Artificially inducing regular crack fronts should, therefore, be avoided.

It is important to note that large hot reducing strains at the mill will eventually create an unacceptable inclusion density for a sulphide bearing steel, even if modified by rare-earth additions. For good through thickness properties in thin, rolled plate or pipe, initial melt must show sulphur contents equivalent to those of steel D which showed less than 0.005% S by weight, Table (2).

CHAPTER 5

THE EFFECTS OF THE PLASTIC ZONE ON FRACTURE

To ensure valid plane strain fracture toughness testing according to ASTM E399-74 and BS 5447 (19, 20) requirements would involve the use of prohibitively large specimens, especially for ductile engineering materials. For this reason, subsized and manageable specimens were used from which meaningful fracture toughness characterisations one attempted to extract.

The widespread use of COD and J Integral testing of specimens in the general yielding mode has gained rapidly in complexity. This has led to ambitious claims from authors for the industrial applicability of various concepts. Relating COD and J Integral results to design curves, used in estimating tolerable crack lengths for structures under various conditions, has made a study of specimen geometry and loading conditions of major importance.

Chapter 2 gave an introduction to the problems associated with the dependence of the measured toughness and transition temperature on the specimen size. Also noted, was the difficulty in defining the point of crack initiation, and the difficulties associated with measuring the crack opening at such points.

The specimen size and geometry dependence of the ductile to brittle transition temperature for small ductile steel specimens was investigated. In doing so, more importance was attached to the measurement of strains and the plastic zone size rather than limit loads or stress analyses. Various techniques were used to study the crack tip strains in an effort to calibrate them. The works of other investigators in this field were reviewed in detail in an attempt to find common ground for the geometry related fracture transition behaviour.

The significance of the method of load application was also investigated. The author chose to compare between bending and

tensile loading effects on the measured toughness, that is, between three point bend specimens (SENB) and single edge notched specimens pulled in tension by fixed grips (SENTfg).

Finally, the industrial relevance of small sized fracture toughness specimens was investigated by comparing with the fracture behaviour of larger welded steel plates.

5.1. PLASTIC ZONE SIZE MEASUREMENTS

Orowan's slip line field analysis for calculating peak tensile streses, using the Tesca yield criterion in a notched bar (107), gave:

$$\sigma_x = 2\ T_Y\ (1 + \pi/2) = 2.57\ \sigma_Y \qquad \ldots.5.1$$

where T_Y is the shear yield stress.

From equation [2.29], using the definition of plane strain to calculate σ_z and the von Mises criterion one obtained:

$$\bar{\sigma} = 0.4\ \sigma_x$$

where the mean stress was equated to the yield stress, one obtained:

$$\sigma_x = 2.5\ \sigma_Y \qquad \ldots.5.2$$

for plane strain conditions. Hence, the principal stresses at the crack tip can exceed σ_Y under conditions of plane strain.

Using the principle of temperature independent brittle fracture stress, σ_f, Orowan plotted the σ_Y-temperature dependence for uniaxial tensile specimens and added the peak tensile stresses obtainable in a notched specimen by a simple multiple of 2.5 σ_Y. The plot is given in Figure (47) and the interaction of the two yield traces with σ_f represented the points of transformation from ductile to brittle behaviour.

To expand further on Orowan's work, one defined the point of intersection of the uniaxial σ_Y with σ_f at T_a in Figure (47), as the lowest temperature of transformation possible for the material. T_b, which represented the intersection of the plane strain (maximum attainable) principal stresses with σ_f, therefore, determined the highest temperature of transformation for a deeply notched specimen. This represented the conditions $\varepsilon_z = 0$ and

and $\sigma_z = 0.6\ \sigma_Y$. Hence, any specimen that exists in a state of stress where $0 < \sigma_z < 0.6\ \sigma_Y$, must lie between the two extremes of a uniaxial tensile specimen and a plane strain condition. That is, a fracture toughness specimen will show a trend intermediate to the two curves of Figure (47). More to the point, the transition temperature will exist, for most laboratory specimens, in between T_a and T_b.

Knott (117) identified T_b (and presumably T_a) as being equivalent to T_{gy} of Figure (48), where the general yielding coincided with brittle fracture. Below T_b or T_a brittle fracture took place after successively smaller amounts of yielding, locally at the crack tip. Knott pointed out that Orowan's theory did not distinguish between general and local yielding in the specimen.

Figure (48) plots general yielding loads, P_{gy}, as a function of temperature for notched specimens (108). The point of interaction between P_{gy} and the fracture load, P_f, represented the transition temperature T_{gy} which delineated the onset of brittle fracture. Again, no indication was given by the plot of the amount of strain incurred in the specimen, except to distinguish the point T_{gy} at which general yielding of the specimen coincided with brittle fracture. It can be seen, from the notch root strain of the same figure, that strain was continuous and no abrupt behaviour was distinguished at T_{gy}.

The plastic zone size, r_p, was known to reflect the measured toughness and had been used to identify valid plane strain conditions when its ratio to crack length approached zero. Studies of the plastic zone have led to the identification of a process zone that had been related to critical crack tip strains and inter-inclusion spacing (134). However, with the acceptance of critical crack tip strains as non-material parameters but to be geometry related, the validity of associating crack tip strains with material variables, such as inclusions, come under doubt.

In the present work, r_p was known to be large and to extend through the specimen ligament at higher temperatures. This was

used as a definition by Knott (117) to represent general yielding conditions. For higher temperatures, all specimen sizes considered in BS 4360 50D steel may be considered to be generally yielded, that is, from Figure (31) up to W = B = 75mm.

In this section, the behaviour of r_p was investigated experimentally with respect to changing temperature, material inhomogeneity and specimen size. The latter point was discussed in further detail below.

5.1.1. EXPERIMENTAL

Microhardness determination of r_p was found, in this work, to be more versatile than etching or optical surface determinations of the plastic zone. Two specimen sizes were considered, 10 x 10mm and 18 x 18mm, although results from Kamath et al (141) were called upon.

To estimate the crack tip strains, 18mm thick parent plate sections were taken and cold-rolled to various strains. The hardness measured from 25 readings of the centre of each piece was plotted against the strain suffered. Continuous strain-hardness curves were thus constructed.

To observe specimen surface deformations, the polished surface after loading was observed and photographed using polarised light. The resulting micrograph showed greater contrast of the surface deformations due to the light interference created by the light reflected from contrasting surface topography.

5.1.2. RESULTS

Microhardness surveys at mid-sections of 10 x 10mm specimens tested to maximum load at 20°C and to the fracture load at -90°C, revealed the plastic zone sizes representative of upper shelf and transition temperatures respectively. Figure (36) shows the extent of the crack tip plasticities. It was observed that the plastic zone consisted of a region of high strain rapidly

decreasing in intensity away from the crack tip. The high strains extended along the planes of maximum shear, at 60° to the crack plane. At 20°C, Figure (49) shows that the zone had microhardness values of 265V adjacent to the crack tip, falling rapidly to 200V at 0.6mm away. The LSS specimen tested at -90°C achieved hardness of 238V adjacent to the crack tip which fell rapidly to 180V at 0.18mm way. The small volume of material showing high hardness values was termed here, the highly strained region and its characteristically small size may be related to the process zone of Section 2.3.4.

To determine the strain, 18mm thick specimens were cold rolled to various thicknesses and sectioned. From the section, twenty five hardness values were taken and the average was plotted against the strain involved; Figure (50) was produced.

As hardness values for the parent plate was between 160-170V, it was clear that the majority of the plastic zone involved very little strain covering the range 170-185V, or a strain of 0.10 to 0.30 for longitudinal specimens of steel D. This can be found by using Figure (50).

Using Figure (50) one obtained an estimate of the strains achieved at a deforming crack tip for different conditions. From these calibrated curves, strains exceeding 0.64 were measured for hardness exceeding 223. Such strains were measured at the tips of cracks growing in a stable, ductile manner at 20°C in ZTD specimens. For the same specimens at -90°C, where cracking occurred by brittle cleavage mechanisms after a limited amount of ductility, the hardness registered was equivalent to a strain of 0.58. This can be seen in Figure (36A, B) for ZTD and ZTS specimens. The drop in strain measured at cryogenic temperatures was not as large as would have been expected.

Taking LSS and LSD specimens at 20°C and loading to various values of COD from 0.1mm to 0.6mm and performing a microhardness survey of a central section, one obtained Figure (51). This revealed that the maximum value of strain at the crack tip did not

increase but the lateral extension of the highly strain region increased as plastic loading continued.

Figure (51) also shows that the maximum hardness of steel D at the crack tip was 230-240V while that for steel S was 255-265V. Relating these values to the calibration curves of Figure (50) showed that the steel D average hardness corresponded to a strain of 0.83 and for steel S a strain of 0.80. The higher strains of steel D from the calibration curves was in spite of the lower hardnesses registered at the crack tip. This correctly reflected the higher COD values measured for the clean steel.

Figure (36B) shows the size of the plastic zone ahead of the crack tip in a through thickness dirty steel specimen (ZTS). It can be seen that the highly strained region and the extensive plastic zone were much reduced in size in comparison to clean steel.

General yield loads (P_{gy}) and fracture loads (P_f) for 18 x 18mm specimens are given in Figure (52A, B) respectively, for various a/W values. P_{gy} was found to increase as temperature dropped, associated with the increase in σ_y. The increase of P_{gy} with decreasing a/W was gradual and did not show an abrupt change at any temperature tested. The greatest increase of P_{gy} occurred for a/W = 0.22. However, the crack length this represented would not have been sufficient to limit yielding to the unbroken ligament and gross yielding would have occurred. The fracture loads were seen to decrease slightly with temperature drop.

Plates (8 to 11) show the interaction of inclusions with the plastic zone and their behaviour within the plastic zone. The optical micrographs were taken under polarised light.

Plates (12 to 14) show the effect of inclusions on crack deformations at the centre of through thickness specimens. These plates were taken using conventional optical micrography. The elongated inclusions of plate (14) were obtained by hot rolling steel S of plate (13). Plate (12) shows the crack tip in clean steel.

5.1.3. DISCUSSION

The highly strained region within the plastic zone was seen from Figures (36, 49) to show a sharp fall in strain away from the crack tip. The size of the highly strained region was of the size of the crack tip opening displacement. Size rather than intensity of strain of the high strained region were shown to be highly temperature dependent, Figures (36, 49). Since the δ_i values of 18mm specimens were shown to be both geometry and size dependent, Figure (33), it is likely that plastic strain and the size of the highly strained region are similarly dependent.

From Figure (36) it is observed that the size of the yielded zone was considerably reduced at lower transition temperatures. Figure (49) shows that although the lateral extend of yielding was reduced in size, the fracture strain at 0.58 was not a significant drop. This supports the work of Knott, Figure (48) which shows considerable ductilities associated with brittle fracture. However, although the size of the yielded zone was reduced, the actual strain was not reduced, if one used a sufficiently small gauge length. This suggests that the fracture strain, over the transition, was more constant than previously thought.

At upper shelf temperatures, the large plastic zone, lower yield strength and blunted crack tip profiles combined to create low crack tip constraints. The principal stresses at the crack tip were low and ductile cracking continued in a stable manner.

Associated with the plastic zone decrease over the transition temperature, there was a corresponding decrease in the amount of stable ductile cracking prior to fast fracture. The ductile cracking was considered necessary to increase the crack tip constrains sufficiently for brittle fracture to occur. It has been generally accepted that ductile crack growth increased the crack tip constraints by the effects of tunnelling. It was shown above that the cracking also increased constraints by creating sharper crack tip profiles. Plate (12) shows the early

development of a fissure ahead of the deforming crack tip in the clean steel. These fissures, grew in strain hardened material, had sharp profiles and grew into the blunted crack tip. The principal stresses formed at the new crack tip would be higher than at the original blunted crack tip. It was shown above that the upper transition region exhibited considerable crack tip plastic deformations. Even at -90^{o}C, which represented lower transition temperatures, Figure (36) showed that the plastic zone still existed and the intensity of strain at 0.58 in the ZTD specimen was still quite considerable. For lower transition temperatures, brittle fracture occurred at the critical fracture stress which did not vary significantly, Figure (52B). At higher temperatures, which were characterised by large plastic deformations and extensive crack tip blunting, the brittle fracture conditions were met by the combination of an increase in the yield stress (by material work hardening) and the increase in constraints (by ductile crack growth). At lower shelf temperatures, the plastic zone size was greatly reduced and the crack tip would be sufficiently sharp to elevate the stresses to the critical fracture level. Figures (24, 25) show that the uniaxial yield strength increase over the range considered was small. However the uniaxial yileld strength cannot realistically be compared to a notched specimen. The presence of a crack, even under plane stress conditions, represented a situation of considerably higher constraints. The significant change in the crack tip blunting, considered above, suggests that the plastic zone was considered to be highly sensitive to small changes in yield stress and, hence, the temperature range of the transition zone.

The ductile to brittle transition was viewed, from the above, to be caused by the dissipation or concentration of stresses at the crack tip due to the size of the plastic zone and not necessarily the level of strain within the plastic zone. The plastic zone was shown to depend not only on the state of stress and, hence, on specimen thickness, but also on material properties, the rate of load application, the presence of free surfaces adjacent to the

crack tip, the presence of inclusions and also on the specimen geometry as will be shown below, in section 5.2.

If the plastic zone size is considered to be the important parameter in the ductile to brittle transition then the brittle, lower toughness shelf cannot be considered to represent a shift to plane strain conditions. The plastic zone size was shown to be dependent not only on through thickness strains (e_z) but also on e_y, by the inclusion of free surfaces in that direction. Below, the plastic zone size will also be shown to depend on e_x.

The size of the plastic zone was shown to be dependent on inclusion content in the through thickness specimen, Figure (36) and Plate (4). As load increased and yielding occurred at the fatigue crack tip, the sulphide inclusions were noted to delaminate at low strains. The resulting sharp form of the void caused considerable stress concentration and plastic strains at the apices. The intervening matrix would shear and the crack front would assume a new position locally. The result would be crack growth at lower loads and hence smaller plastic zone sizes.

Where inclusions lay within the plastic zone, but remote from the fatigue crack tip, the inclusions would debond, show increasing strain at the apices, shear the inter-inclusion matrix and create a sharp new fissure ahead of the crack. Plate (8A) is a polarised light micrograph of two inclusion interacting within a large plastic zone. The edge of the plastic zone is clearly seen in Plates (8A, B). Outside the plastic zone the larger inclusion was already showing debonding. Plates (9, 10, 11, 15) show crack growth caused by the shearing at the inclusion apices. Note also that although strain had increased at the inclusion apices, there was a distinct strain decrease at the sides of the inclusion due to the void opening.

Plate (12) shows the development of fissures ahead of the blunted crack tip in a clean steel specimen in the through thickness direction. Plate (13) shows the development of large cracks ahead

of the crack tip at inclusion clusterings in a moderately dirty steel. These cracks will create favourable out-of-plane extension planes for the crack tip. Finally, the very dirty steel shows large void formation ahead of the crack front, Plate (14). The plastic zone was shown to decrease as one progressed from Plate (12 to 14) and this was shown in Plate (4).

It can be seen from Plates (1, 2) that the controlled rolling operations left a banded structure in the through thickness direction of the two steels. The inclusions of plate S were not considered to be randomly distributed. Rather, they tended to cluster and show a degree of banding. This can be seen in Plates (2, 13). The separation of two inclusion bands was usually about 0.1mm but could have exceeded this and separations of 0.25mm were not unusual. The crack front was shown to follow prominent inclusion bands in Chapter 4. In some cases the fatigue crack tip may have terminated at the end of such an inclusion band. The next nearest inclusion band was likely to be about 0.1mm to either side. The inter-inclusion spacing within the plane was likely to have exceeded this since the steel plates had undergone considerable thinning in the mill which resulted in large inter-inclusion separations. Referring to Figure (36B) it was shown that the ZTS crack tip strain was greatly limited in size at $-90^{o}C$. The value of r_p at this temperature for the ZTS specimen was less than 0.1mm for a strain of 0.26. At such temperatures, therefore, it is possible that the plastic zone may have existed entirely within clean steel matrix but surrounded by dirty steel. Such a situation would give COD values approximating to clean steel properties and may explain the large scatter shown for ZTS specimens at cryogenic temperatures, Figure (30).

5.2. THE EFFECTS OF SPECIMEN GEOMETRY, LOADING ACTION AND TEMPERATURE ON FRACTURE TOUGHNESS TESTING

It was apparent from section 5.1 that the measured toughness was related to the plastic zone size. This suggests that upper shelf toughness would relate to the unbroken ligament in general yielding situations. For ductile structural steels, such as BS 4360 50D, general yielding conditions were shown to prevail for very heavy sections. It was, therefore, necessary to show the geometry and size dependence of the measured toughness. A review of the literature on this subject served to show the depth of disagreement on the geometry related dependence. It was expedient to scrutinize a few published works in depth.

At lower temperatures, corresponding to the transition temperatures, the size and geometry dependence of toughness became more difficult to determine due to the difficulties associated with temperature control. Further difficulties were introduced due to the non-standardisation of the term 'specimen size' since this can mean increases in specimen thicknesses, width and crack length.

The mode of deformation normally suggested in fracture toughness testing was bending. The mode of deformation in engineering structures is usually by a combination of forces. It was, therefore, considered plausable to study the differences between bending and tensile modes of deformation in fracture toughness specimens.

5.2.1. EXPERIMENTAL

Two materials were chosen for experimentation in the chapter, BS 4360 50D steel with low inclusion content, termed steel D. The steel was tested in the LS direction. The other material chosen was plasticine, used for obvious time saving advantages.

Two specimen types were also chosen for investigation. A comparison between tensile and bending load action was made. The three point, single edge notched, bend specimen (SENB) and the single

edge notched specimen loaded in tension by fixed grips (SENT fg) represented the two types.

The SENB specimens were prepared and tested as described in Chapter 4. Clip gauge opening was traced autographically against load. A further series of tests involved SENT specimens, pulled by fixed grips in a tensile mode. For such specimens, load was recorded against time. Here, COD was measured at maximum load by the rubber infiltration technique, in the on-load and off-load conditions. Crack opening was measured at the imprint of the fatigue crack tip using a travelling microscope. All tests were carried out at ambient temperatures.

The plasticine, however, proved a little difficult to use as its sensitivity to temperature was high and it showed negligible work-hardening capacity. Forming the specimens, the plasticine was continually rolled out in a rolling mill until the consistency was assured. The crack was introduced by forcing a fine wire through the material. The specimens were kept at a constant $10^{o}C$ for several hours before testing, to aid in its handling.

Load application for the plasticine specimens was a manual operation and, hence, no recordings could be made. Crack opening could only be measured at the first visible point of ductile tearing. Measurements of COD were again made using the travelling microscope in the 'off-load' condition.

Through thickness strains (e_z) were measured using point micrometers to determine the notch tip contraction. The strain was obtained as a ratio to the original specimen thickness.

5.2.2. RESULTS AND DISCUSSION

5.2.2.1. SITUATIONS OF EXTENSIVE PLASTICITY

High a/W values were presumed to produce a more restrictive geometry; in as much as toughness appeared to decrease with increasing a/W ratio (75, 76, 109). It is this point that was investigated more thoroughly.

Figure (54) shows the decrease of δ_m with increasing a/W ratio for small 10 x 10mm specimens of BS 4360 50D steel. Figure (55), collected from the present research and that of de Castro (203), shows variation of δ_m, δ_u and δ_c with a/W for 18 x 18mm specimens of the same steel; the same trend was followed. Many other researchers found this behaviour and their work will be discussed in greater detail.

In view of the work done so far in this thesis, concerning the proximity of free surfaces to a straining crack tip, an anomaly is apparent. If a free surface in the y-direction was considered to reduce the triaxial stress state by facilitating flow and manifesting itself in terms of increasing δ_m and the shift of the transition to lower temperatures, how then does the proximity of a free surface in the x-direction show itself in terms of increasing constraints and decreasing COD and K?

The reason given by de Castro for the toughness decrease with a/W increase was that the state of triaxiality increased. This view was the only natural conclusion that could be reached by other authors, although only few have been as bold to commit themselves (*75, 76, 109). As a measure of the triaxiality increase, de Castro chose to validate his view by considering two experimentally determined parameters; the limit loads which were supposed to shift from plane stress to plane strain values, with increasing a/W, when compared to theoretical values of the limit load calculated by the slip line field theory of Green and Hundy (207). The scatter observed was too high and no significant conclusions could reasonably be reached. The other parameter chosen was e_z (defined as the notch root contraction divided by specimen thickness) plotted against a/W. This showed a linearly decreasing e_z with increasing a/W.

It was accepted that e_z was directly proportional to COD. This dependence is supported by the present work for 10 and 18mm specimens in Figures (56 and 57). Since COD decreased with a/W increase or temperature decrease, so then did e_z show the same trend. It is, therefore, a foregone conclusion that e_z should

not be taken as a measure of a change in the state of stress any more than should COD. However, if the relationship between the two varies producing higher e_z values for the same COD, then a shift to plane stress could be so defined and vice versa. This is schematically shown in Figure (58).

To do this, values of NRC and COD against temperature were taken from various sources (141, 203, 204) and rearranged to plot e_z against COD for various geometries. The result is shown in Figure (59). This does, indeed, show the trend predicted in the schematic representation of Figure (58).

What was interesting here, was that for any one geometry, there was no change in slope from upper shelf to lower shelf temperatures; again, because e_z was directly equivalent to COD. Hence, e_z cannot be used, as a tool in itself, to show changes in stress state as a/W varies or as temperature decreases for a single specimen geometry.

The toughness variation with a/W should be viewed from a different prospective. The plastic zone size (r_p) had been used in Chapter 4 to explain the influence of free surfaces upon the deforming crack tip region. It was well established that the size of the plastic zone was seen to influence the measured toughness in the stress approach, a plastic zone was viewed as a blunting influence on the crack tip and ρ, the crack tip radius of equation [2.1] was directly applicable. For the strain approach, such as COD, the strain at the crack tip was proportional to the plastic strain in the specimen ligament.

Section 4.2 showed how r_p was related to COD for materials with varying through thickness toughnesses as a result of varying inclusion contents. Above, r_p measurements were shown to reflect the COD transition of the upper and lower temperature shelves. Hence, large r_p reflected high toughnesses at the crack tip.

In fracture toughness testing of engineering materials at their design temperatures, the specimens tested nearly always

deformed under general yielding conditions. The point of non-linearity on a load-displacement trace of COD, J or K_Q testing represented a point of extensive plasticity. The initiation of ductile tearing at the crack tip was well within the general yielding regime, where plasticity penetrated the unbroken ligament to the far surface. Hence, the relationship between (W - a) and δ becomes a logical one.

For any given set of parameters such as material, specimen thickness (B), temperature, method of loading and rate of load application, there exists a representative plastic zone size, at the critical value, termed, r_c^*. This r_c^* can easily be altered in various ways in laboratory testing of materials. This was done by geometrical changes, addition of side grooves, free surfaces etc. The point of the exercise was to achieve a higher crack tip constraint and hence, a more conservative fracture toughness characterisation. Of interest here is the specimen geometry, specifically, changes of W and (a).

It is important to stress the point made in the above paragraph referring to a representative plastic zone size r_c^*. The inference there is that there exists, in a sufficiently large plate under critical conditions, a representative plastic zone size at a critical value which can be very large for ductile materials. Where (W - a) is very large, this r_c^* is fully accomodated. Where a/W values approach unity, the resulting small unbroken ligament will limit the full capacity of the plastic zone size. The result is to limit the strain at the crack tip and hence, the toughness measured.

The plastic zone is not a homogeneously strained region. Microhardness techniques were used to measure the plastic zone for samples taken at midsection of specimens loaded to the first attainment of maximum load. Figures (49, 51) show that the plastic zone consists of a highly strained region adjacent to the crack tip with the strain falling rapidly away from the crack. That is, most of the strain contributing to crack opening takes place in a

small proportion of the volume of the plastic zone.

The above, views the problem in terms of uncracked ligament length, (W - a). For upper shelf temperatures, high a/W ratios resulted in small (W - a) and low toughness values due to smaller volume of material available to deform and vice versa. Upper shelf temperatures were quoted because the plastic zone size was known to be large and fully penetrated the ligament.

For the full range of tests on BS 4360 50D steel, the relationship between COD and a/W was seen to increase with absolute value of ligament length, as presented in Figures (54, 55). This suggested that r_c^* was always larger than the (W - a) ligament.

As a measure of the plastic zone size, using equation [2.25] for plane stress:

$$r_p = (1 / (2\pi)) (K / \sigma_Y)^2 \qquad ....5.3$$

substituting equation [2.18] to obtain an equation in terms of G:

$$r_p = (1/(2\pi)) (E G)/(\sigma_Y)^2 \qquad ....5.4$$

since G = J where $J = m \sigma_Y$ from equation [2.58], and m varies from 1.0 to 3.0 one can assume an average of m = 2, thus:

$$r_p = (E \delta)/(\pi \sigma_Y) \qquad ....5.5$$

Let σ_Y = 260 MN/m^2 and E = 210,000 MN/m^2, thus for a material where δ_i = 0.3mm

r_p = 77mm

This empirical analysis gives an approximate expression to the large plastic zone size associated with the initiation COD values of a 10 x 10mm specimen, obtained for this ductile steel at upper shelf temperatures. The available results were conducted on specimens with (W - a) values very much smaller than the 77mm required from the above expression. It is therefore, foreseen that the toughness will continue to increase with (W - a) for B = 10mm

specimens.

The above argument leads to the assumption that where the ligament exceeds the predicted critical plastic zone size, the toughness values measured will become independent of further increases in (W - a).

It is interesting here to turn to the ASTM test for plane strain fracture toughness of metallic materials, E399-74, where the (W - a) was also studied in terms of reproduction of results. The conclusion was that the ligament should exceed a critical size:

$$(W - a) > (W - a)_c = 2.5\ (K_Q/\sigma_Y)^2 \qquad \ldots.5.6$$

This view was also reported by Munz (208) in ASTM STP 668, again on the subject of LEFM testing. It naturally follows that if (W - a) was being defined to a specific minimum value, then it must imply that the larger (W - a) values represented a condition necessary for plane strain testing. In all cases, as (W - a) decreased, K_Q was also seen to decrease.

Tests were performed to establish the validity of the (W - a) effect on toughness. Initially δ_m was measured for 10 x 10mm specimens for various crack lengths, results shown in Table (27) and Figure (53). For comparison, de Castro's 18mm results were considered and plotted in Figure (54) along with the 10mm results. For greater variability, 18 x 8.2mm specimens were tested and the results given in Table (28).

Figure (60) represents the behaviour of three specimen sizes of the same thickness (B) and a/W ratio, only the absolute value of W and hence (W - a) varied. In all cases B = 18mm and a/W = 0.5. To eliminate a lot of the ductile crack growth effects, δ_u was measured in a range of $-77^{\circ} \pm 3^{\circ}C$. The specimens were fully ductile at these temperatures. The figure clearly shows that the larger the absolute value of (W - a), the higher the measured δ_u. Thus, suggesting that the uncracked ligament was more significant a parameter than the a/W ratio.

The increase of (W - a), even for a constant a/W ratio, increased the volume of material available for deformation. The temperature used for the test at -77^{o}C represented upper transition temperatures where, although incorporating a general yielding environment, the amount of ductile cracking prior to fracture was limited. Thus, although the δ_R curves would be different for varying specimen width, the amount of the difference would be limited by the temperature and would not account for the significant variation in δ_u.

To find the full effect of specimen width, and specifically the effect of (W - a) on toughness, would involve very expensive and time consuming testing. Furthermore, the results would be valid for one specimen type, that is, the SENB. It is known that the many types of test specimens available behave differently as the loading action varies in a range from essentially tension in centre cracked (CC) to bending in SENB specimens. The bend specimens which include SENB and CTS specimens, involve rotation around a hinge point situation in the (W - a) ligament, the position of which varies and necessarily affects the measured toughness. Haig and Richards (209) gave an account of the various specimens available.

To ensure that extreme loading conditions were met, the best choice would be centre cracked (CC) and single edge notched bend (SENB) specimens. However, the choice of CC specimens in this test program would have involved very great loads for testing. Consequently, a special design of specimen was used to include an essentially tensile mode of deformation. This took the form of single edge notched tensile specimens with the ends held by fixed, crocodile-jaw grips, which did not allow rotation of the specimen, here termed SENT fg. The deformation is as in CC specimens but requires only half the load. The toughness was measured as crack opening displacement at first attainment of maximum load. The silica gel replica method (58), taken on-load and off-load, was used to measure the crack openings.

The room temperature COD results for steel specimens of 18 x 8.2mm geometry with varying a/W values were made in two sets of identical specimens. The first set was loaded to maximum load in three point bending and the COD measured by using both a clip-gauge for crack mouth opening and also the off-load rubber infiltration techniques. These results were compared to the second set of tests in SENT fixed grip mode, measured at maximum load by rubber infiltration on-load and off-load.

The results are tabulated and shown graphically in Table (28) and Figure (61A, B). It was seen that off-load measurements were slightly lower than on-load COD values, as noted in Chapter 2. It was evident from the results that δ_m increased with (W - a). It was also evident that the specimens in tension showed higher toughness values at maximum load than their SENB equivalents. This was associated with the very much larger plastic zones that developed in SENT fg specimens as shown in Plate (16). Furthermore, there was a contribution of strain from the free surface in x-direction as a result of the lack of compressive strains caused by bending within the ligament.

This supports the discussion above which related the toughness measured directly to the amount of material plastically deformed. With the SENB specimens, the plastic zone was limited to a near-cylindrical shaped region within the unbroken ligament but with SENT fg specimens, the plasticity extended considerably in the y-direction. In the x-direction the mode of strain changed, leading to higher crack tip strains. Thus, the SENB specimens showed more restrictive behaviour than SENT fg specimens which led to more conservative results being obtained with laboratory specimens loaded in bending.

For very short (W - a) lengths, the tensile specimens show an unusual reversal in the COD trend. From Figure (61A) it is evident that the δ_m trend shows a reversal and increases as a/W approaches unity. This was associated with high strains in the x-direction which more than compensated for the reduction of (W - a).

With bend specimens the crack tip strains, measured as a COD, were strains mainly in the y-direction. From constant volume considerations, these strains were equal to half the total strains in the x and z-directions. In the SENB specimens, there existed the hinge position (H) ahead of the crack around which rotation was considered to occur, calculated by Green and Hundy (207) as:

$$H/W = 0.55\ (1 - a/W) \qquad \ldots.5.7a$$

for $a/W \geq 0.295$

but probably would make more physical sense if expressed as:

$$H = 0.55\ (W - a) \qquad \ldots.5.7b$$

The important point to be observed was that roughly half the volume of material ahead of the crack flowed under tensile loadings to areas of greatest strain. Beyond the hinge, the material was under compressive loading and tended to expand laterally away from the crack tip. The measure of this lateral expansion was related to the fracture processes at the crack tip and was used as a measure of toughness in Charpy impact testing. Since the material in the ligament of a ductile material, under general yielding conditions, flowed in opposing directions about the hinge, the hinge may be considered to act as a barrier to flow of material to the crack tip in the x-direction.

In bend specimens, the proximity of the free surface in the x-direction did not facilitate flow of material because of the physical barrier set up by the bending action. The stress, σ_x, did not tend to zero with proximity of the surface, whereas σ_y did tend to zero as the holes drilled in the y-direction approach the crack tip.

In the tensile specimens, the centre of rotation was removed and flow in the x-direction was very apparent, as can be seen in Plates (16, 17). This contributed to the strain at the crack tip, thus, increasing the measured COD for very short ligament lengths. In this case, the free surface in the x-direction did act as a free

surface and suppressed the stresses in the x-direction.

To obtain a more complete understanding of the effect of geometry on COD, the plasticine specimens were rolled out to a single thickness, B, of 12mm with various values of W and a/W. Bend and tensile results are given in Table (29). The COD results were plotted against (W - a) irrespective of W and (a) in Figure (62A, B, C). It is evident that three regions exist for the SENT fg specimens.

(i) For very large (W - a) ligaments, in excess of the size of r_c* (measured for this thickness at 22mm) the COD was stabilized at 3.1 $\pm$ 0.3mm. This was the expected behaviour and was in agreement with the plane strain toughness testing recommendations, equation [5.6]. This region was not observed for steel specimens in Figure (61) as the (W - a) was of insufficient size.

(ii) An intermediate region where the plastic zone size was limited by (W - a). In SENT fg specimens the x-direction strain was not significant due to the relatively large (W - a). This region also found for SENB specimens and the toughness decreased with decreasing (W - a) in a linear manner for both sets. This was also shown in steel specimens of Figure (61A, B).

(iii) The end region for very small (W - a) where the effect of e_x tended to increase the strain at the crack tip. This region showed greatest scatter due to the difficulties in applying very small loads and in identifying the point of ductile cracking. This region was not noticed for SENB specimens. Figure (61A, B) shows the beginning of such a zone (dashed lines) for steels of SENT fg specimens.

In general, SENT fg specimens showed overall higher COD

values in both steel and plasticine specimens, for reasons discussed earlier relating the effects of e_x and larger plastic zone proportions under tensile loading. In steel specimens, the (W - a) ligament never exceeded the plastic zone size and hence, no levelling out of the curve was observed. The worked example of equation [5.5] showed r_p^* to be 77mm, far in excess of experimental (W - a).

Since many papers published on this subject have tended to treat the measured toughness dependence on geometry in terms of, primarily, a/W ratios but also crack length (a) and, to a lesser extent, specimen width (W), it would seem practical to re-analyse their work in terms of the present hypothesis.

A very useful set of experimental results were published by Bradshaw and Wheeler (210). The work considered resistance curves of K for four aluminium alloys, two of which exhibited very tough characteristics. Fortunately, their work used similar specimen constraints as used in this work, that is, centre notched (CC) and compact tension (CTS) geometries. These compared tensile to bending loading actions respectively. Various specimen widths and crack lengths were employed. The results were originally interpreted in terms of K dependence on specimen width and to a lesser extent to crack length. It is useful and surprising that the authors also considered the plastic zone size in terms of resistance to crack growth. Their opinions can be summarised by their own figure represented here as Figure (63).

Replotting their results in terms of (W - a) one obtains the very distinctive behaviour, seen in Figure (64). This figure ignores results for the very smallest crack length of the CC specimens for the two ductile alloys since the plasticity would not have been contained by crack lengths of 13mm.

The toughness for both CC and CTS specimens, for all alloys, increased with increasing (W - a) until a critical ligament, r_c^*, length was reached, at which the toughness stabilised. This $(W - a)_c$ was smaller, the less ductile the alloy. Thus,

Bradshaw's work supports the hypothesis which distinguishes the (W - a) as the important variable, contrary to his conclusions. Furthermore, it covered a sufficiently large range of (W - a) in the CC specimens to distinguish the intermediate range (of increasing toughness dependence with increasing (W - a) and the range in which the ligament exceeded $(W - a)_c$ (where the toughness was independent of ligament length).

Although Bradshaw's work did show that the highest K values measured were for the CC specimens, this was not found to be the trend over the intermediate range for all specimens. K was calculated for the two specimens by different techniques which could have accounted for the inability to correlate the results directly.

The range of ligament lengths tested in CC specimens did not cover very small (W - a) values, where the effect of e_x would have been noticeable and caused a reversal in the toughness trend. The smallest ligament tested in CC specimens was 64mm, hence, for a sheet thickness of 1.6mm and maximum plastic zone size measured at 150mm, it would not have been expected for any straining in the x-direction to influence the toughness significantly. The 64mm ligament would be characteristic of the intermediate range, (ii) above, and this is clearly shown in Figure (64).

The plastic zone sizes were experimentally determined by Bradshaw and are included in Figure (64). It was seen that the plastic zone ranged in size from 20 to 150mm in radius. The method of plastic zone size determination used by Bradshaw, was the difference between the compliance and optical crack extensions and not a direct measurement of the plastic zone size. It was shown from their work that $(W - a)_c$ increased as r_p^* increased for different materials. For the two ductile materials $(W - a)_c$ was roughly 175mm and the corresponding r_p^* was approximately 150mm. For the two less ductile alloys $(W - a)_c$ was between 40 to 60mm and r_p^* was approximately 21mm.

Kaufman et al (211) studied the specimen size effect on toughness in an aluminium alloy at ambient temperatures. Maximum load and 5% offset secant stress intensity values, K_m and K_Q respectively, were calculated from CTS specimens. Both specimen thickness and width were varied in their work but a/W remained constant. Most of the work was in the plane stress regime and only three results satisfied the $P_m/P_Q \leq 1.1$ criterion for plane strain (ASTM STP 559, page 79, erred in presenting the criterion as being satisfied when it exceeded 1.1).

Kaufman et al concentrated on the idea that K_Q and K_m increased with increasing (a). This is a surprising view to hold, since most workers appear to accept the reverse.

From Kaufman's work, Figure (65) shows how K_Q increases with (a) and Figure (66) shows the independence of K_Q on B. It was the evidence of these plots that led Kaufman et al to make their conclusions. Figures (67, 68) show the behaviour of K_m with (a) and B.

One would expect the fracture toughness parameter, K_c, to decrease with increasing B until plane strain conditions were reached; although previous indications of a constancy in K_c with thickness increases was previously noted in several materials by Sullivan et al (212) to support Kaufman's results in Figure (66).

It is apparent that if the thickness, B, were to increase while keeping a constant geometry, the measured toughness would tend to increase as a consequence of the (W - a) increase. To study the effect of an increasing thickness, the ligament must remain constant in size. Although most workers tend to ignore this, Kaufman supplied enough data to establish K_Q and K_m dependence on B. Kaufman's results showed that K_Q was constant for increasing B but K_m decreased with increasing B, Figures (66, 68). This was probably due to the decrease of stable crack growth tolerated as the stored energy increased with specimen size.

From Kaufman's results, it was shown conclusively that upper shelf a/W values did not determine the toughness. For all thickness of 12, 25, 37 and 51mm the K_Q and K_m values (measured at a constant a/W ratio of 0.5) increased with increasing ligament lengths. Figures (65, 67) show the increase of K_Q and K_m respectively, with increasing (W - a). $(W - a)_c$ was reached for K_Q at about 2 inches.

Kaufman's only reason for choosing the crack length as being the important variable in their tests was because of an unfortunate choice of a/W = 0.5 where crack length was always equal to the ligament length. Had they chosen an additional ratio or series of ratios, they would have established the importance of (W - a) for upper shelf behaviour.

Nevertheless, Kaufman's results, when reanalysed in terms of (W - a), prove useful to this thesis in three aspects:

(i) They clearly demonstrate, as ineffectual, the variable a/W at upper shelf temperatures.

(ii) That, given the standard fracture specimen of W = 2B = 2a, an increase in size of such specimen will affect the measured toughness because both B and (W - a) have increased.

(iii) They support the existence of $(W - a)_c$ for both the K_Q and K_m measurements.

May et al (213) have documented extensive work on the effect of specimen geometry on toughness of various steels. They held that δ_i, δ_m, J_i and J_m increased with specimen size and in particular with increasing B. They also found that δ_i decreased with increasing crack length.

Taking, initially, the increase of toughness measured against thickness, it is apparent that they measured P_Q and δ_i as a function of increasing specimen size. That is, they considered specimens with increasing B when totally neglecting the consequent increase of (W - a). This oversight led May et al to

conclude that δ_i increased linearly with B.

What of the actual relationship between toughness and B? As May et al made no attempt to study the effect of varying B with constant (W - a) on toughness, it was difficult to establish. However, because of the sheer number of tests conducted by May et al it was possible to collect such results for two batches of steel. δ_i values were given in most cases and P_Q values were converted to K_Q by the use of:

$$K_Q = Y P_Q / B W^{\frac{1}{2}}$$

for their CTS specimens. The results are given in Table (30) and are plotted against B in Figure (69). These results show a high degree of scatter and not the linear increase portrayed in Figure (70) for K_Q dependence on increasing B. These results lend support to Kaufman's view that increasing B did not significantly affect the measured toughness.

May et al also considered the decrease of δ_i and δ_m with increasing crack length (a). Again, May et al overlooked the fact that for those particular specimens considered, a/W = 0.5. This obliges them to differentiate between COD dependence on (a) and on (W - a).

To view this problem realistically, it was decided to use their results to test the validity of (a) as a controlling parameter. Fortunately, steel 5 of their classification (a pipeline steel) was tested at various values of W and (a) with B limited to 12.5mm in all cases. The results were plotted in three forms: as δ_i vs(a), δ_i vs a/W and δ_i vs (W - a), see Figure (71A, B, C). It is quite conclusive that, allowing for scatter, only δ_i vs (W - a) shows any trend at all. This again supports the author's own work and shows a linearly increasing relationship.

It was shown above, that the plastic zone size depended on (W - a) for upper shelf temperatures. The plastic zone increased

in size until a critical value of $(W - a)_c$ was reached. Above $(W - a)_c$, the plastic zone and hence, the measured toughness would be independent of ligament length. It was also shown that as the ligament length became very small, the specimens loaded in pure tension would reflect the increased strains from an adjacently situated free surface.

5.2.2.2. SITUATIONS OF LIMITED PLASTICITY

The plastic zone size had already been shown to be sensitive to many material and experimental variables. In fracture toughness testing, the most commonly used variable was that of r_p dependence on temperature. Laboratory specimens of ductile engineering materials exhibited plastic zone sizes greatly in excess of the unbroken ligament, $(W - a)$. For the BS 4360 50D used, the critical plastic zone size and, hence, $(W - a)_c$ was calculated at 77mm. Generally, for the lower transition region, the plastic zone can be shown to be measurably smaller in size. At such low temperatures, the zone was seen to be contained within the $(W - a)$ ligament, as shown in Figure (36A, B).

The δ_m values contain a measure of ductile crack growth which will be shown to be very dependent on the specimen size, geometry, stiffness of the system and the testing temperature. These variables determine the amount of stored elastic energy and, hence, the amount of ductile cracking tolerated and will be discussed in greater detail below.

Assuming that, for a given specimen thickness and transition temperature, there existed a contained plastic zone within the $(W - a)$ ligament then it is likely that an increase in the size of $(W - a)$ would create an equivalent increase in the stored elastic energy of the system. The increased stored energies would result in a reduction of the amount of ductile crack growth tolerated prior to catastrophic failure. The effect of this on the transition curve has not been fully determined. However, it can be shown that for small increases in stored energy resulting from increased compliance of the system or increased size of $(W - a)$ in small

scale laboratory specimens would reduce the amount of ductile tearing prior to fast fracture and results in a steeper transition curve. Figure (31) by Kamath et al (41) shows the effect of specimen size increase on producing sharper transition curves. This was due to an increase in stored energy brought about by an equivalent increase in both B and (W - a). Figure (68) also shows the reduction of K_m as the specimen size and stored energy increased.

The effect of stored energy on statically loaded, precracked, fracture toughness specimens has not been fully determined experimentally over the transition zone. Studies were conducted with small changes in (W - a) over the transition region (56, 203, 215) and these results showed small changes in the shape of transition curve. What was not conclusively shown was whether the transition temperature shifted to significantly higher temperatures with significant changes in (W - a) and, hence, the stored energy of the system. The question asked is whether the initiation of ductile cracking is affected by the stored energy of the system. This question is relevant since if initiation is seen to be affected by the stored energy then the laboratory measured transition temperature of statically loaded, precracked specimens, can be of no relevant industrial applicability.

Whilst considering the transition temperature effects of increasing stored energy brought about by increasing (W - a) one should not ignore the possible effects caused by changing (a) and (a/W).

Dawes (56) and de Castro (203) suggested that a/W ratios were significant in predicting a transition temperature shift. Both authors considered that there was a shift to plane strain conditions as the a/W increased. The results from de Castro contained excessive scatter to be able to make any such observation. The evidence given by Dawes to support his hypothesis was, arguably, inconsistent. Initial observations revealed that his choice of a/W of 0.2 was unfortunate for a ductile BS 4360 50C steel. It was shown above how ratios less than 0.23 would be

insufficient to limit plasticity to the uncracked ligament, at least for higher temperatures. It was also apparent that his maximum load values, representative of upper shelf behaviour, did not reflect the ligament length. Yet all other works considered here provide irrefutable evidence of the dependence of upper shelf general yielding toughness measurements on the ligament length. Again, there is good argument to suggest that his two a/W = 0.5 geometries of Figure (72) should not be represented by one curve but two. That is, the wider specimen showed a greater number of results lying towards higher temperatures. Finally, Figure (73) for machine notched specimen toughness values clearly showed that transformation shifted to higher temperatures as crack length and (W - a) increased. The mere increase of notch root radius cannot, in itself, account for this anomaly. Hence, it can be assumed from Dawes' own work that a transformation shift to higher temperatures is more likely to be associated with an increase in crack length (a) or (W - a) than with an increase in the a/W ratio.

The work of Chell and Gates (214) and Chell and Davidson (72) were conducted on high temperature, high strength low alloy steels within the transition temperature range. Both works showed a measured toughness increase with decrease in crack length. However, it may be considered that their study was more indicative of upper transition temperatures and considerable crack tip plasticities.

More recently, Milne and Curry (215) have conducted a series of experiments on BS 1501-271 steel to show the transition dependence on specimen size. From their experiments investigating the crack length, no noteworthy conclusion could be made concerning the transition temperature dependence. At higher temperatures, the measured toughness could be shown to depend on the (W - a) ligament. There was evidence, from their results, that specimens with larger W and (a) suggested a transformation at higher temperatures. The larger specimen was twice the width of the smaller and was of smaller a/W ratio. Nevertheless, their results showed much scatter and no firm conclusion can be made.

From de Castro (203), a significant number of BS 4360 50D, 18 x 18mm specimens were tested in the transition temperature region. There was also a wide range of a/W ratios tested. The results were used in an attempt show a shift to plane strain conditions with high a/W ratios, by plotting COD against a/W at -10, -80, -90 and -100^{o}C, Figure (55). These results are replotted as COD against temperature for different a/W ratios, in Figure (75). It is clear from this figure that large (W - a) ligaments showed a sharper ductile to brittle transformation. Such behaviour adds support to work conducted on stored energy (Section 5.3). Larger specimens require higher loads for fracture and as the crack starts to grow, the high stored energy will drive the crack to fast fracture. Thus, the transition fracture of large specimens will not tolerate large amounts of ductile cracking. Figure (75) also suggests that the transformation temperature shifted to the right as (W - a) was increased. However, the scatter is high and a larger variation in (W - a) would be required to support such a phenomenon. Nevertheless, it can be said that in the transition region, the plastic zone is observed to reduce in size with temperature drop. Hence, if the ligament is small, the plastic zone will hit the end of the specimen. Alternatively, a large (W - a) would result in the plastic zone surrounded by elastically loaded material. Not only does the latter case store more energy to be released on crack initiation, it may even prove to be a situation of higher constraint.

Milne and Curry's experiments on B were of more value. Such tests were conducted on a range of B = 20 to 75mm. The important point was that the (W - a) ligament was kept constant at 48mm. Their results showed no difference in toughness for increasing B over both upper shelf and transition regions. However, they did go on to say that crack tip ductilities did decrease with increasing thickness. The relative unimportance of increasing B on measured toughness was also noted previously from Kaufmann's work (211). Figure (74) also adds support to this observation. Here, 10mm and 18mm thick BS 4360 50D specimens with equal (W - a) were shown to have similar upper-shelf values. Similarly,

Figure (54) shows a greater range where (W - a) and COD are equal for B = 10mm and 18mm specimens. Over the transition range, Figure (74) suggests that, although overlapping, the 18mm specimens did show a slight shift to higher temperatures.

It is apparent that most of the works reviewed showed a transition temperature dependence on specimen size and, hence, on stored energies. There have been exceptions, but in such cases the scatter was large. The work presented by Dawes can be re-interpreted to show a toughness dependence on (W - a) at low temperatures. Chell and Gates (214), Chell and Davidson (72) and Milne and Curry (215) gave some support to the significance of ligament length. It should be remembered that most of the works were conducted on small increases in specimen widths and showed a correspingly small shift in transition temperature. From the available work it was not possible to confidently predict a significant change in transition temperature with (W - a) increase. Hence, from the work reviewed, it was considered that the (W - a) increase resulted in increased stored energy in the system which reduced the amount of crack growth that occurred prior to fast fracture in the transition region. As a result a steeper transition was observed which resulted in a shift in the transition to higher temperatures.

5.3. STORED ENERGY AND WELDED STRUCTURES

Throughout the discussions above, the effect of (W - a) on the measured toughness was said to exist at upper shelf temperatures where high ductility was exhibited at the crack tip. As the ligament length increased so did the stored energy of the system. The stored energy of a system can be increased by other means, such as by increasing the compliance of the system and by increasing the rate of load application and by reducing temperature.

Research by Spurrier et al (216) on the stored energy of a system was conducted on large tensile specimens of BS 4360 50B steel. The 50 x 12.5mm specimens were tested at various temperatures and the fracture appearance transition temperature (FATT) and reduction of area (%RA) was determined against temperatures Plate (18). The procedure was repeated with a 10mm weld bead deposited on the plate, longitudinally. The weld deposit was of high strength, brittle, hard-facing metal. It was determined that a considerable shift in the transition temperature resulted, as well as a reduction of upper shelf ductilities. Further tests by the author were conducted on 20mm and 50mm wide plate with a deposit of rutile weld rods on chilled plates that were either quenched immediately after welding or allowed to cool in air.

The effect of chilling the plate to $-30^{o}C$ and quenching the weld resulted in a well defined, brittle HAZ as seen in Figure (76). The effect of the brittle weld and HAZ was to shift the transition temperature further into higher temperatures and to reduce the upper shelf ductility. The ductile weld bead HAZ was not shown to have such dramatic effects. The results are given in Figure (77).

The introduction of a brittle weld/HAZ resulted in an increase in load bearing capacity of the tensile specimen by virtue of increasing the cross-sectional area. The weld acted as a crack initiator or crack equivalent. At upper shelf temperatures the weld fractured at loads above the yield load of the parent metal. The crack was arrested by the ductile parent material and stable

growth continued until failure. This cracking resulted in a decrease of the overall ductility of the specimen. Several cracks appeared at upper shelf temperatures, since the initial cracks stabilised before maximum load was reached, thus facilitating initiations of other cracks along the weld.

At lower temperatures the weld's yield strength was increased, failing at higher loads in an unstable manner. This led to a sudden release of energy which, due to colder temperatures, occurred at higher loads. If this energy release was sufficient enough, it would continue the crack growth through the parent plate in a catastrophic manner, leading to a drastic decrease in ductility (measured as %RA).

The stored energy of the system was not associated with the weld bead as such but with the much larger volume of parent plate, since the smaller specimens (W = 20mm) did not lead to a significant shift in transition temperature when weld beads were deposited, quenched and tested.

The importance of the brittle weld bead or HAZ Figure (76), lay in its ability to introduce a dynamic crack suddenly and at high loads. It was shown above that a static crack did not lead to a comparable shift in transition temperature. The dynamic crack must, therefore, have affected the yielding conditions, locally at the crack tip, in a manner similar to impact testing conditions. This resulted in a very significant shift of the transition to higher temperatures, Figure (77).

It must be stressed that bad welding practices can lead to an embrittled HAZ by a fast run of small gauge welding electrode on thick plate in cold conditions. These conditions are met in welding large structures outdoors in cold weather. The large heat sink will cause rapid cooling and an embrittled HAZ. In such cases, fracture toughness results from standard specimens will not predict the transition temperature of badly welded structures.

In high temperature applications a group of Cr-Mo-V steels

have been used for their good creep resistance properties. These steels are usually welded with a high pre-heat temperature. Failure to do so usually resulted in a martensitic structure. Again, this could lead to brittle fracture conditions being observed well above the transition temperature of the parent plate.

5.4. CRACK LENGTH CONSIDERATIONS

It was noted that K_Q, COD and J varied significantly at upper shelf temperatures when a/W and B were kept constant whilst varying W. It appeared that the measured toughness depended on (W - a) rather than thc absolute value of (a) at these temperatures.

It is normal to specify a minimum a/W ratio in GYFM which served to limit plasticity to the unbroken ligament. Knott (117), using slip line field theory found an a/W ratio in excess of 0.3, necessary to contain plasticity. Generally, a/W values are quoted as 0.3 or 0.5, for normal SENB specimens.

As testing temperatures decreased and transition temperatures encountered, the plastic zone sizes, measured by microhardness studies of Figure (49), became very small. It must naturally be assumed that the necessary crack length to contain plasticity also decreased. A single value in terms of an a/W ratio for all materials, irrespective of the material toughness and the temperature, is not valid. It would be safe to assume that an a/W ratio of 0.1 or much less would be sufficient for glass, very high strength steel, or even tough steels at temperatures characteristic of the lower temperature toughness shelf.

Thus, a valid description of crack length sufficient to contain plasticity within the ligament would be to describe it in terms of the plastic zone size. From the tests conducted in this programme on 10 x 10mm and 18 x 18mm specimens, the plastic zone at upper shelf temperatures was considered to affect the entire unbroken ligament. Since the plasticity was found to escape to the upper surface of the specimen at 2.3mm and 4mm for 10 x 10mm and 18 x 18mm specimens respectively, it can be said that the minimum crack length to contain plasticity is roughly a quarter the unbroken ligament, where general yielding is applicable.

Where the plastic zone size is smaller than the ligament length due to cryogenic temperatures or the use of brittle materials, the crack size necessary for containing plasticity

would be a function of the plastic zone size rather than the ligament length. Following from the discussion above, it was suggested that the crack length should be not less than a quarter the diameter of the plastic zone.

From Chell and Davidson (72), working on the effect of small crack lengths on K_{IJ} testing of Durchete 1055 bainitic 1% Cr Mo V alloy, it was given that σ_Y was 565 MN/m^2. For standard specimens with large cracks, K_{IJ} was measured at 100 $MN/m^{3/2}$ as an upper value approximation of the scatter. From equation (5.8) for plane stress,

$$r_p = 1 / (2\pi) \quad (K_{IC}/\sigma_Y)^2$$

$$r_p = 5mm$$

From their work, Chell and Davidson found that the measured toughness increased with crack lengths smaller than 7mm. This minimum size of crack length was considered necessary to contain plasticity and is within the range of the calculated plastic zone size. The calculated value of (a) necessary for plane strain toughness testing (19, 20) greatly exceeds this.

Elsander et al, working on the same material (218) found that K_{IJ} increased with cracks smaller than 4mm. From their work K_{IJ} was 70 $MN/m^{3/2}$ for large crack lengths and r_p is calculated at 2.4mm. Again some correlation between calculated r_p and the measured crack length does exist.

Both the above examples show that by limiting the crack length as a function of plastic zone size as a method of containing plasticity to the ligament does prove useful. However, the calculated values of the crack length necessary to contain plasticity were found to exceed those predicted from their associated plastic zone sizes.

5.5. SUMMARY OF DISCUSSIONS ON THE EFFECT OF THE PLASTIC ZONE SIZE

The work in this chapter has concentrated on studying the plastic zone size dependencies on temperature, specimen geometry, material and testing materials. The behaviour of the plastic zone in relationship to its geometric surroundings and the flow within the plastic zone has given a better understanding of the behaviour of ductile materials.

At upper shelf temperatures, the behaviour of ductile engineering materials, as small sized laboratory specimens, showed a marked dependence of the measured fracture toughness parameter on the plastic zone size. Under general yielding conditions this was shown to depend linearly on (W - a), Figures (60, 61, 62, 64, 65, 71C). It was suggested that for a given thickness, the material would show a characteristic plastic zone size r_c^*. For the toughness to be independent of specimen geometry, (W - a) should exceed r_c^*, as shown in Figures (62A, 64, 65).

For δ_m and δ_u measurements, there existed a measure of ductile crack growth. These toughness measurements showed a dependence on the stored energy of the system and, hence, on specimen size. The effect of increasing the specimen ligament caused a shift in the transition to higher temperatures by exhibiting a steeper transition zone. Whether the stored energy would influence the initiation results was not fully ascertained, although Figures (72, 73, 75) suggest that this could be a possibility.

The increase of specimen thickness was shown from the present work, Figure (74), and that of other workers such as Kaufmann, Figure (66) and Milne and Curry (215) not to affect the upper shelf values. However, Figure (74) did show a shift to a higher transition temperature with increasing thickness. It is important here to show the effect of specimen thickness independently of width, unlike that shown in Figure (31) where specimen thickness, width and crack length were all seen to vary.

Generally yielded specimens loaded under a bending moment showed greater restrictions to material flow than specimens loaded in pure tension. It was found that the free surface in the x-direction contributed to material flow under tensile conditions. Under bending conditions the free surface was in compression and did not contribute to the crack tip flow processes. It was, therefore, shown that free surfaces within the plastic zone would contribute to crack tip ductilities whether placed in the x, y or z-directions, Figures (62A, 37, 44) respectively. Thus, it was concluded that through thickness cracks lying adjacent to the surface would be less dangerous than at the plate centre.

Critical fracture stresses at the crack tip would be achieved when the temperature was sufficiently low to increase σ_Y or where the crack tip conditions were sufficiently severe to create stress triaxiality to a degree sufficient to elevate the maximum stresses above the critical conditions. In both cases the plastic zone size would be of very small size. The crack tip would not deform and blunt and hence, a higher stresses concentration would be achieved. Ductile materials at upper shelf temperatures suffered crack blunting, Plate (12) and dissipation of stresses. After sufficient strain in the specimen, small cracks appeared ahead of the crack tip which, due to the high work hardening in the plastic zone adjacent to the crack tip, had sharper apices. These continued to grow in a ductile manner until either the crack tunnelling caused enough constraint for fast fracture or the ligament suffered plastic collapse.

Brittle fracture at upper transition temperatures showed decreasing amounts of ductile cracking necessary to elevate the stresses to critical levels. At lower transition temperatures the microhardness measurements showed much reduced plastic zone sizes, Figures (36, 49), but the actual strain level was not significantly reduced. If sufficiently small gauge lengths were assumed at the crack tip, the strain to fracture would not be shown to alter significantly over the transition region. It was the volume of material within the plastic zone that diminished that was the more

significant factor for the transition.

The measured through thickness strain, e_z, was found to be directly related to COD, Figures (56, 57, 58, 59). The e_z studies were only considered to reflect a change in the state of stress when it was shown that there was significant variation from the strain in the y-direction. Figures (58, 59) plotted e_z against COD for various specimen sizes and at various temperatures. From these it was shown that a shift towards plane strain was observed by increasing specimen size (B, W and a) but no variation in the e_z - COD dependence was observed as transition temperatures and brittle fractures were encountered. It was, therefore, suggested that the transition temperature reflected only the crack tip processes in terms of the plastic zone size and the amount of ductile cracking involved rather than a shift towards plane strain conditions, Figure (36).

5.6. CONCLUSIONS

1. Ductile engineering materials at upper shelf temperatures showed large plastic zones upon general yielding. The plastic zones consisted of small highly strained regions at the crack tip which extended along the planes of maximum shear. Strains up to 0.78 were registered during ductile fracture and up to 0.58 at brittle fracture conditions Figure (36A, B). The extensive plastic zone extended throughout the uncracked ligament and registered a much lower strain which decreased rapidly with distance from the crack tip, Figures (49).

2. For generally yielded ductile materials, upper shelf toughness measurements related directly to (W - a) and, hence, the plastic zone size. To obtain geometry independent toughness values, (W - a) should exceed the characteristic plastic zone size (r_c*) for the given thickness and temperature.

3. In the absence of inclusions, the crack tip blunting resulted in the dissipation of maximum stresses. Critical stresses for fracture could not be achieved and excessive loading led to strain hardening and new crack formation ahead of the fatigue crack tip. The new crack had sharp apices and grew ahead of the fatigue crack tip, which it then extended into. The extended crack tip achieved higher constraints due to sharper profile and the effect of tunnelling, Plate (12).

4. Where MnS inclusions existed in through thickness specimens, sharp cracks formed at inclusions at very low strains. The extensive plastic zone and highly strained region were reduced in size but the maximum strains achieved at the crack tip were not significantly affected. The reduction in r_p due to the ease of crack growth into suitably aligned inclusions which lead to a reduction in post-yield, load bearing capacity of the unbroken ligament. The constraints were further increased for through thickness cracks in dirty steels due to crack tunnelling locally into elongated sulphide

ribbon-like clusters. The plastic zone size decrease with increasing inclusion content in the through thickness direction is clearly seen in Plate (4) and Figure (36A, B).

5. At lower transition temperatures, the extensive plastic zone and highly strained region were significantly reduced in size. The maximum strains achieved at the crack tip at fracture were not significantly reduced. The crack tip blunting was very limited and the maximum stresses at the crack tip were high. This, in addition to slightly higher yield stresses due to the temperature drop, allowed brittle fracture conditions to be met.

6. At intermediate temperatures of the upper transition, the plastic zones were quite large. The behaviour approximated to upper shelf behaviour. At such temperatures ductile cracking occurred which increased the constraints sufficiently in the strain hardened material to meet critical fracture stresses. At such temperatures it was shown that ductile cracking occurred before brittle fracture. The amount of ductile cracking tolerated was limited by increasing the stored energy of the system, hence δ_m and δ_u were sensitive to increases in B and (W - a). However, whereas an increase in B was shown to shift the transition to higher temperatures due to an increase in plane strain conditions, evidence from increases in (W - a) were not sufficient to confirm its effect on initiation values of toughness.

7. The effects of B on toughness measurements should be conducted independently of (W - a) and (a). Results have shown that upper shelf increases in B did not significantly affect toughness, Figure (74). This was supported by Milne (215) and Kaufmann (211). However, increasing B led to higher stored energies and crack tip constraints which caused a shift in transition temperatures to the right, Figure (31, 74).

8. It was considered that the state of stress was not indicated by the absolute values of e_z, COD or the plastic zone size.

It was shown how an increase in plane strain conditions could only be indicated by a decrease of e_z with respect to COD. This suggested that transition temperature crack tip behaviour was not indicative of a shift to plane strain conditions since, for a given specimen geometry, no change in e_z-COD behaviour was noted, Figure (59).

9. Specimens loaded in tension gave higher maximum load COD values than those loaded in bending. This occurred because the plastic zone size was larger under tension and also because the free surface deformation in the x-direction aided in crack opening. The bend specimen had a centre of rotation within the ligament that acted as a barrier to material flow to the crack tip, Plate (16) and Figures (61A, 62A).

10. Three zones could be distinguished for geometry related fracture toughness for small, generally yielded specimens.

    i) where the ligament length exceeded the characteristic plastic zone size; no geometry dependence was noted.

    ii) where the ligament was smaller than plastic zone size; the measured toughness was linearly dependent on (W - a).

    iii) where the ligament was much smaller r_c^* for SENT fg specimens; the influence of e_x (the high strains from the free surface ahead of the crack tip) caused the measured toughness to increase.

All three regimes are shown in Figure (63A) for plasticine. This behaviour is partly seen in Figure (61) for steel and and Figure (64) for various aluminium alloys.

11. Crack length necessary to contain plasticity to the unbroken ligament was related to the plastic zone size and, hence, the toughness of the material. Fracture, under conditions of limited yielding, should not necessarily be limited to the highly conservative specimen geometries of a = 0.3W. Under

general yielding conditions, this geometry was found to be sufficient to limit the plasticity to the uncracked ligament.

12. The brittle fracture of a weld in a large specimen caused the sudden release of high stored energies. The fast growing crack caused a shift in the transition temperature of the parent plate material to higher temperatures, Figure (77). The transition temperature shift can be very significant and can lead to brittle fracture of, an otherwise, ductile material.

CHAPTER 6

SUMMARY OF CONCLUSIONS AND SUGGESTIONS FOR FURTHER WORK

6.1. SUMMARY OF CONCLUSIONS

The major conclusions are listed below.

1) A method was detailed to determine valid fracture toughness measurements for plates below 50mm in thickness which constituted a problem in through thickness testing. Friction welding of 'dummy ends' at either side of the plate proved the best solution to the problem. The technique involved a minimal heat imput which created a small HAZ. The constraints on through thickness cracks of thin plate materials diminished as free surfaces approached the crack. This was due to the ease of flow of material in the y-direction towards the crack tip region which led to the increase in measured COD. Figure (37) and plates (3A, B) show the effects of the proximity of simulated free surfaces to the crack front. The simulated stress-free, free surfaces deformed and caused increased flow to the deforming crack tip, only when it interacted with the plastic zone ahead of the crack tip. Hence, on welding of 'dummy ends', the free surfaces were removed. This resulted in increased constraints. To study the through thickness behaviour of a plate, independently of the effects of the free surfaces or the 'dummy ends', it was recommended that the limiting factor was applied for upper shelf temperatures:

$$(W - a) \geq T - 3$$

where T was the plate thickness and measurements in millimetres. The constant 3 represented the burn-off and HAZ and would, naturally, vary with the welding parameters and size. This limited the geometry so that the plastic zone size would not interact with the embrittled areas of the HAZ.

2) Hot-rolled plates containing sulphide inclusions showed a small through thickness directionality associated with the highly

elongated inclusions, that is, a ZR and ZT anisotropy existed. With hot-rolling operations, ZR and ZT planes showed a small variation in total inclusion length per unit area, Appendix A, and this accounted for the anisotropy. The average length of inclusions in the two orientations varied very significantly but the length to inter-inclusion separation ratio did not vary in the two directions as rolling increased. Appendix A was used to measure the total inclusion length per unit area, $\Sigma l/A$, taking greater account of crack front migration out-of-plane as a result of observed crack front behaviour. With increasing hot reduction, ZT directions showed greater $\Sigma l/A$ values than ZR directions due to inclusion interaction out-of-plane, facilitated by specimen thinning and inclusion elongation. Plates (7, 13 and 14) serve to illustrate the fracture surface formed by local crack tip jumps to various levels following suitable inclusion clusters within the plastic zone.

The maximum load COD was shown to decrease exponentially with increasing $\Sigma l/A$, in the through thickness direction, Figure (45). If Cotton's approximation (196) of 20% RA of the through thickness direction necessary to avoid lamellar tearing is accepted, then Figure (45) suggests that this corresponded approximately to 1 to 1.5mm/mm^2 of $\Sigma l/A$ and a δ_m value of 0.4. Steel S variety of BS 4360 50D contained 2.5mm/mm^2 of inclusions and a corresponding δ_m value of 0.2mm and was, thus, unacceptable.

In general, to obtain medium to low thickness rolled plate or pipe with good through-thickness toughness characteristics, one must start off with a steel melt with low sulphur content.

Where inclusions are present in plate or pipe, the fullest advantage should be taken of the slightly superior ZR orientation characteristics by welding attachments in that direction, where possible.

3) Laboratory specimens of structural engineering materials exhibited extensive plasticity at the crack tip. The plastic zone was shown to contain a small, highly strained region at the crack

tip which registered high strains and which extended along the lines of maximum shear. The extensive plastic zone registered very small strains, these decreased away from the crack tip. The plastic zone size was shown to depend on the temperature, Figures (36, 49) and inclusion content plate (4). However, the maximum strains reached at the crack tip were only marginally affected. The temperature related plastic zone size affected the fracture behaviour of the material as follows:-

a) At upper shelf temperatures, general yielding occurred for ductile materials and the plastic zone became limited by the (W - a) ligament in small specimens, as shown in plate (16). Under such conditions the measured toughness was dependent on (W - a). Only when (W - a) exceeded the characteristic plastic zone size (r_c*) for the given thickness, could the measured toughness be independent of specimen geometry, as shown in Figures (61A, 62A and 64). At such temperatures the highly strained region was large and the crack tip blunting was extensive. The maximum attainable stresses at the crack tip were, therefore, low and even extensive material work hardening did not permit critical fracture stress conditions to be met. Ductile crack fissures formed ahead of the crack tip, created sharper crack fronts and ran into the blunted crack tip by shearing of the intervening matrix, as in plate (12). This led to ductile crack growth, of a stable nature.

b) For low temperatures, below the transition, the plastic zones were found to be greatly reduced in size, Figure (36A). Due to the high stress concentrations achieved by the sharp notch and the elevated yield stresses of the material at cryogenic temperatures, critical fracture stress conditions were met and brittle fracture occurred. Insufficient evidence was available to suggest a shift in transition to higher temperatures due to the higher constraints created by large elastically loaded ligaments containing a small plastic zone.

c) At intermediate temperatures of the upper transition, extensive plasticity was noted, with crack blunting dissipating the maximum attainable stresses. Some amount of crack growth was necessary before brittle fracture occurred. The combination of ductile cracking (which led to higher constraints and sharp crack fronts) and material work hardening led to higher principal stresses at the crack tip. At these temperatures the effect of stored energy was significant. Large specimens with high stored energy, sufficient to support fast fracture from the first creation of a moving crack, would reduce the necessity for ductile cracking and effectively create a steep transition as seen in Figures (31, 75).

4) Inclusions in the through thickness direction delaminated at very low strains, forming sharp stress concentrators ahead of the fatigue crack tip. These elevated stresses led to higher strains forming at each end of the inclusions and favoured shearing of the inter-inclusion matrix and crack growth, plates (13, 14). This led to a reduction in the applied loads necessary for crack growth and, hence, limited the plastic zone size, plate (4). The sides of an easily delaminated inclusion showed the effects of locally reducing the strains in the transverse direction, plates (9, 10, 11). Constraints further increased in the through thickness direction by crack tip tunnelling along inclusion ribbons which formed frond like crack extensions. These acted as constraining factors on the intervening matrix, plate (6).

At low temperatures, the highly strained region was greatly reduced in size. Where the fatigue crack ended between two well spaced inclusion bands in through thickness direction of a dirty steel, the highly strained region could have existed entirely within clean matrix material. The effect was that at transition temperatures, COD for steel S showed a greater amount of scatter and at times showed toughness values corresponding to those of clean steels, Figure (30).

For LT orientations, Figure (44), large inclusions had the effect of creating a laminar or composite structure ahead of the crack tip. This resulted in an increase of the low temperature ductilities by means of the high ductilities associated with locally reduced specimen thicknesses, as shown in Figure (30).

5) A computer model, based on polynomial approximations of δ_m dependence on $\Sigma 1/A$ was included in Appendix B to predict through thickness toughness behaviour in a scalar manner. Using toughness values obtained experimentally from longitudinal specimens and measuring the total inclusion length/unit area in the direction of interest, the model will predict through thickness toughness values. The model is restricted in use to small specimen sizes, nearly equiaxed grain structure and easily debonded inclusions.

6) It was considered that a shift in the state of stress could only be accompanied by a shift in the rate of change of COD with respect to through thickness strain, e_z. It was found that for a single specimen geometry, e_z was linearly dependent on COD even though the ductile to brittle transition, as shown in Figures (56, 58, 59). A shift towards plane strain conditions should be accompanied by an increase of measured COD relative to e_z. This increase was clearly noted by increasing specimen size in Figure (59) and not by the transition itself.

7) The effect of a sudden release of stored energy, from the fracture of an embrittled weld or HAZ, resulted in a dynamic crack propagating in a brittle manner through otherwise ductile parent material. This led to a very significant shift in the ductile to brittle fracture temperature to higher temperatures as shown in Figure (77).

It was shown that two factors were necessary to achieve the transition temperature shift:-

a) High stored energy was required, as in a specimen of sufficient size or a highly compliant system. This was achieved by using a tensile specimen of 50mm in width loaded on a hydraulic tensile testing machine.

b) Sudden release of stored energy from the fracture of a brittle weld or HAZ leading to a dynamically growing crack.

The absence of either sufficient stored energy or a fast crack initiator did not result in a significant shift in fracture behaviour. In practice, fast deposition of weld bead on cold plate in conditions likely to cause rapid cooling and an embrittled HAZ, as shown in Figure (76), should be avoided by the use of a suitable preheat.

OTHER CONCLUSIONS

For tensile specimens of ductile structural materials at upper shelf temperatures where the point of rotation lay outside (W - a), the COD values were consistently higher than for specimens loaded in bending, as in Figures (61, 62, 63). This was due to (i) the formation of a larger plastic zone for the tensile specimens and (ii) the effect of the free surface ahead of the crack tip which, under tension, deformed resulting in e_x or flow of material towards the straining crack tip, as shown in plates (16, 17). In bending, the effects of the free surface in the x-direction were not realised since the deformations were compressive, away from the crack tip.

At upper shelf temperatures δ_m tended to decrease with increasing temperature. This may have been as a result of decreasing yield stress as temperature increased. High temperature design using room temperature toughness values would lead to unsafe structures.

The effect of specimen thickness (B) on fracture toughness testing should be conducted so that both crack length (a) and unbroken ligament (W - a) be kept constant. This limitation was necessary since toughness depended on the plastic zone size and, hence, (W - a), as described in conclusion 3(b). The large transition temperature and upper shelf toughness variations with increased specimen size, shown in Figure (31), would not be as significant if (W - a) was kept constant. Figure (77) shows the small variations in toughness as a result of increasing only B.

Other investigators (211, 213, 215) also observed, or it was shown from their results, that the effect of increasing only B did not result in a significant effect on measured toughness.

BS 5762 (40) should not limit COD testing to specimens containing regular crack fronts as this would preclude the testing of high sulphur steels in the through thickness direction.

BS WEE 37 should give interaction of inclusions in the out-of-plane direction equal prominence to in-plane interaction as suggested by Appendix A (iii).

Crack length necessary to limit plasticity to the unbroken ligament should be a function of the plastic zone size rather than geometry. Crack lengths greater than one quarter the diameter of the plastic zone was found to be sufficient to contain plasticity. In generally yielded specimens at upper shelf temperatures it is permissible to set a geometrically dependent a/W value. However, at lower transition temperatures the plastic zone was very limited in size for ductile materials. For high strength low toughness materials the plastic zone size was small even at upper shelf temperatures and for such cases one need not set a geometrically dependent crack length to limit the plasticity to the ligament.

6.2. SUGGESTIONS FOR FURTHER WORK

Automated methods of inclusion counting should be used to calculate $\Sigma l/A$. The Quantimet apparatus suggests the most hopeful method of developing this field, if background scatter can be reduced to an acceptable level. The difficulty with Quantimet results was that large areas of steel surface must be surveyed to obtain reasonable $\Sigma l/A$ evaluations. Using small magnifications of the polished steel surface resulted in high scatter to an unacceptable level. Alternatively, using high magnifications reduced the level of background scatter but made the number of readings required tediously large. To account for the interaction of inclusions according to Appendix A (i) and (iii), the results could be modified by a simple conversion factor which relates to the

average inclusion length.

The geometry dependence of toughness in the transition zone was suggested to depend on specimen size and hence on the stored energy of the system. The increase of specimen thickness was shown to shift the transition to higher temperatures by increasing the constraints. Increasing (W - a) created a larger force behind the growing crack which caused the transition to occur over a narrower temperature range. The research reviewed and that conducted in this program were not exhaustive and no firm conclusion could be made on the dominating effect of any one variable. A short research program is envisaged using specimens of one thickness and of various geometries tested at cryogenic temperatures over the transition range. The limiting factor in such experimentation was the absence of dependable temperature regulating equipment necessary for such testing. The specimens should cover a very wide range of unbroken ligament lengths thus ensuring a wide range of stored energies. The results should confirm the independence, or otherwise, of initiation toughness values on specimen geometry for a single thickness, over the transition range.

REFERENCES

REFERENCES

(1) INGLIS, C.E.
Trans. Inst. Nav. Archit. 60, 219, (1913).

(2) GRIFFITH, A.A.
'The phenomenon of rupture and flow in solids', Phil. Trans. Roy. Soc. A221, 163, (1920).

(3) IRWIN, G.R.
'Fracture Dynamics' in Fracturing of Metals ASM Cleveland, 147 (1948).

(4) OROWAN, E.
Rep. Prog. Phys. 12, 185 (1949).

(5) OROWAN, E.
Weld. J. Res. Suppl. 20, 157 (1955).

(6) IRWIN, G.R., and KEIS, J.A.
Weld. J. Res. Suppl. 31, 95s (1952).

(7) SRAWLEY, J.E., JONES, M. and GROSS, B.
'Experimental determination of the dependence of crack extension force on crack length for a single-edged-notch tension specimen', NASA TND-2396 (1964).

(8) DAY, E.E.
'Strain energy release rate determination for some perforated structural members', Weld. J. Res. Suppl. 21, 60s (1956).

(9) LOVE, A.E.
Mathematical Theory of Elasticity, 4th ed. (Dover, New York) (1944).

(10) IRWIN, G.R.
'Analysis of stress and strains near the ends of a crack traversing a plate', J. Appl. Mech. 24, 361 (1957).

(11) IRWIN, G.R.
'Relation of stresses near a crack to the crack extension force', 9th Int. Cong. Appl. Mech. Brussels, (1957).

(12) WESTERGAARD, H.M.
'Bearing pressures and cracks', J. Appl. Mech. 6, A49 (1939).

(13) PARIS, P.C. and SIH, G.C.
'Stress analysis of cracks' in Fracture Toughness Testing and its Applications, ASTM STP 381, Phila. (1965).

(14) KRAFFT, J.M., SULLIVAN, A.M. and BOYLE, R.W.
'Effect of dimensions on fast fracture instability of notched sheets', Proc. Cranfield Crack Propag. Symp. Vol.1, 8 (1961).

(15) BROWN, W.F. and SRAWLEY, J.E.
ASTM Spec., Tech. Pub. No.381, 133 (1965).

(16) TETELMAN, A.S. and McEVILY, A.J.
Fracture of Structural Materials, Wiley, New York (1967).

(17) BRIDGMAN, P.W.
Large Plastic Flow and Fracture. McGraw Hill, New York (1952).

(18) LUDWIG, P.
Z. Metallk. 18, 269 (1926).

(19)
Test for Plane-Strain Fracture Toughness of Metallic Materials. ASTM E 399-74 (1974).

(20)
Methods of Testing for Plane Strain Fracture Toughness (K_{IC}) of Metallic Materials BS 5447-1977.

(21) BERNARD, L. et al
'Inclusions in steel plane and mechanical anisotropy', Met. Tech. 2, 11, 512 (1975).

(22) MAXEY, W.A.
Fracture Initiation, Propagation and Arrest. 5th Symp. on Line Pipe Research, Pipeline Research Committee of AGA. Houston, Texas, Nov. (1974).

(23) ROLFE, S.T. and BARSOM, J.M.
Fracture and Fatigue Control in Structures. Prentice-Hall, (1977).

(24) IWADATE, T., KARAVSHI, T. and WATANABE, J.
'Prediction of fracture toughness K_{IC} of 2.1/4 Cr IMo pressure steels from Charpy V notch test results'.
Flow Growth and Fracture, ASTM STP 631 (1977).

(25)
Symp. on Crack Propagation in Pipelines. Inst. of Gas Engineers, Newcastle Upon Tyne (1974).

(26) FEARNEHOUGH, G.D., DICKSON, D.T. and JONES, D.G.
'Dynamic toughness determination in ductile materials'.
Dynamic Fracture Toughness International Conf. The Welding Inst. (1976).

(27) DICK, J.A., JAMIESON, P. McK. and WALKER, E.F.
Symp. on Crack Propagation in Pipelines. Inst. of Gas Engineers, London (1974).

(28) RITCHIE, R.O.
'On the relationship between fracture mechanics and CVN energy in ultra high strength steel', AIMA Winter Mt., Denver, Proc. of Conf. (1978).

(29) COTTRELL, A.H.
'Theoretical aspects of radiation damage and brittle fracture in steel pressure vessels'. Iron and Steel Inst. Spec. Report No.69, p.281 (1961).

(30) WELLS, A.A.
'Application of fracture mechanics at and beyond general yield'. Brit. Weld. J., 10,11, 563, (1963).

(31) EFTIS, J. and LIEBOWITZ, H.
'On fracture toughness evaluation for semi brittle fracture'. Eng. Fract. Mech. 7, 101, (1975).

(32) DUGDALE, D.S.
'Yielding in sheets containing slits'. J. Mech. Phys. Solids 8 (1960).

(33) BARENBLATT, G.I.
Advances in Appl. Mech. 7, 55 (1962).

(34) WELLS, A.A.
Proc. Cranfield Crack Propagation Symposium, 1, 210 (1961).

(35) WELLS, A.A.
'Notched bar tests, fracture mechanics and the brittle strengths of welded structures', Houdremont Lecture, Brit. Weld. J. 12, 2 (1965).

(36) BURDEKIN, E.M. and STONE, D.
'The COD approach to fracture mechanics in yielding materials'. J. Strain Analysis, 1, 2, 145 (1966).

(37) HAYES, D.J. and WILLIAMS, J.C.
Int. J. Fracture Mech. 8, 239 (1972).

(38) WELLS, A.A.
J. Eng. Fract. Mech. 1 (1968).

(39) B.S.I. Draft for Development DD19 Methods for Crack Opening Displacement (COD) Testing (1972).

(40) Methods of Crack Opening Displacements (COD) Testing. BSI Publication BS 5762: 1979 (1979).

(41) WELLS, A.A.
'The status of COD in Fract. Mech.', 3rd Canadian Conf. on Applied Mech. Calgary, p.59 (1971).

(42) INGHAM et al
Practical application of fracture mechanics to pressure vessel technology. I.M.E. London (1971), p.200.

(43) EWING, D.J. and HILL, R.
'The plastic constraint of V notched tension bars'. J. Mech. Phys. Solids, 15, 2, 115, (1967).

(44) KNOTT, J.F.
J. of Iron and Steel Inst., 204, 104 (1966).

(45) DAWES, M.G. and KAMATH, M.S.
'The COD design curve approach to crack tolerance'. Tolerance of Flaws in Pressurised Components. IME Conf. Publ. 10, 27 (1978).

(46) DAWES, M.G.
'Elastic-plastic fracture toughness based on the COD and J-contour integral concepts'. Elastic Plastic Fracture ASTM STP 668, (1979).

(47) NICHOLS, R.W., BURDEKIN, F.M., COWAN, A., ELLIOT, D. and INGHAM, T.
'The use of critical COD techniques for the selection of fracture resistant materials'. Practical Fracture Mech. for Structural Steel. Proc. Conf. Risley, UKAEA and Chapman and Hall (1969).

(48) HICKSON, V.M.
'A replica technique for measuring plastic strain'. J. Mech. Eng. Sci. 1, 2, 171 (1959).

(49) VISOKOVSKY, O.
'Displacements and strain at the crack tip', Int. J. of Fract. Mech. 4,3, 321, (1968).

(50) KOBAYASHI, A.S., ENGSTROM, W.L., and BRAY, J.W.
'COD and normal strains in centrally notched plates'. Experimental Mechanics, 163, April (1969).

(51) LOW, I. and BRAY, J.W.
'Strain measurements using Moire fringes', Engineer, 213, 566, (1962).

(52) HAHN, G.T., KANNINEN, M.F., and ROSENFIELD, A.R.
'Ductile crack extension and propagation in steel foil'. Proc. 2nd Int. Cont. on Fracture, Brighton, Chapman and Hall, p.58 (1969).

(53) HAHN, G.T. and ROSENFIELD, A.R.
'Local yielding and extension of a crack under plane stress'.
Acta Met. 13, 3, 293 (1965).

(54) KANAZAWA, T., MACHIDA, S., MOMOTA, S. and HAGIWARA, V.
'A study of the COD concept for brittle fracture initiation'.
Proc. 2nd Int. Conf. on Fracture, Brighton, Chapman & Hall,
1 (1969).

(55) VEERMAN, C.C. and MULLER, T.
'The location of the apparent rotation axis in notched bend testing'. Eng. Fract. Mech. 4, 25 (1972).

(56) VANTABE, M. MUKAI, Y. KAGA, S. and FUJIHARA, S.
Proc. 3rd Int. Conf. on PV Technology, Tokyo, Part II,
ASME, New York, 677, (1977).

(57) OTSUKA, A., MIYATA, T. and NISHIMURA, S.
Fr. Mech. and Tech. G.C. Sih and C.L. Chow Editors.
Sithoff and Noordhoff Int. Publ. 1, 539 (1977).

(58) ROBINSON, J.N. and TETELMAN, A.S.
'Measurement of K_{1C} on small specimens using critical CTOD'.
Fracture Toughness and Slow Stable Cracking, ASTM STP 559,
139 (1974).

(59) FIELDS, B.A. and MILLER, K.J.
'A study of COD and crack initiation by a replication technique'. Eng. Fr. Mech. 9, 137 (1977).

(60) GREEN, G., SMITH, R.F. and KNOTT, J.F.
'Metallurgical factors in low temperature slow crack growth'.
BSC Conf. on Mechanics and Mechanisms of Crack Growth.
Camb. 58, April (1973).

(61) BROEK, D.
'Correlation between fracture toughness and stretch zone size'. 3rd Int. Conf. on Fracture. Munich April (1973)

(62) ELLIOT, D.
'Simplified COD testing for industry', BISRA Report
MG/52/71, May (1971).

(63) FREDERICK, G. and SALKIN, C.V.
'Fracture mechanics assessment of steel plates to brittle fracture'. Paper C35/71 I.M.E. Conf. on Practical Applications of Fr. Mech. to P.V.T. London 136 (1971).

(64) GRAY, T.G.
'Notch root contraction as a fracture measurement'.
Int. J. of Fr. Mech. 8, 3, 277 (1972).

(65) KAMATH, M.S.
M.Sc. Thesis, Cranfield (1975).

(66) INGHAM, T., EGAN, G.R., ELLIOT, D., and HARRISON, T.C.
'The effect of geometry on the interpretation of COD test data'. Paper C54/71 I.M.E. Conf. on Pract. Applic. of Fr. Mech. to P.V.T. London (1971).

(67) ELLIOT, D., WALKER, E.F. and MAY, M.T.
'The determination and applicability of COD test data', Paper C77/71 I.M.E. Conf. on Pract. Applic. of Fr. Mech. to P.V.T. London (1971).

(68) ARCHER, G.L.
'The relationship between notch tip and notch mouth displacement is SENB fracture toughness specimens'. W.I. Report E/63/75, March (1975).

(69) CLARK, G., ELSOUDANI, S., FERGUSON, W.G., SMITH, R.F. and KNOTT, J.F.
'Ductile Crack Initiation in Pressure Vessel Steels'. Tolerance of Flaws in Pressurised Components. Paper C 80/78 I.M.E. Conf. (1978).

(70) BURDEKIN, F.M.
'Crack opening displacement: a review of principle and methods'. Pract. Fr. Mech. for Struct. Steel UKAEA & Chapman and Hall, Risley, 1969.

(71) BUCCI, J.R., PARIS, P.C., LANDES, J.D. and RICE, J.R.
ASTM STP 514, 40 (1972).

(72) CHELL, G.G. and DAVISON, A.
'A post yield fracture mechanics analysis of SENT specimens', Mat. Sci. and Engineering, 24, 45 (1976).

(73) SMITH, R.F. and KNOTT, J.F.
Proc. Conf. on Pract. Application of Fr. Mech. to Pressure Vessel Technology. IME 65 (1971).

(74) GREEN, G. and KNOTT, J.F.
'On effects of thickness on ductile crack growth in mild steel'. J. Mech. Phys. of Solids 23, 167 (1975).

(75) CHIPPERFIELD, C.G.
'Some observations on ductile crack initiation and propagation in fracture toughness specimens'. OECD/NEA Spec. Mtg. on Elastoplastic Fract. Mech. Daresbury, May (1978).

(76) de CASTRO, P.M., SPURRIER, J. and HANCOCK, P.
'An experimental study of the a/W ratio dependence of the COD test'. 11th Nat. Synp. on Fract. Mech., Virginia, USA, June 1978.

(77) SMITH, R.F.
PhD. Thesis, Cambridge.

(78) COWAN, A. and KIRBY, N.
'The application of COD measurement to large scale test behaviour'. Practical Fract. Mech. for Struct. Steels. Published by Chapman and Hall and UKAEA, Risley (1969).

(79) BURDEKIN, F.M. and TAYLOR, T.E.
'Fracture in spherical pressure vessels'. J. Mech. Eng. Sci., 11, 5, 486, (1969).

(80) FEARNEHOUGH, G.D., CEES, G.M., LOWES, J.M., and WEINER, R.T.
Paper 71, IME Conf. on Practical Applications of Fracture Mechanics to Pressure Vessel Technology.

(81) FEARNEHOUGH, G.D. et al
Churchill College Cambridge, April (1973). Conf. on Mechanics and Mechanisms of Crack Growth.

(82) BARR, R.R., ELLIOT, D., TERRY, P. and WALKER, E.F.
'The measurement of COD and its application to defect significance', Metals Construction Dec. (1975).

(83) BERRY, G. and BROOK, R.
'On the measurement of COD when slow crack growth precedes rapid fracture'. Int. J. of Fract. 11, 6, Dec. (1975).

(84) KAMATH, M.S.
'The R curve approach to fracture', The Welding Institute, Res. Bull. June p.145 (1977).

(85)
ASTM Spec. Tech. Publ. No.527, Symp. on Fracture Toughness Evaluation by R Curve Methods (1973).

(86) GARWOOD, S.J.
PhD. Thesis, Imperial College, Univerity of London.

(87) GARWOOD, S.J., PRATT, P.L. and TURNER, C.E.
'Measurement of slow crack growth in structural steel and prediction of unstable fracture'. CSM 132. UKAEA DECD Paper 11 (1978).

(88)
Conclusion of Meetings on Application of Reliability Technology to Nuclear Power Applications. IAEA Symp.

(89) THAULOW, C.
'Comparison between COD at initiation of ductile crack growth and max load of submerged arc weld material'. Int. J. Fract. 15 (1977).

(90) McCABE, D.E.
'Determination of R curves for structural materials using non linear mechanics'. ASTM STP 631 (1977).

(91) SERVER, W.L.
'Static and dynamic fiberous initiation toughness results for nine pressure vessel materials". ASTM STP 668 (1979).

(92) WITT, F.J.
'Equivalent energy procedures for predicting gross plastic fracture'. 4th Nat. Symp. on Fracture. Carnegie Mellon Univ. Aug. (1970).

(93) WITT, F.J. and MAGER, T.R.
Nucl. Eng, Design, 17, 91 (1971).

(94) CHANG, S.J. and WITT, F.J.
Fracture Analysis, ASTM STP 560 (1979).

(95) HARRISON, R.P., LOOSEMORE, K. and MILNE, I.
'Assessment of the integrity of structures containing defects'. CERL Report R/H/R6, April 1977.

(96) RICE, J.R.
Trans. ASME, J. Appl. Mech. 35, 379, (1968).

(97) RICE, J.R.
Fracture - An Advanced Treatise, Vol.2. Ed. H. Liebowitz, New York, Academic Press, p.1 (1968).

(98) DRUCKER, D.C. and RICE, J.R.
Eng. Fract. Mech. 1, (1970).

(99) BUCCI, J.R., PARIS, P.C., LANDES, J.D. and RICE, J.R.
BSI Draft for Public Comment, Doc. 75/77081 DC April (1976).

(100) RICE, J.R., PARIS, P.C. and MERKLE, J.G.
ASTM STP 668 (1979).

(101) TURNER, C.E., and BURDEKIN, F.M.
'Review of current status of yielding fracture mechanics'. Atomic Energy Review IAEA, Vienna, 12, 3, (1974).

(102) TURNER, C.E.
'Yielding fracture mechanics', J. of Strain Analysis, 10, 4, 207 (1975).

(103) SUMPTER, J.D. and TURNER, C.E.
Int. J. of Fracture Mechanics, 9, 3, 320 (1973).

(104) SUMPTER, J.D. and TURNER, C.E.
'Cracks and fracture', ASTM STP 601, (1976).

(105) RICE, J.R.
'The mechanics of fracture', AMD Vol.19, ed. F. Erdogan, New York (ASME) (1976).

(106) BROBERG, K.B.
J. Mech. Phys. Solids, 19, 407 (1971).

(107) OROWAN, E.
Trans. Inst. Engnrs. Shipbuilders Scot., 89, 165 (1945).

(108) KNOTT, J.F.
'Effect of second-phase particles on the mechanical properties of steel' 44, The Iron and Steel Inst. (1971).

(109) SMITH, E.
Int. J. Fracture 14, 125, (1978).

(110) SCHWALBE, K.H.
'Some properties of stable crack growth'. Engng. Fract. Mechanics 11, 331 (1979).

(111) COTTON, H.C.
'How to conduct COD tests and utilise the results in practice'. 1st Int. Symp. Japan Welding Soc. Tokyo III B9.1, Nov. (1971).

(112) GARLAND, J.G. and KIRKWOOD, P.R.
'The selection and fabrication of steels for off-shore structures'. Int. Off-shore Techn. Conf. London Oct. (1974).

(113) HICKS, J.S.
'A study of material and structural problems in offshore installations'. Welding Inst. Reprint E/55/74 Jan (1974).

(114) TURNER, C.E.
'Notes on experimental verification of J_{IC} and K_C. 6th Int. Post Experience Course on Yielding Fracture Mech. June (1976).

(115) PARIS, P.C., BUCCI, R.J. and LOUSHIN, L.L.
'Dynamic compact tension testing for fracture toughness'. ASTM STP 559 (1974).

(116) WILKOWSKI, G.M., MAXEY, W.A. and EIBER, R.J.
Canadian Met. Quart. 19, 59 (1980).

(117) KNOTT, J.F.
'Fundamentals of Fracture Mechanics', Butterworths Group (1973).

(118) RADON, J.C. and TURNER, C.E.
J.I.S.I. 204, 842 (1966).

(119) BARSOM, J.M. and ROLFE, S.T.
ASTM STP 466, 281 (1970).

(120) HERTZBERG, R.W.
Deformation and Fracture Mechanics of Engineering Materials, John Wiley & Sons (1976).

(121) KALTHOFF, J.F. et al
'Measurements of dynamic stress intensity factors for fast, running and arresting cracks'. ASTM STP 627 (1977).

(122) OSTENSSON, B.
IAEA Sympos. on Applications of Reliability Technology to Nuclear Power Plants. Paper No. 1A EA SM 218/17.

(123) KRAFFT, J.M.
Appl. Mater. Res. 1, p.88 (1964).

(124) YODER, G.R.
Met. Trans. 3, p.1851 (1972).

(125) BARSOM, J.M. and PELLEGRINO, J.V.
Eng. Fract. Mech. 5, p.209 (1973).

(126) HAHN, G.T. and ROSENFIELD, A.R.
ASTM STP 432 (1968).

(127) WEISS, V.
Proc. of the Int. Conf. on Mechanical Behaviour of Materials, p.458 (1972).

(128) GARRET, G.G.
PhD. Thesis, Cambridge (1973).

(129) FIELDS, B.A. and MILLER, K.J.
'Fibrous crack initiation and propagation in prestrained HY100 steel'. Engng. Fract. Mech. (1976).

(130) CHIPPERFIELD, C.G.
'Detection and toughness characterisation of ductile crack initiation in 316 stainless steel'. Int. J. Fract. 12, 873 (1976).

(131) KIM, Y.H., FINE, M.E., and MURA, T.
'Plastic yielding at the tip of a blunt notch during static and fatigue loading'. Eng. Fract. Mech. 11, 536 (1979).

(132) McCLINTOCK, F.A.
Int. J. Fract. Mech., 4, 101 (1968).

(133) BROEK, D.
Engng. Fract. Mech, 5, 55 (1975).

(134) CHIPPERFIELD, C.G. and KNOTT, J.F.
'Microstructure and toughness of structural steels'.
Metals Tech. 45, Feb. (1975).

(135) MYLONAS, C. Proc. 11th Int. Conf. for Appl. Mech. 652 (1964).

(136) ORNER, G.M. and MARTBOWER, C.E.
Weld. Res. Suppl. p.405s, (1961).

(137) LEREIM, J. and EMBURY, J.D.
ASM Publcn. Proc. of Conf. on 'What does the Charpy test really tell us?'. Colorado, Feb. (1978).

(138) RITCHIE, R.O.
ASM Publcn. Proc. of Conf. on 'What does the Charpy test really tell us?'. Colorado, Feb. (1978).

(139) WILKOWSKI
ASM Publcn. Proc. of Conf. on 'What does the Charpy test really tell us?'. Colorado, Feb. (1978).

(140) DAWES, M.G.
'Fractural control in high yield strength weldments'.
Weld. J. Res. Suppl. Vol.53, 369s (1974).

(141) KAMATH, S., SPURRIER, J. and HANCOCK, P.
'Influence of specimen geometry on the fracture toughness of 50D steel'. Dept. of Materials, C.I.T., Internal Report.

(142) KIESSLING, R. and LANGE, N.
'Non-metallic inclusions in steel'. Part II Iron and Steel Inst. Publ. 100, London (1966).

(143) KIESSLING, R. and WESTMAN, C.
J. of Iron and Steel Inst. 204, 377 (1966).

(144) KIESSLING, R. and WESTMAN, C.
J. of Iron and Steel Inst. 208, 699 (1970).

(145) MALBERG, T. et al.
'The addition of Se and Te to carbon steels, their recovery and effect on inclusions and machinability'. Scand. J. of Metall. 3,4, 16 (1974).

(146) SIMS, C.E.
Trans. A.I.M.E. 215, 367 (1959).

(147) BARKER, T.J. and CHARLES, J.
J. of Iron and Steel Inst. 210, 702 (1972).

(148) FREDRIKSSON, H. and HILLERT, M.
Scand. J. of Metall. 2, 125 (1973).

(149) BAKER, T.J.
Sulphide Inclusions in Steel, ASM Publ. (1974).

(150) FREDRIKSSON, H. and HILLERT, M.
J. of Iron and Steel Inst. 209, 109 (1971).

(151) MAUNDER, P. and CHARLES, J.
J. of Iron and Steel Inst. 206, 705 (1968).

(152) CHAO, H. and VAN VLACK, L.
Trans. A.I.M.E., 233, 1227 (1965).

(153) MOORE, C.
M. Met. Thesis Univ. of Sheffield (1968).

(154) TABOR, D.
Rev. Phys. Techn. 1, 145 (1970).

(155) BAKER, T., GROVE, K. and CHARLES, J.
Metals Techn. April (1977).

(156) GROVE, K. and CHARLES, J.
Metals Tech. 1, 279 (1974).

(157) GOODIER, J.
Trans. A.I.M.E. 55, 39 (1933).

(158) SUNDSTROM, B.
J. Compos. Matter. 5, 8, 277 (1971).

(159) ZEISLOFT, R. and HOSFORD, W.
Trans. A.I.M.E. 62, 297 (1969).

(160) BERNARD et al
'Inclusions in steel plate and mechanical anisotropy'.
Met. Tech. 2, 11, 512 (1975).

(161) PUTTICK, K.E.
Phil. Mag. 4, 964, (1959).

(162) ROSENFIELD, A.R.
Met. Rev. 13, 121, 29 (1968).

(163) McCLINTOCK, F.A.
Fracture, Ed. H. Liebowitz, Academic Press, New York, 3, 106 (1971).

(164) RICE, J.R. and TRACEY, D.
J. Mech. Solids, 17, 201 (1969).

(165) BERG, C.A.
Inelastic Behaviour of Solids. Eds. M. Kanninen et al.
M.I.T. Press, Cambridge Mass. 307 (1970).

(166) McCLINTOCK, F.A.
Physics of Strength and Plasticity. Ed. A.S. Argon,
M.I.T. Press, Cambridge, Mass. 307 (1969).

(167) RITCHIE, R.O., KNOTT, J.F. and RICE, J.R.
J. Mech. Phys. Solids 21, 395 (1973).

(168) PLAMER, I.J. and SMITH, G.C.
Met. Soc. A.I.M.E. Conf. Oxide Dispersion and Strengthening.
Gordon and Breach, New York, 47 (1966).

(169) BARNABY, J.J.
Acta. Met., 15, 903 (1967).

(170) GURLAND, J. and PLATEAU, J.
Trans. A.S.M., 56, 442 (1963).

(171) TANAKA, K., MORI, T. and NAKAMURA, T.
Phil. Mag. 21, 267 (1970).

(172) ASHBY, M.F.
Phil. Mag. 14, 1157, (1966).

(173) McCLINTOCK, F.A.
Ductility A.S.M. Publ., Metals Park, Ohio, 255 (1968).

(174) EDELSON, B. and BALDWIN, W.
Trans. A.S.M. 55, 230 (1962).

(175) GLADMAN, T.
Sulphide Inclusion in Steels. A.S.M. Publ. (1974).

(176) BAKER, T.J.
Proc. of B.S.C. Conf. 'Inclusions and Their Effects on Properties'. Leeds, Paper 2 (1974).

(177) BAKER, T.J., GROVE, K.B. and CHARLES, J.A.
Metals. Tech. 183 (1975).

(178) ASHBY, M.F.
Met. Soc. A.I.M.E. Conf. Oxide Dispersion Strengthening.
Gordon and Breach, New York 143 (1966).

(179) BROWN, C.Y. and STOBBS, V.M.
Phil. Mag. 23, 1201 (1971).

(180) ROESCH, L.
Mem. Sci. Rev. Met. 66, 29, (1969).

(181) ARGON, A.S., IM, J. and SOFOGLU, R.
Met. Trans. A. 6A, 825 April (1975).

(182) GLADMAN, T., HOLMES, B. and McIVOR, I.D.
'Effect of second phase particles on mechanical properties of steel'. Iron and Steel Inst., London 68 (1971).

(183) FRENCH, I.E. and WEINRICH, P.F.
Met. Trans. 6A, 785 (1975).

(184) ARROWSMITH, J.M.
Proc. of B.S.C. Conf. Inclusions and Their Effects on Properties. Leeds, Paper 7 (1974).

(185) CLAYTON, J.Q.
Dissertation for the Board of Graduates, Cambridge Univ. (1973).

(186) De ARDO, A.J. and HAMBURG, E.G.
'Sulphide inclusions in steel', 309 (1975).

(187) HODGE, J., FRAZIER, R. and BOULGER, F.
Trans. A.I.M.E. 215, 10, 745, (1959).

(188) FRANKLIN, A. et al
J. of Iron and Steel Inst. 292, 7, 588 (1964).

(189) BROWNRIGG, A. and CHAMBERS, F.M.
J. of Iron and Steel Inst. 298, 12, 1078 (1970).

(190) HEISTERKAMP, F. et al
Stahl. u. Eisen, 90, 22, 1255 (1970).

(191) ERRIKSON, K.
'Fracture Toughness and the Distribution of Inclusions".
Scandanavian J. of Met. 4, 4, (1975).

(192) LEHTINEN, B. and EASTERLING, K.E.
'Dynamic observation on cavity nucleation and growth at MnS/ferrite interfaces in steel".

(193) NICHOLLS, D.M.
'Lamellar tearing in hot rolled steel'. British Weld. J. p.103 March (1968).

(194) FARRAR, J.C., DOLBY, R.E. and BAKER, R.G.
'Lamellar tearing in welded structural steels', Welding J. p.274s July (1969).

(195) DRURY, M.L. and JUBB, J.E.M.
'Lamellar tearing and the slice bend test', Welding J.. p.88s, Feb. (1973).

(196) COTTON, H.C.
'Material requirements for offshore structures'. Rosenhain Centenary Conf. Royal Soc. London p.53 (1976).

(197) HUGUET, C. and RICHTER, J.
Revue de Metallurgie, April 321 (1974).

(198) McMAHON, C.J.
Fundamental Phenomenon in Materials Science. Plenum, New York, 14, 247 (1967).

(199) Turkdogan, E.T.
Sulphide Inclusions in Steels. A.S.M. Publ. (1974).

(200) ASHTON, J.D. et al
J. of Metals. April, 47 (1964).

(201) MIYASHI, S. et al
Revue de Metallurgie, Apr. 395 (1974).

(202) HARRISON, J.D. et al
'Cod approach and its application to welded structures'. Symp. on Elastoplastic Fracture, Atlanta USA, ASTM STP (668) 1977.

(203) de Castro P.M.S.T.
PhD. Thesis, Dept. of Materials, Cranfield Inst. of Tech. (1980).

(204) AL-HADITHY, N.A.J.
M.Sc. Thesis, Dept. of Materials. Cranfield Inst. of Tech. (1977).

(205) TOBLER, R.I., MIKESELL, R.P. and REED, R.P.
'Cryogenic effects on the fracture mechanics parameters of ferritic nickel alloy steels'. Preliminary Report (1978).

(206) MAY, M.J., TIBBOT, A., BANKS, T.M. and WALKER, E.F.
'The evaluation of the effects of inclusion form and distribution on the fracture of C-Mn steels'. BSC Report PT/6787/3/77/A. (1977).

(207) GREEN, A.P. and HUNDY, B.B.
'Initial plastic yielding in notched bend test'. J. Mech. and Phys. of Solids 4, 128 (1956).

(208) MUNZ, D.
'Minimum specimen size for the application of LEFM'. Elastic Plastic Fracture, ASTM STP 668 (1979).

(209) HAIG, J.R. and RICHARDS, C.E.
'Yield point loads and compliance functions of fracture mechanics specimens'. CEGB Report RD/C/M/461 June (1974).

(210) BRADSHAW, F.J. and WHEELER, C.
RAE Technical Report 73191 March (1974).

(211) KAUFMAN, J.G. and NELSON, F.G.
'More on specimen size effects in fracture toughness testing'. ASTM STP 559. Fract. Toughness and Slow Stable Cracking (1974).

(212) SULLIVAN, A.M. and STOOP, J.
'Further aspects of fracture resistance'. ASTM STP 559. Fract. Toughness and Slow Stable Cracking (1974).

(213) MAY, M.J., WEBSTER, S., BANKS, T.M. and WALKER, E.F.
'Influence of yield strength and tensile strength on fracture toughness testing and defect tolerance calculations.
BSC Report SH/PT/8239/--/78/B (1978).

(214) CHELL, G.G. and GATES, R.
Int. J. of Fract. 14, 223 (1972).

(215) MILNE, I. and CURRY, D.A.
3rd Colloquium on Fract. Imperial College Sept (1980).

(216) SPURRIER, J., SANTAROSSA, P. and HANCOCK, P.
Eng. Fract. Mech. 13, 829 (1980).

(217) de CASTRO, P.M., SPURRIER, J. and HANCOCK, P.
Int. J. of Fracture 26, 3 (1980).

(218) ELSENDER, A., POYNTON, A. and BATTE, D.
Obtained from Chell and Gates ref (214).

TABLES

TABLE 1 - Chemical Analyses of the Steels

	Element Weight %																
	C	S	P	Si	Mn	Ni	Cr	Mo	V	Cu	Nb	Ti	Al	B	Pb	Sn	Co
Steel D																	
Clean Steel	0.11	<0.005	0.012	0.47	1.36	0.06	0.05	0.01	<0.01	0.07	0.28	<0.01	0.02	<0.001	<0.01	0.02	<0.01
Steel S																	
Dirty Steel	0.19	0.016	0.02	0.38	1.40	0.06	0.11	0.03	<0.01	0.07	0.03	<0.01	0.032	<0.001	<0.01	0.02	<0.01

TABLE 2 - Inclusion and Grain Size Variation Through the Steels

Inclusion distribution through the thickness in the rolling direction for the 51mm thick plate of steel S.

Distance from Surface	NUMBER OF INCLUSIONS > 0.25mm	>0.5mm	Maximum Inclusion Length (l)mm	
2mm	6	0.0	0.25	2.68
8mm	10	3.0	0.30	2.46
12mm	12	4.0	0.90	2.40
17mm	16	4.5	1.50	2.40
25mm	16	10.0	1.50	2.38

Mid-thickness 1 mm /mm^2 ZTS = 2.38mm/mm^2
Mid-thickness 1 mm/mm^2 ZRS = 1.84mm/mm^2

Thus 23% variation from ZRS to ZTS orientations.

Steel S 0.50 strain hot rolling
ZTS 1 mm/mm^2 = 5.80
ZRS 1 mm/mm^2 = 3.70

Steel S 0.75 strain hot rolling
ZTS 1 mm/mm^2 = 7.89
ZRS 1 mm/mm^2 = 5.30

Steel D 0.00 strain
ZTD 1 mm/mm^2 = 0.20
ZRD 1 mm/mm^2 = 0.15

Steel D 0.50 strain
ZTD 1 mm/mm^2 = 0.29
ZRD 1 mm/mm^2 = 0.18

Steel D 0.75 strain hot rolling
ZTD 1 mm/mm^2 = 0.32
ZRD 1 mm/mm^2 = 0.20

GRAIN SIZE VARIATION

Dirty steel S
Longitudinal to transverse 20%
Centre to surface 0%

Clean steel D
Longitudinal to transverse 30%
Centre to surface 10%

TABLE 3 - Tensile Test Results, Longitudinal Specimens, Steel D *

Temperature °C	Yield Strength σ_Y N/mm^2	Tensile Strength σ_{UTS} N/mm^2	Reduction of Area %RA
18	336	497	78
18	352	510	77
-40	364	542	77
-58	384	565	75
-91	395	575	74
-91	405	580	74
-196	760	850	5
-196	771	862	4

TABLE 4 - Tensile Test Results, Through Thickness Specimens Steel D

Temperature °C	Yield Strength σ_Y N/mm^2	Tensile Strength σ_{UTS} N/mm^2	Reduction of Area %RA
18	336	497	68
18	342	505	68
18	349	510	65
-58	372	557	62
-62	393	567	62
-80	387	571	62
-80	400	582	63
-196	740	812	4

* all tests at 1.27mm/min

TABLE 5 - Tensile Test Results, Longitudinal Specimens Steel S

Temperature °C	Yield Strength σ_Y N/mm^2	Tensile Strength σ_{UTS} N/mm^2	Reduction of Area %RA
18	285	430	69
18	285	444	67
-87	360	522	69
-119	388	560	-
-196	628	715	3
-196	638	720	3

TABLE 6 - Tensile Test Results, Through Thickness Specimens Steel S

Temperature °C	Yield Strength σ_Y N/mm^2	Tensile Strength σ_{UTS} N/mm^2	Reduction of Area %RA
18	290	340	6.9
18	295	343	6.6
-98	360	432	3.5
-130	428	439	3.1
-196	440 *		3
-196	458 *		3

* Fracture Strength

TABLE 7 - Charpy V Notch Impact Test Results
Steel D

Temperature °C	LS Specimens (ft lbs)	ZT Specimens (ft lbs)
18	160.0	111.5
	166.0	108.5
	163.0	
	163.0	
	160.0	
-45		54.5
		23.0
-50		45.5
-56		23.0
-60	103.0	36.5
	94.5	
-63		24.5
-65	104.0	
-69	54.5	
-73	20.0	
-75		

TABLE 8 - Charpy V Notch Impact Results
Steel S

Temperature °C	LS Specimens (ft lbs)	ZT Specimens (ft lbs)
18	134.5	23.0
	131.5	20.0
	126.0	
	137.0	
	128.5	
-28	114.5	
-40	117.0	
	88.5	
	106.0	
-47	74.5	
-50	71.5	
-55	48.5	
-61	40.0	
-64	48.5	5.5
-74	8.5	

TABLE 9 - COD Values for LS Oriented Steel (D)
Specimens a/W Values from 0.25 - 0.35
W = B = 10mm.

Temperature °C	COD Type	COD Value mm	Scatter of COD due to 0.5% Load Variation	mm
48	δ_m	0.65	± 0.05	
20		0.80		
		0.90		
		0.90		
		0.85		
		0.88		
18		0.72	0.09	-0.02
		0.95	± 0.08	
1		1.00		
-30		0.90		
-45		1.04	0.09	-0.08
-60		0.97		
-60		0.78		
-70		0.80		
-80		0.93		
-80		0.80		
-85		0.78		
-87		0.84	0.11	-0.04
-90		0.75		
-93		0.80		
-93	δ_c	0.53	0.00	-0.04
-95		0.63		
-98		0.30	± 0.00	
-98		0.35		
-100		0.30	± 0.00	
-128		0.09	± 0.00	
-139		0.12		
-196*		0.07		

* Calculated from notch root contraction

TABLE 10 - COD Values for ZT Oriented Steel 'D'
Specimens a/W Values from 0.25 - 0.35
W = B = 10 mm

Temperature °C	COD Type	COD Value mm	Scatter of COD due to 0.5% Load Variation mm	
20	δ_m	0.73		
		0.72		
		0.80	0.13	-0.02
		0.82	0.10	-0.05
		0.73		
		0.72		± 0.02
		0.76		
		0.73	0.12	-0.02
		0.74	0.09	-0.02
		0.90		
		0.75		
		0.76		± 0.20
18		0.74		
		0.74	0.06	-0.04
		0.80		
		0.78		
10	δ_m	0.75		
-15		0.78		
-25		0.81	0.15	-0.02
-35		0.72		
-42		0.70	0.15	-0.02
-50		0.75	0.12	-0.05
-68		0.78		± 0.03
-68		0.70	0.13	-0.09
-72		0.77		
-72		0.77		
-79		0.90		
-80		0.70		
-83		0.65		
-85		0.75		
-87		0.75		
-90		0.75	0.11	-0.06
-90	δ_u	0.62		± 0.00
-91		0.43		± 0.00
-92		0.39		
-97		0.32		
-97		0.29		
-98		0.30		
-102		0.30		
-104		0.20		
-147		0.10		
-147		0.12		
-150		0.07		
-196		0.07		± 0.00

* Calculated from notch contraction

TABLE 11 - COD Values for ZR Oriented Steel (D)
Specimens a/W Values from 0.25 - 0.35
W = B = 10 mm

Temperature °C	COD Type	COD Value mm	Scatter of COD due to 0.5% Load Variation		Scatter of COD due to 0.5% mm
20	δ_m	0.96	0.04		-0.12
		0.86	0.07		-0.03
		0.82		± 0.07	
		0.86			
18		0.77	0.11		-0.04
		0.80			
		0.85			
0		0.78		± 0.07	
-15		0.86			
-25		0.80			
-47		0.83			
-69		0.71			
-69		0.74			
-75		0.87	0.13		-0.09
-80		0.84	0.15		-0.13
-83		0.74			

TABLE 12 - COD Values for LS Oriented Steel (S)
Specimens a/W Values from 0.25 - 0.35
W = B = 10 mm

Temperature °C	COD Type	COD Value mm	Scatter of COD due to 0.5% Load Variation	mm
20	δ_m	0.70		
		0.72		
		0.79	0.07	-0.13
		0.78	0.15	-0.08
		0.66		
		0.65		
		0.71		
		0.65		
		0.63		
0		0.77	0.15	-0.20
-10		0.76		
-15		0.72		
-18		0.66		
-48		0.60	± 0.13	
-66		0.60		
-69		0.83	0.13	-0.04
-85		0.74	0.04	-0.09
-85	δ_u	0.49	0.00	-0.09
-88	δ_c	0.24	± 0.00	
-196		0.10	± 0.00	

TABLE 13 - COD Values for ZT Oriented Steel (S)
Specimens a/W Values from 0.25 - 0.35
W = B = 10 mm

Temperature °C	COD Type	COD Value mm	Scatter of COD due to 0.5% Load Variation mm
20	δ_m	0.22	
		0.19	
		0.23	
		0.18	± 0.02
		0.16	
-12		0.20	
-18		0.19	± 0.01
-25		0.17	
-31		0.14	
-32		0.16	
-34		0.17	
-67		0.17	± 0.02
-69		0.19	
-80	δ_u	0.10	
-85	δ_u	0.10	
-85	δ_m	0.28	
-86	δ_u	0.15	
-94	δ_u	0.12	
-110	δ_c	0.04	

TABLE 14 - COD Values for ZR Oriented Steel (S)
Specimens a/W Values from 0.25 - 0.35
W = B = 10 mm

Temperature °C	COD Type	COD Value mm	Scatter of COD due to 0.5% Load Variations mm	
20	δ_m	0.18	± 0.03	
		0.25	0.00	-0.04
		0.24		
		0.19		
0		0.22		
-17		0.28	0.00	-0.04
-31		0.25	± 0.03	
-40		0.22		
-50		0.20		
-55		0.19		
-88		0.27		
-92	δ_u	0.14	± 0.00	

TABLE 15 - COD Values for LS Oriented, Steel (D)
Specimens W = B = 18mm

Temperature °C	COD Type	COD Value mm	Scatter of COD due to 0.5% Load Variation	mm
20	δ_m	1.77	± 0.12	
		1.80	0.12	-0.10
		1.62	0.22	-0.11
-10		1.66		
		1.62	± 0.08	
-48		1.69		
-54		1.59		
		1.85		
-75	δ_u	1.30	± 0.05	
-81		0.73		
-85		0.55		
-90		0.70		
-90		0.60		
-112	δ_c	0.50	± 0.00	
-112		0.41	± 0.00	

TABLE 16- COD Values for ZT Oriented, Steel (D)
Specimens W = B = 18mm

Temperature °C	COD Type	COD Value mm	Scatter of COD due to 0.5% Load Variation	mm
20	δ_m	1.50		$\pm$ 0.16
20		1.65		
20		1.72		
-50		1.49		
-50		1.68		
-63		1.50		
-68		1.29	-0.22	0.05
-80	δ_u	0.62		
-85		0.75		
-95	δ_c	0.40		$\pm$ 0.00
-97		0.38		$\pm$ 0.00

TABLE 17 - COD Resistance Curves for Two Steels. All Tests at 18°C, Crack Length Varies Between 2.85 - 3.15mm W = B = 10 mm

Specimen	Average Crack Growth Δ a, mm	NRC mm	COD $a=a_f$	COD $a=a_f+\Delta a$
LSD	0.00		0.12	0.12
	0.00	0.24	0.23	0.23
	0.00	0.32	0.26	0.26
	0.00	0.33	0.32	0.32
	0.20		0.51	0.49
	0.40		0.60	0.55
	0.58		0.66	0.58
	0.81		0.78	0.65
	1.19		0.79	0.60
	1.92	1.20	0.93	0.57
ZTD	0.00	0.13	0.14	0.14
	0.00		0.25	0.25
	0.00		0.30	0.30
	0.36		0.61	0.58
	0.75	0.79	0.77	0.66
LSS	0.00		0.05	0.05
	0.00		0.12	0.12
	0.00	0.40	0.17	0.17
	0.00	0.30	0.25	0.25
	0.10	0.35	0.38	0.37
	0.23		0.46	0.44
	0.58		0.60	0.52
	1.12		0.61	0.47
	1.50	0.75	0.68	0.48
	2.15		0.75	0.44
ZTS	0.00		0.04	0.04
	0.68		0.11	0.10
	0.90		0.12	0.10
	1.60		0.18	0.12

TABLE 18 - Charpy V Notch Impact Results for Short Specimens (50mm) *

Under Size ZTD (ft lbs)	Full Size ZTD (ft lbs)	Under Size LSD (ft lbs)	Full Size LSD (ft lbs)
111.5	111.5	166.0	166.0
108.5	108.5	166.0	163.0
108.5		163.0	163.0
106.0		160.0	160.0
		160.0	160.0

* all tests at 18 C

TABLE 19 - Charpy V Notch Impact Results LSS Specimens with Holes Drilled Below Notch. *

Distance Below Notch (mm)	Distance Between Hole Centres (mm)	Charpy V Impact (ft lbs)	Strain of Hole in y-Direction
5.0	9.5 x	134.5 x	
5.0	11.0	131.0	
5.0	12.0	165.5	0.16
5.0	12.0	165.5	0.16
5.0	13.5	144.0	0.09

x fracture of material separating holes and crack tip.

* all tests at 18 C

TABLE 20 - Charpy V Notch Impact Results LSD Specimens with Holes Drilled Below Notch.*

Distance Below Notch (mm)	Distance Between Hole Centres (mm)	Charpy V Impact (ft lbs)	Strain of Hole in y-Direction
5.0	8.0	207.5	0.30
5.0	8.5	165.0	0.26
5.0	10.7	177.5	0.07
5.0	12.3	162.5	0.06
3.5	11.2	173.0	0.17
3.5	11.5	167.0	0.18
3.5	13.5	163.0	0.09
3.0	9.3	163.0	0.18

* all tests at 18 C

TABLE 21 - Effect of Free Surfaces in the y-Directionon the COD of W = B = 10mm LSS & LSD Specimens at18°C

Specimen	COD_m mm	Free Surface to Notch Separation mm
LSS	0.72	5.00
	0.75	4.50
	0.74	4.25
	0.76	3.65
	0.92	3.50
	1.00	3.00
	1.15	2.75
	1.26	2.55
	1.88	2.15
LSD	0.88	4.50
	0.90	4.25
	1.00	4.20
	0.93	4.05
	1.08	3.30
	1.10	3.10
	1.21	2.90
	1.24	2.90
	1.97	2.50
	1.99	2.50
	0.94*	2.00

* Ductile shear rupture of ligament between notch tip and hole.

TABLE 22- Results from Undersized, As-Welded Specimens showing COD Variations with position in plate
W = B = 10mm.

For ZTD

δ_m As-Welded 25mm Central Section	δ_m As-Welded 12.5mm Central Section
0.74mm EBW	0.74mm EBW
0.78mm EBW	0.74mm EBW
0.72mm FW	0.74mm FW
0.84mm FW	0.80mm FW
As-Welded 25mm Edge Section	**As-Welded 12.5mm Edge Section**
0.70mm EBW	0.72mm EBW
0.78mm EBW	0.80mm EBW
0.78mm FW	0.82mm FW
0.72mm FW	0.72mm FW

For ZTS

As-Welded 25mm Central Section	As-Welded 12.5mm Central Section
0.22mm EBW	0.22mm EBW
0.19mm EBW	0.20mm EBW
0.22mm FW	0.15mm FW
0.20mm FW	0.23mm FW
As-Welded 25mm Edge Section	**As-Welded 12.5mm Edge Section**
0.20mm EBW	0.20mm EBW
0.14mm EBW	0.15mm EBW
0.22mm FW	
0.18mm FW	

All tests conducted at 18°C

TABLE 23 - COD Values for Quenched and Tempered Specimens of Parent Plate Steel D
W = B = 10mm

Specimen	Temperature °C	CODmm	COD Type
LSD	20	0.53	δ_m
	20	0.59	
	-40	0.58	
	-70	0.62	
	-130	0.53	
	-130	0.58	
	-145	0.20	δ_c
	-145	0.18	δ_c
ZTD	20	0.54	δ_m
	20	0.49	
	20	0.55	
	-130	0.57	
	-132	0.59	
	-150	0.15	δ_c

TABLE 24 - COD Values for Quenched and Tempered Specimens of Parent Plate Steel S
W = B = 10mm

Specimen	Temperature °C	CODmm	COD Type
LSS	20	0.50	δ_m
	20	0.53	
	20	0.56	
	-130	0.57	
	-130	0.49	
	-149	0.15	δ_c
ZTS	20	0.13	δ_m
	20	0.15	
	20	0.15	
	-132	0.13	
	-159	0.09	δ_c

TABLE 25 - COD Values for Hot Rolled, Welded and Quenched and Tempered Specimens of Steel D
W = B = 10mm

Hot Rolling Strain	Specimen	Welding Technique	Temperature °C	CODmm	COD Type
0.75	LSD	FW	20	0.59	δ_m
		FW	10	0.65	
		EBW	-35	0.65	
		EBW	-130	0.46	
		FW	-145	0.12	δ_c
0.50	ZTD	FW	20	0.49	δ_m
		EBW	20	0.43	
		EBW	20	0.42	
		FW	-30	0.50	
		FW	-79	0.45	
		FW	-136	0.32	δ_c
0.75	ZTD	FW	20	0.45	δ_m
		EBW	20	0.50	
		EBW	20	0.40	
		FW	-110	0.48	
		FW	-117	0.40	
		EBW	-147	0.19	δ_c

TABLE 26 - COD Values for Hot Rolled, Welded and Quenched and Tempered Specimens of Steel S
W = B = 10mm

Hot Rolling Strain	Specimen	Welding Technique	Temperature °C	CODmm	COD Type
0.50	ZTS	FW	20	0.06	δ_m
			20	0.07	
			20	0.07	
			-100	0.04	δ
0.50	ZRS	FW	20	0.08	δ_m
			20	0.12	
			20	0.04	
			-60	0.06	δ
0.75	ZTS	FW	20	0.06	δ_m
			20	0.05	
			20	0.05	

TABLE 27 - Variation of COD with Crack Length (a) for 10mm, Three Point Bend, ZR and ZT Orientated, Clean Steel (D) Specimens

Crack Length (a) mm	COD (δ_m) mm	Specimen
2.22	1.10	ZTD
2.30	1.05	ZTD
2.58	0.96	ZRD
2.78	0.82	ZTD
2.84	0.84	ZRD
2.85	0.90	ZRD
2.87	0.86	ZRD
2.92	0.89	ZTD
2.94	0.76	ZTD
3.05	0.86	ZTD
3.16	0.80	ZTD
3.25	0.74	ZTD
3.33	0.75	ZTD
3.35	0.78	ZTD
3.38	0.73	ZTD
3.40	0.80	ZRD
3.44	0.72	ZTD
3.51	0.76	ZRD
3.68	0.64	ZRD
3.70	0.70	ZTD
3.83	0.69	ZRD
4.05	0.64	ZTD
4.48	0.59	ZTD

All tests at 18°C

TABLE 28 - COD Variation with Ligament Length (W - a) for 18 x 8.2 x 72 Specimens in Three Point Bend and Fixed Grip Tension. Tests at 20°C.

Specimen	Ligament Length (W - a) mm	COD δ_m Calculated mm	COD δ_m Rubber Infiltration mm
LSD SENB	5.0	0.68	0.64
	5.7	0.75	
	7.6	0.98	0.90
	11.9	1.61	1.57
LSD $SENT_{fg}$	5.0		1.10
	7.5		1.13
	7.6		1.48
	11.9		2.13

TABLE29 - Surface COD Measurements for Plasticine in Four Point Bend (SENB4) and Fixed Grip Tension (SENTfg)
B = 10.2mm

W mm	a mm	W - a mm	a/W	$COD_{SENT_{fg}}$ mm	COD_{SENB4} mm
11.0	5.0	6.0	0.45	3.0	2.8
14.0	7.0	7.0	0.50	4.2	3.3
30.0	21.0	9.0	0.70	3.8	2.5
32.0	22.0	10.0	0.69	5.0	2.2
15.0	3.5	11.5	0.23	4.8	2.2
16.0	4.2	11.8	0.26	2.7	2.2
20.0	5.2	14.8	0.26	3.8	3.0
21.0	4.2	16.8	0.20	3.1	3.0
22.0	4.0	18.0	0.18	3.8	2.8
38.0	14.0	24.0	0.37	4.0	3.2
39.0	7.5	31.5	0.20	4.0	3.4

TABLE 30 - The Dependance of K_Q on Specimen Thickness, B, for Constant (W - a) Ligament and for Constant Geometry (W = 2B, a/W = 0.53 - 0.61).

A. For Constant Ligament (W - a)

1. Quenched and Tempered High Strength Steel.

B mm	W mm	a/W	(W - a)	K_Q MN $m^{-3/2}$
25.00	50.00	0.327	34.0	145.0
25.00	50.00	0.339	33.0	141.0
37.70	76.20	0.526	36.0	153.0
37.70	76.20	0.511	37.0	174.0

2. HY 130 Steel

25.00	50.00	0.370	31.5	168.7
38.00	76.00	0.530	35.4	163.4
50.00	100.00	0.620	38.0	184.0
50.00	100.00	0.630	37.0	181.9

B. For Constant Geometry W = 2B, a/W = 0.53 - 0.61

Quenched and Tempered High Strength Steel.

25.00	50.00	0.610	19.5	115.6
25.00	50.00	0.540	23.0	158.4
25.00	50.00	0.530	23.5	176.6
37.00	76.20	0.530	36.0	155.9
76.00	150.00	0.530	70.0	276.0
76.00	150.00	0.530	71.0	266.0

FIGURES

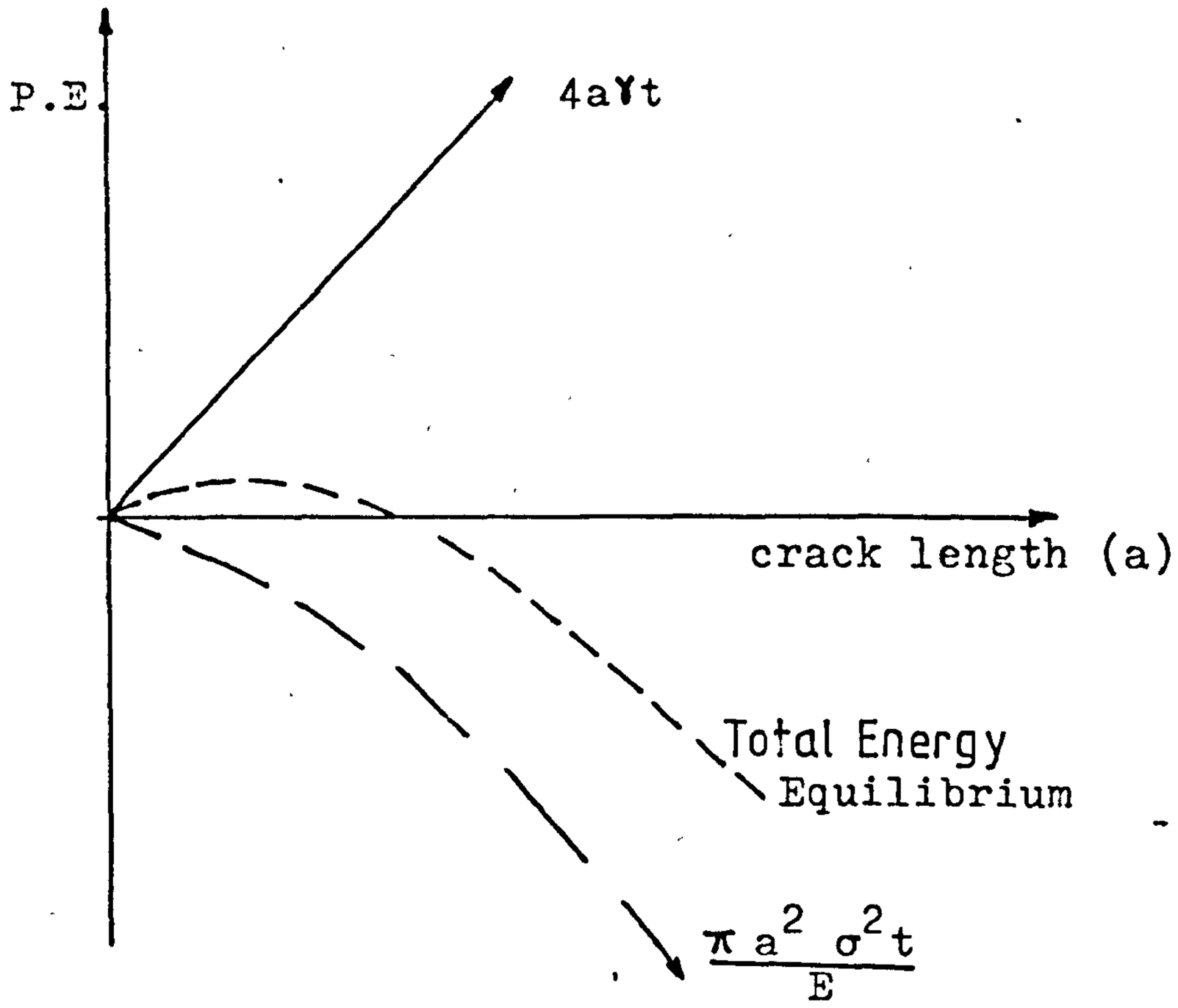

FIG 1. Griffith's Energy Balance Approach to Fracture

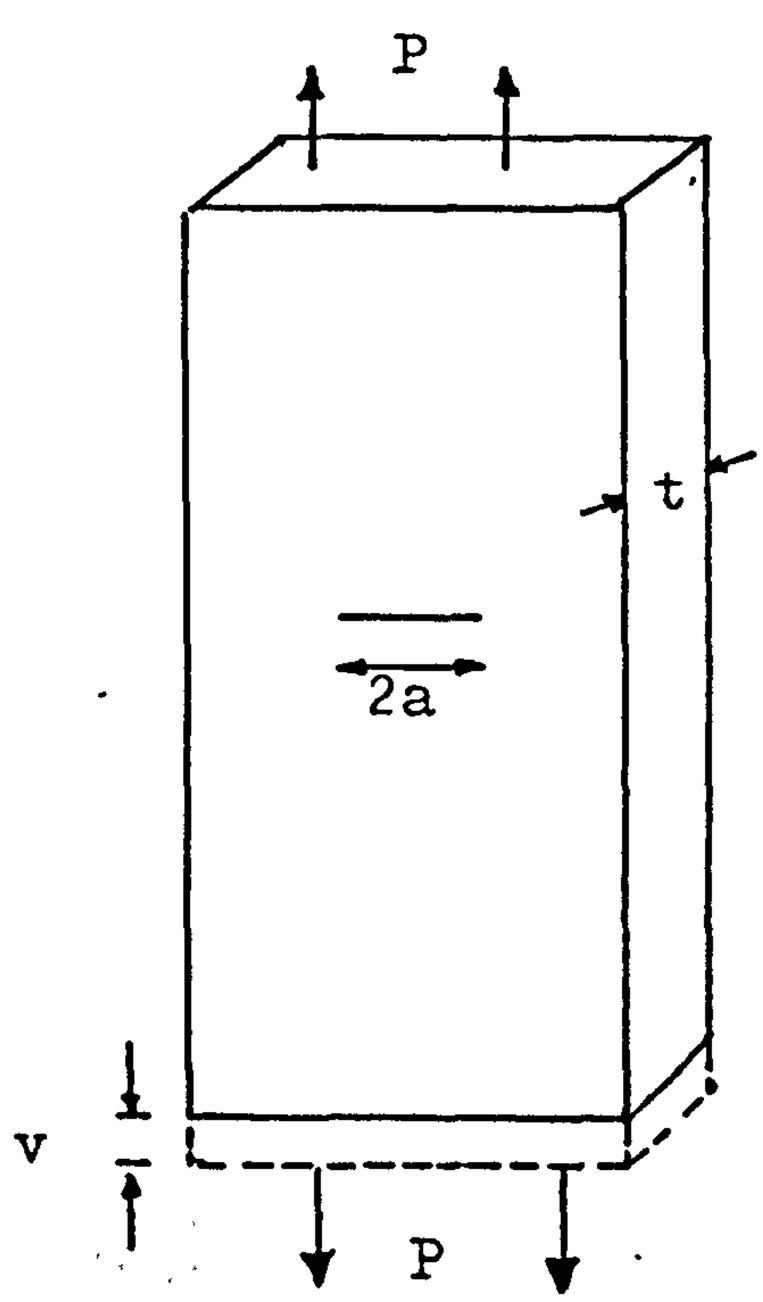

FIG 2 Compliance of a Body with Central Crack

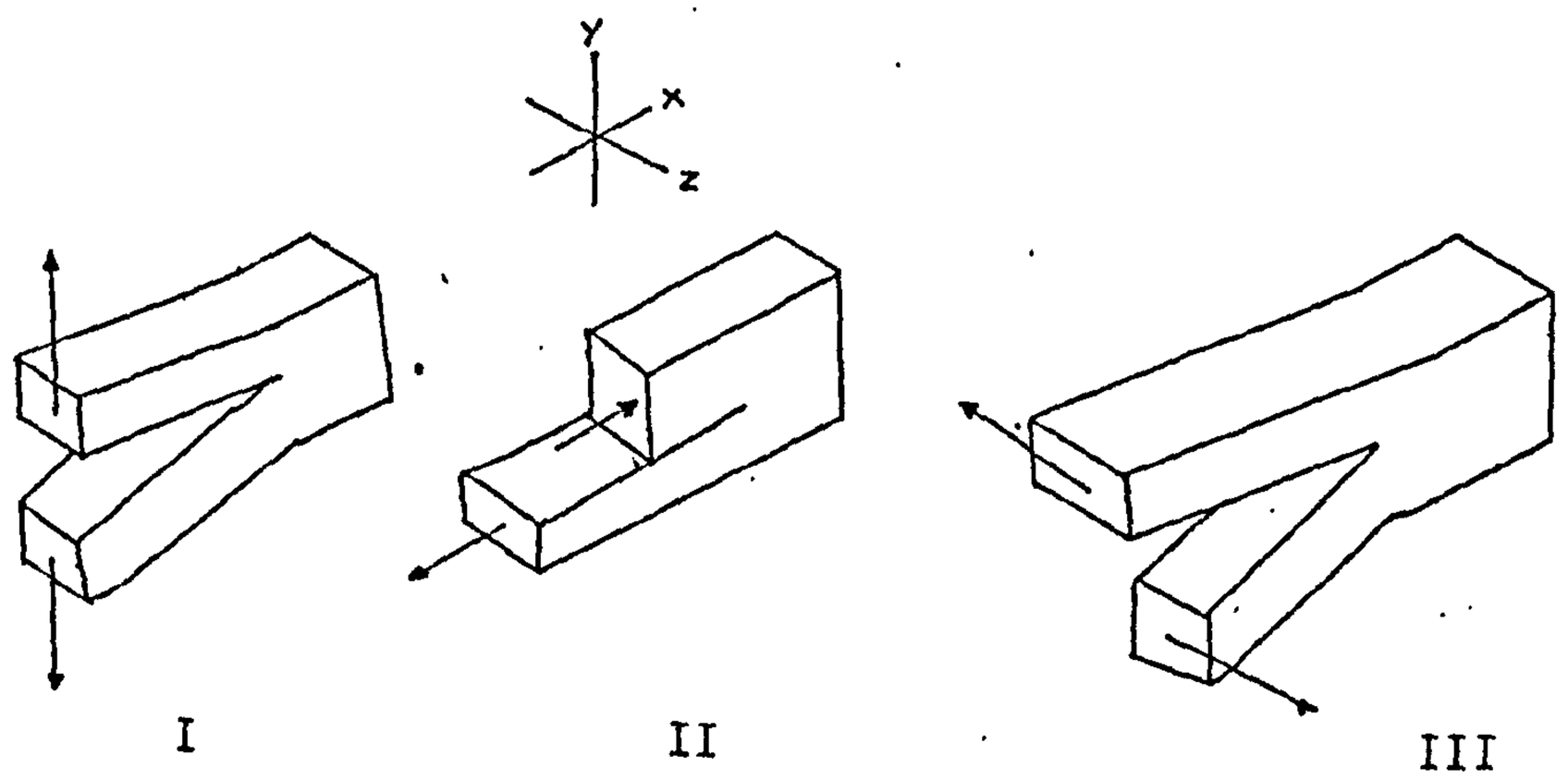

FIG 3. The Basic Modes of Crack Surface Displacements

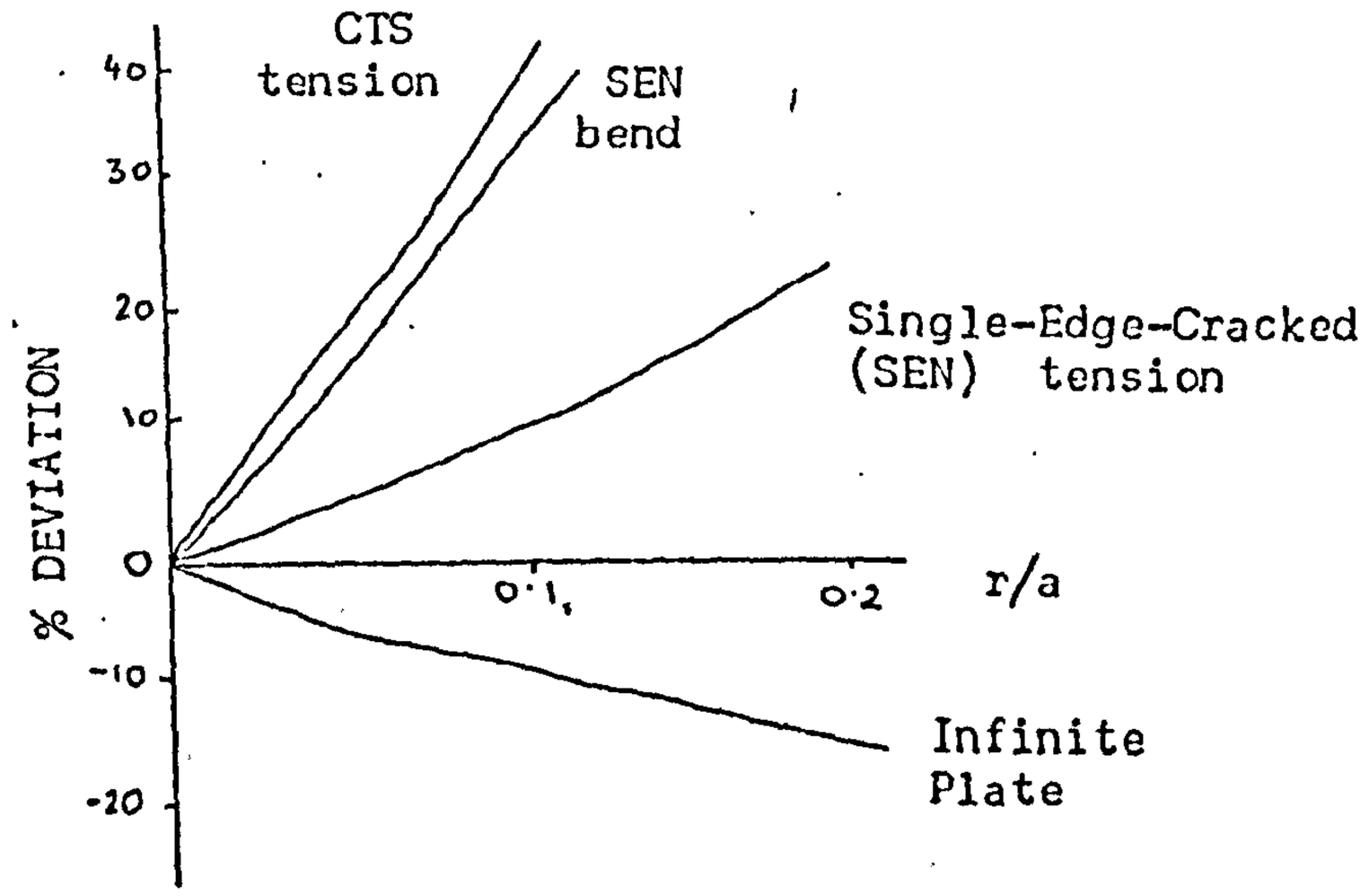

FIG 4. Variation Between Crack Tip Stress as Calculated from K and that Calculated from the Full Series of r, Plotted Against Non-Dimensional Distance Ahead of the Crack Tip, r/a.

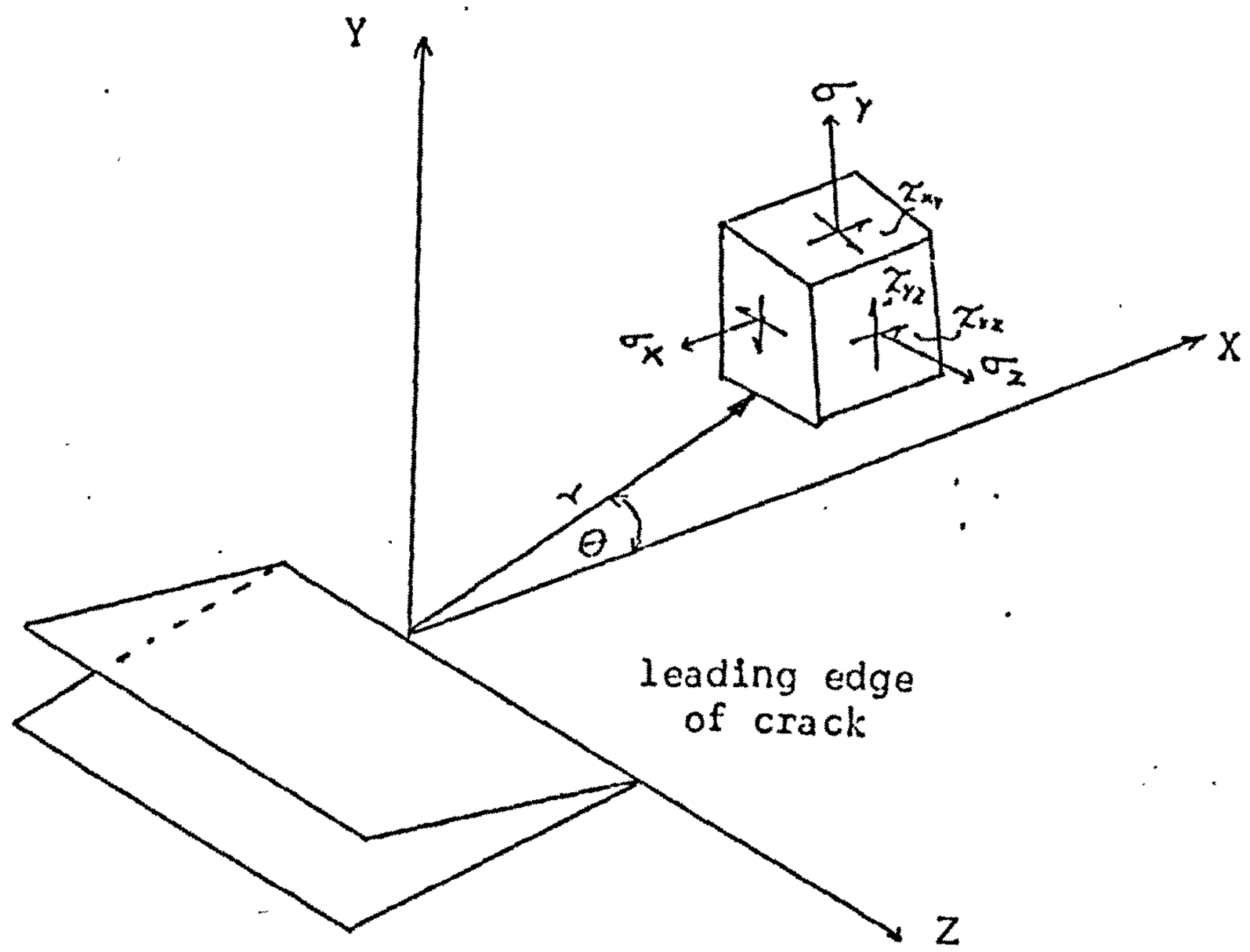

FIG 5. Coordinates Measured from the Leading Edge of a Crack and the Stress Components in the Crack Tip Stress Field.

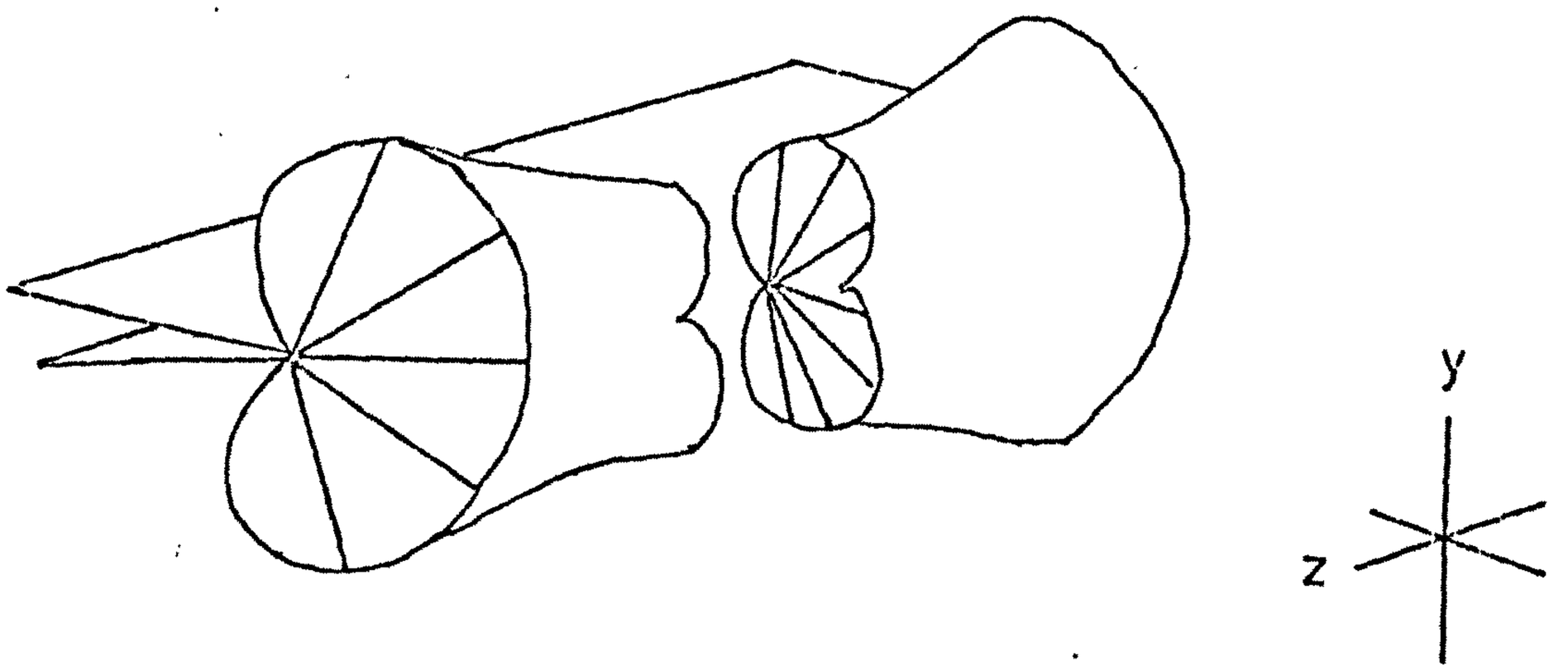

FIG 6. Plastic zone at the crack tip

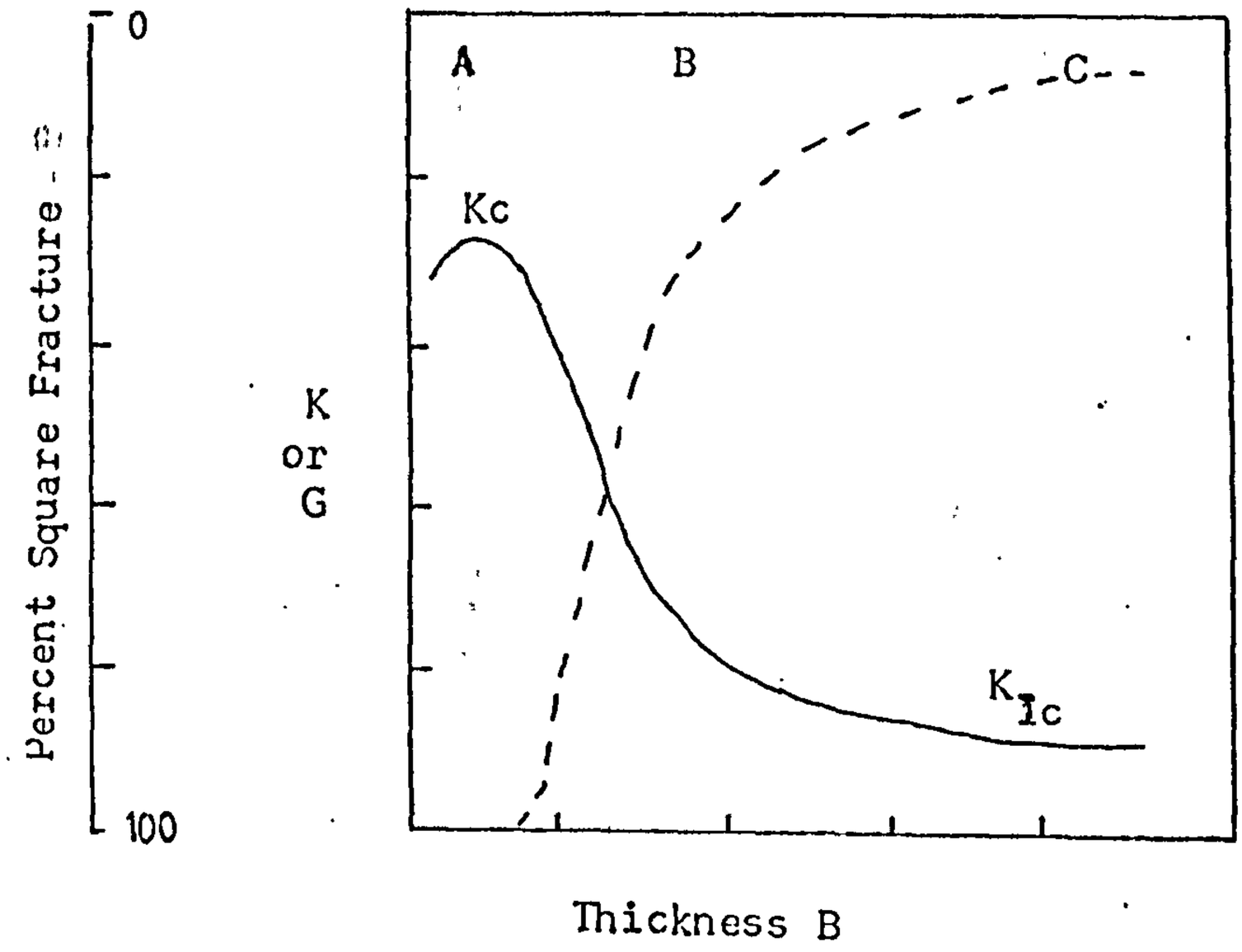

FIG 7. Variation of Toughness with Thickness and Fracture Appearance.

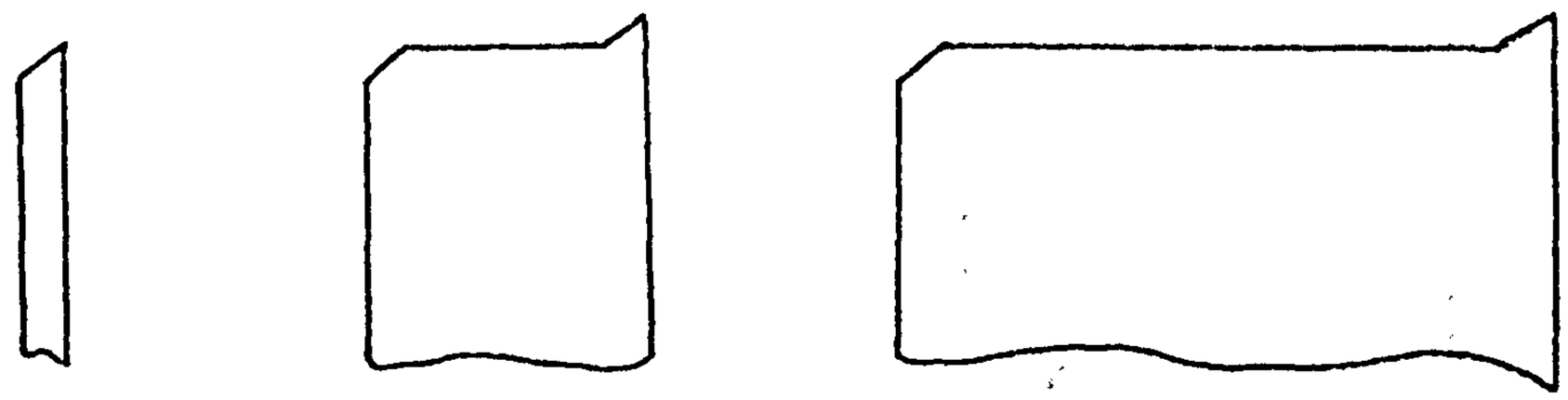

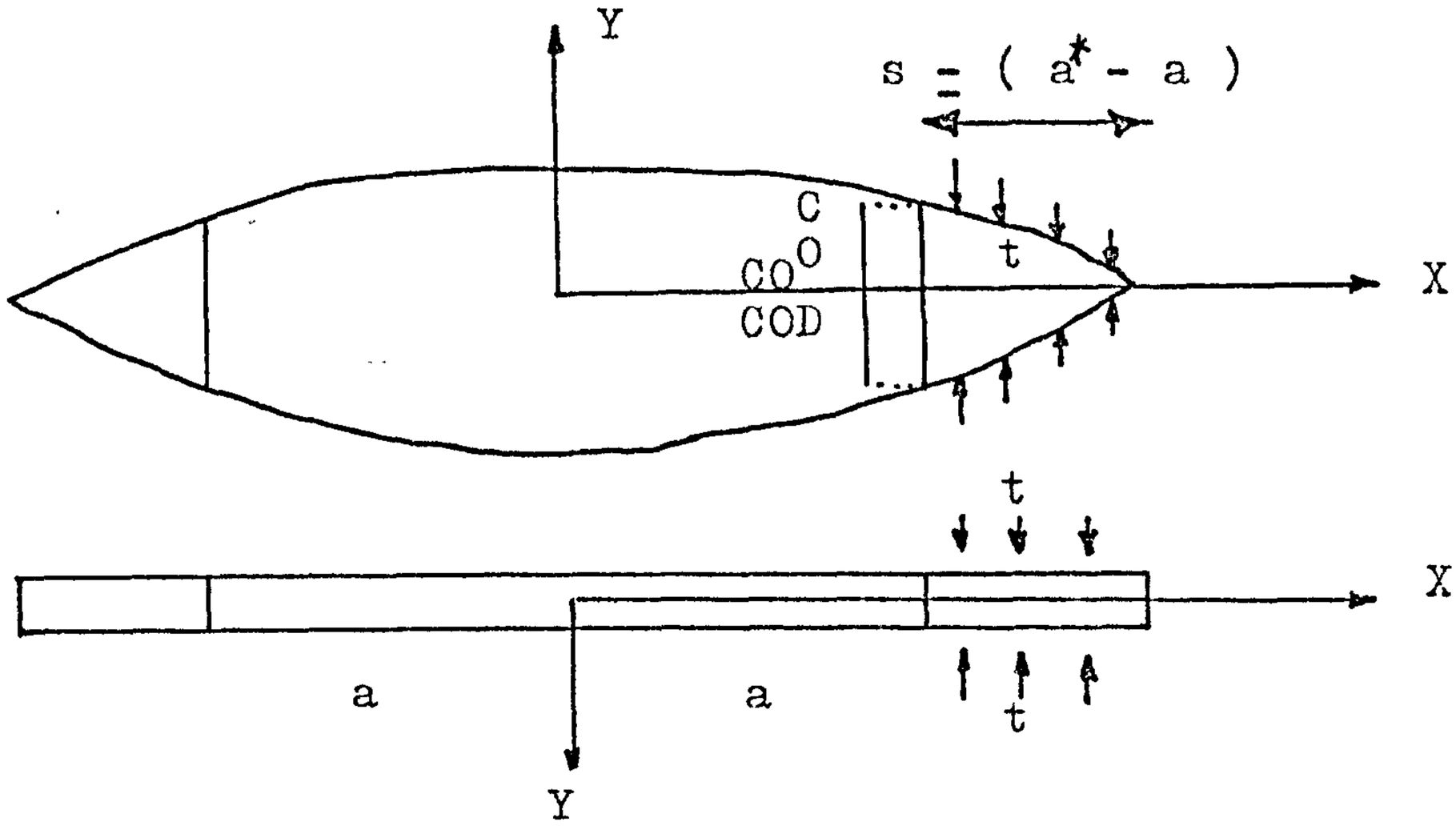

FIG 8. The Dugdale Strip Yield Model for Crack Tip Plasticity

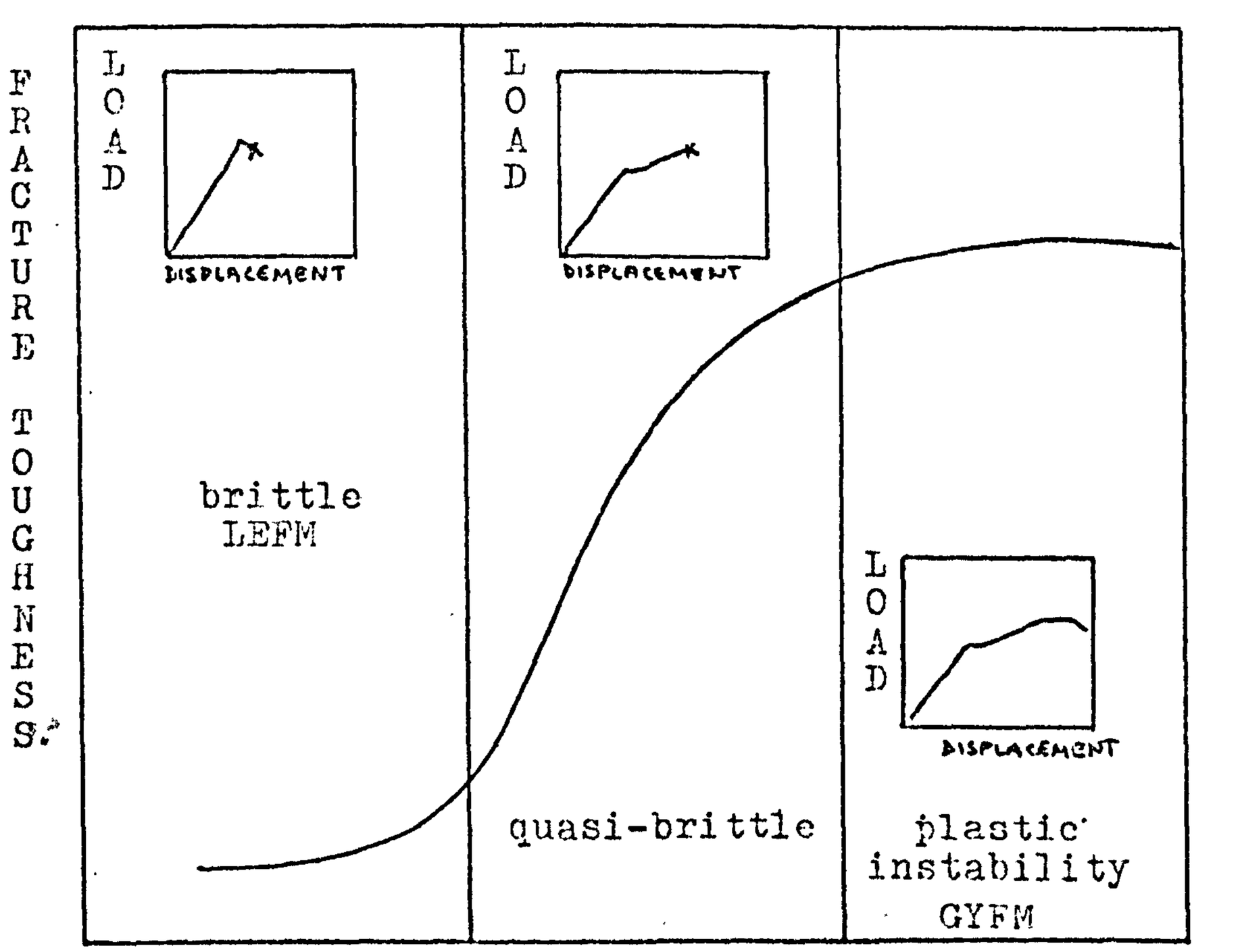

FIG 9. Generalised Models of Instability in Fracture Toughness Testing

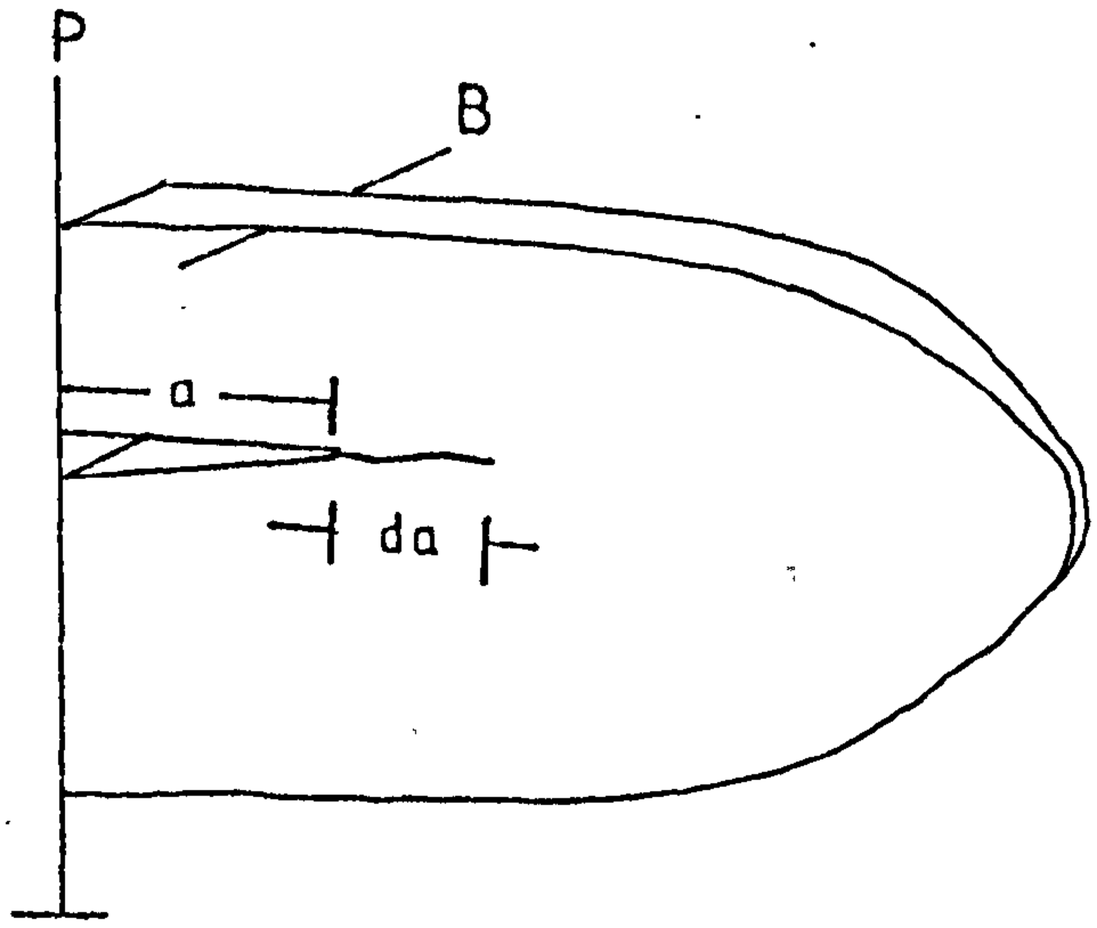

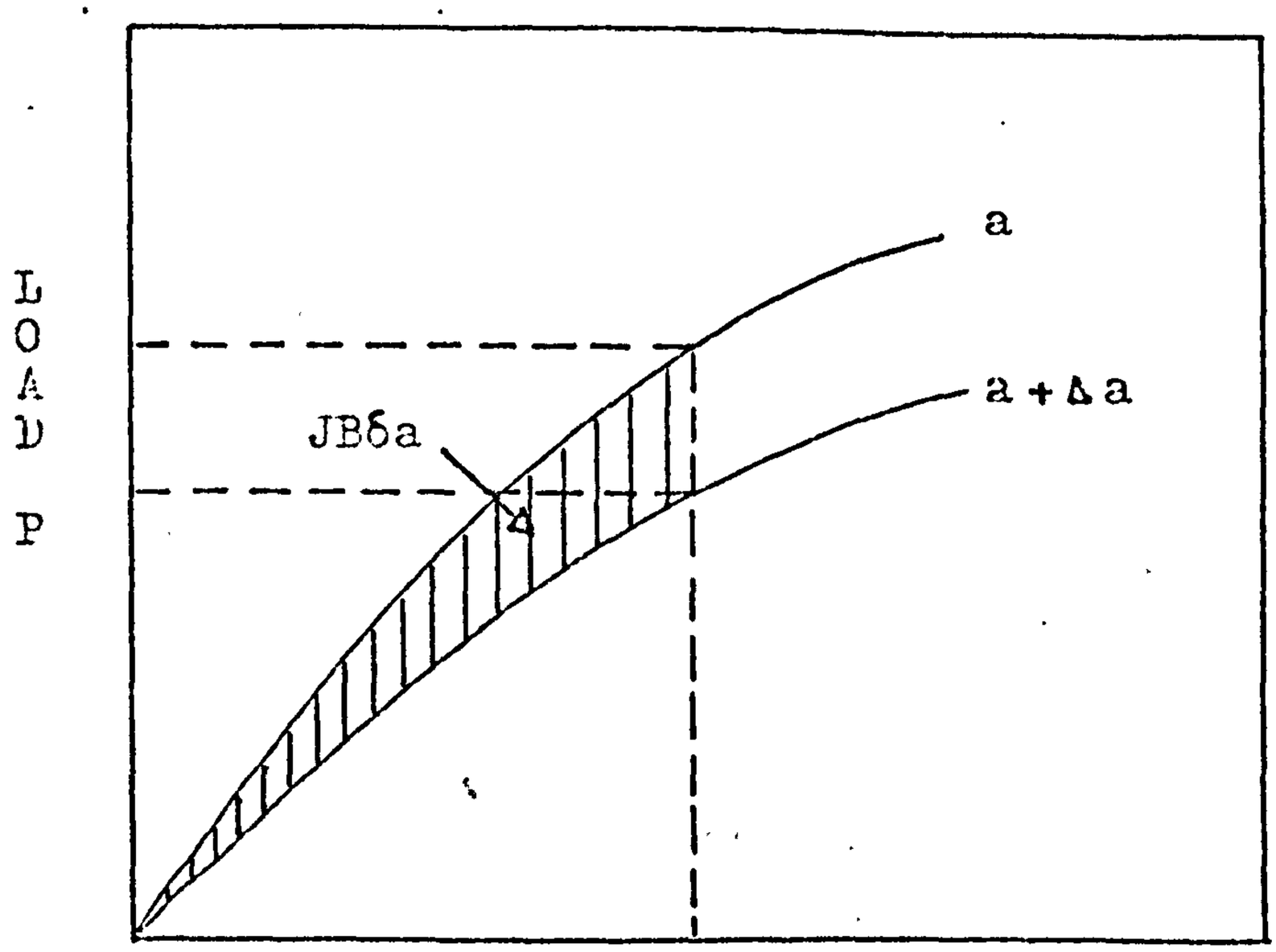

FIG 10. Interpretation of Measured J Integral

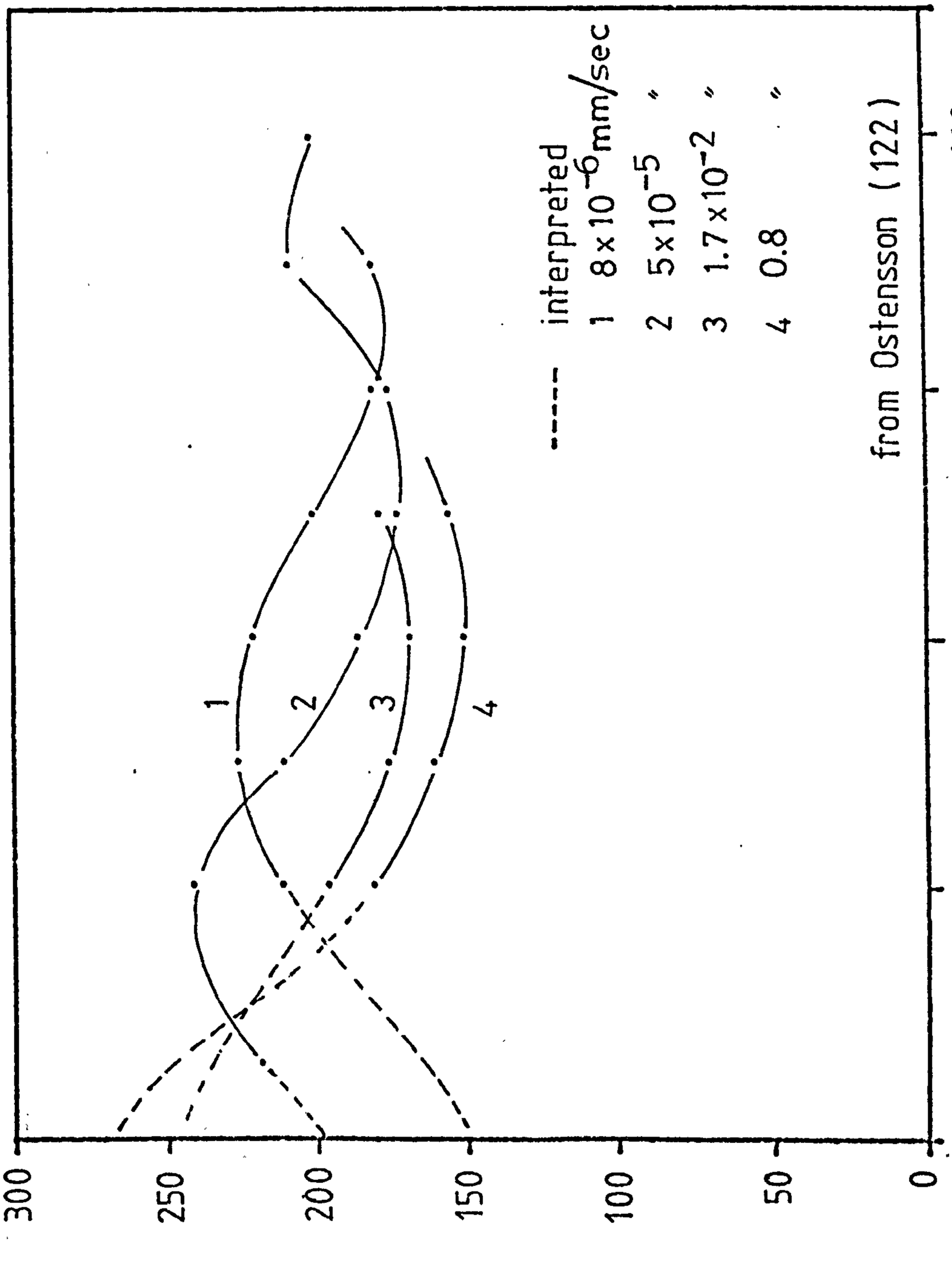

FIG 11. STRAIN RATE EFFECTS ON FRACTURE TOUGHNESS K_{Jc} FOR ASTM A533B STEEL

(for clarity, the plastic zone is omitted in f - h)

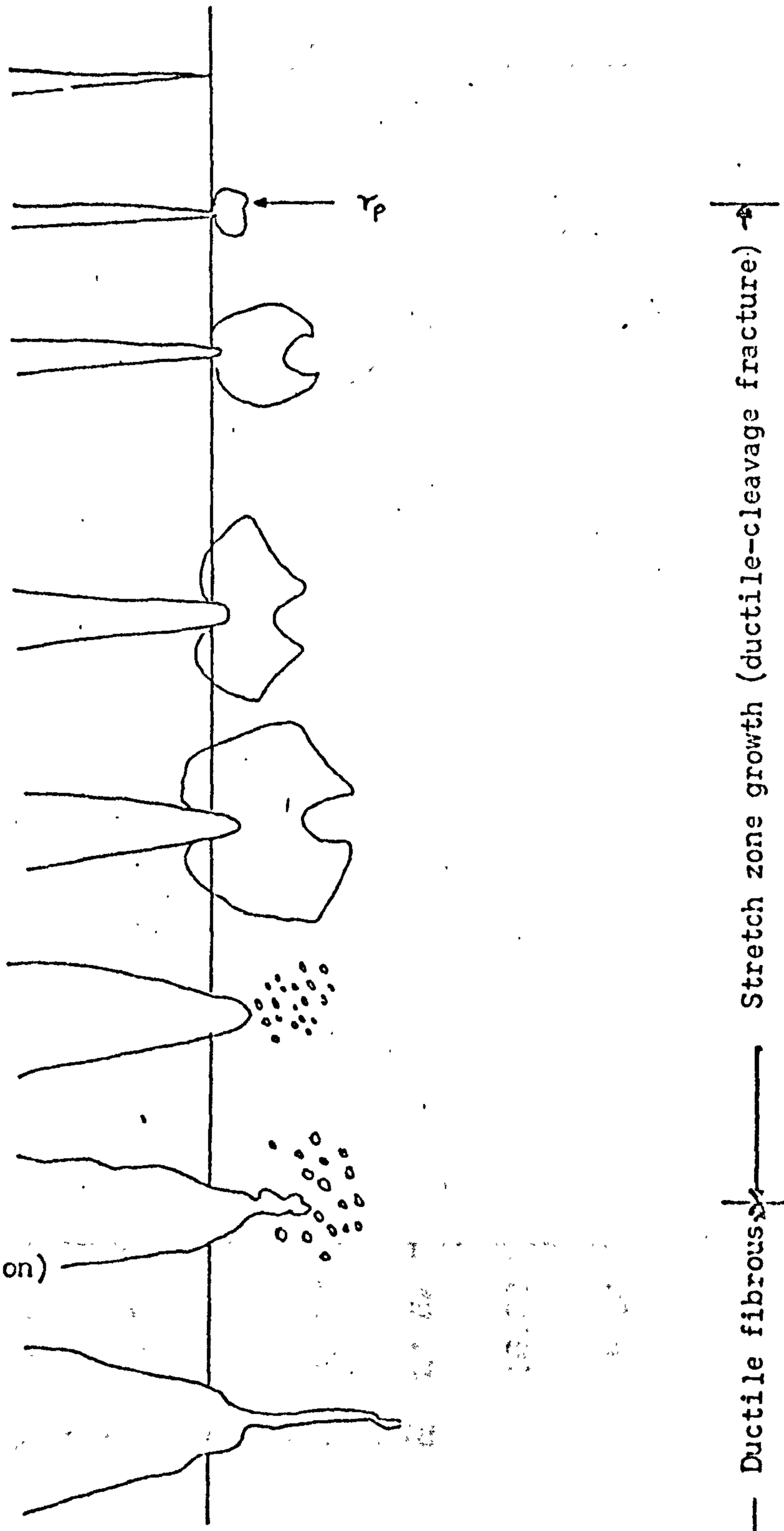

FIG 12. Plastic Zone Developments through Void Formation, Growth and Coalescence Leading to Ductile Crack Growth

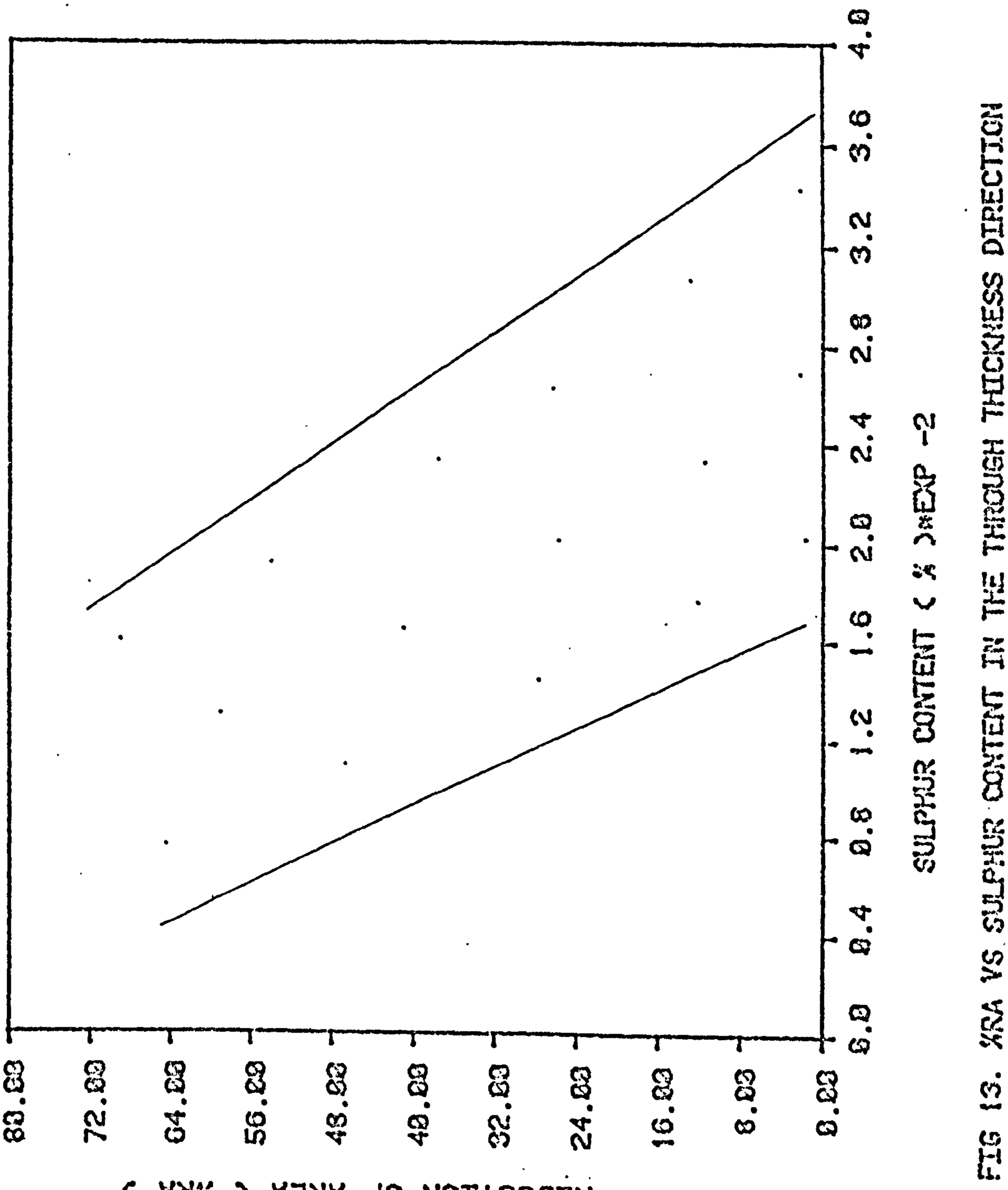

FIG 13. %RA VS SULPHUR CONTENT IN THE

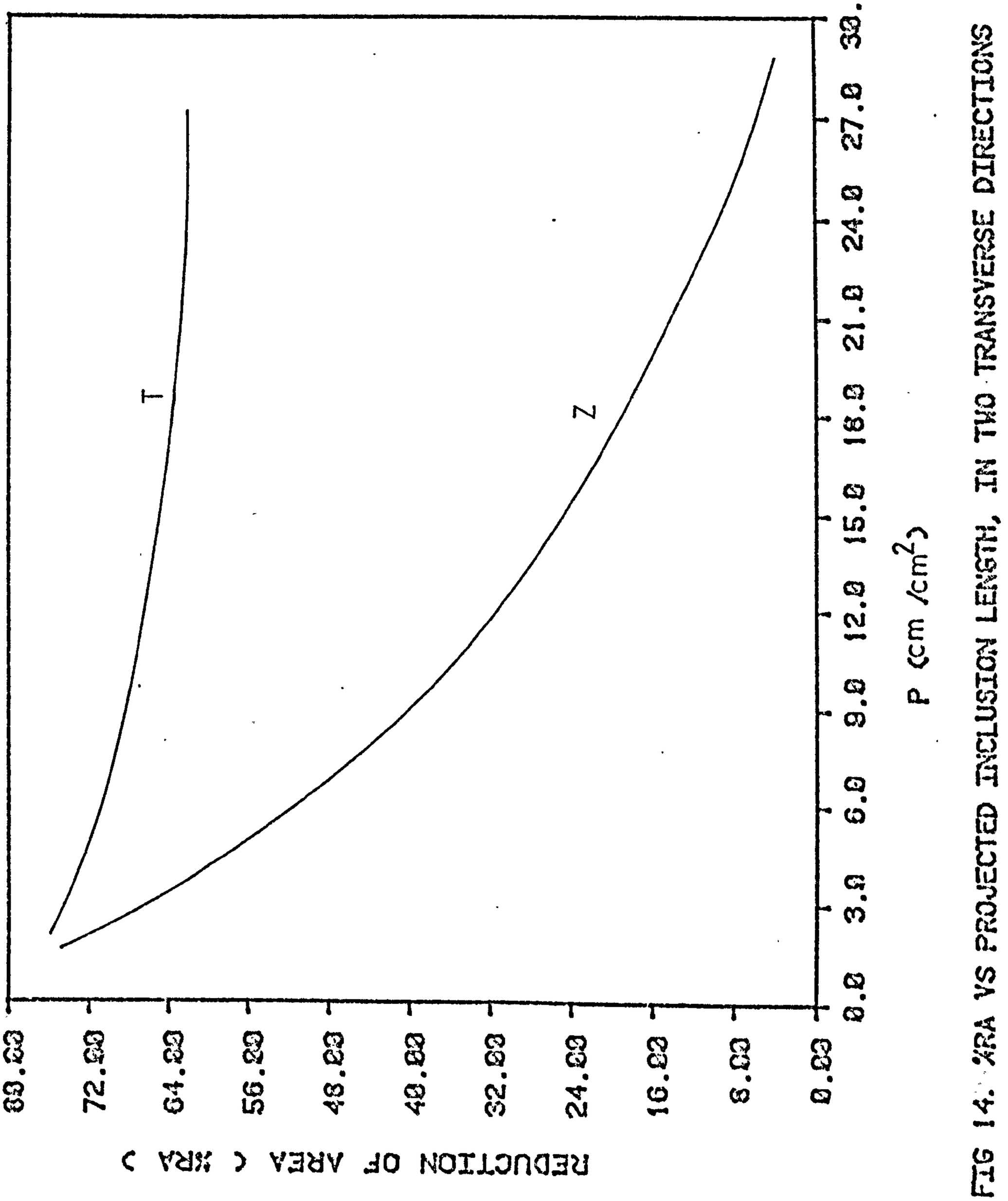

FIG 14: %RA VS PROJECTED INCLUSION LENGTH, IN TWO TRANSVERSE DIRECTIONS

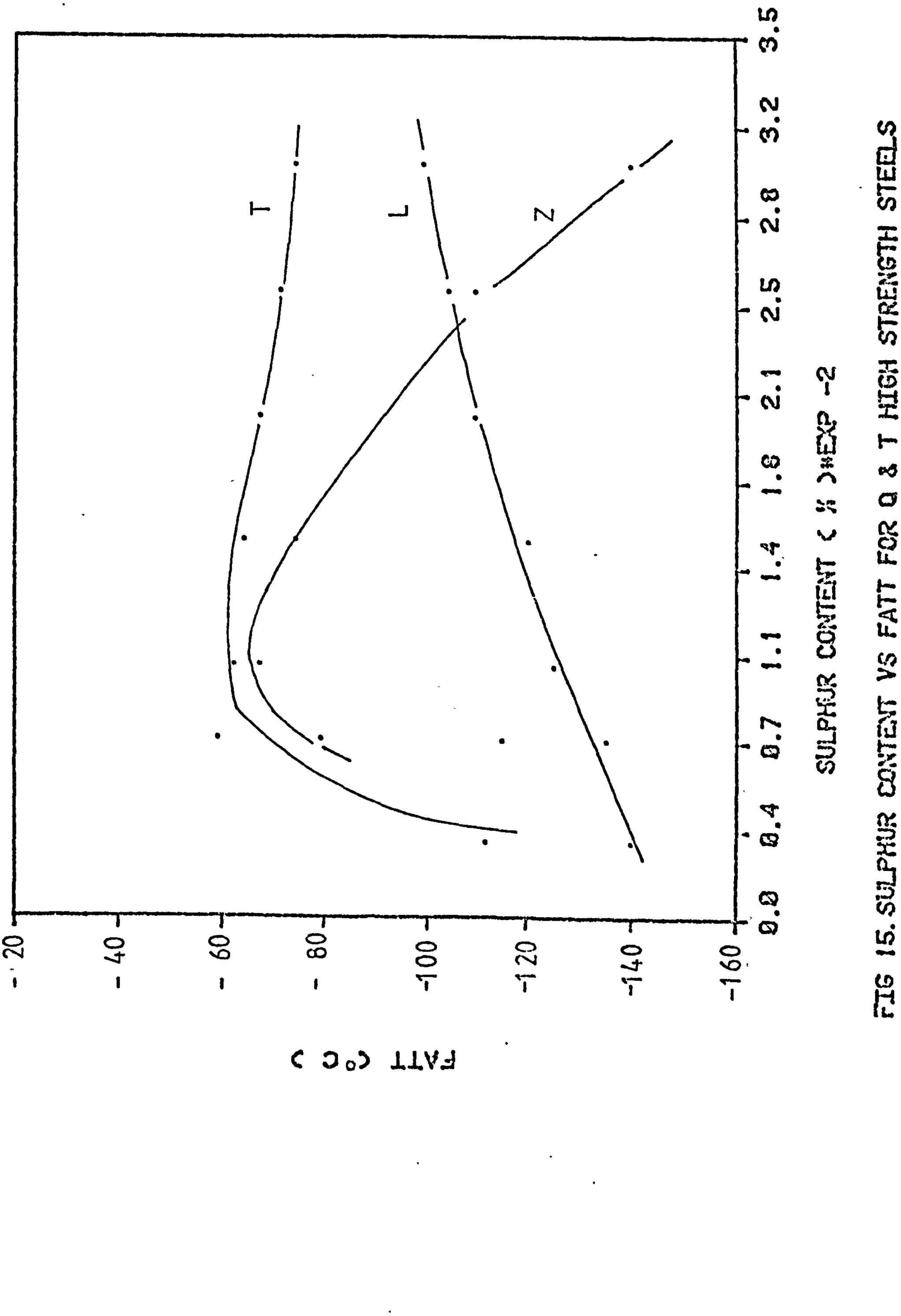

FIG 15. SULPHUR CONTENT VS FATT FOR Q & T HIGH STRENGTH STEELS

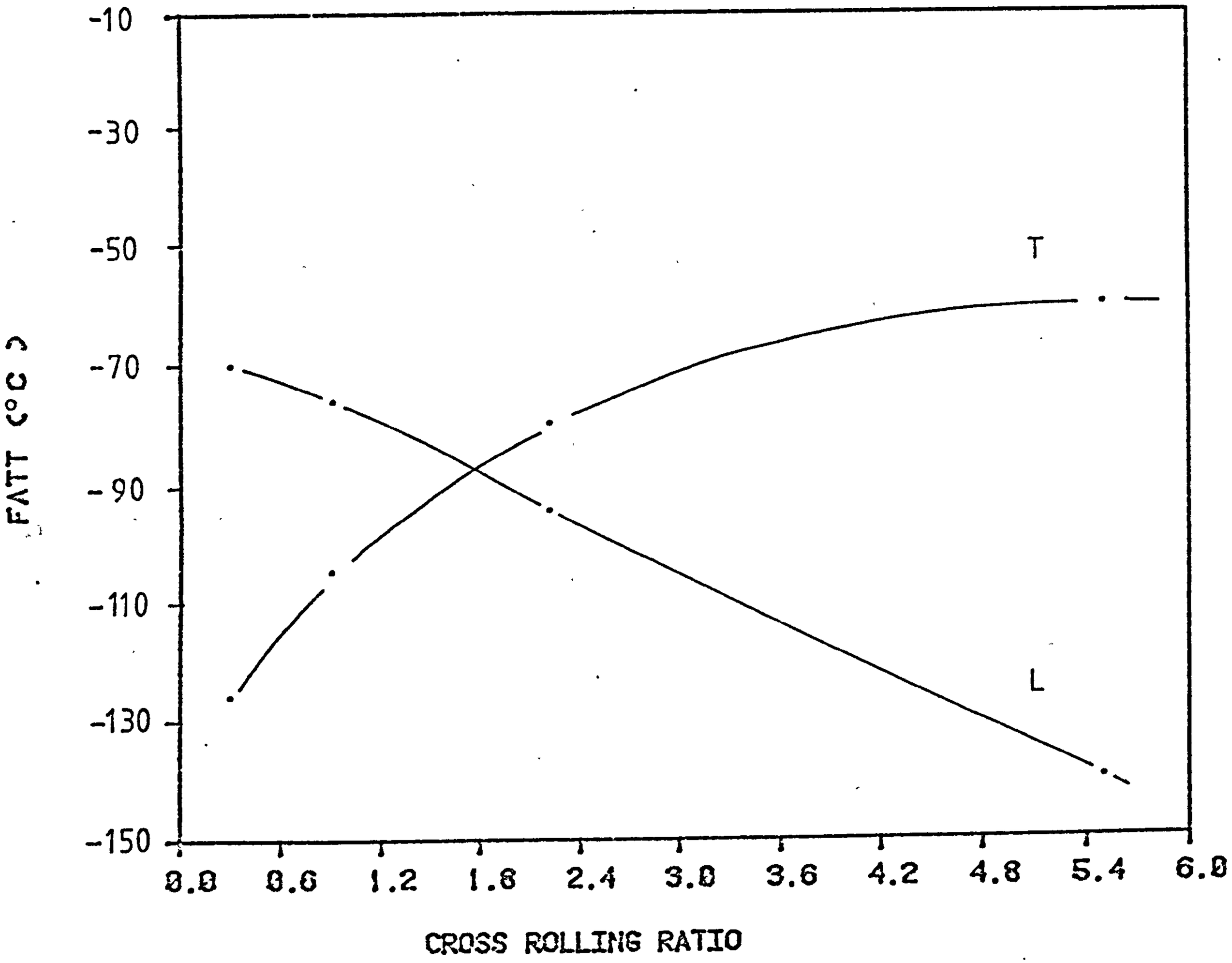

FIG 16. CROSS ROLLING AND THE ANISOTROPY OF FATT

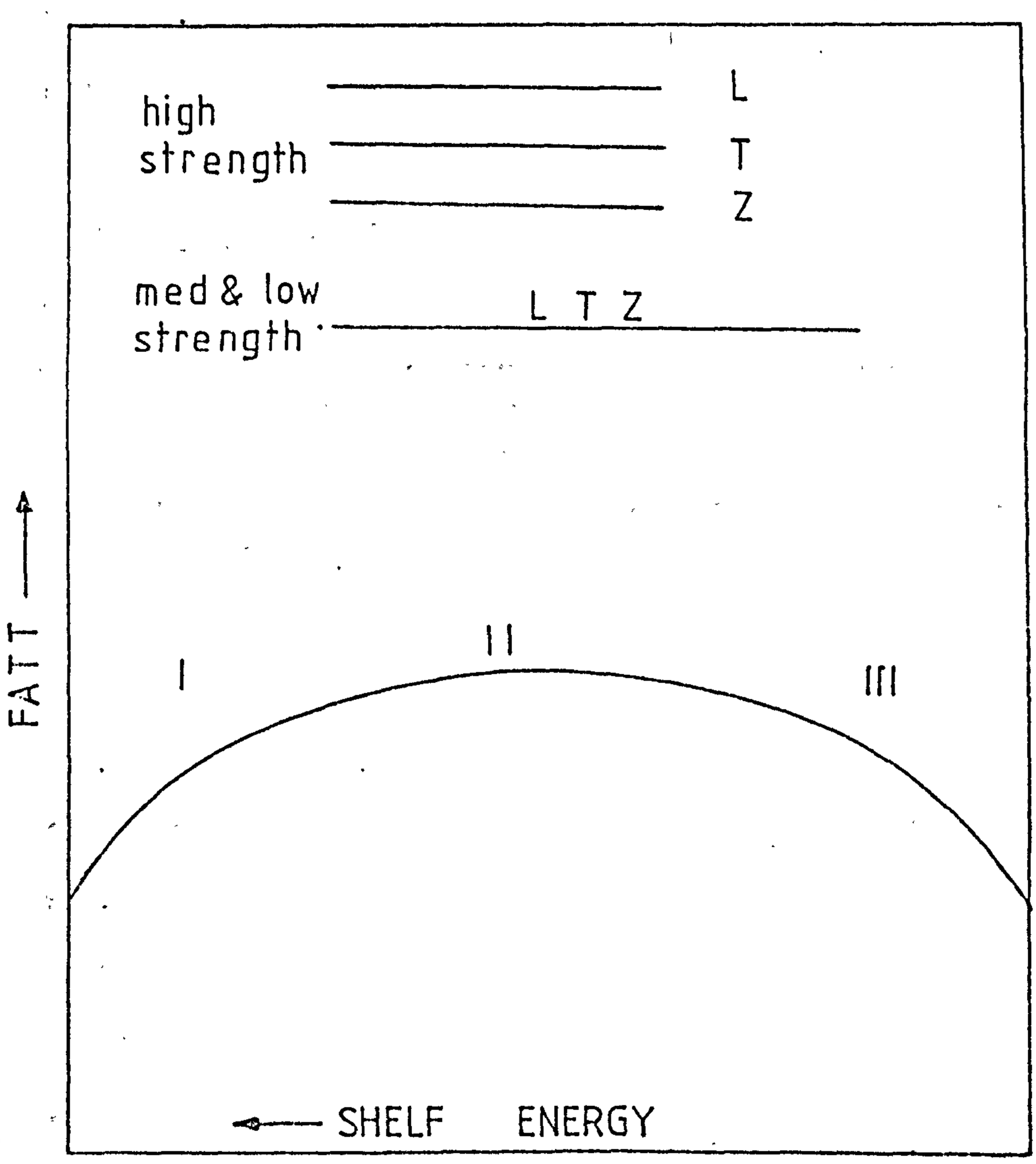

FIG. 17. Generalized Relationship Between Mn S and F.A.T.T.

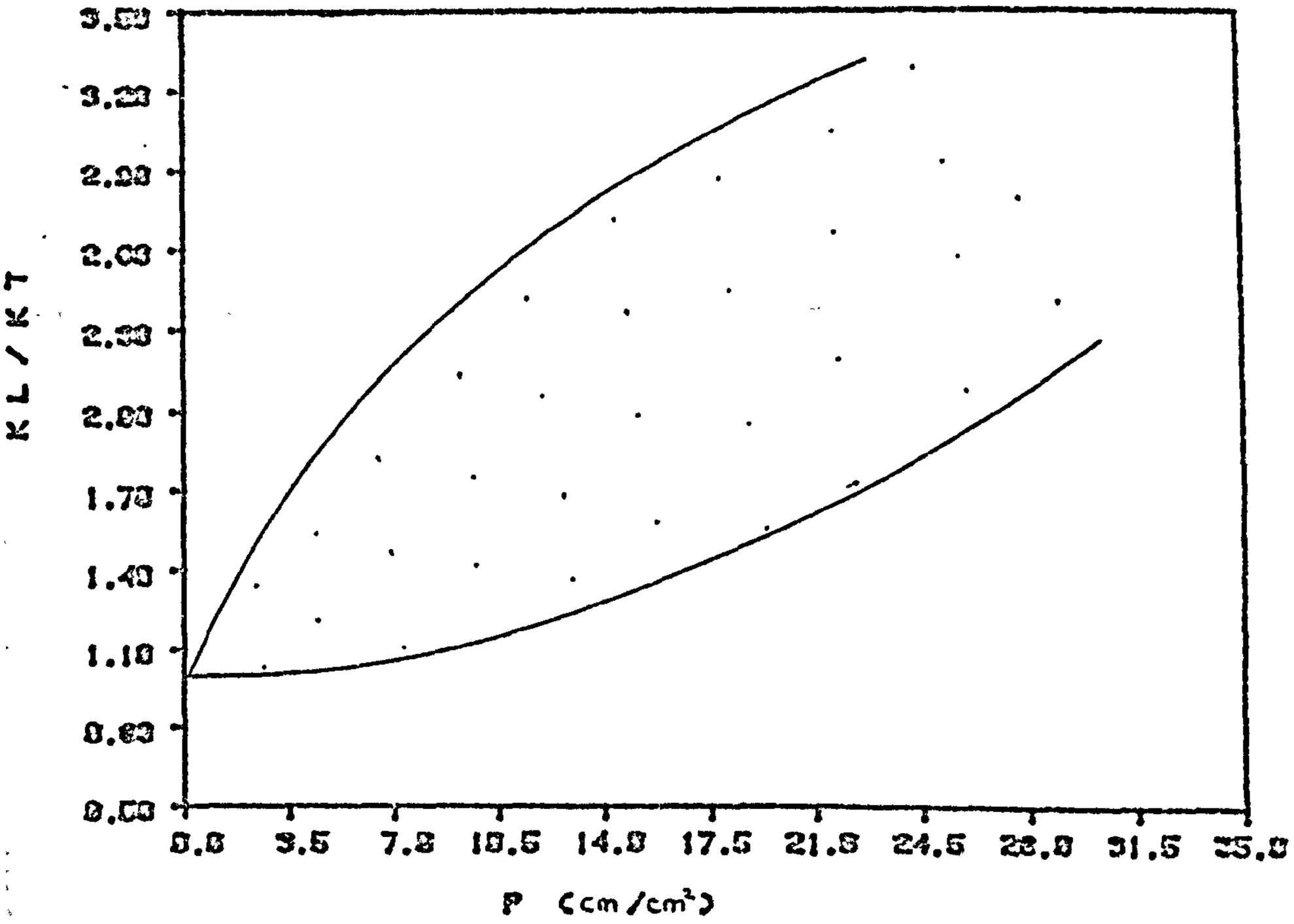

FIG 18 CHARPY ANISOTROPY AS A FUNCTION OF PROJECTED INCLUSION LENGTH

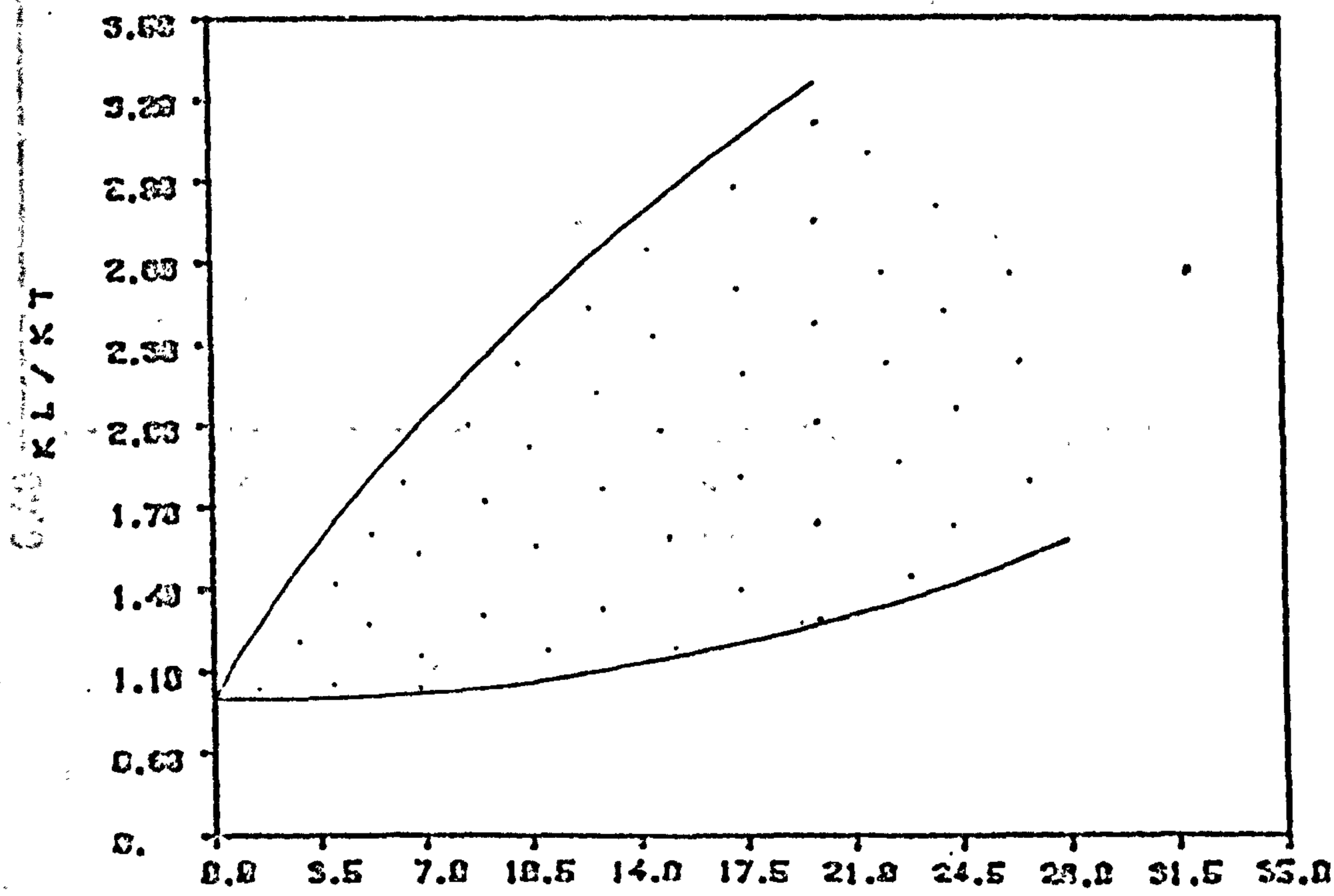

FIG 19 CHARPY ANISOTROPY AS A FUNCTION OF SULFUR CONTENT

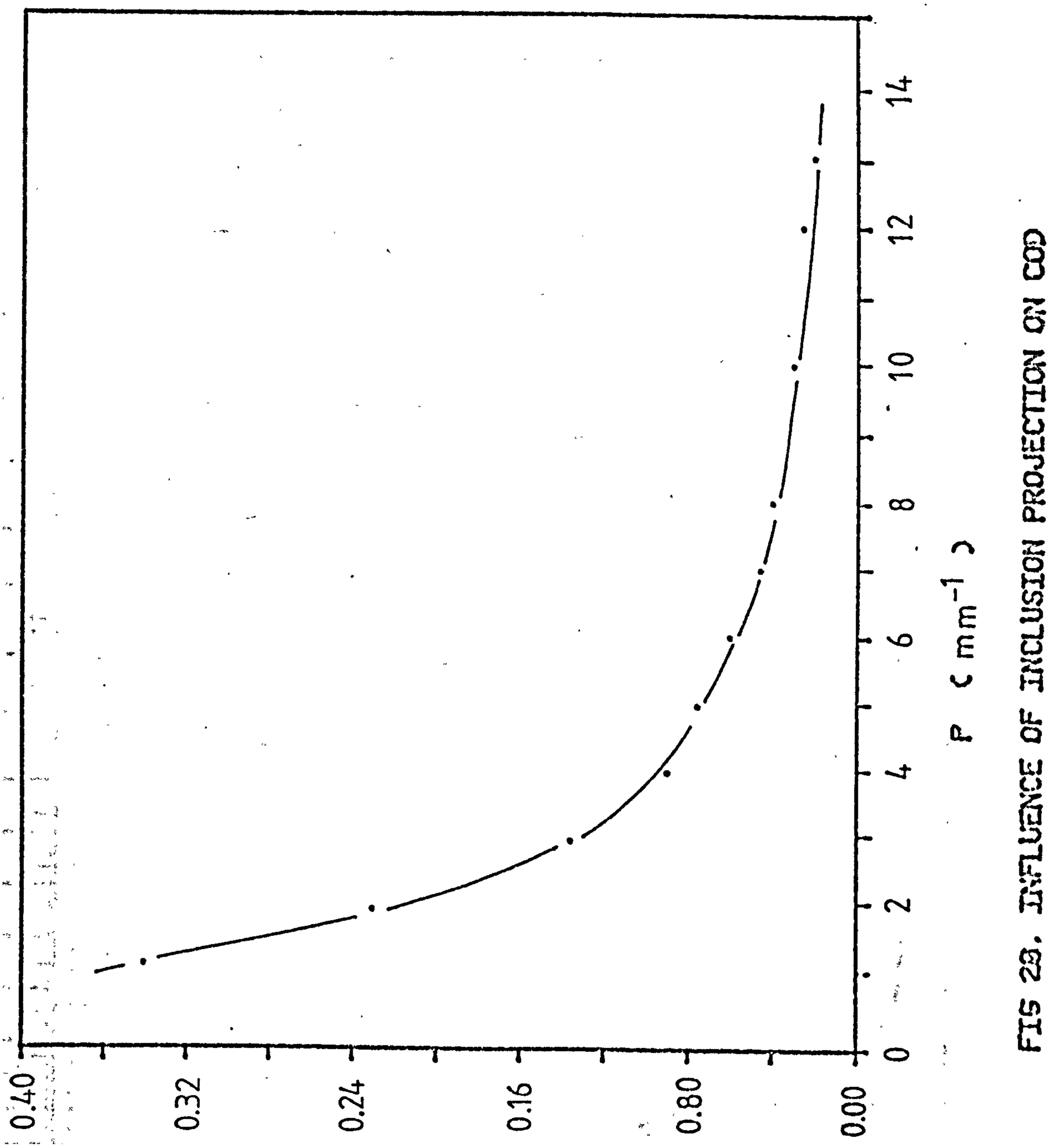

FIG 29. INFLUENCE OF INCLUSION

Laboratory General Atomic Researcher ..... Date .....

Sample .....

KeV ..... Seconds ..... Take off Angle .....

L alpha lines

FE NI ZN GE SE KR SR ZR MO RU PD CD SN TE XE SA CE ND SM GD DY ER Y3 HF W OS PT HG
CO CU GA AS BR RB Y NB TC RH AG IN SB CS LA PR PM EU TB HO TM LU TA RE IR AU

Figure 21 – X-ray Microprobe Analysis of Steel D Showing Complex Oxide Inclusion

O F NE NA MG AL SI P S CL AR K CA SC TI V CR MN FE CO NI CU ZN GA GE

K alpha lines

Researcher _____ Date _____

Sample ZTS R45

KeV _____ Seconds _____ Take off Angle _____

L alpha lines

FE NI ZN GE SE KR SR ZR MO RU PD CD SN TE XE BA CE ND SM GD DY ER YB HF W OS PT HG

CO CU GA AS BR RB Y NB TC RH AG IN SB I CS LA PR PM EU TB HO TM LU TA RE IR AU

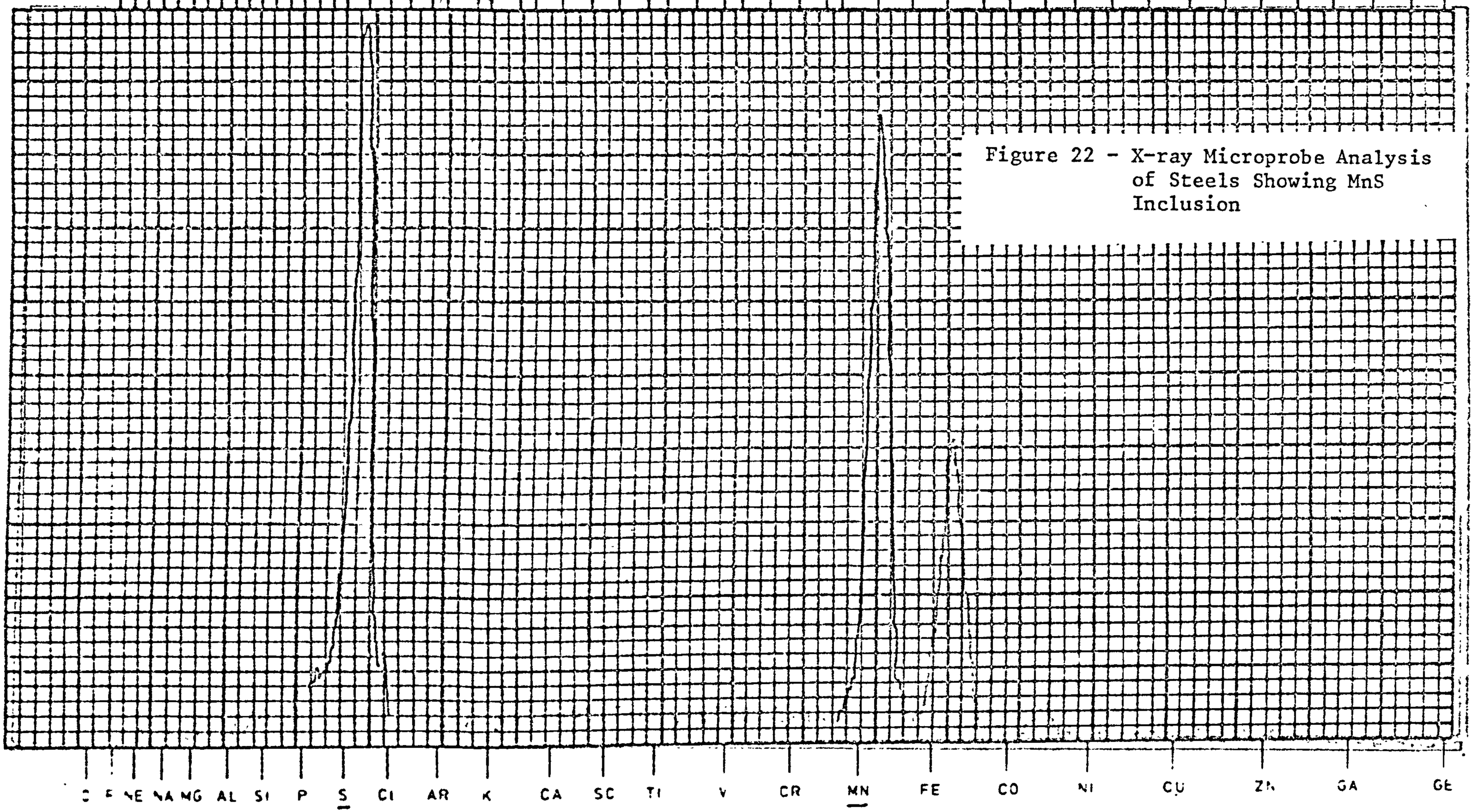

Figure 22 - X-ray Microprobe Analysis of Steels Showing MnS Inclusion

C F NE NA MG AL SI P S CL AR K CA SC TI V CR MN FE CO NI CU ZN GA GE

K alpha lines

Link Systems Ltd X Ray Analysis

(214)

FIG 23. Specimen and Inclusion Orientations with respect to Plate Rolling Direction

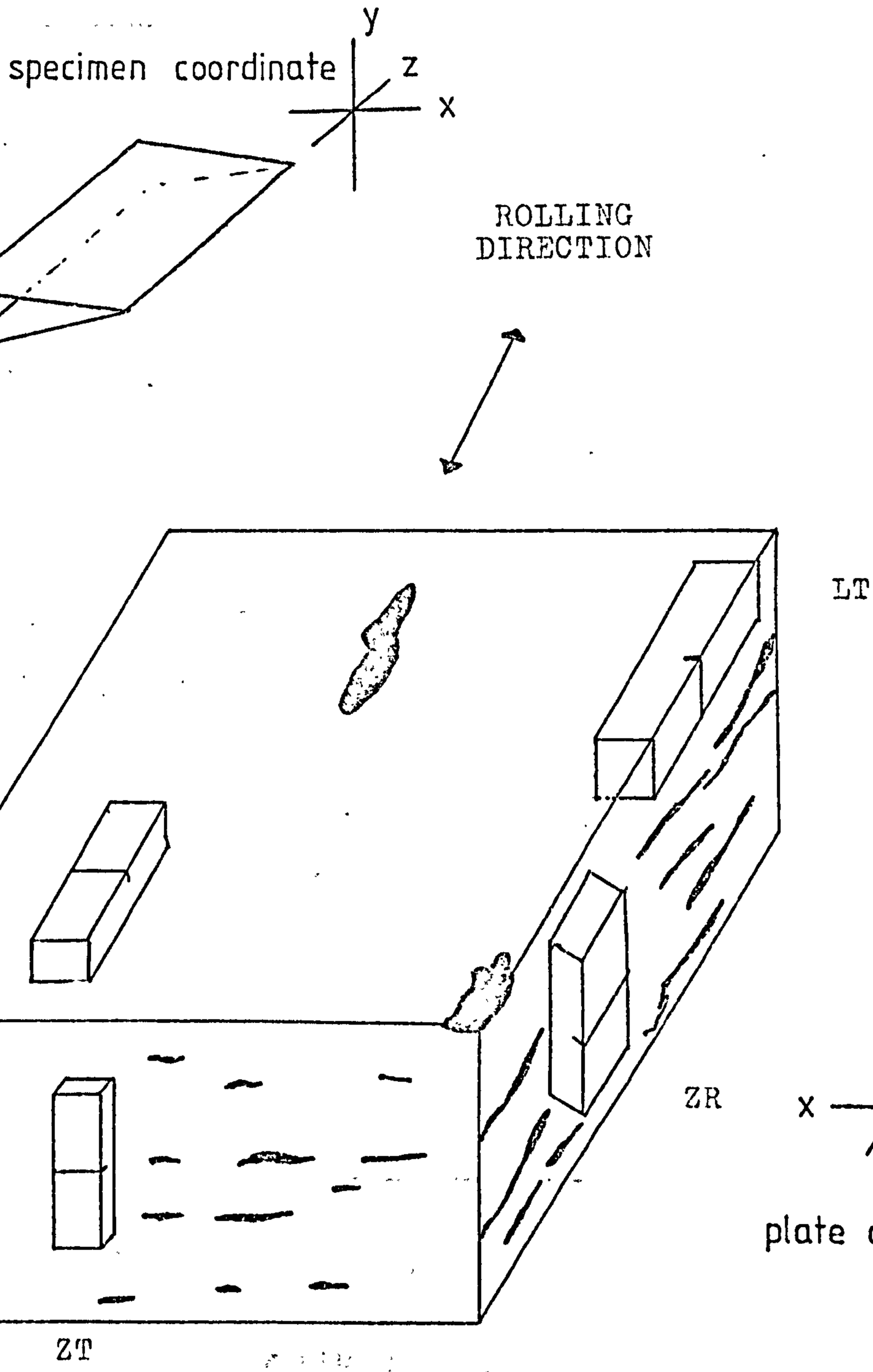

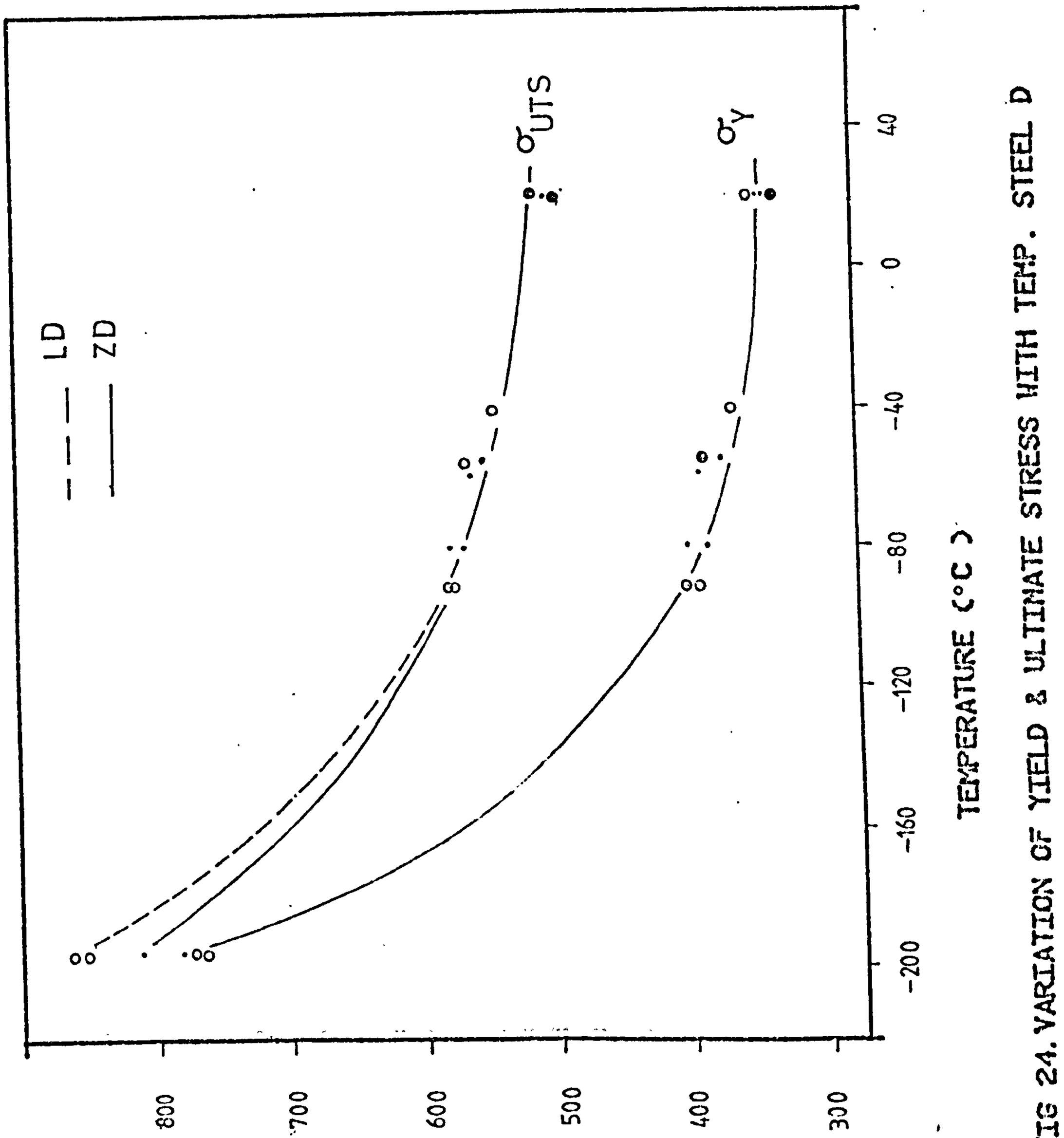

FIG. 24. VARIATION OF YIELD & ULTIMATE STRESS WITH TEMP. STEEL D

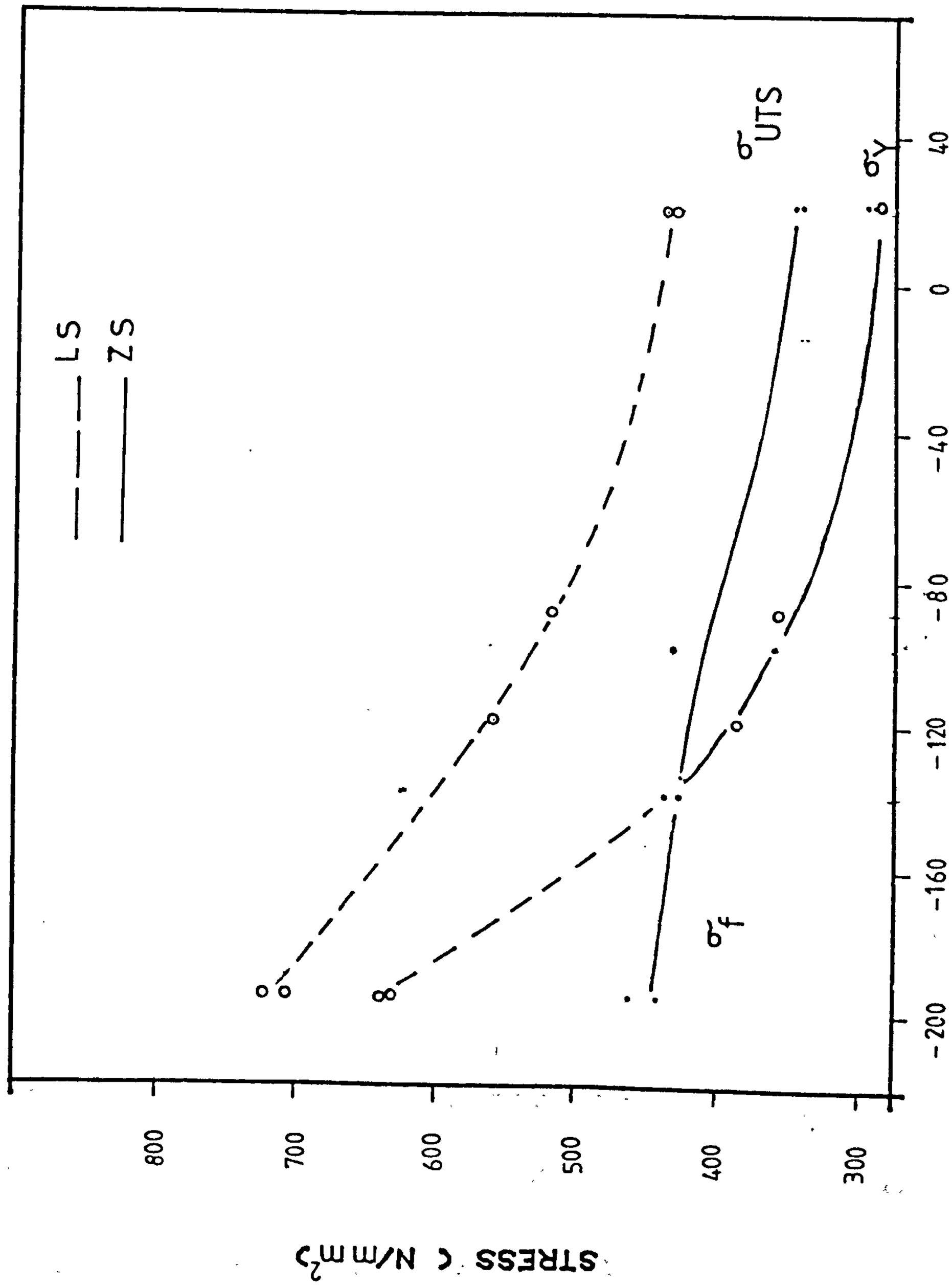

FIG 25. VARIATION OF YIELD & ULTIMATE STRESS WITH TEMP. STEEL S

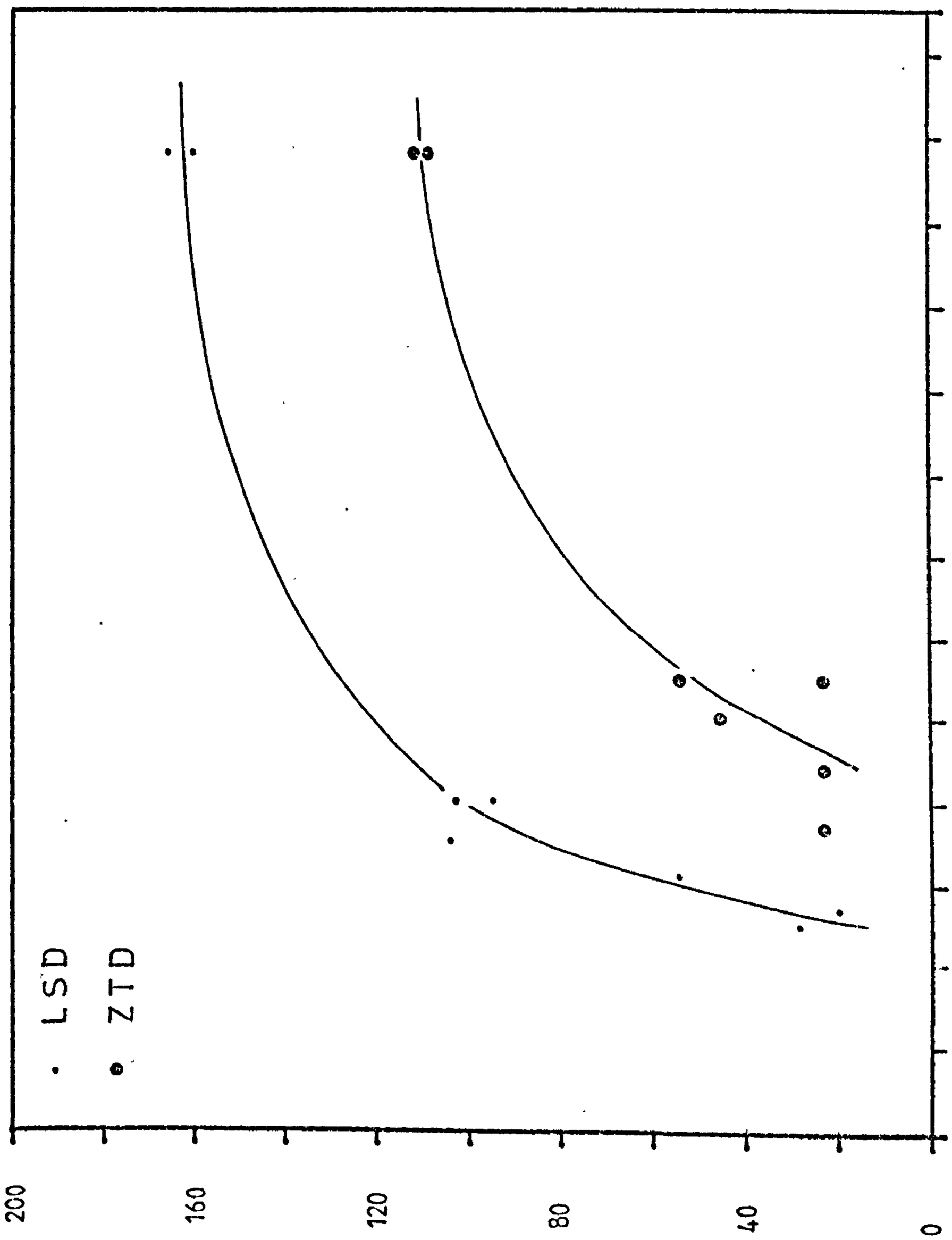

FIG 26. CHARPY V IMPACT TEST DATA FOR STEEL D

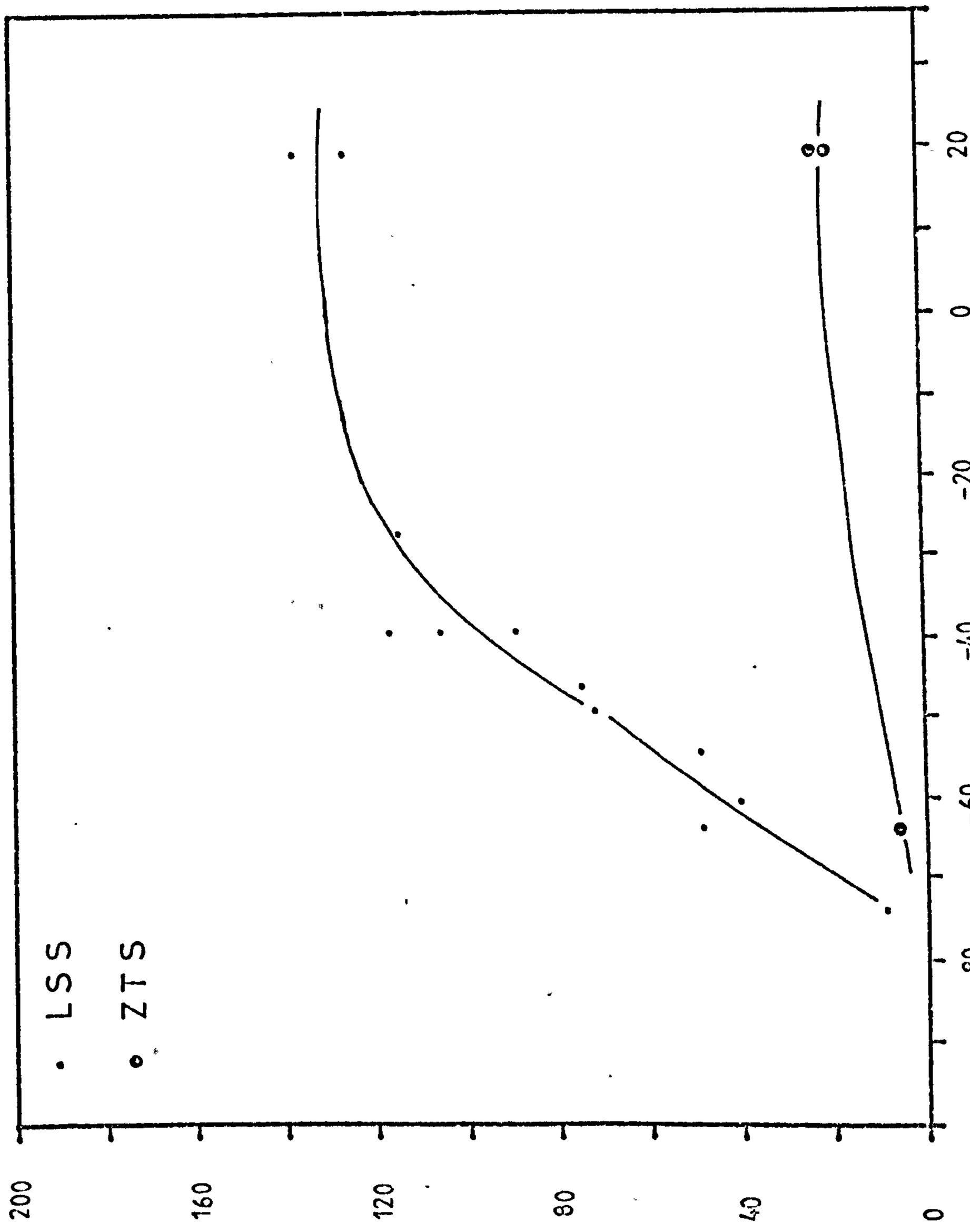

FIG 27. CHARPY V IMPACT DATA FOR STEEL S

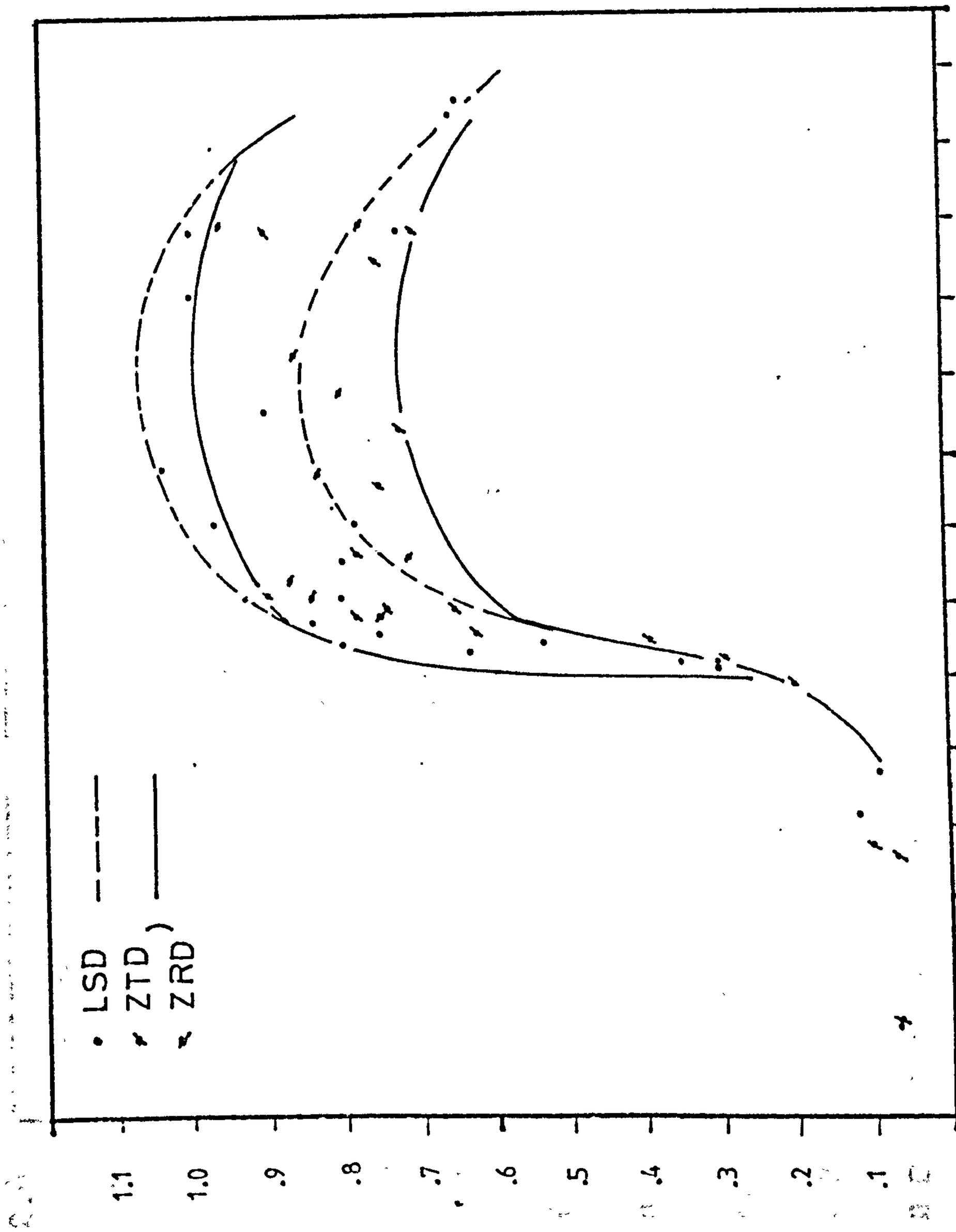

FIG 23. COD DATA FOR STEEL D, H = B = 10 mm

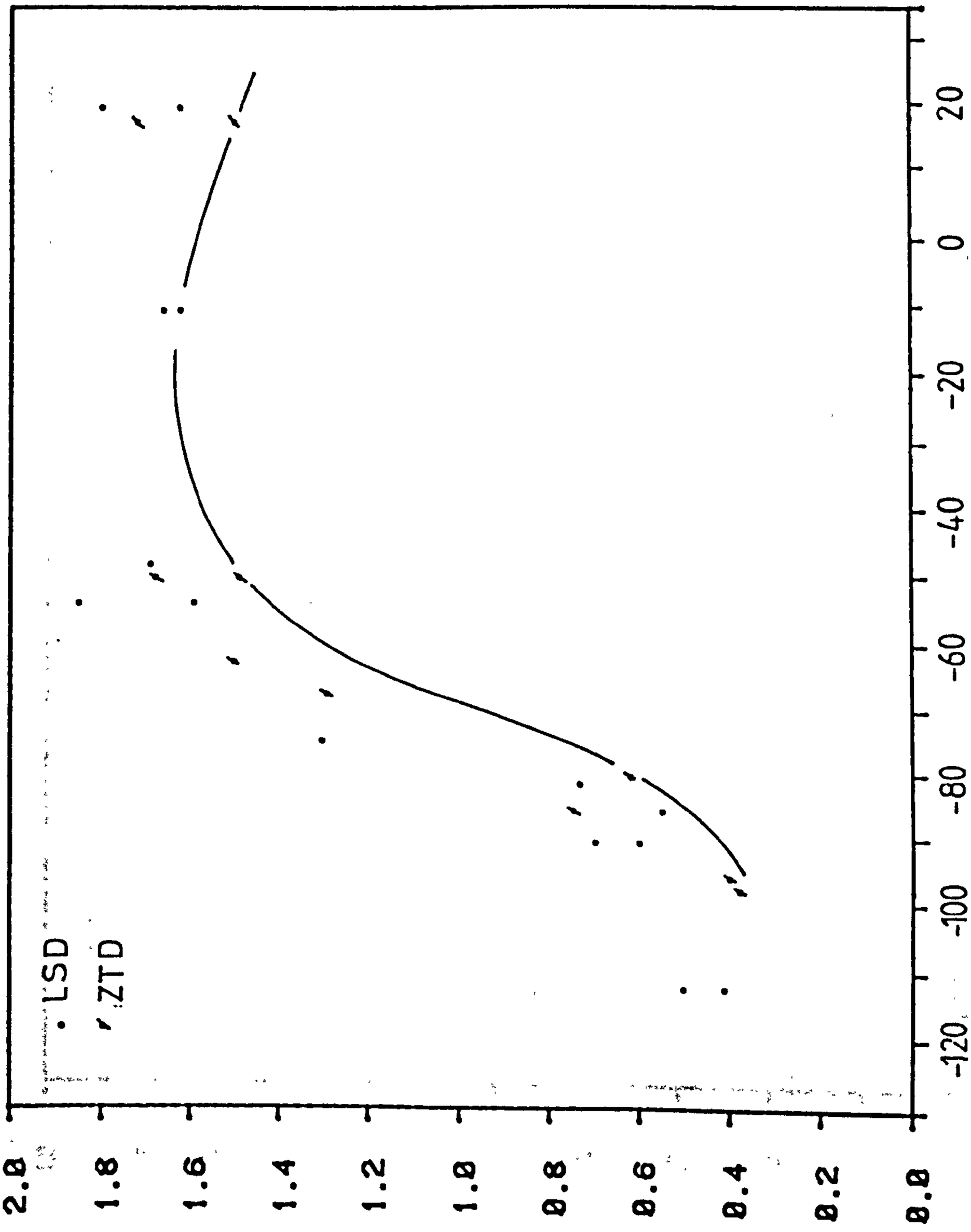

FIG 29. COD DATA FOR STEEL D, W = B = 18 mm

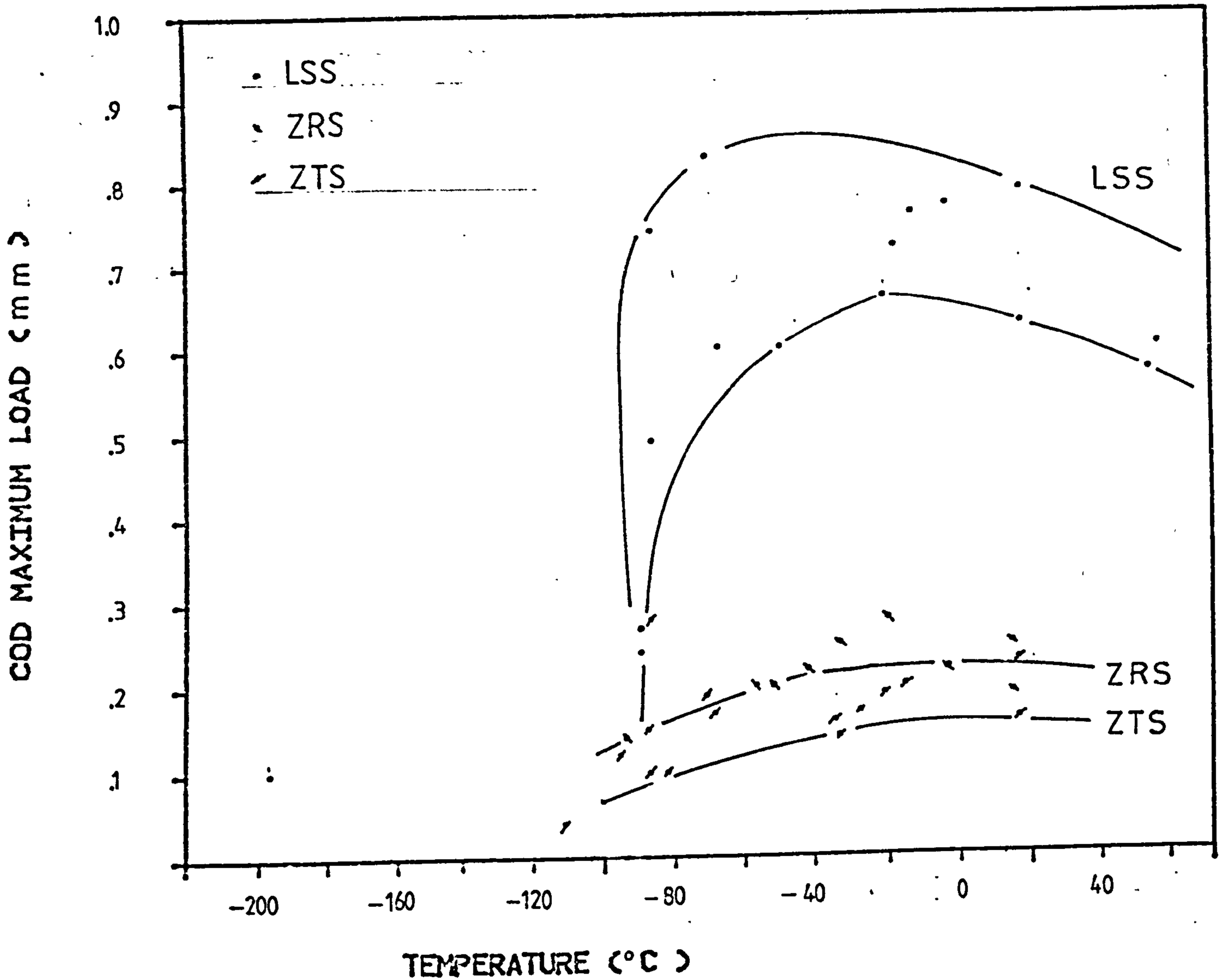

FIG 30. COD DATA FOR STEEL S, W = B = 10mm

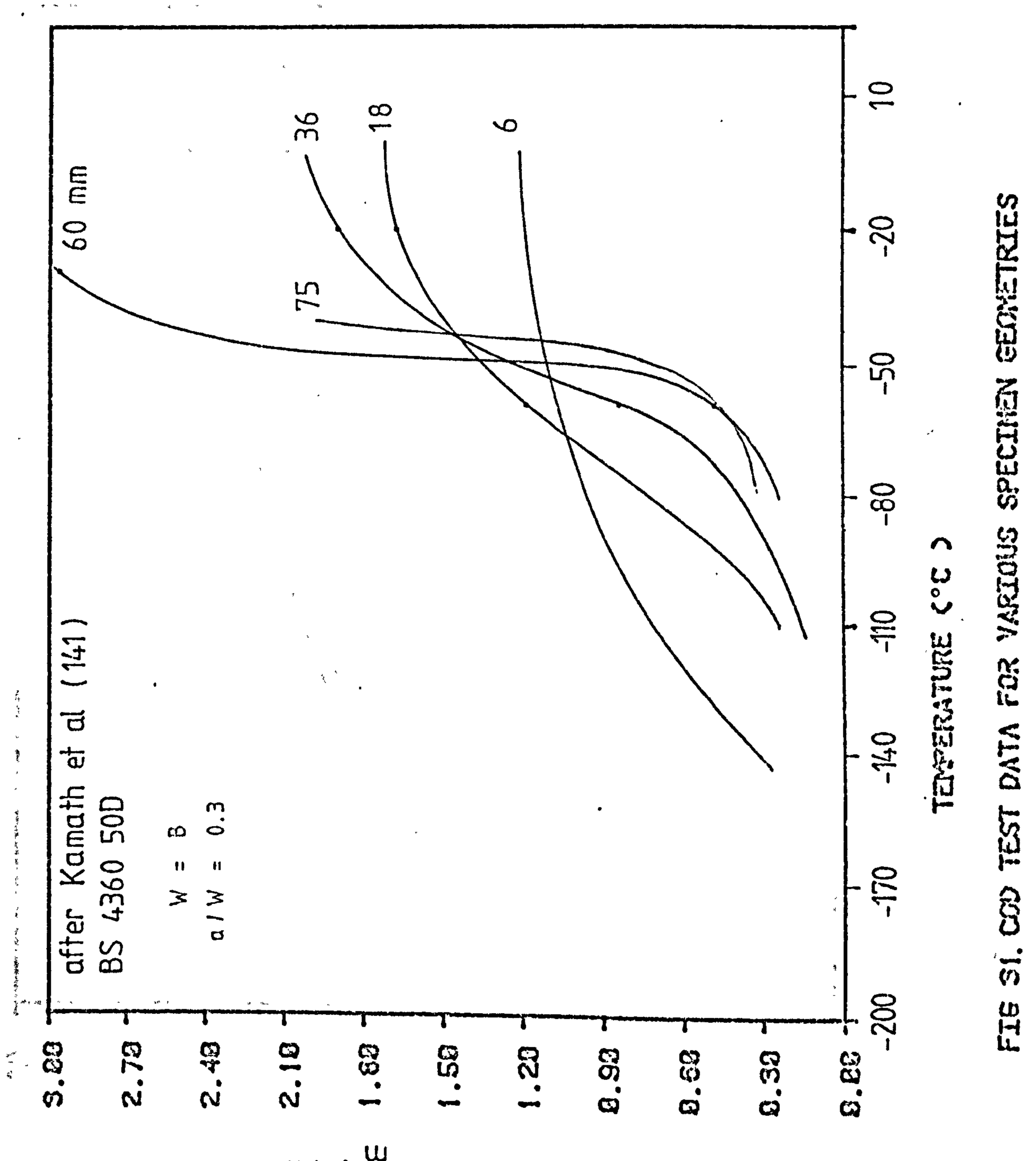

FIG 31. COD TEST DATA FOR VARIOUS SPECIMEN GEOMETRIES

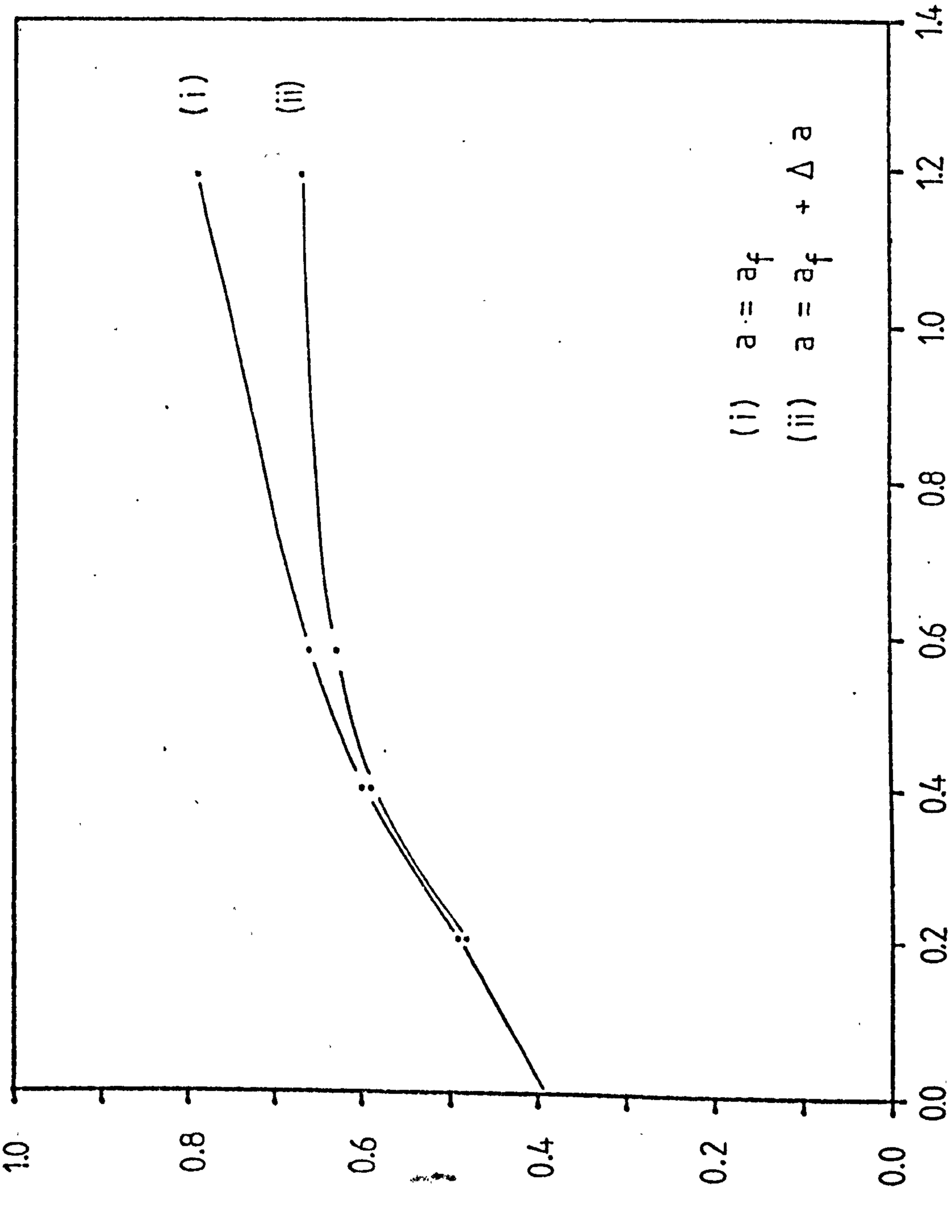

FIG 32. COD RESISTANCE TO CRACK GROWTH, LSD W = B = 18mm

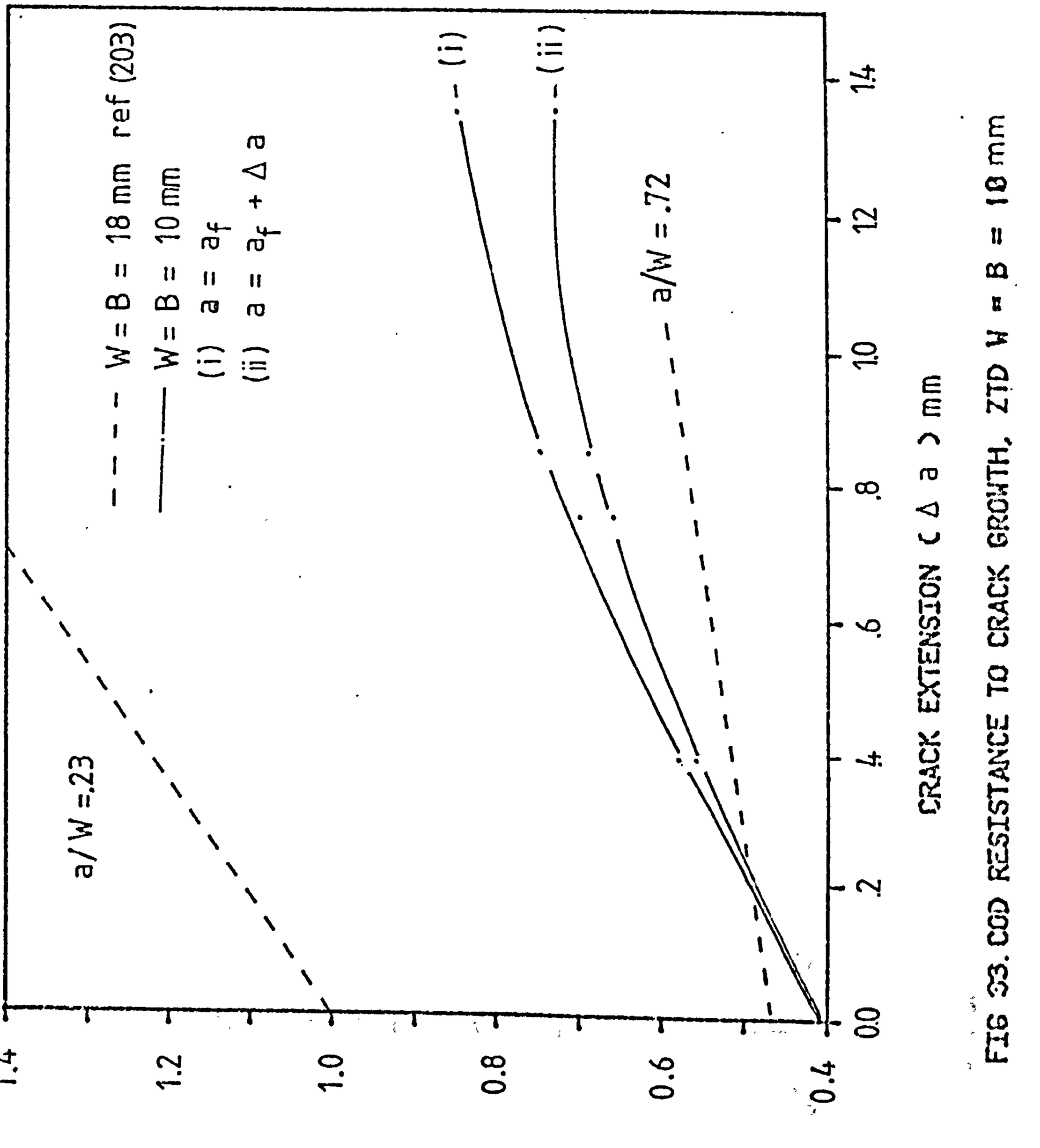

FIG 33. COD RESISTANCE TO CRACK GROWTH, ZTD W = B = 18 mm

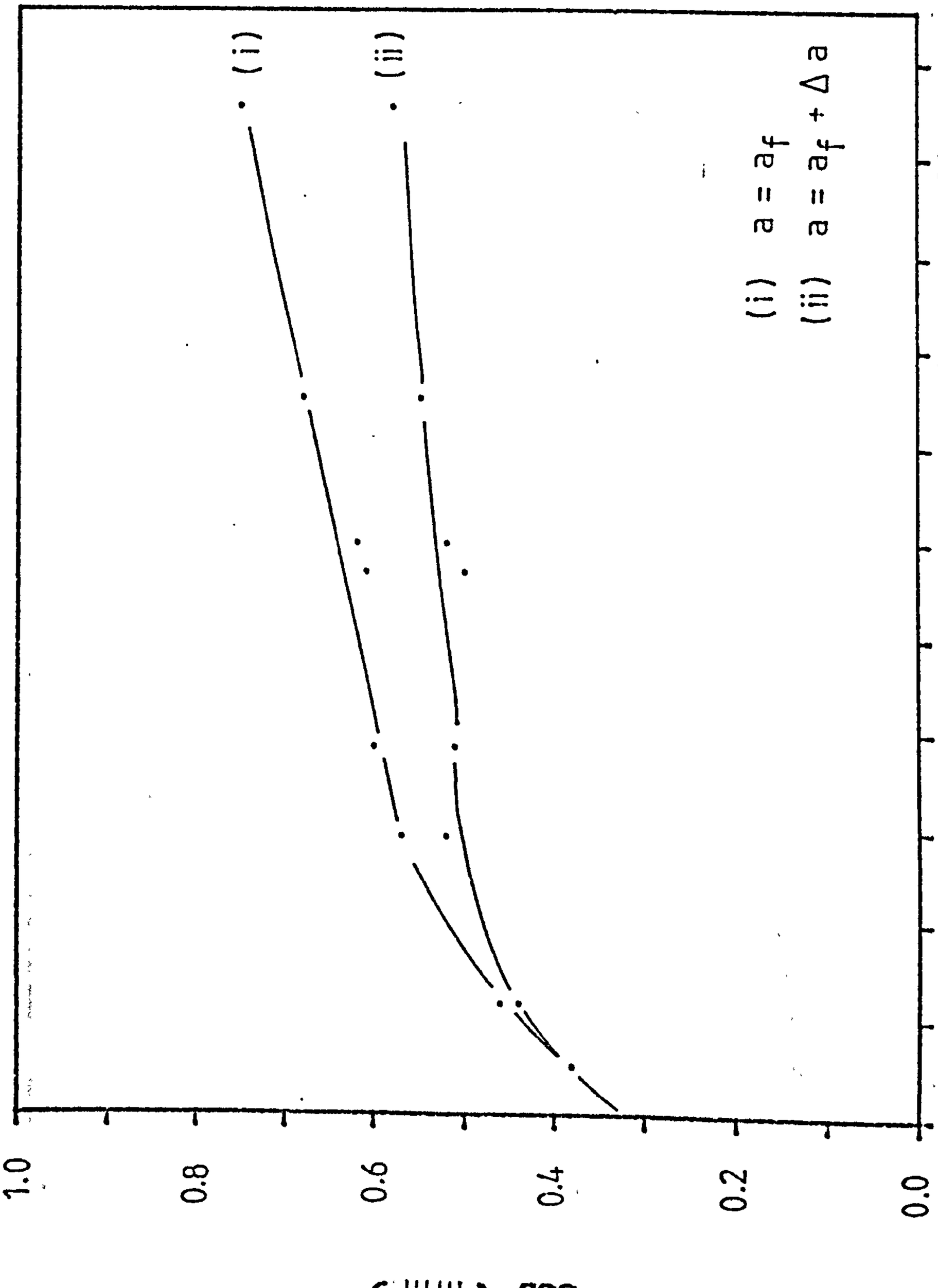

FIG 34. COD RESISTANCE TO CRACK GROWTH, LSS W = B = 10 mm

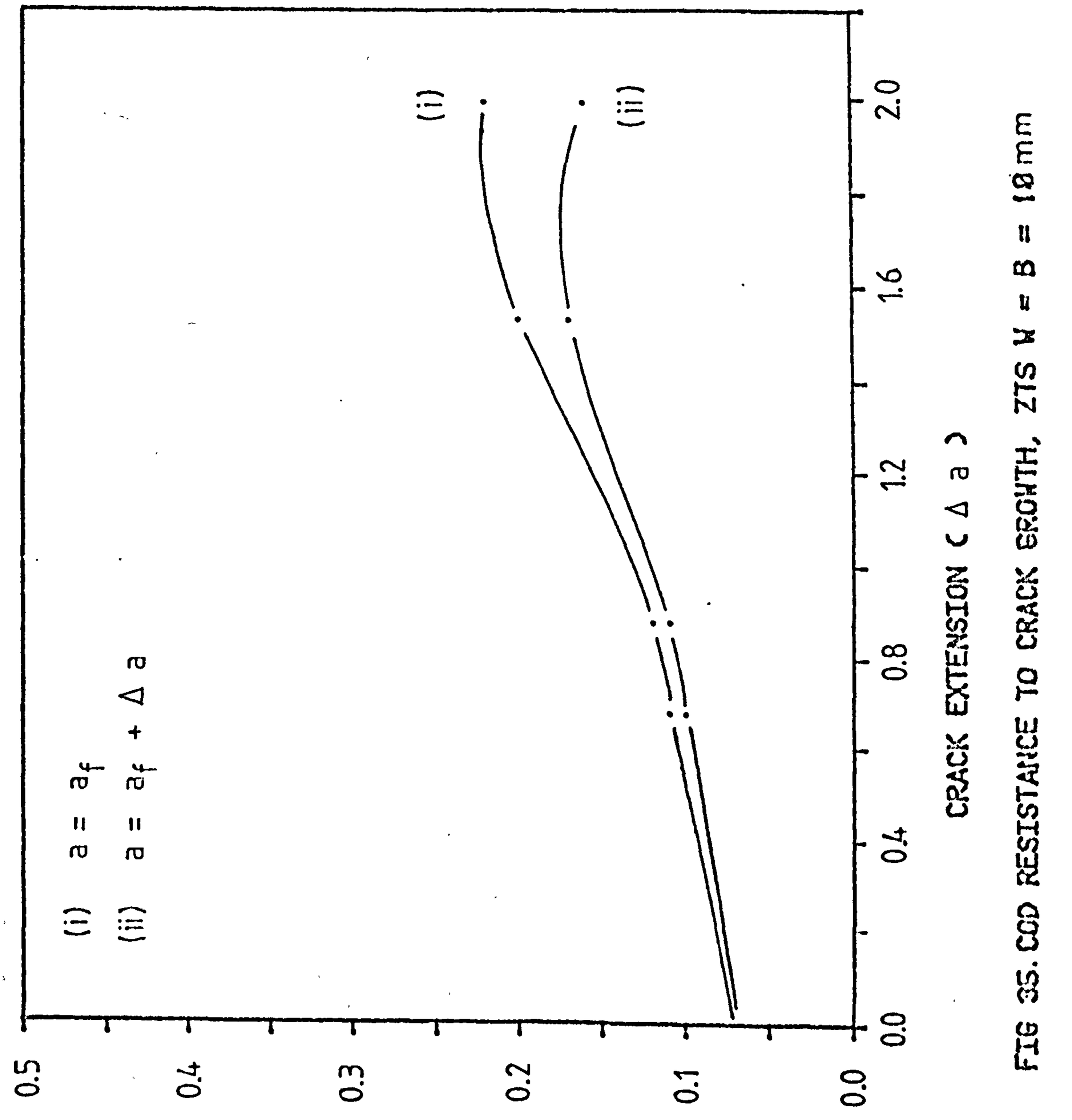

FIG 35. COD RESISTANCE TO CRACK

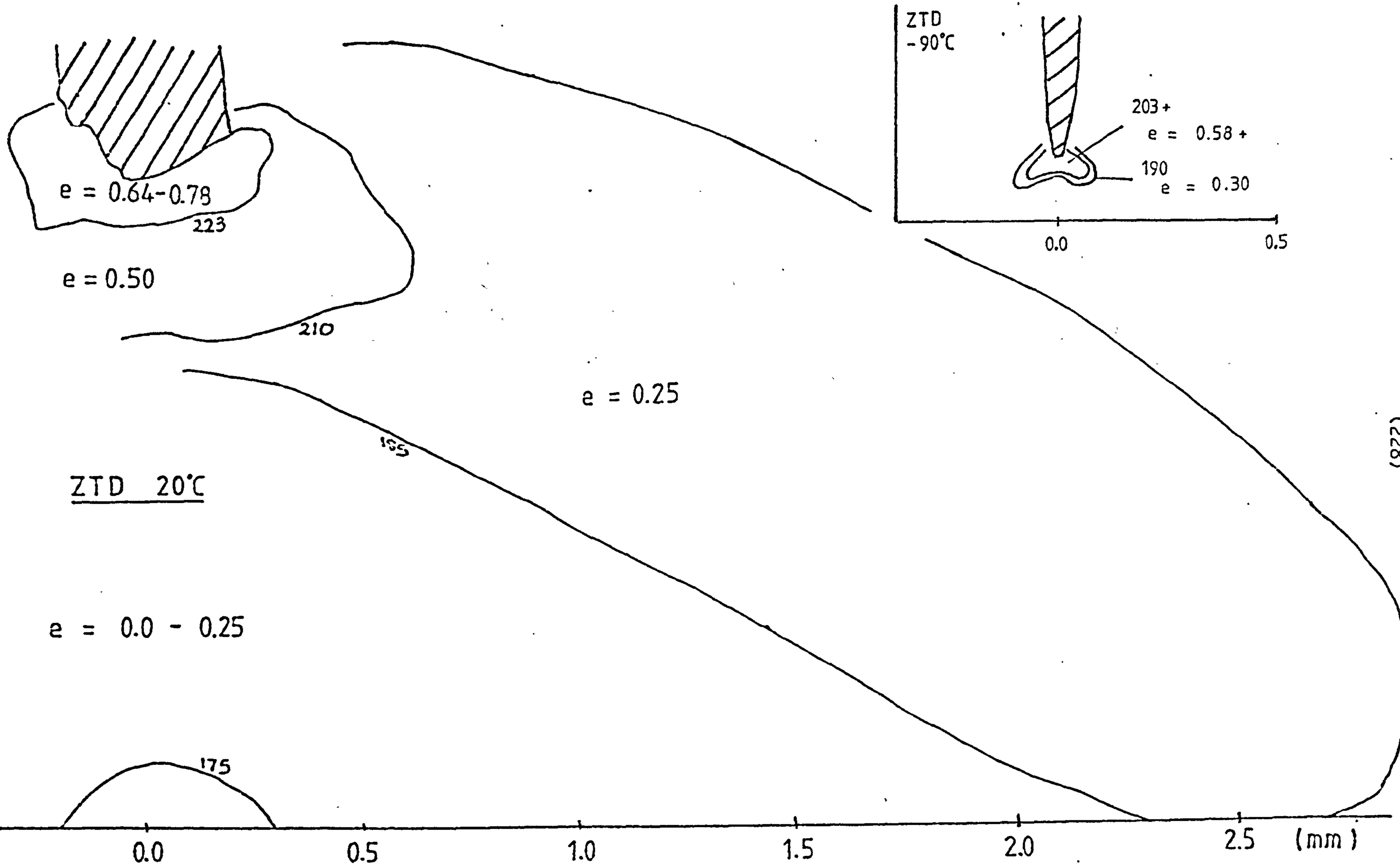

FIG 36A. Plastic Strain Ahead of the Crack Tip , ZTD.

FIG. 36B. Plastic Strain Ahead of the Crack Tip, ZTS.

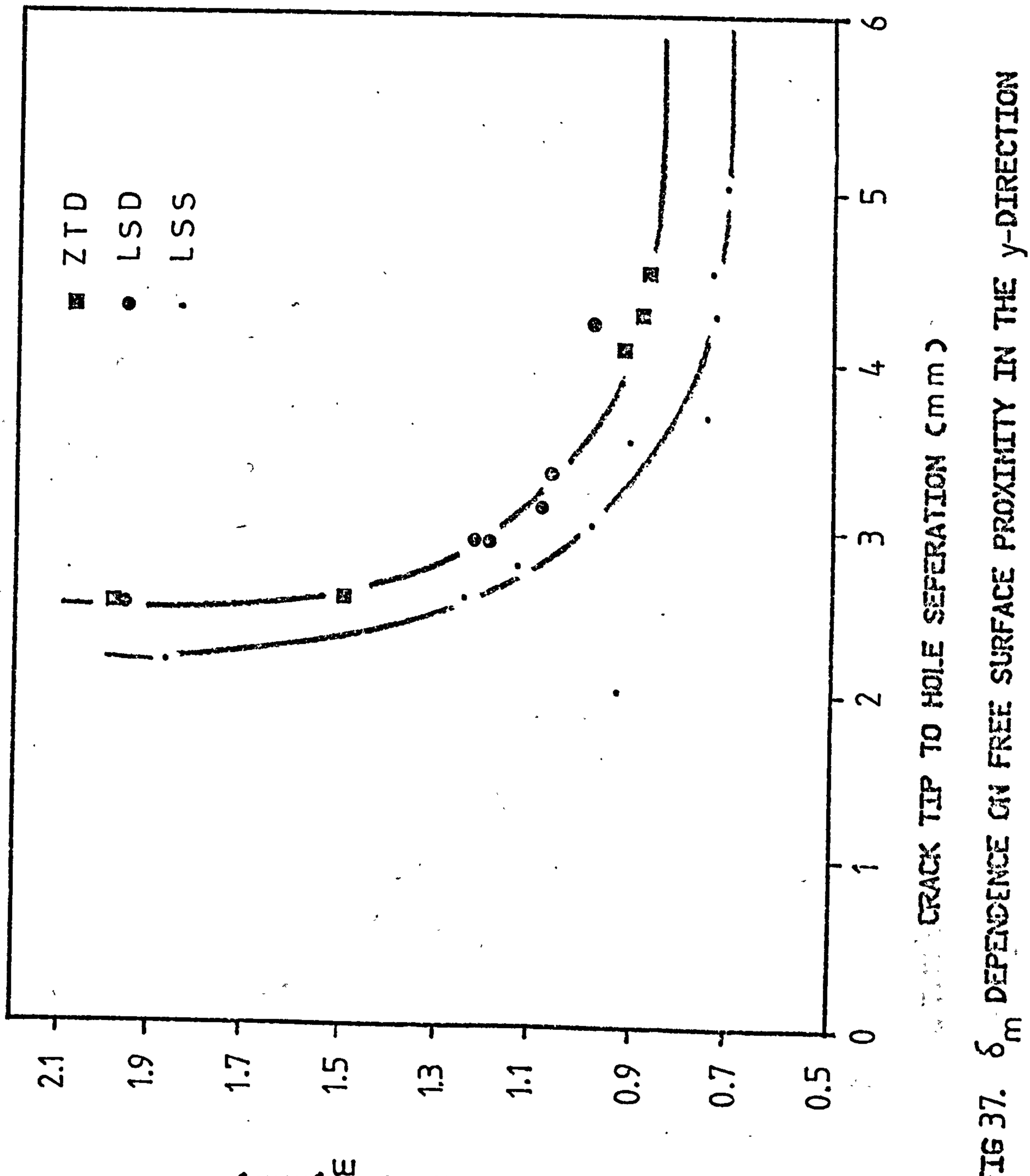

FIG 37. δ_m DEPENDENCE ON FREE SURFACE PROXIMITY IN THE y-DIRECTION

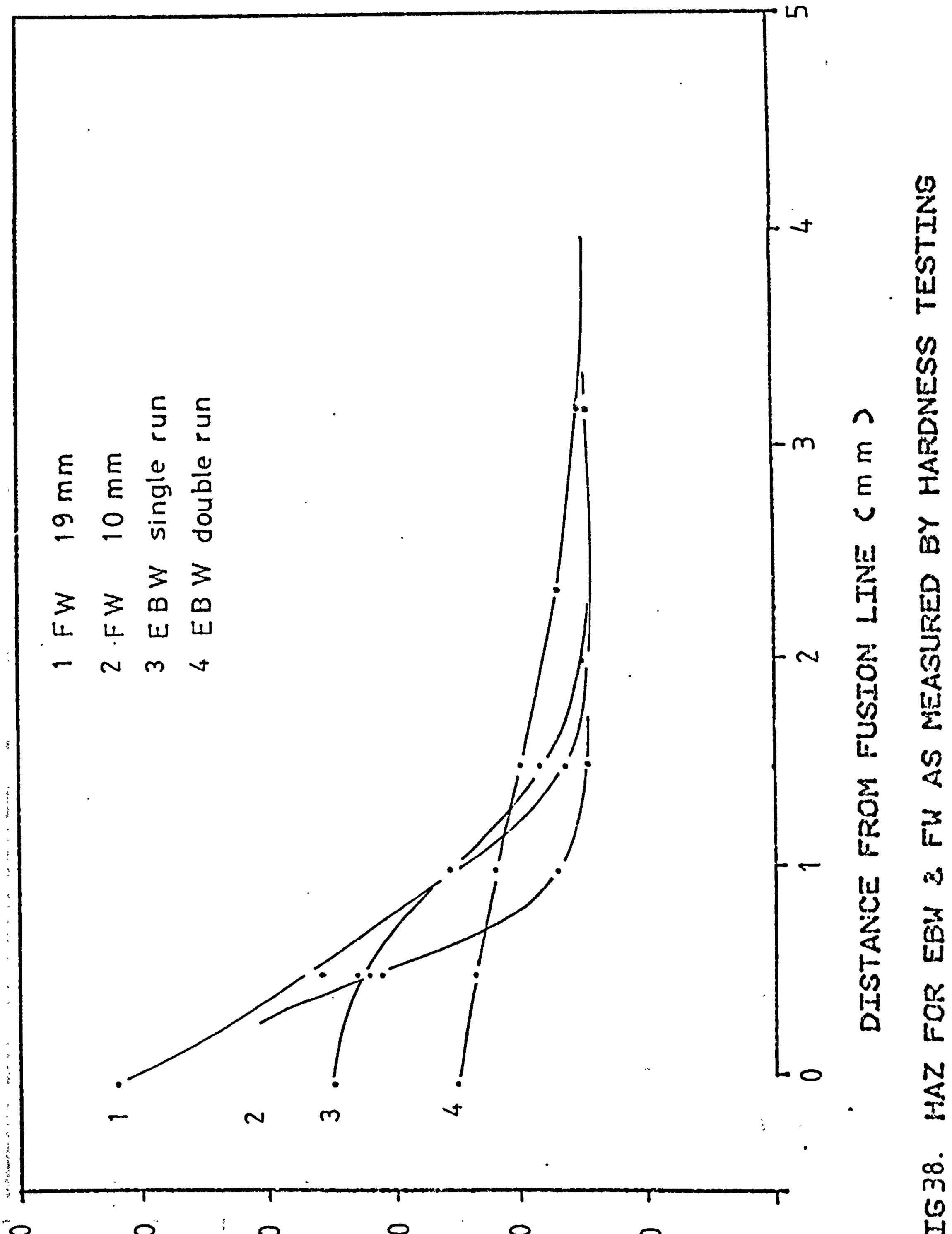

FIG 38. HAZ FOR EBW & FW AS MEASURED BY HARDNESS TESTING

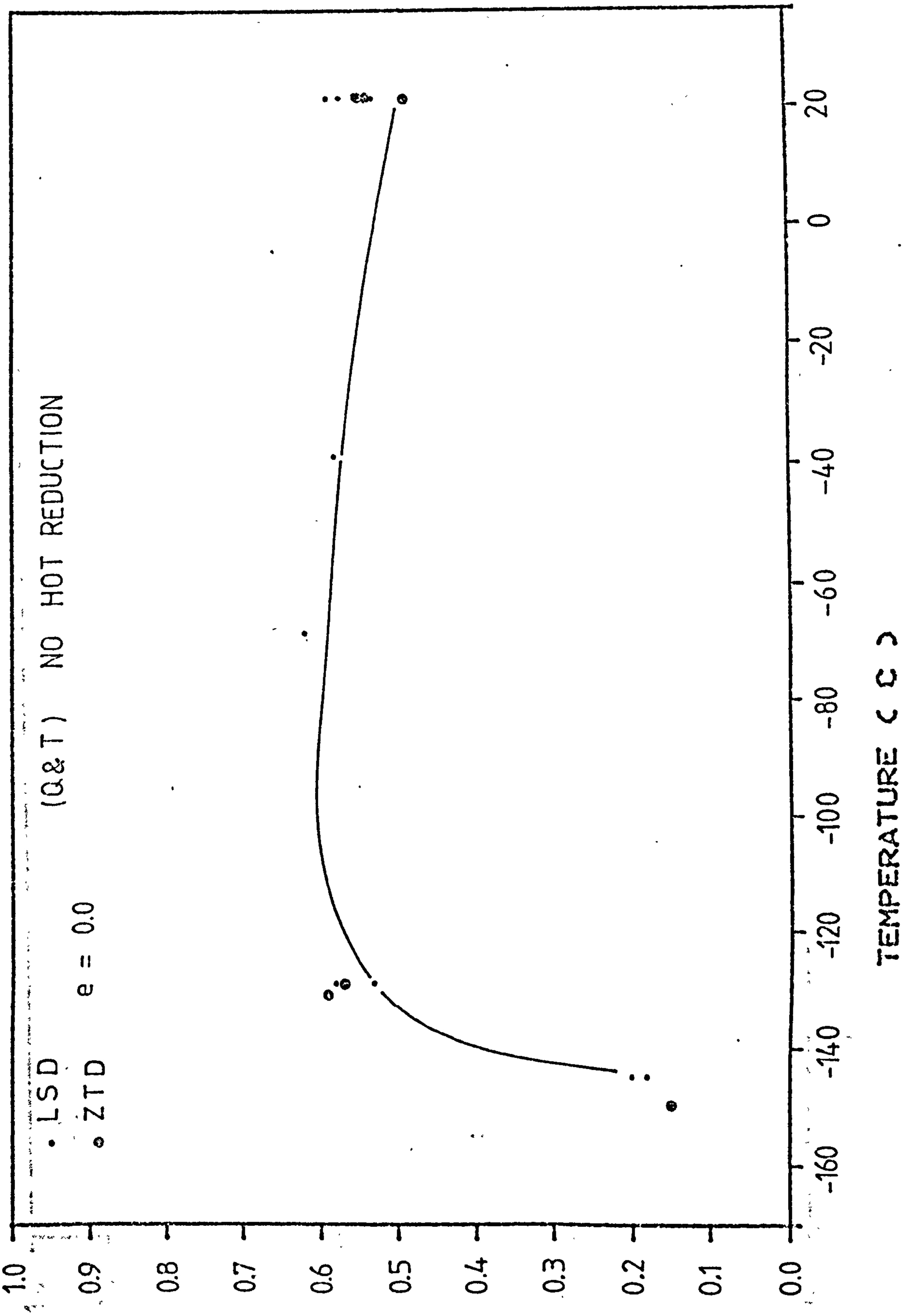

FIG 39. COD VALUES FOR Q & T, P

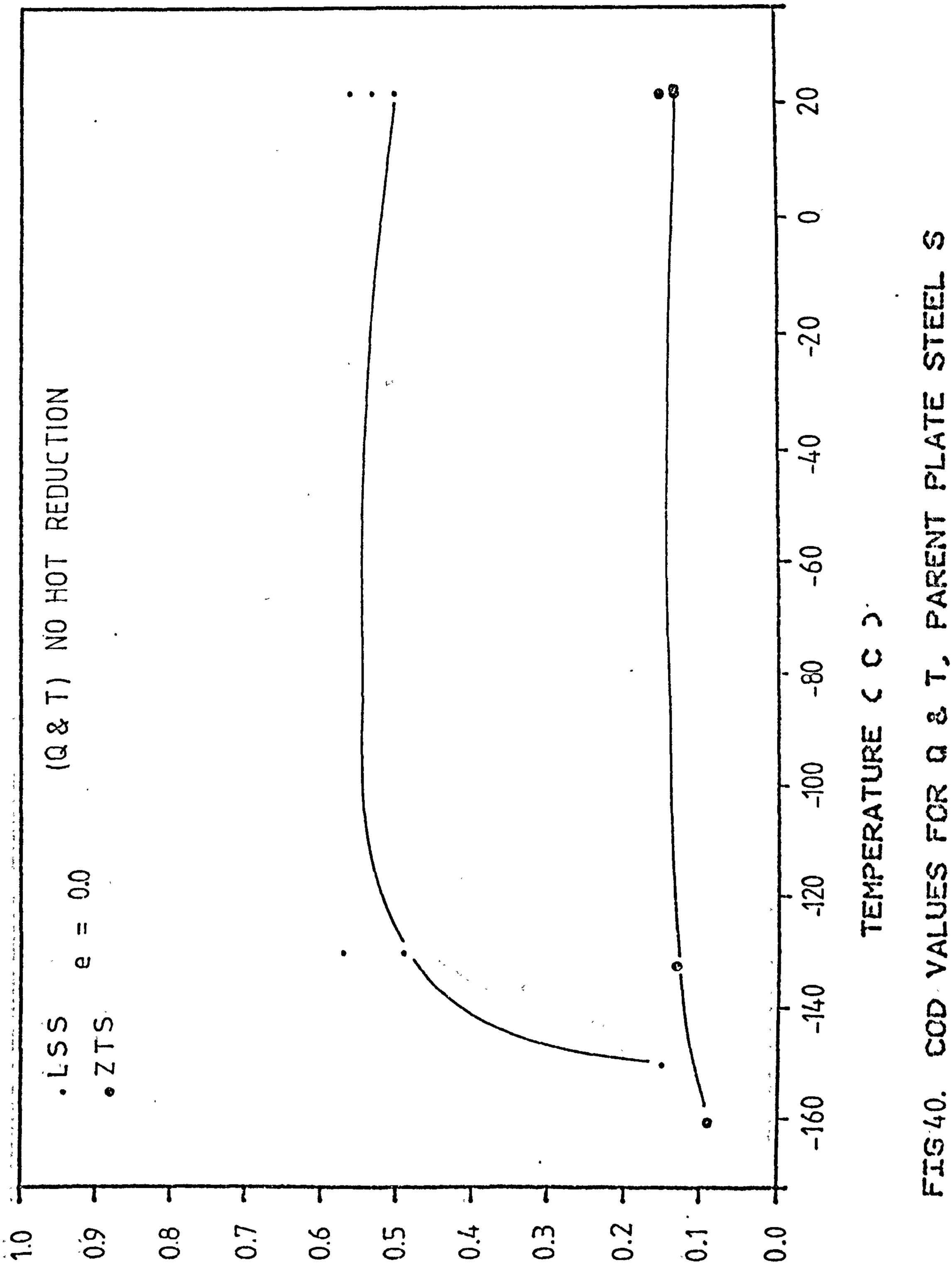

FIG 40. COD VALUES FOR Q & T, PARENT PLATE STEEL

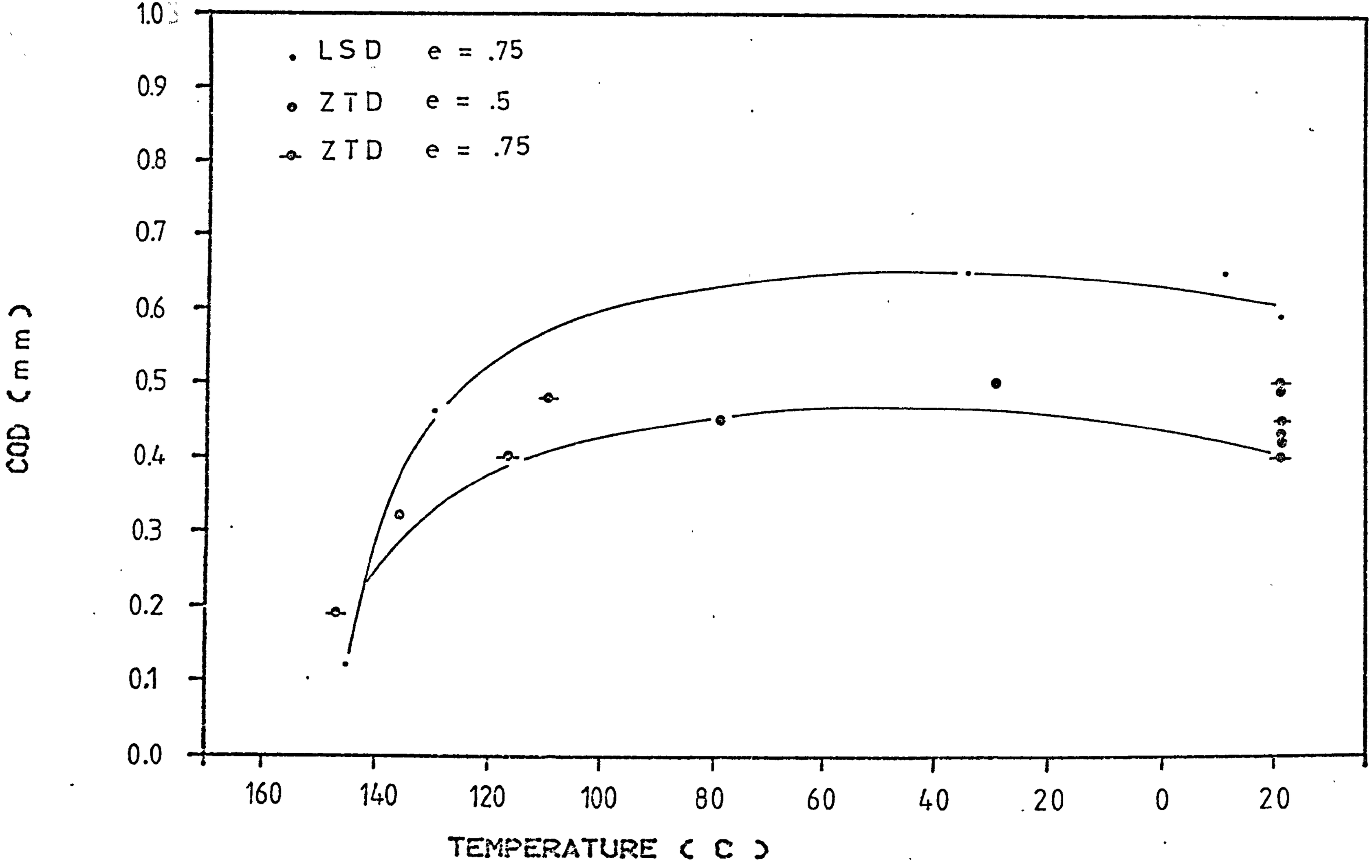

FIG 41. COD VALUES FOR HOT ROLLED, Q & T STEEL D

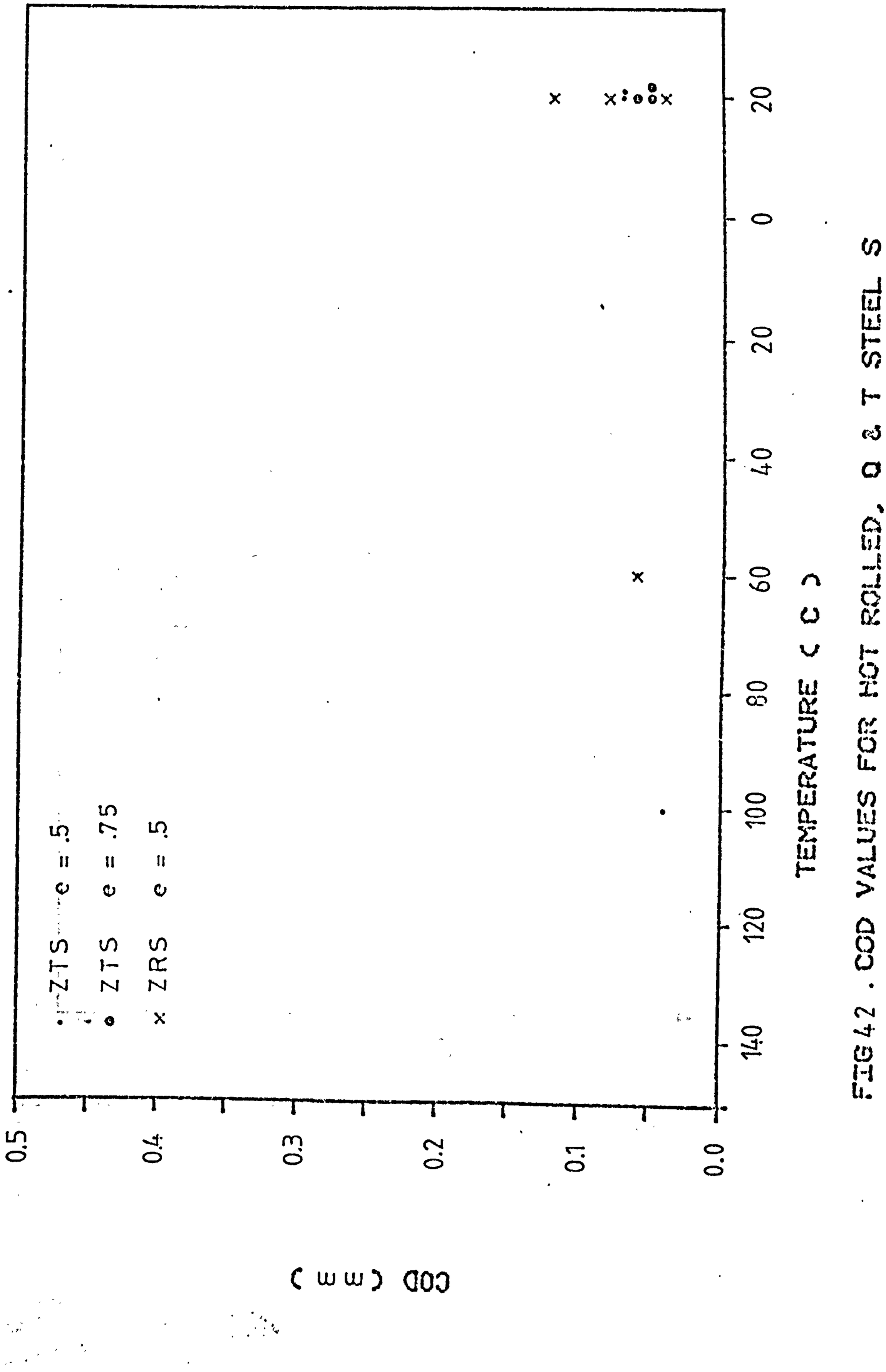

FIG 4.42 . COD VALUES FOR HOT ROLLED, Q & T STEEL S

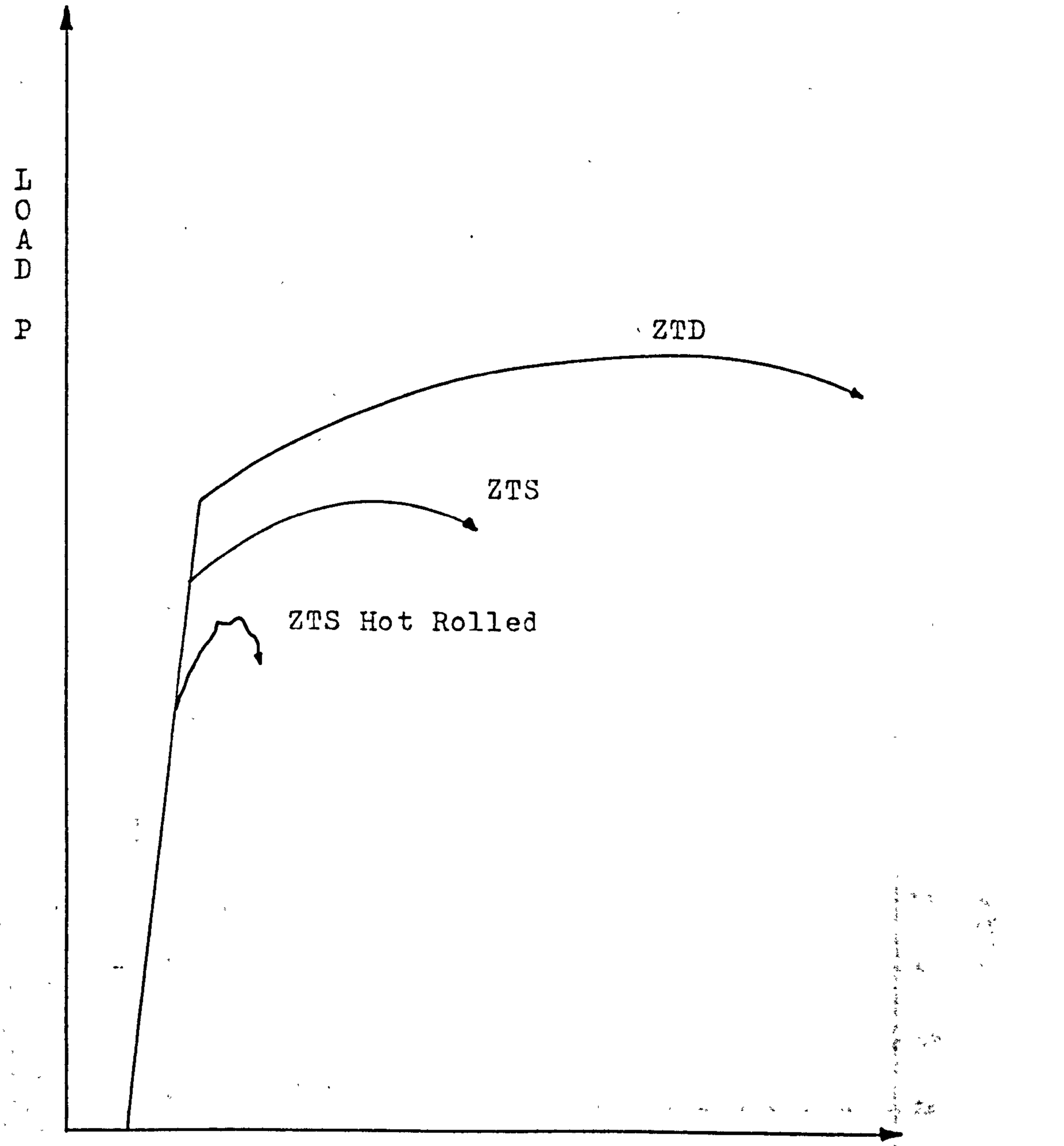

FIG 43. Load vs Clip Gauge Opening for Through-Thickness Directions in Steels Containing Different Inclusion Contents

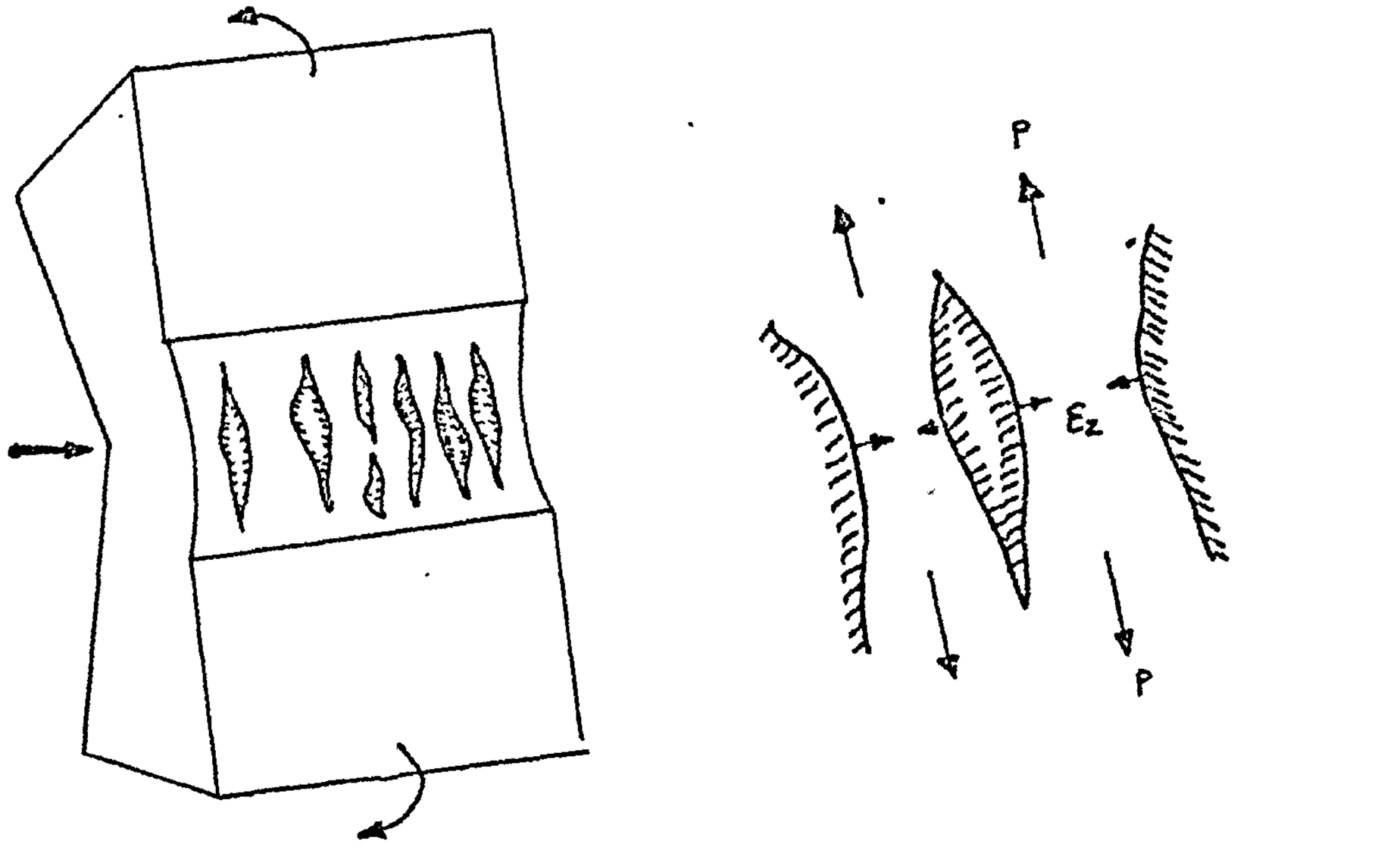

FIG 44. Crack Tip Deformation in an LT Specimen Showing the Effect of Inclusions'Void Expansion

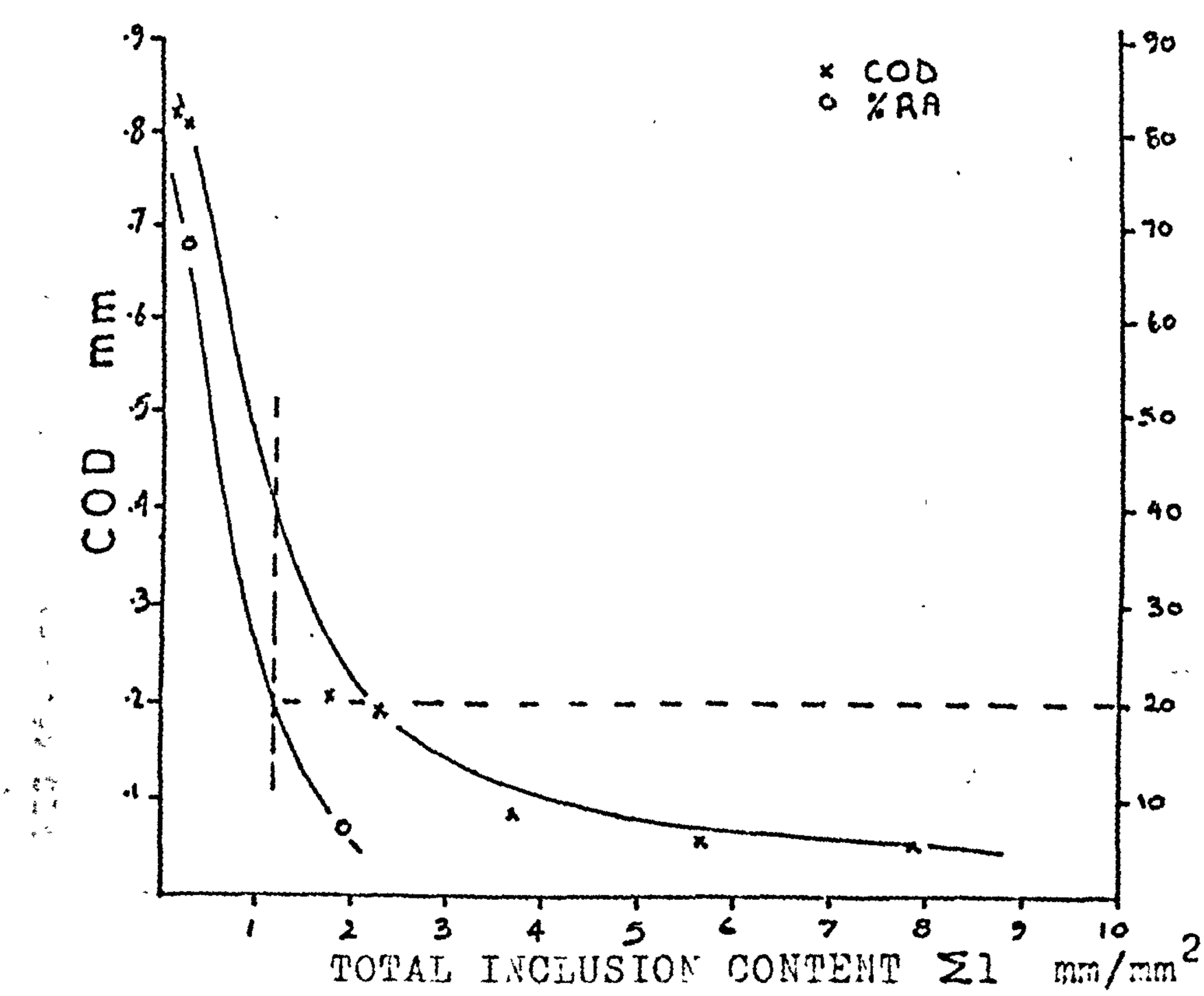

FIG 45, δ_m and %RA Variation with Total Inclusion Content

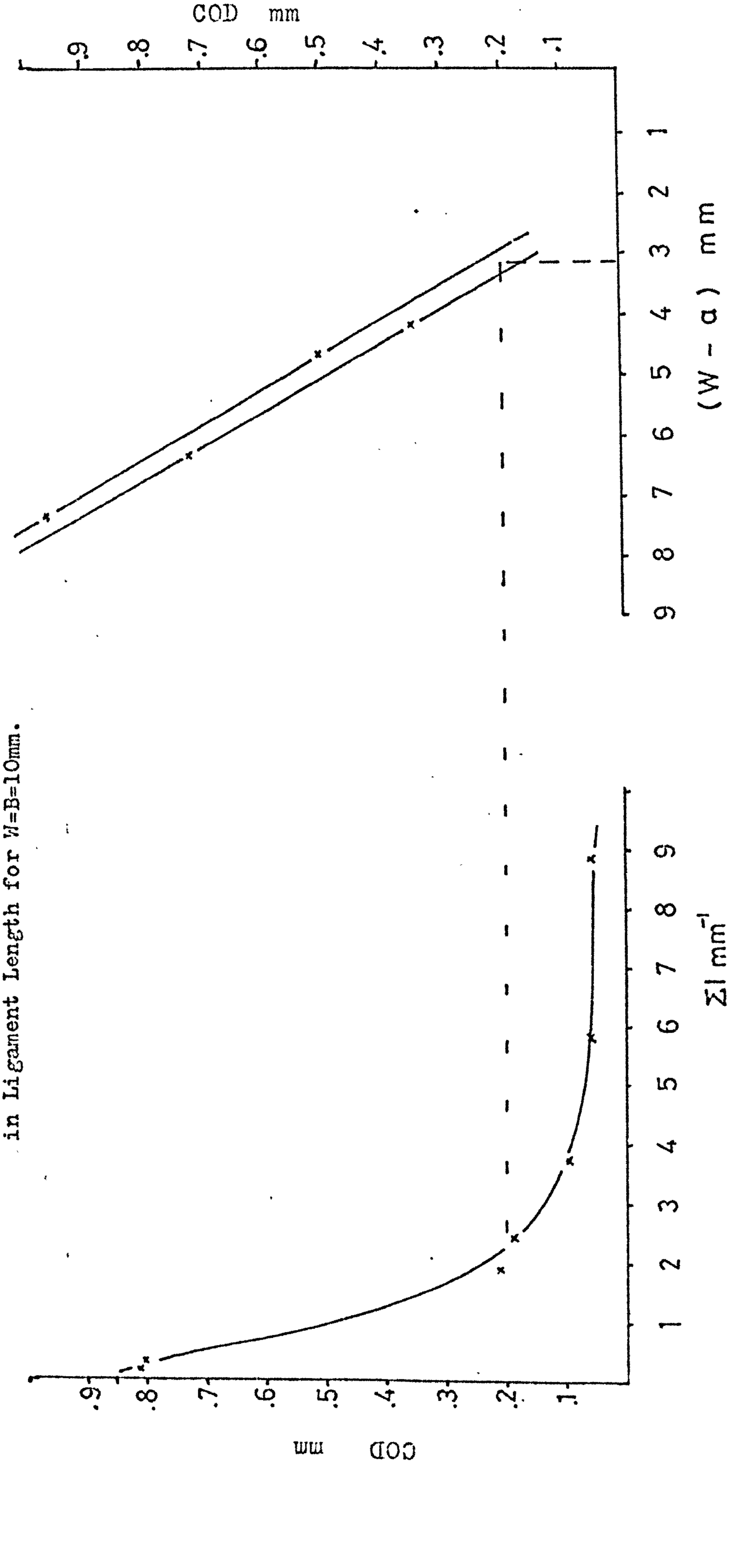

FIG 46. Graphical Method of Equating Inclusion Content to Reduction in Ligament Length for W=B=10mm.

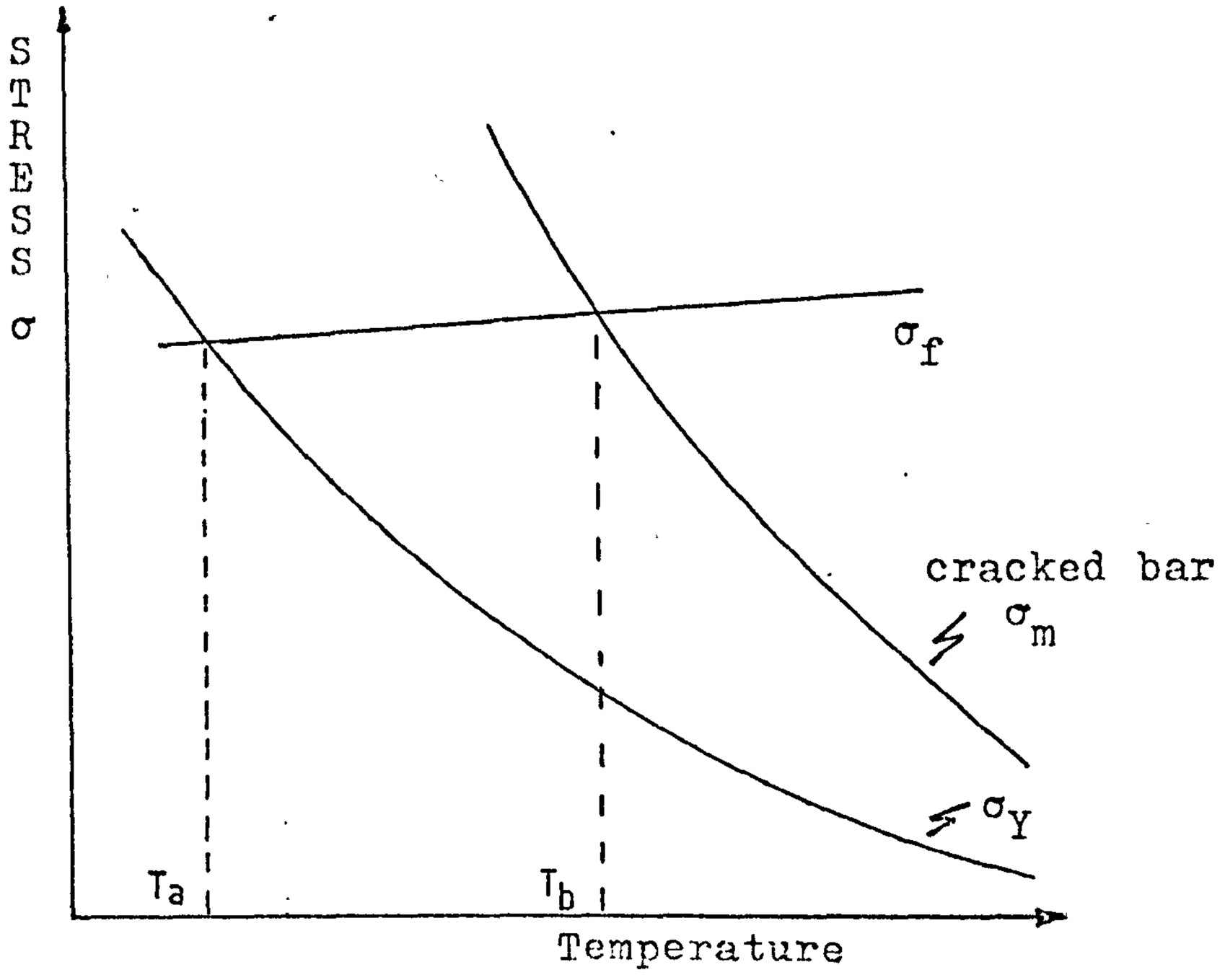

FIG 47 . Orowan's Theory of Brittle Fracture

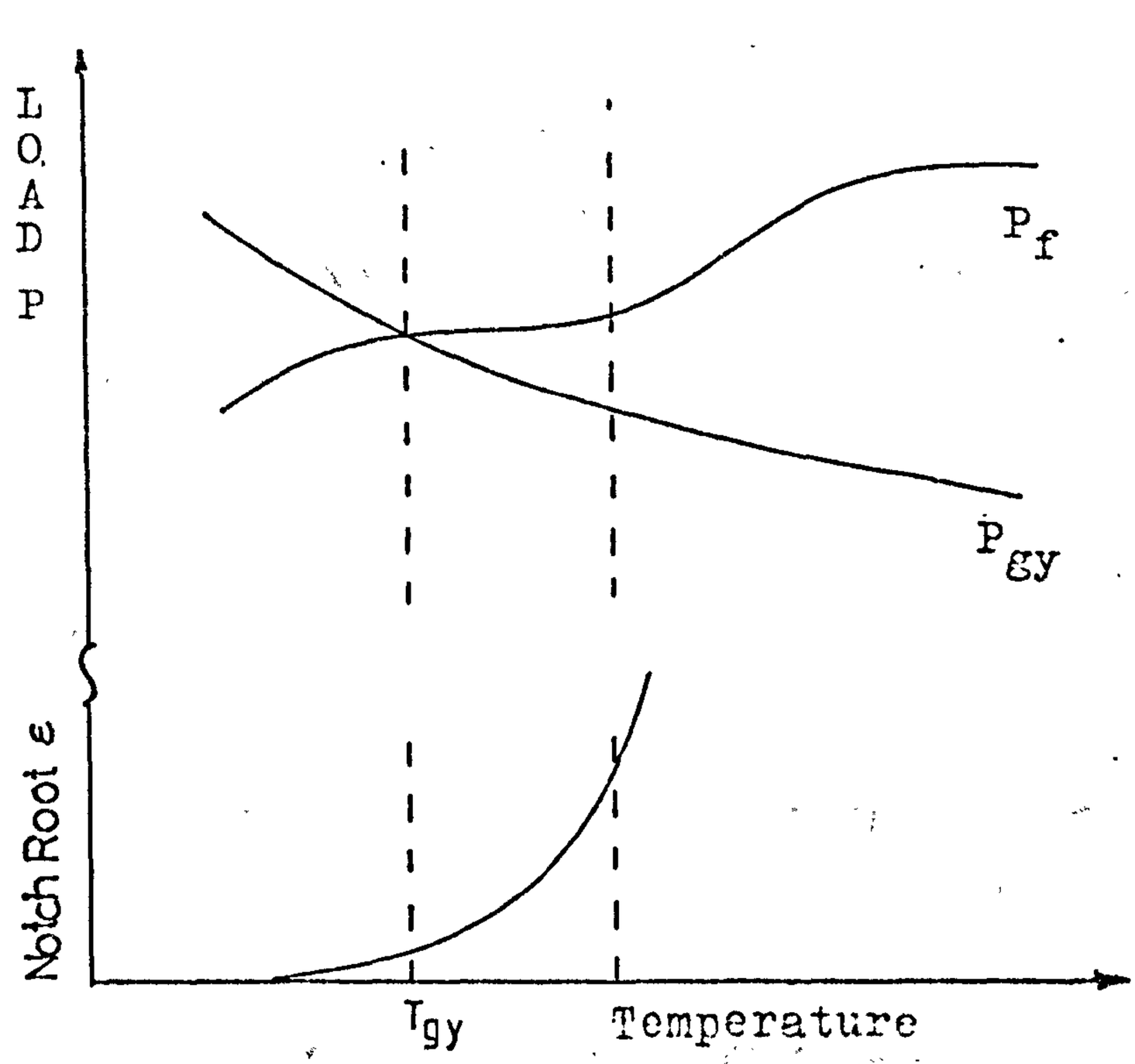

FIG 48 . Schematic Fracture Behaviour with Temperature in Notched Slow Bend Tests

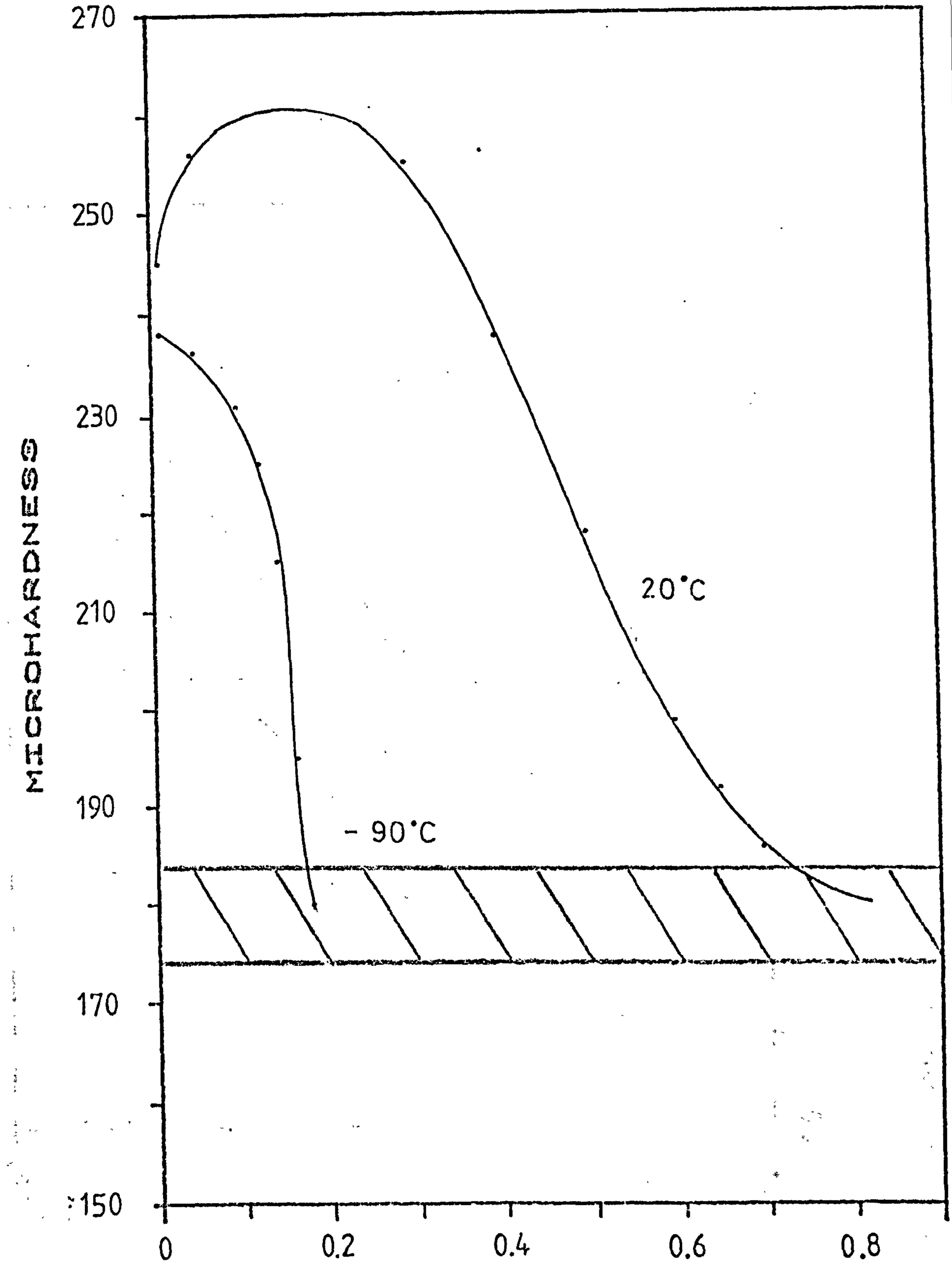

FIG49. r_p DEPENDENCE ON TEMP., LSS, W = B = 10 mm

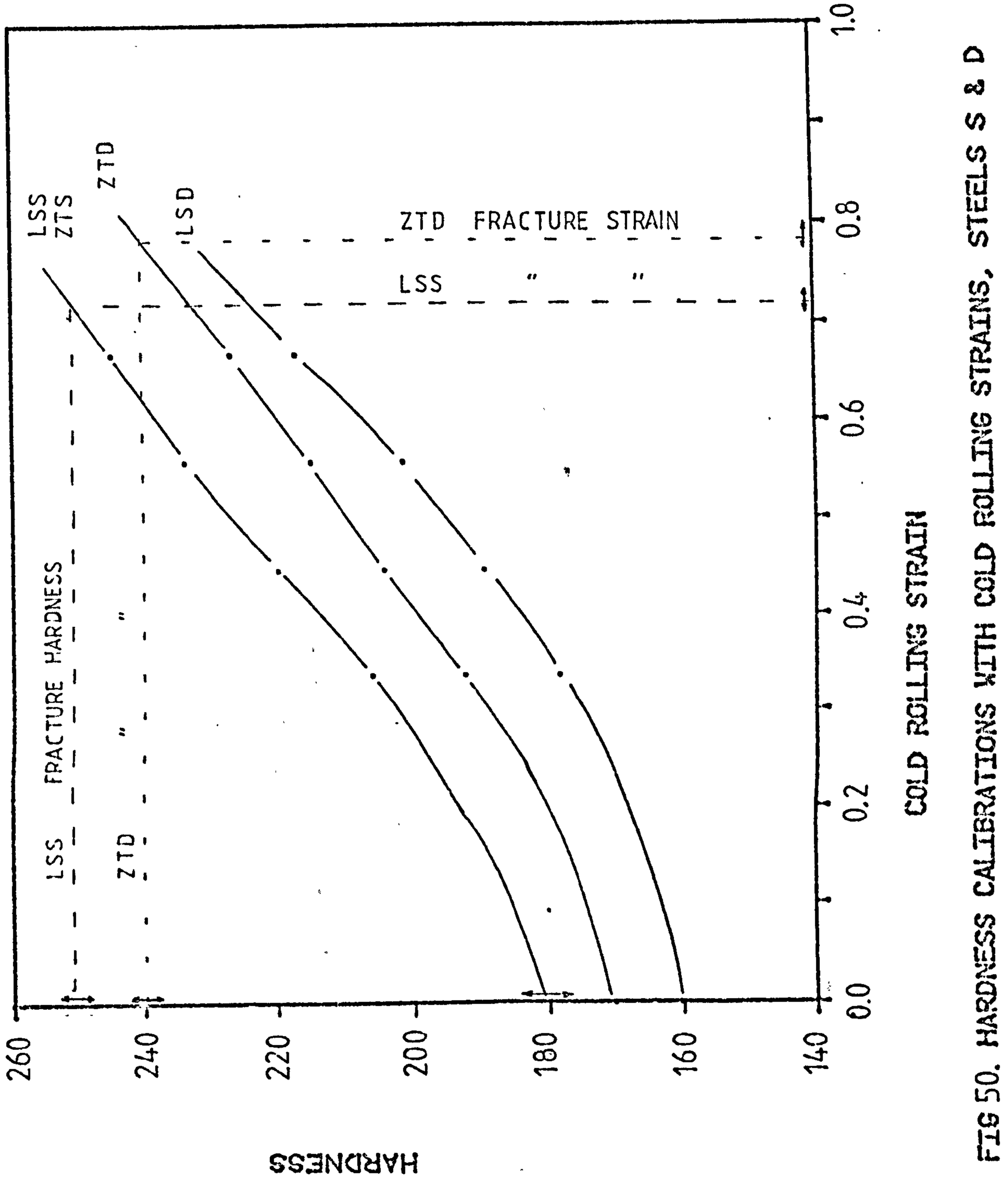

FIG 5. HARDNESS CALIBRATIONS WITH COLD ROLLING STRAINS, STEELS S & D

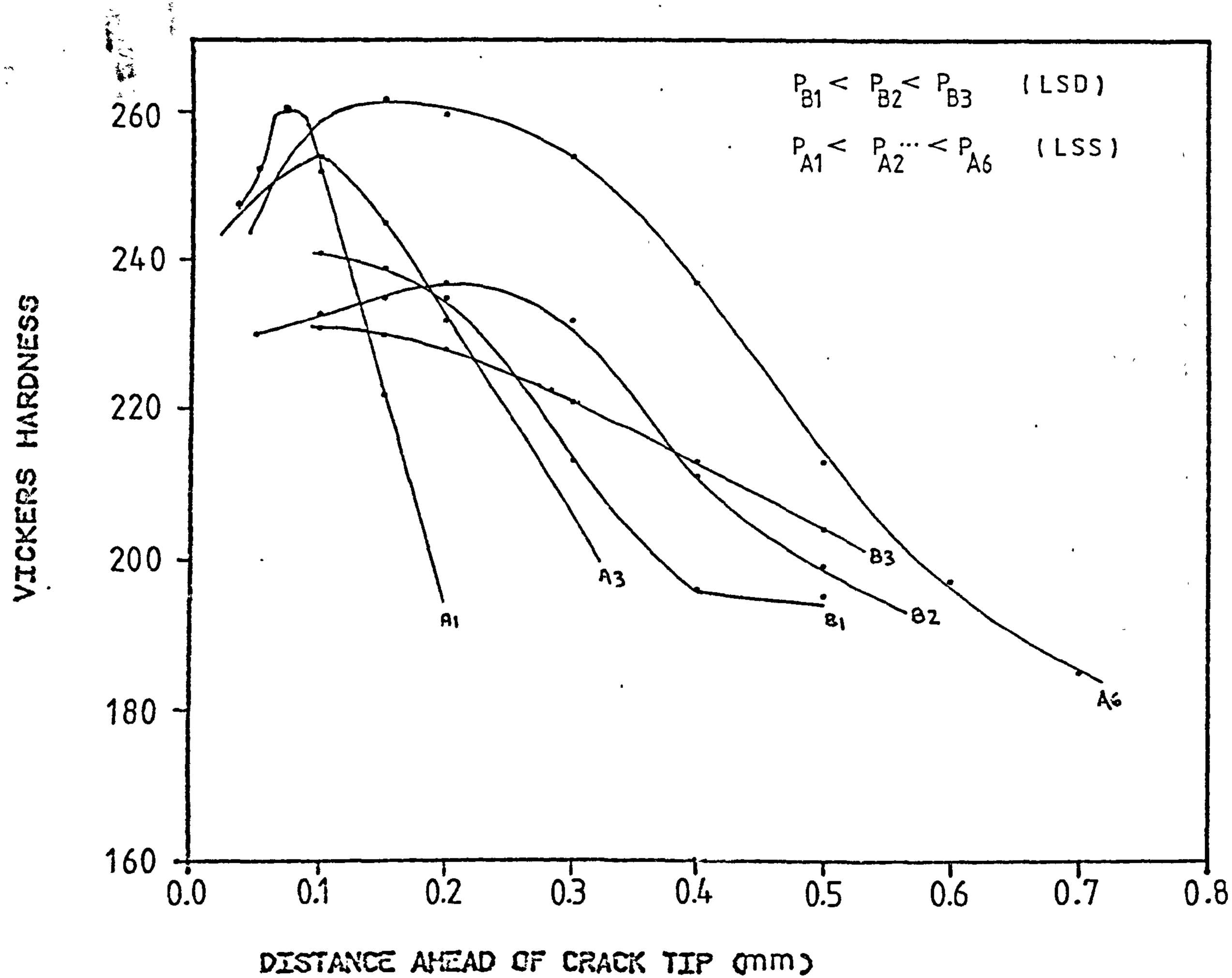

FIG 51 . LOAD DEPENDENCE OF r_p IN W = B = 10mm, LSD & LSS SPECIMENS

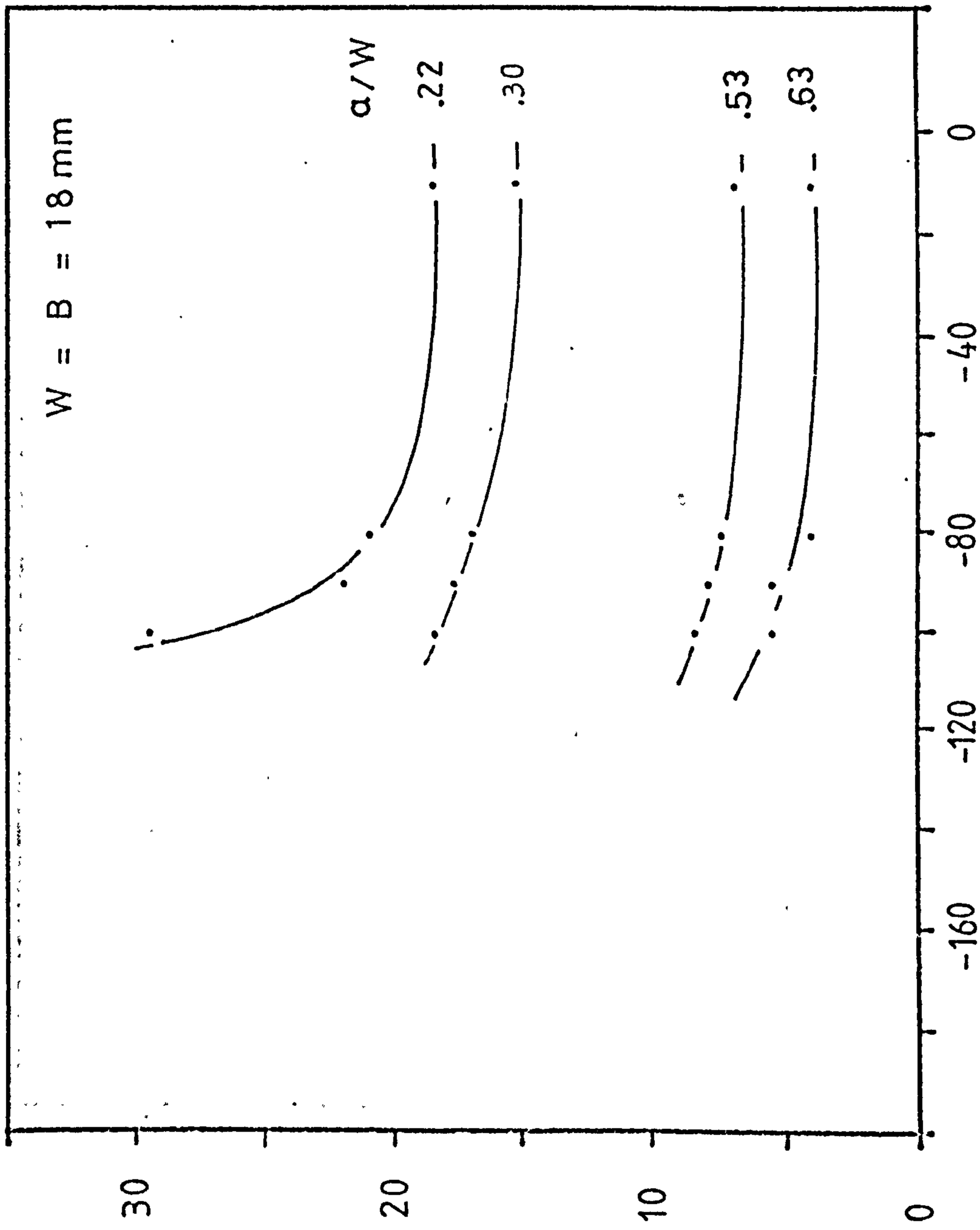

FIG 52A . P_{gy} TEMP. DEPENDENCE

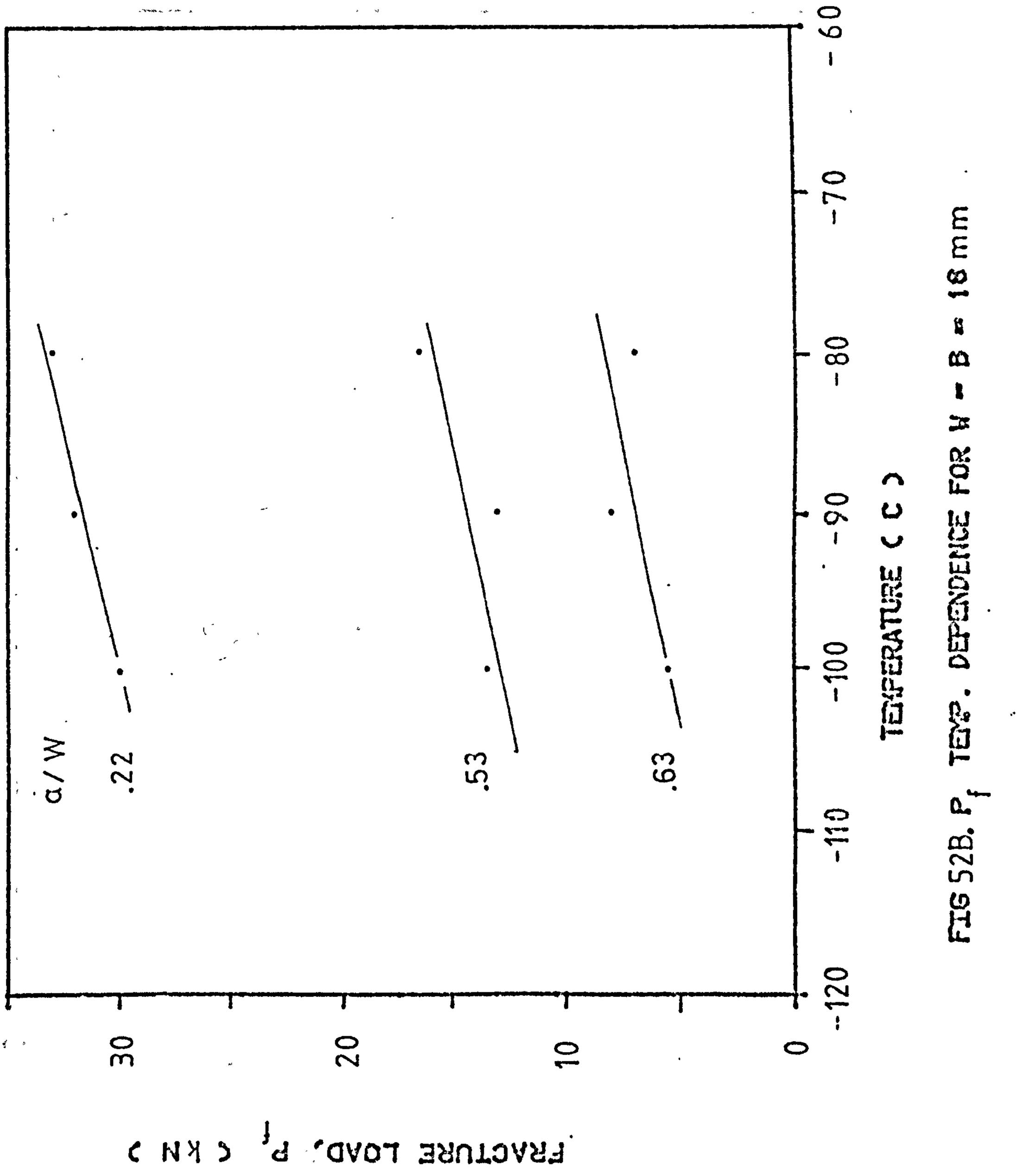

FIG 52B. P_f TEMP. DEPENDENCE FOR W = B = 18 mm

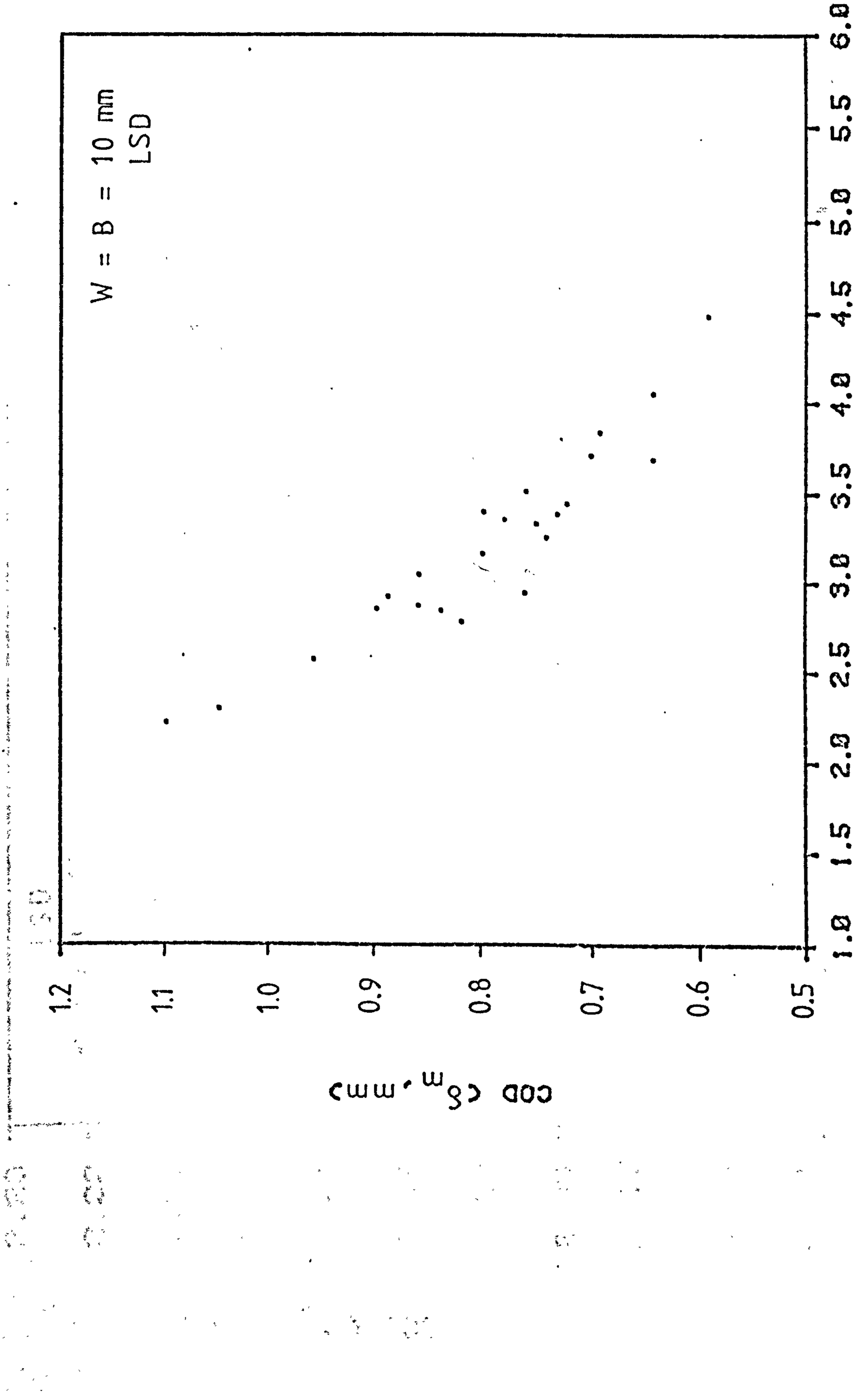

FIG 53. VARIATION OF COD WITH CRACK LENGTH

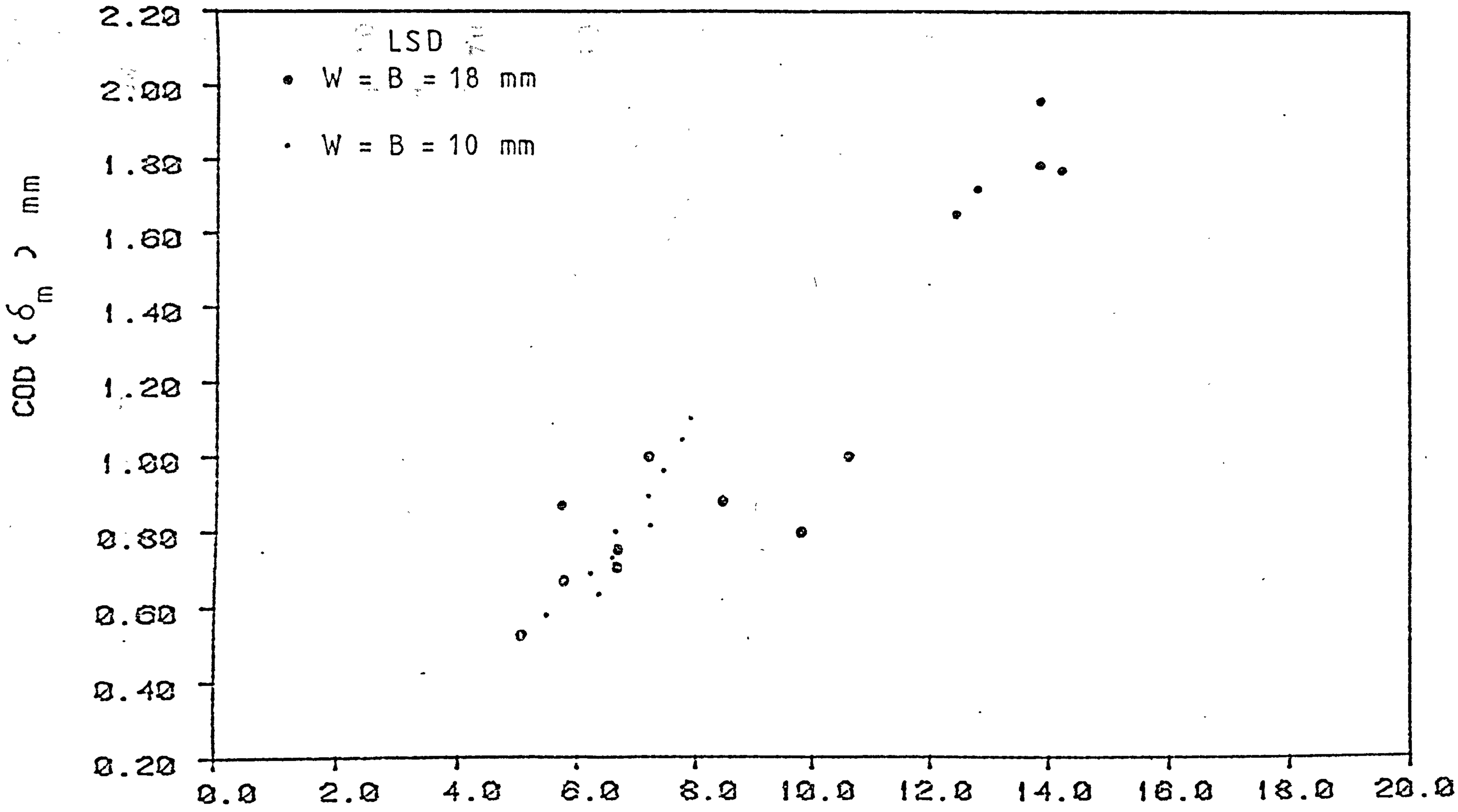

FIG 54. COD VARIATION WITH (W-a)

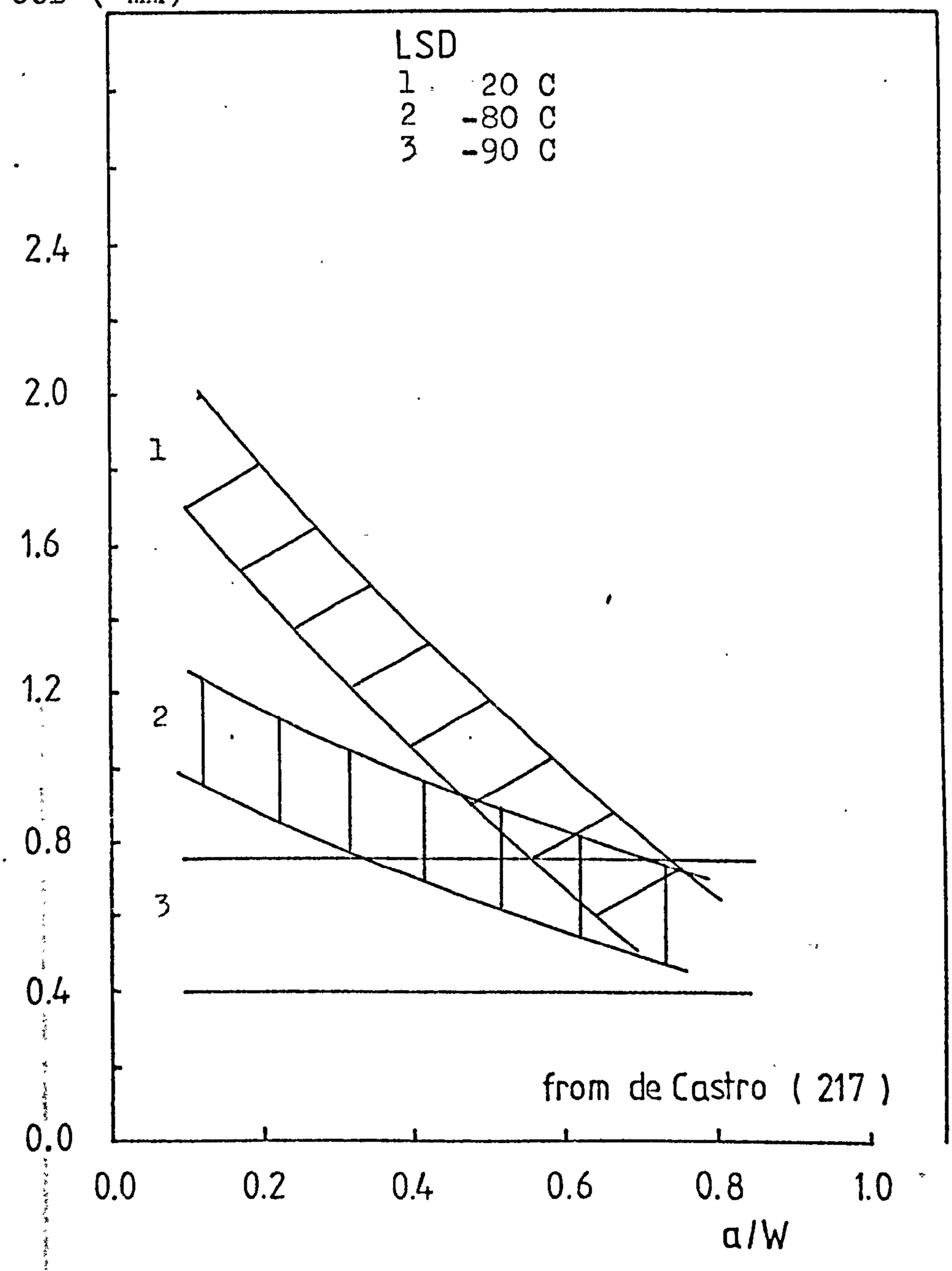

FIG 55. COD DEPENDENCE ON a/W FOR W=B=18mm
LSD SPECIMENS

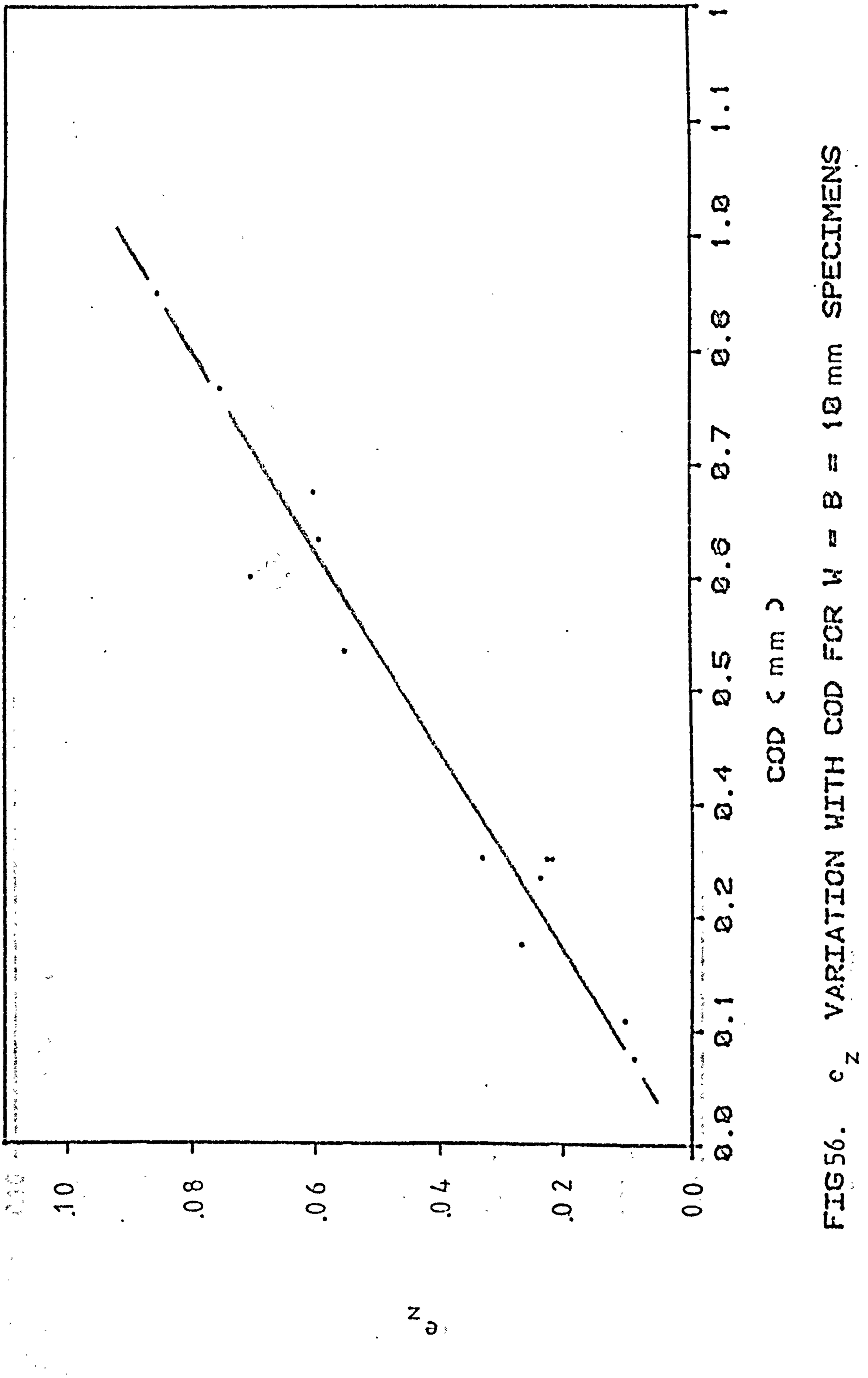
1.2
1.1
1.0
0.9
0.8
0.7
0.6
0.5
0.4
0.3
0.2
0.1
0.0
COD ζ mm
SPECIMENS H = B = 10 mm
VARIATION WITH COD FOR
z_e
z_a
1.0
0.8
0.6
0.4
0.2
0.0

FIG56.

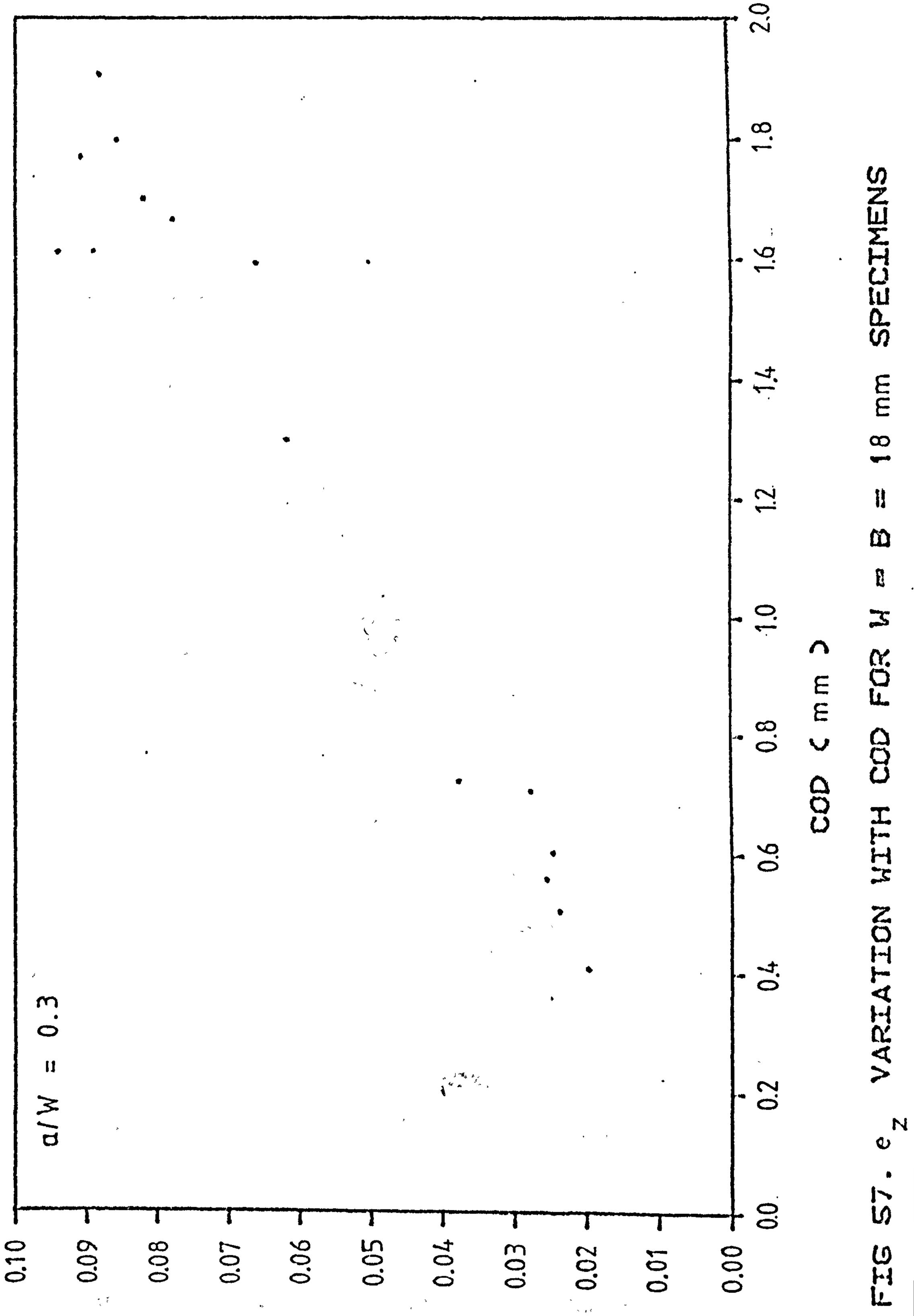
VARIATION WITH COD FOR W = B = 18 mm SPECIMENS
a/W = 0.3
COD ζ mm
e_z
z_e
0.0
0.2
0.4
0.6
0.8
1.0
1.2
1.4
1.6
1.8
2.0
0.00
0.01
0.02
0.03
0.04
0.05
0.06
0.07
0.08
0.09
0.10

FIG 57. e_z

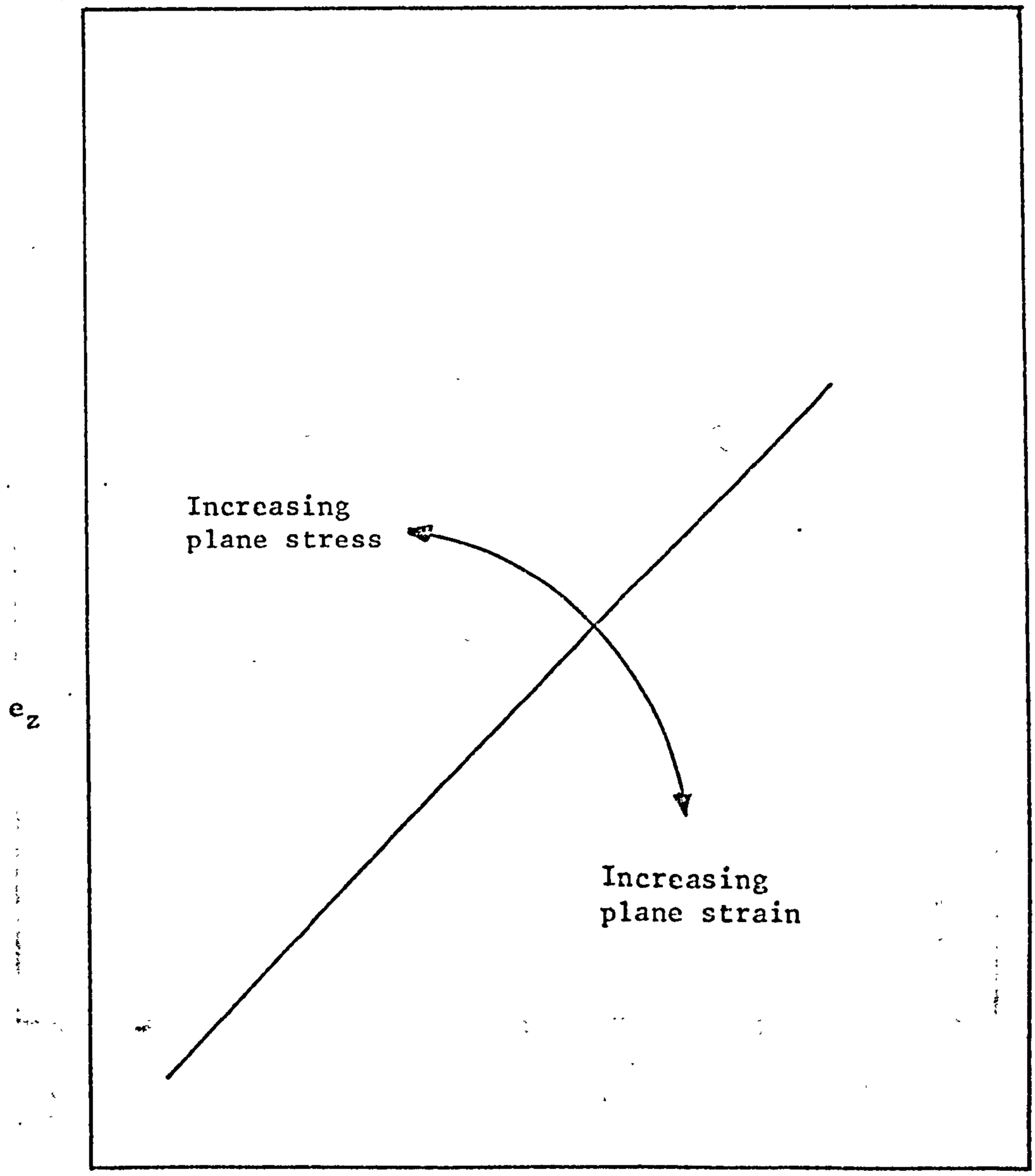

FIG 58. SCHEMATIC REPRESENTATION OF CHANGE IN THE STATE OF STRESS IN THE e_z - COD RELATIONSHIP

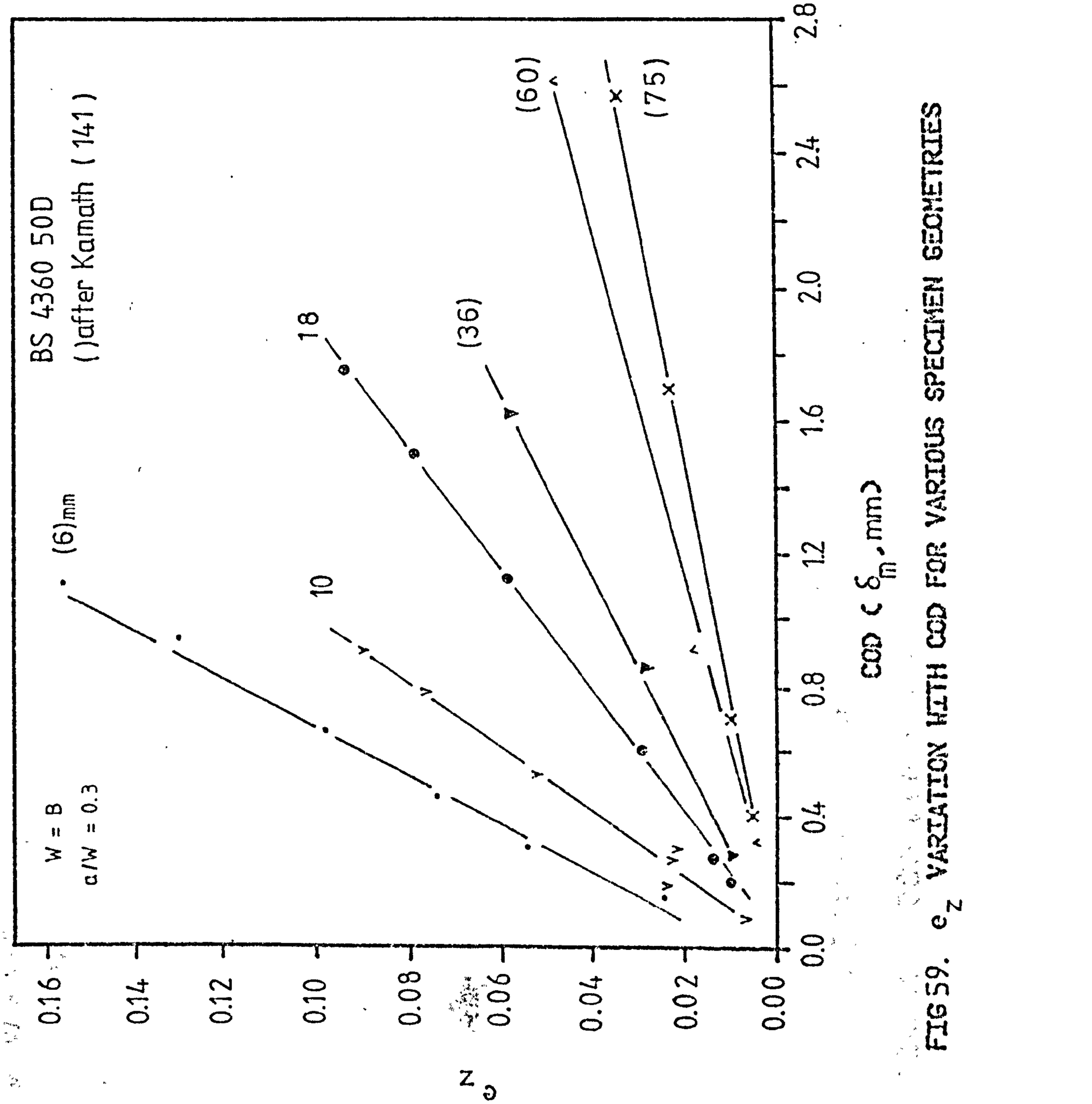
BS 4360 50D
( )after Kamath
(6)mm
W = B
a/W = 0.3
18
10
(36)
(60)
(75)
0.16
0.14
0.12
0.10
0.08
0.06
0.04
0.02
0.00
0.0
0.4
0.8
1.2
1.6
2.0
2.4
2.8
COD ε δm, mm
FIG 59. ez VARIATION WITH COD FOR VARIOUS SPECIMEN GEOMETRIES

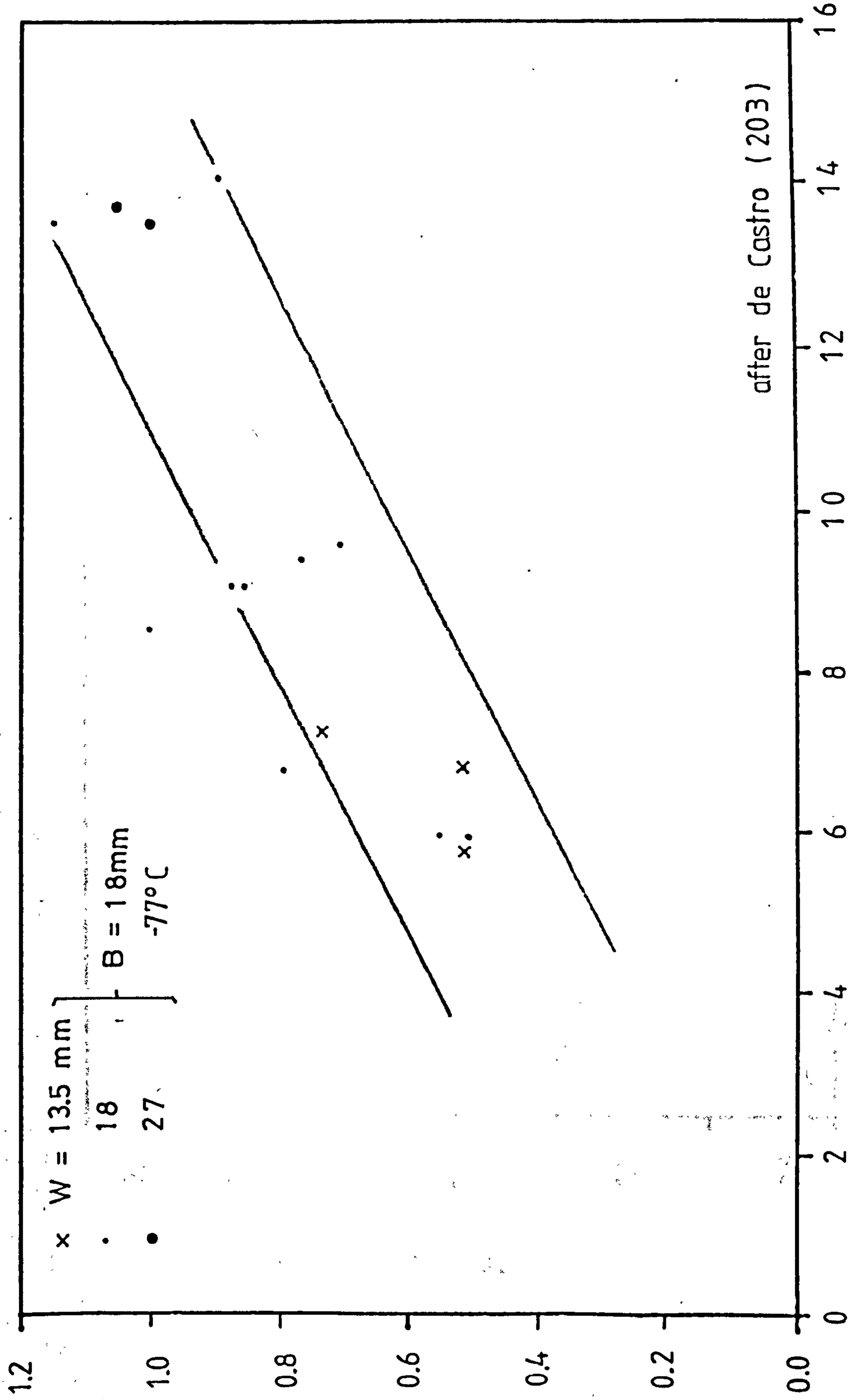

FIG 60. COD DEPENDENCE ON LIGAMENT LENGTH

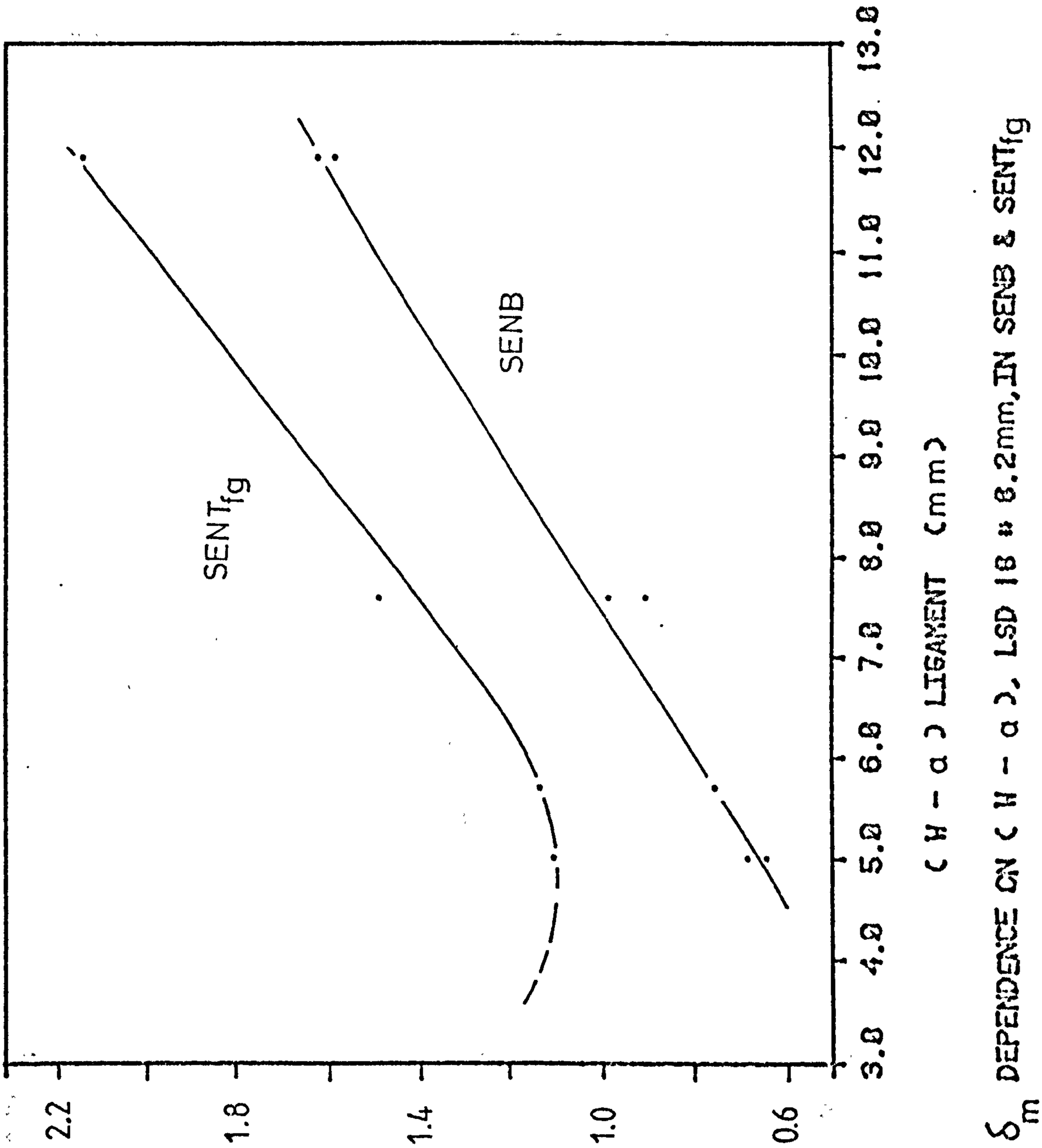

FIG 61A. δ_m DEPENDENCE ON (H - a) AND (H - a) LIGAMENT (mm), LSD 18 * 8.2mm, IN SENB & SENT$_{fg}$

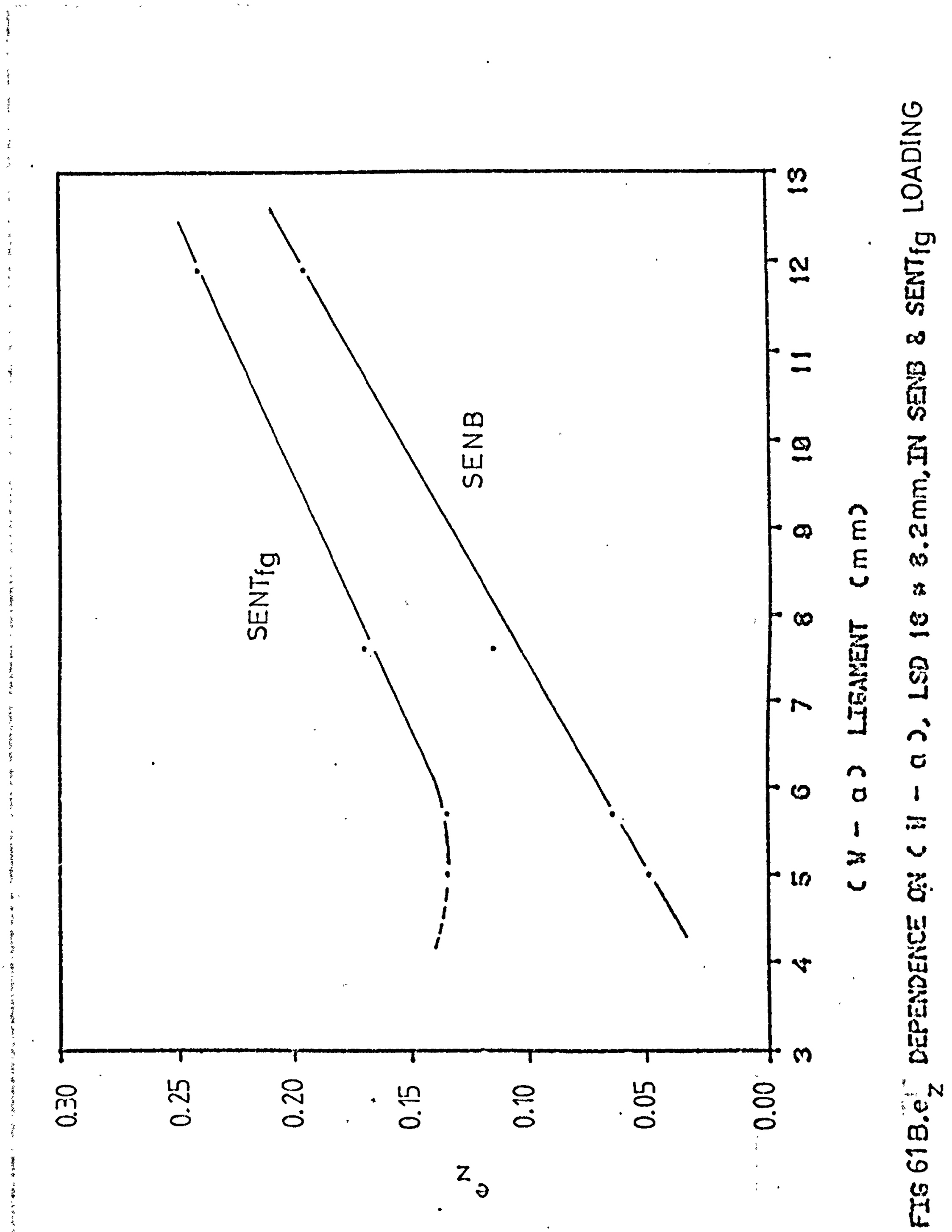
SENTfg LOADING
13
12
10
9
8
7
6
5
4
3
SENTfg
SENB
(W - a) LIGAMENT (mm)
18 x 3.2mm, IN SENB & S
DEPENDENCE ON (W - a), LSD
0.30
0.25
0.20
0.15
0.10
0.05
0.00
N_e

FIG 61B.e$_2$

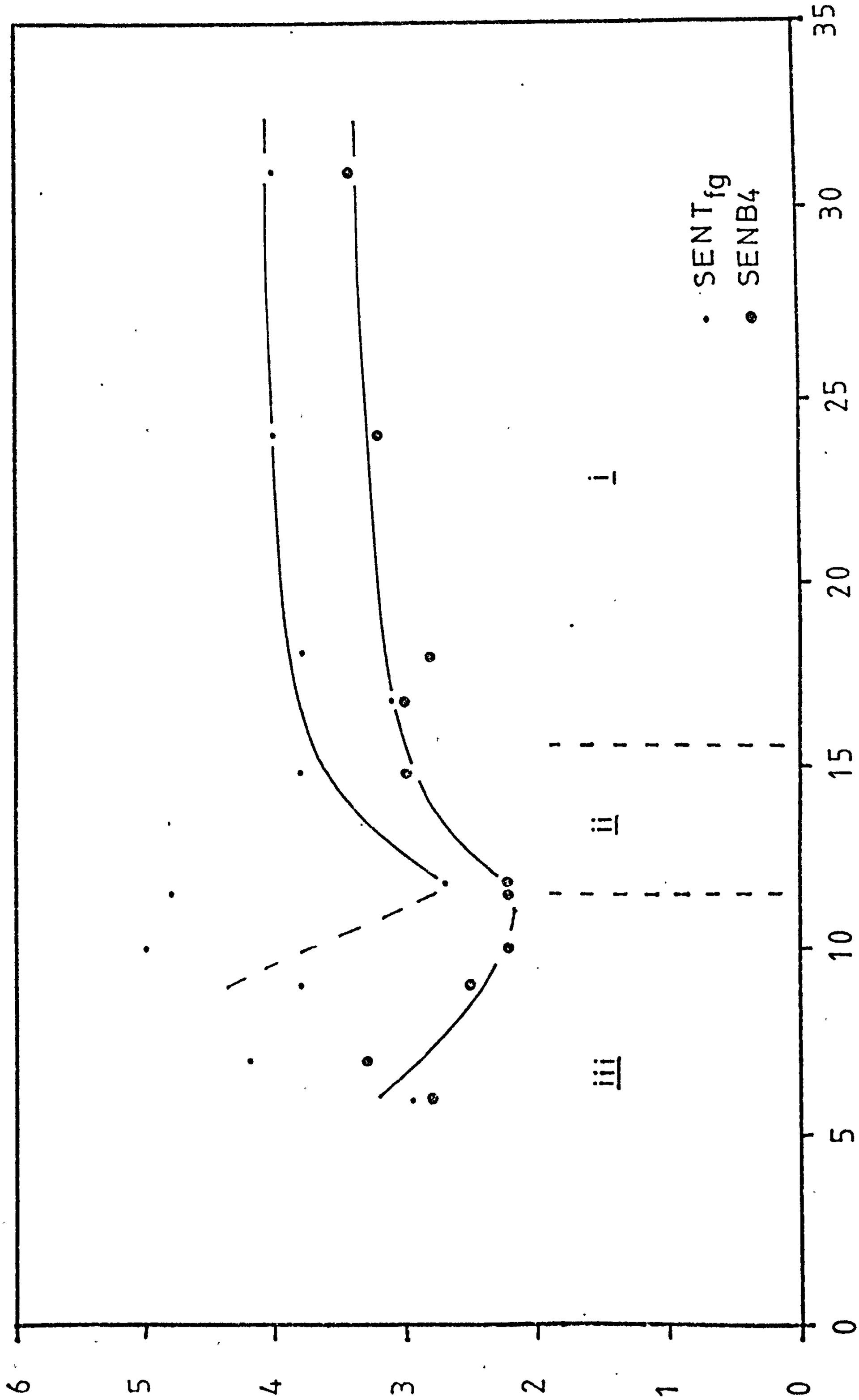

FIG 62A. COD VS (W - a) IN PLASTICINE

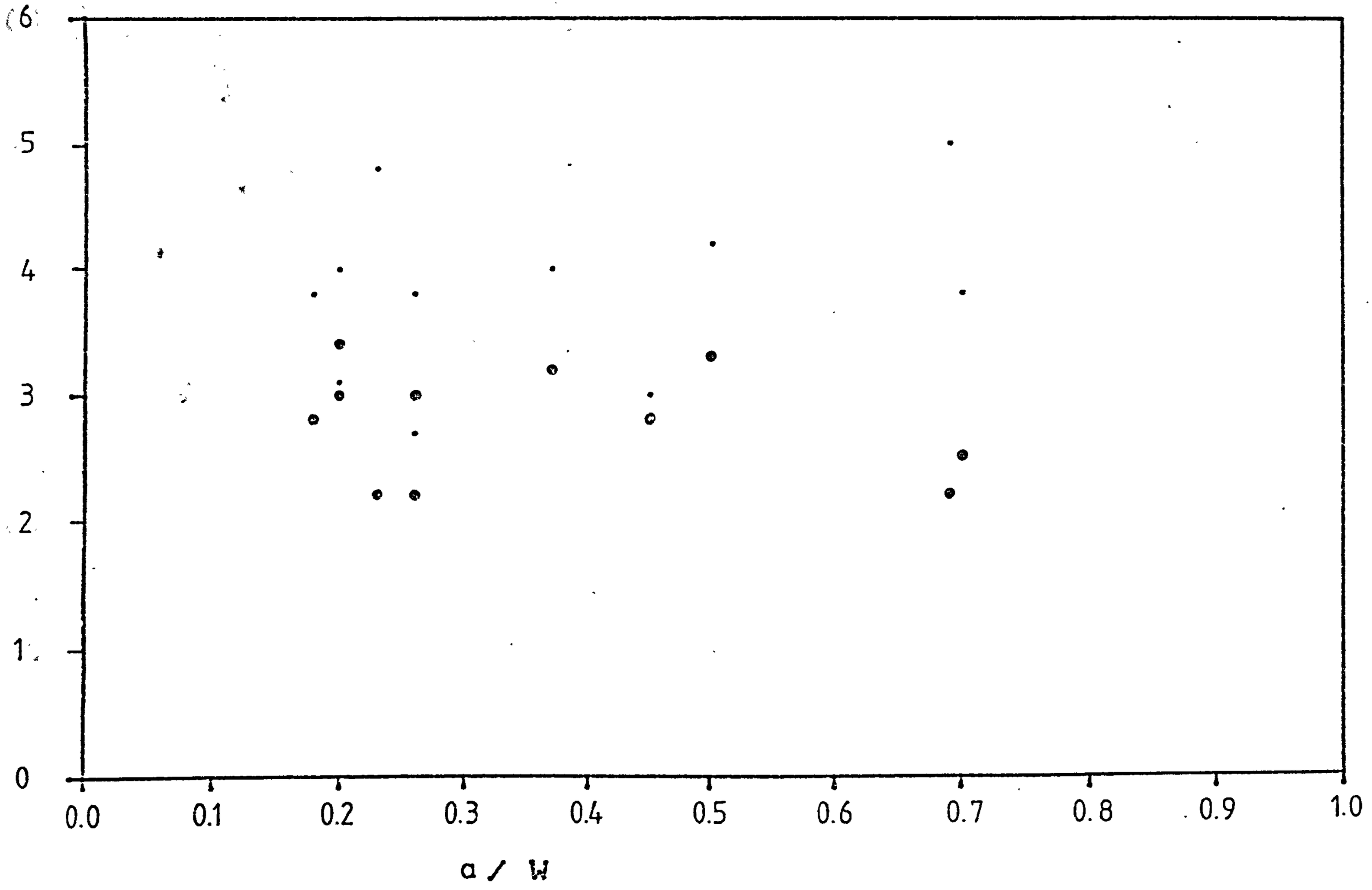

FIG 62B. COD VS a / W IN PLASTICINE

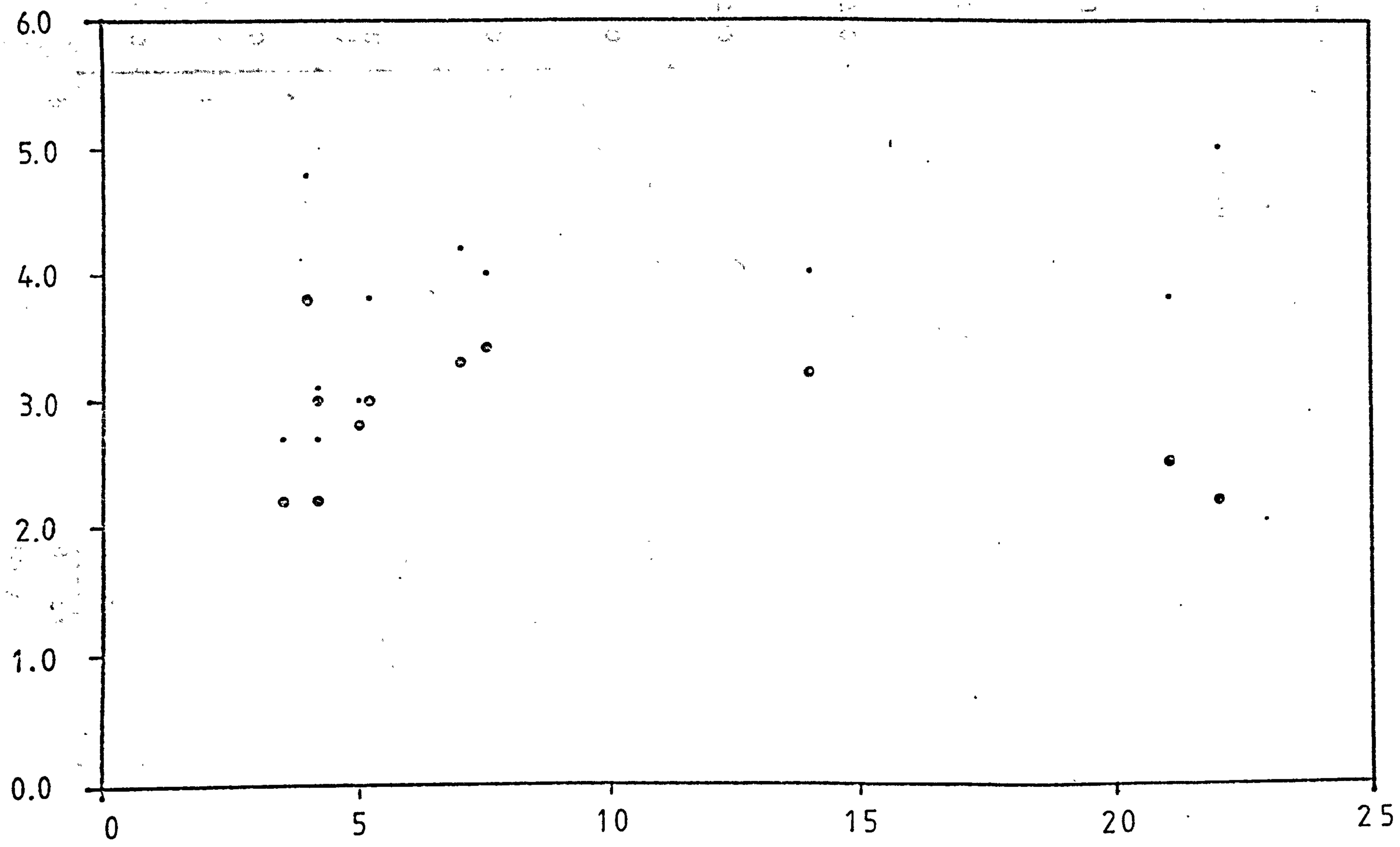

FIG 62C. COD VS (a) IN PLASTICINE

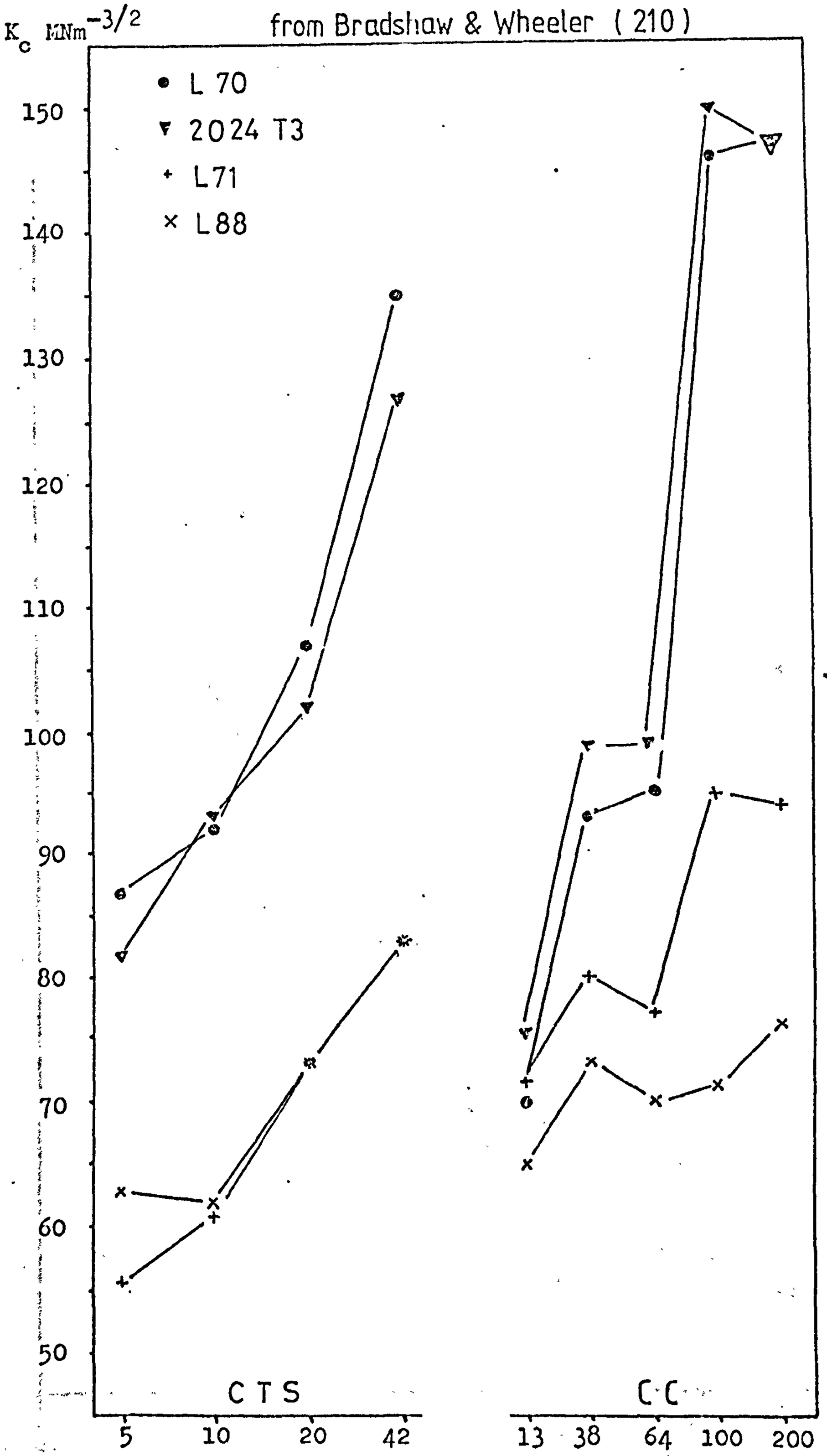

FIG 63. TOUGHNESS DEPENDENCE ON CRACK LENGTH

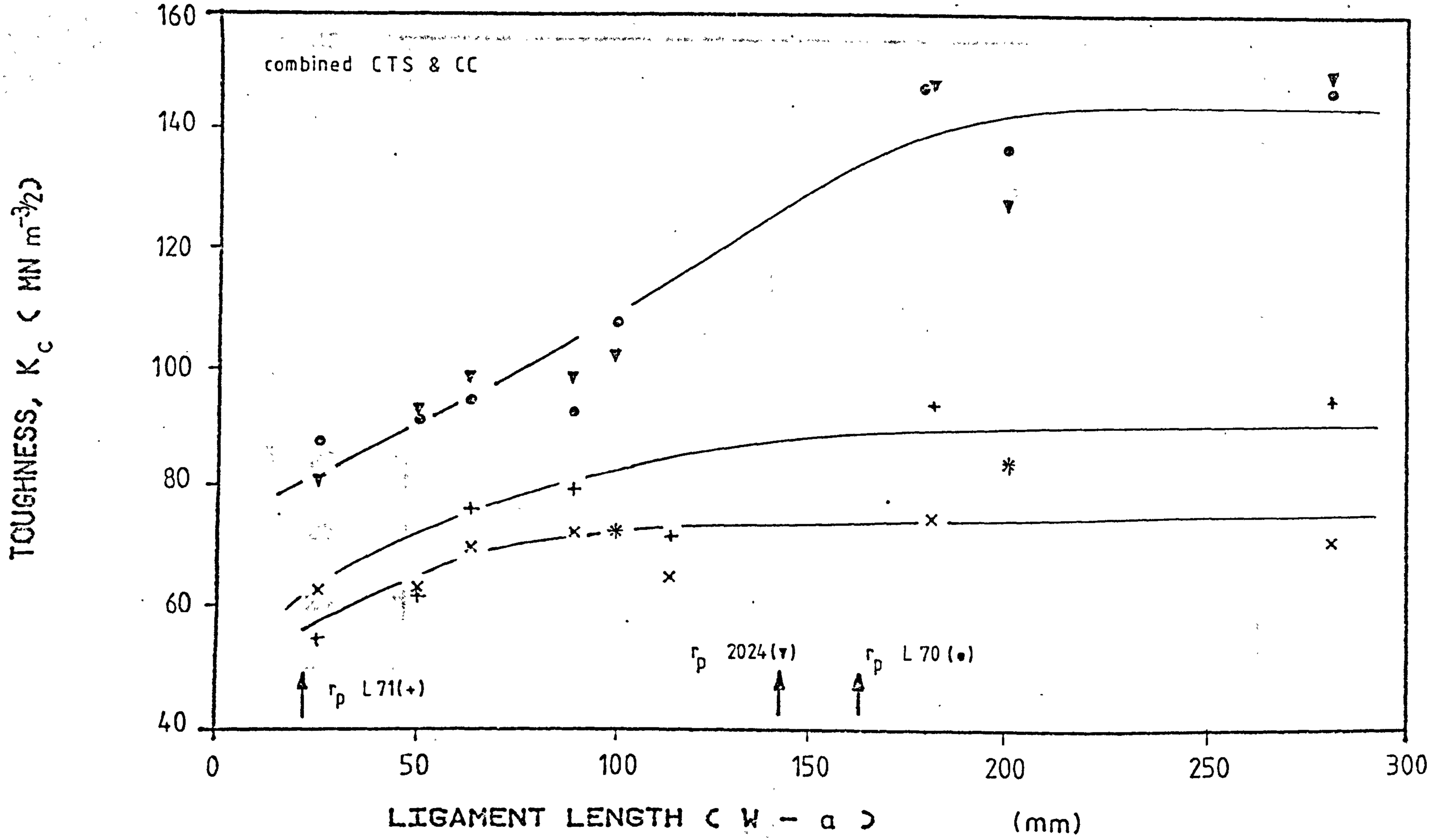

FIG 64. INTERPRETED K_c DEPENDENCE ON (W − a)

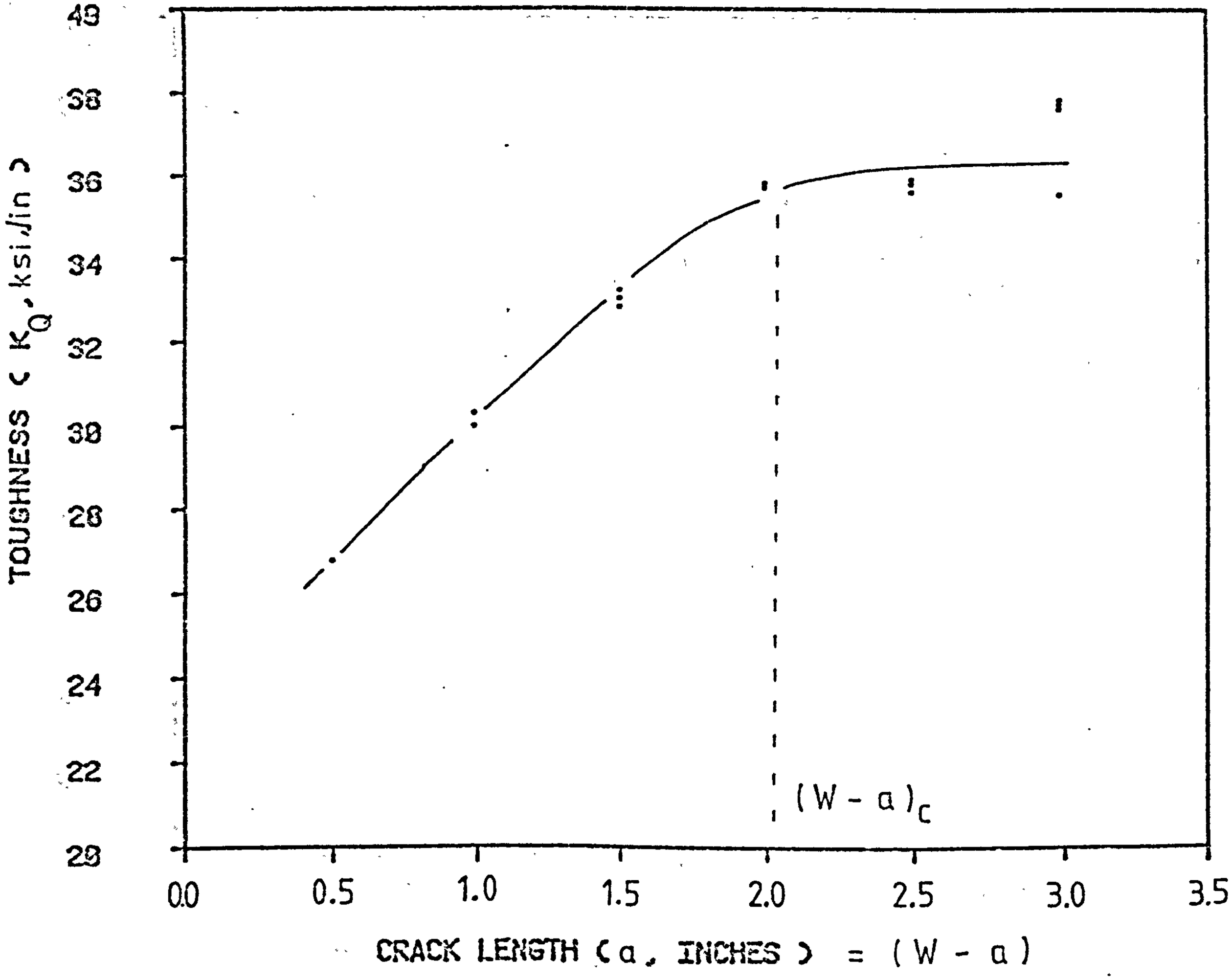

FIG 65. K_Q DEPENDENCE ON CRACK LENGTH FOR AN ALUMINIUM ALLOY

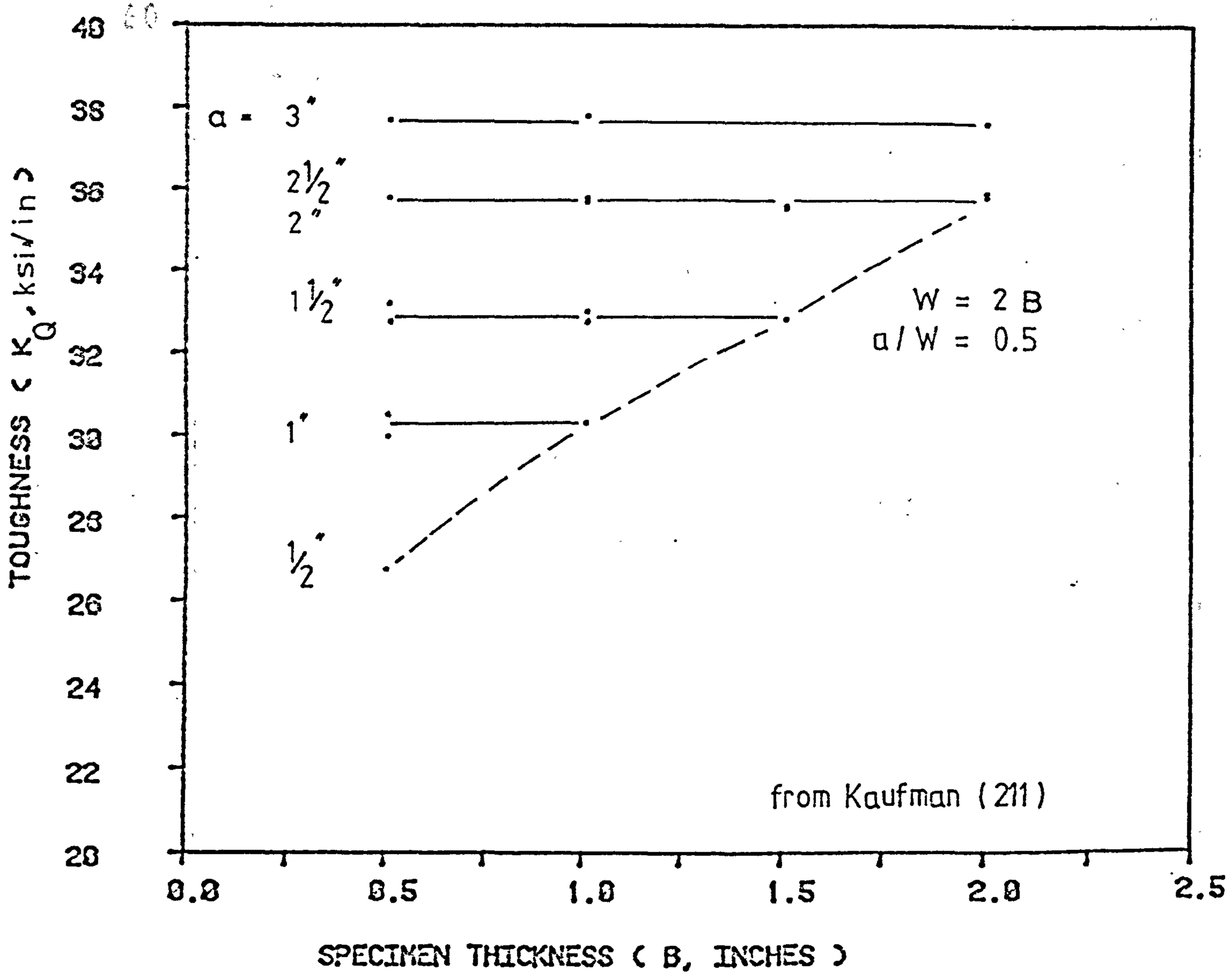

FIG 66. K_Q DEPENDENCE ON SPECIMEN THICKNESS FOR AN ALUMINIUM ALLOY

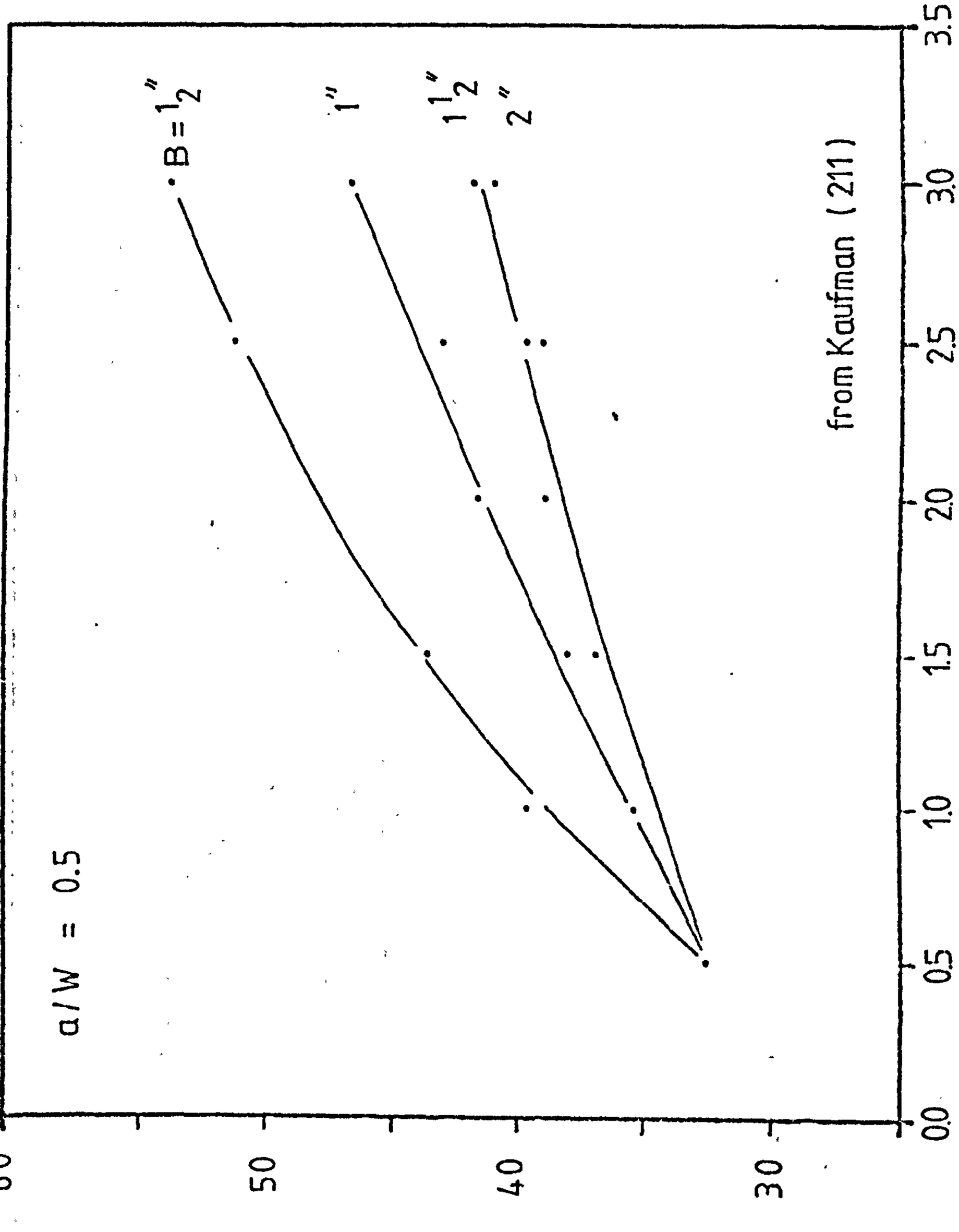

FIG. 67. K_m DEPENDENCE ON CRACK LENGTH FOR AN ALUMINIUM ALLOY

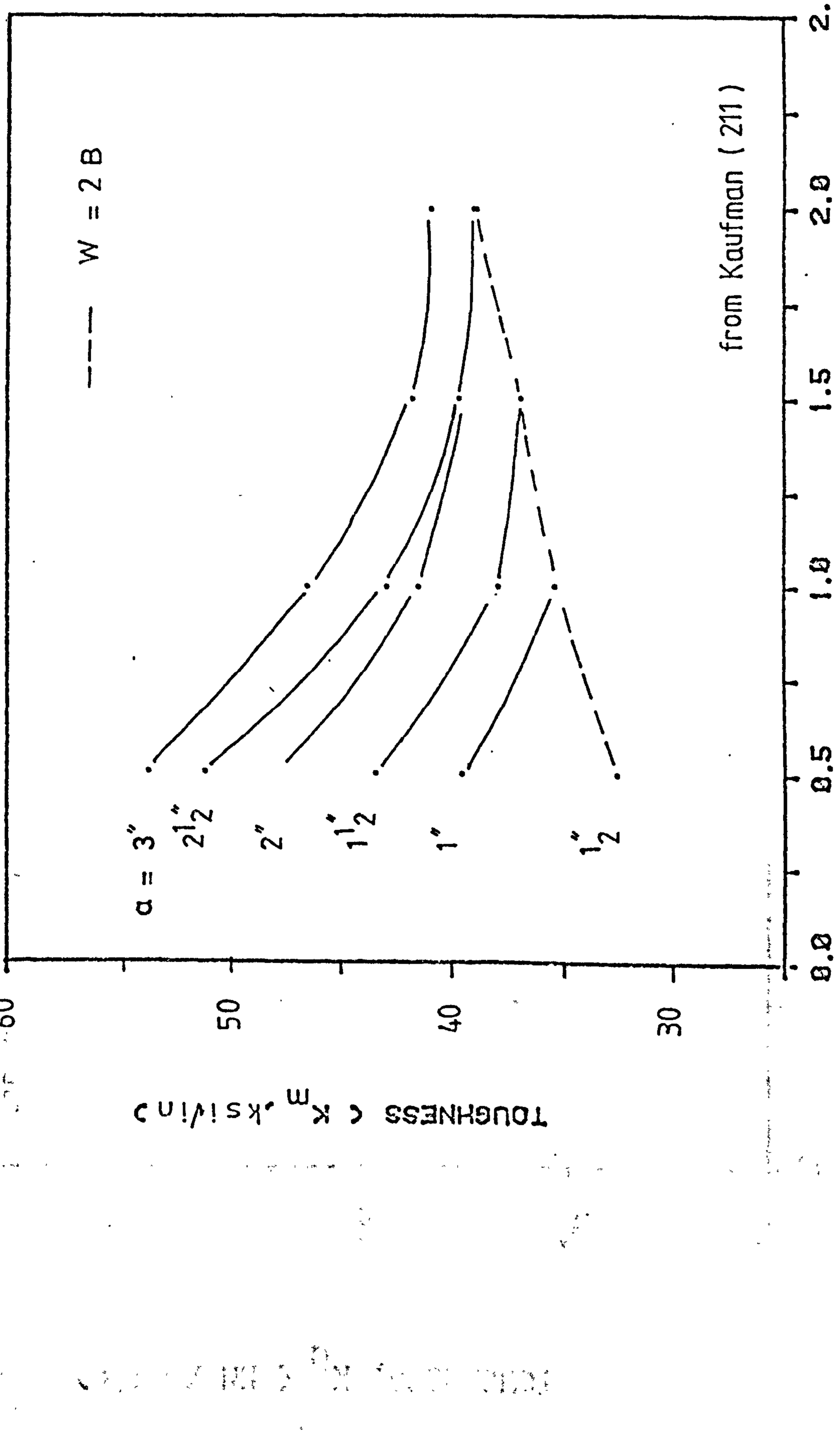
W = 2 B
from Kaufman (211)
THICKNESS FOR AN ALUMINUM ALLOY
SPECIMEN THICKNESS (B, INCHES)
0.0
0.5
1.0
1.5
2.0
2.5
K_m DEPENDENCE ON SPECIMEN
TOUGHNESS (K_m, ksi√in)
60
50
40
30
a = 3"
2 1/2"
2"
1 1/2"
1"
1/2"

FIG 68. K

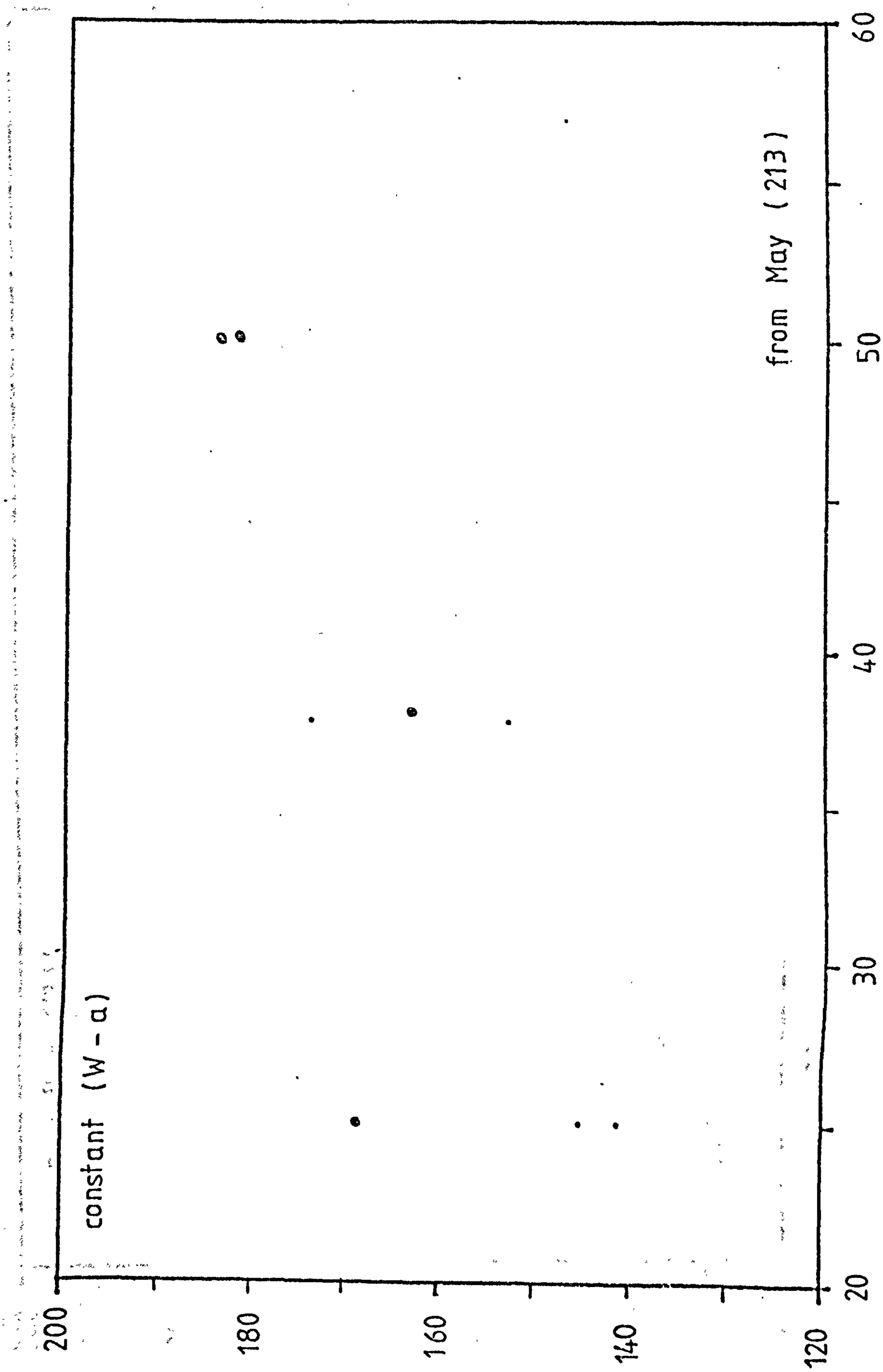

FIG 69 . K_Q DEPENDENCE ON B FOR STRUCTURAL STEELS

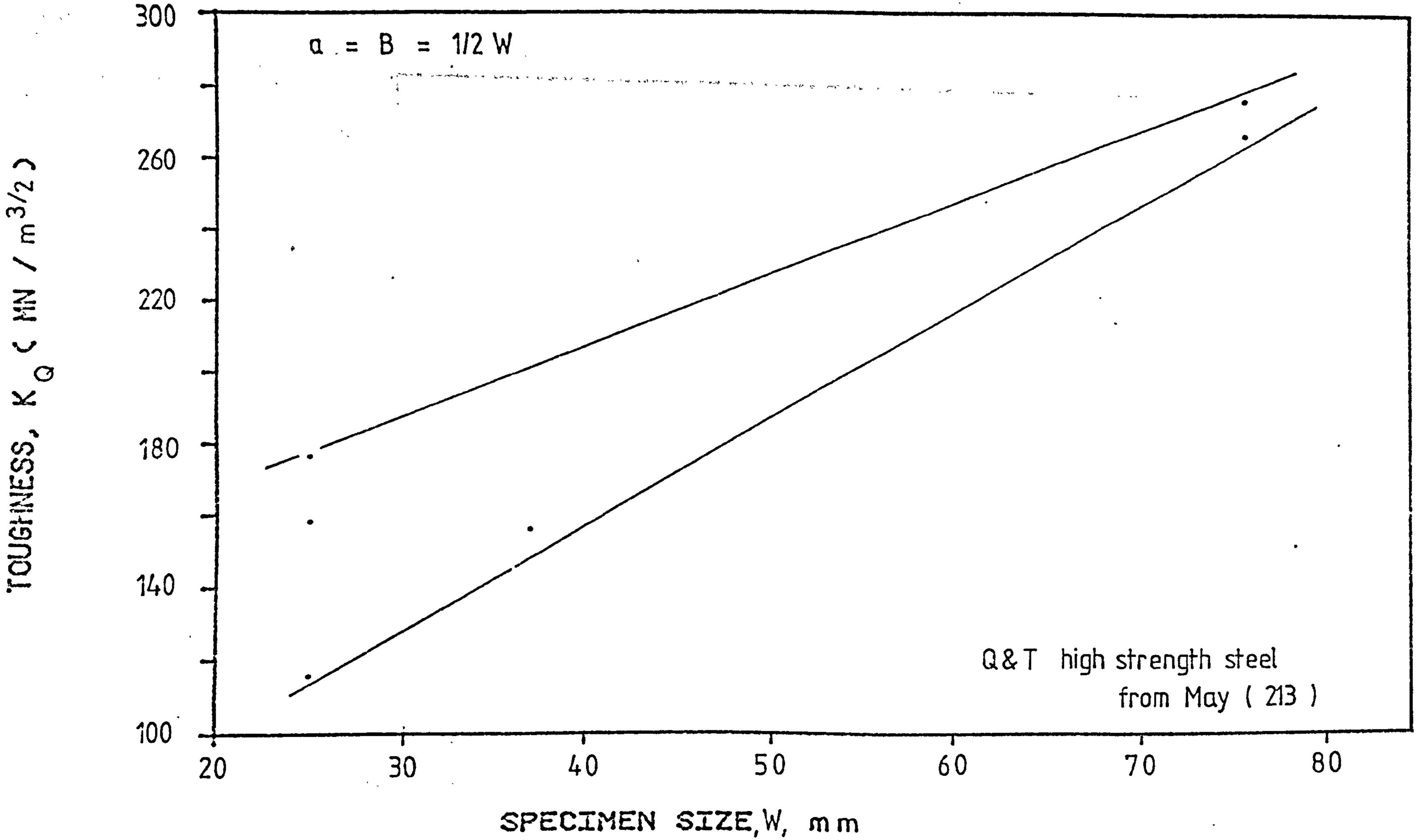

FIG 70 . K_Q DEPENDENCE ON GEOMETRY FOR STRUCTURAL STEELS

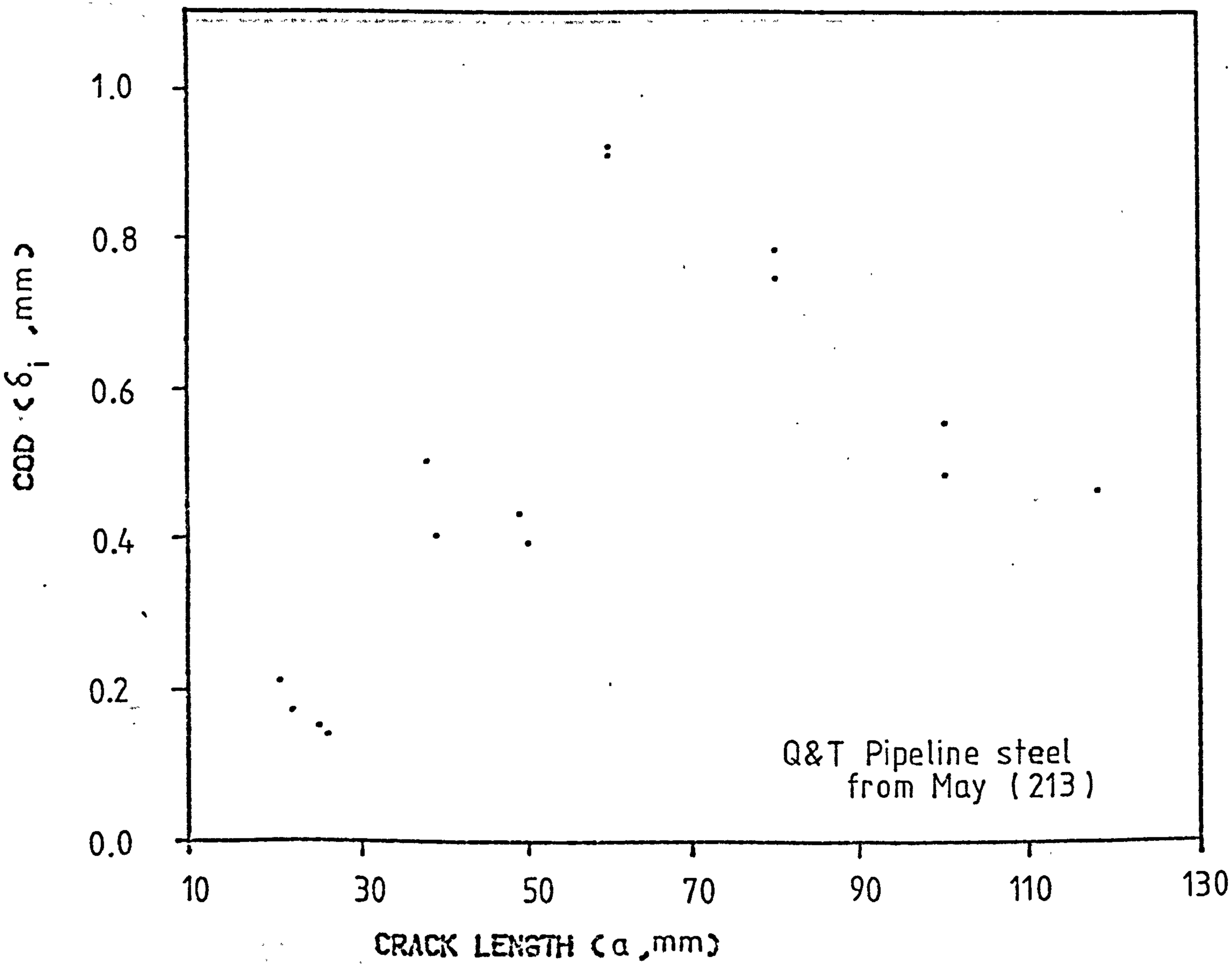

FIG 71A . δ_i DEPENDENCE ON CRACK LENGTH

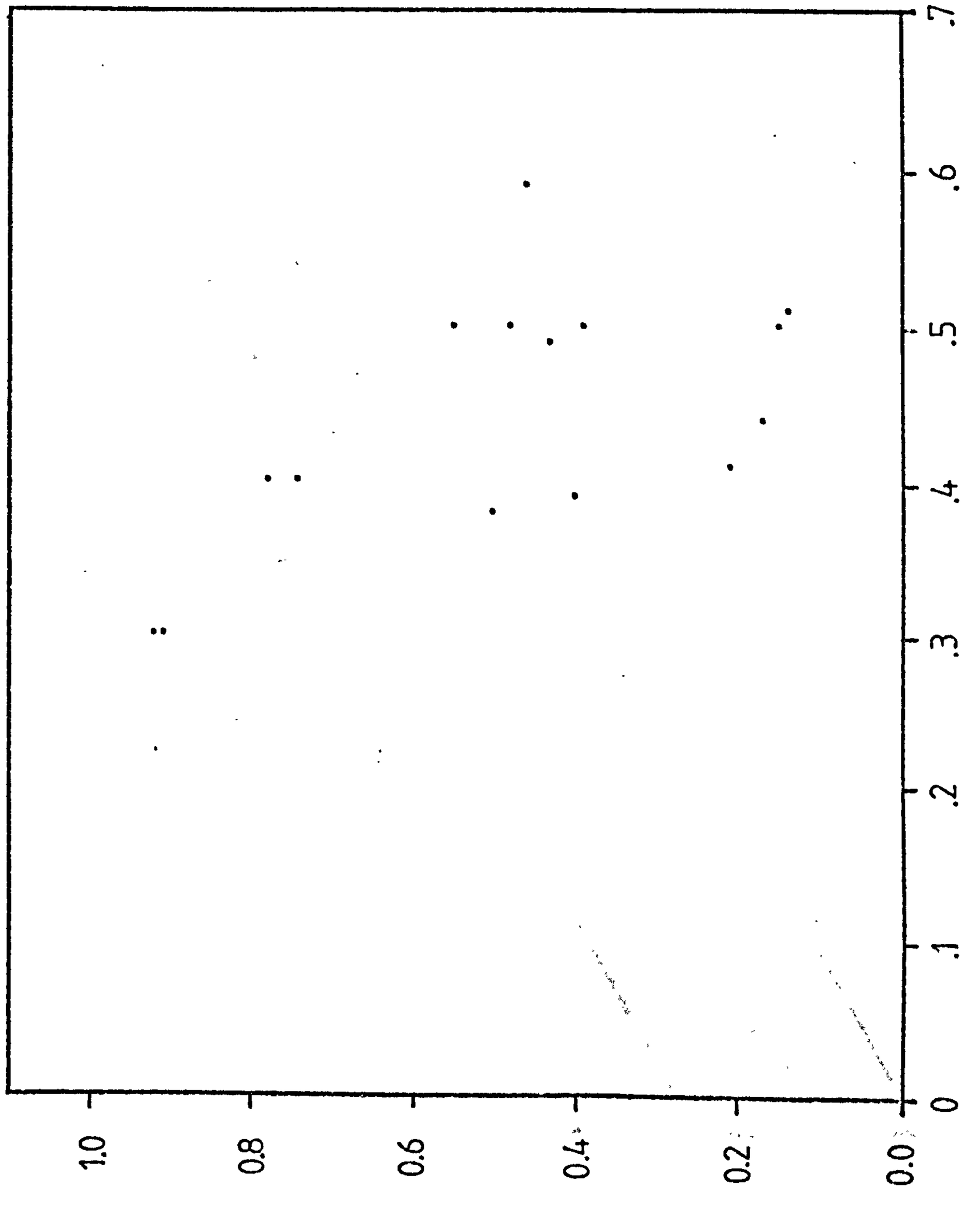

FIG 71B. δ_1 DEPENDENCE ON a/ W RATIO

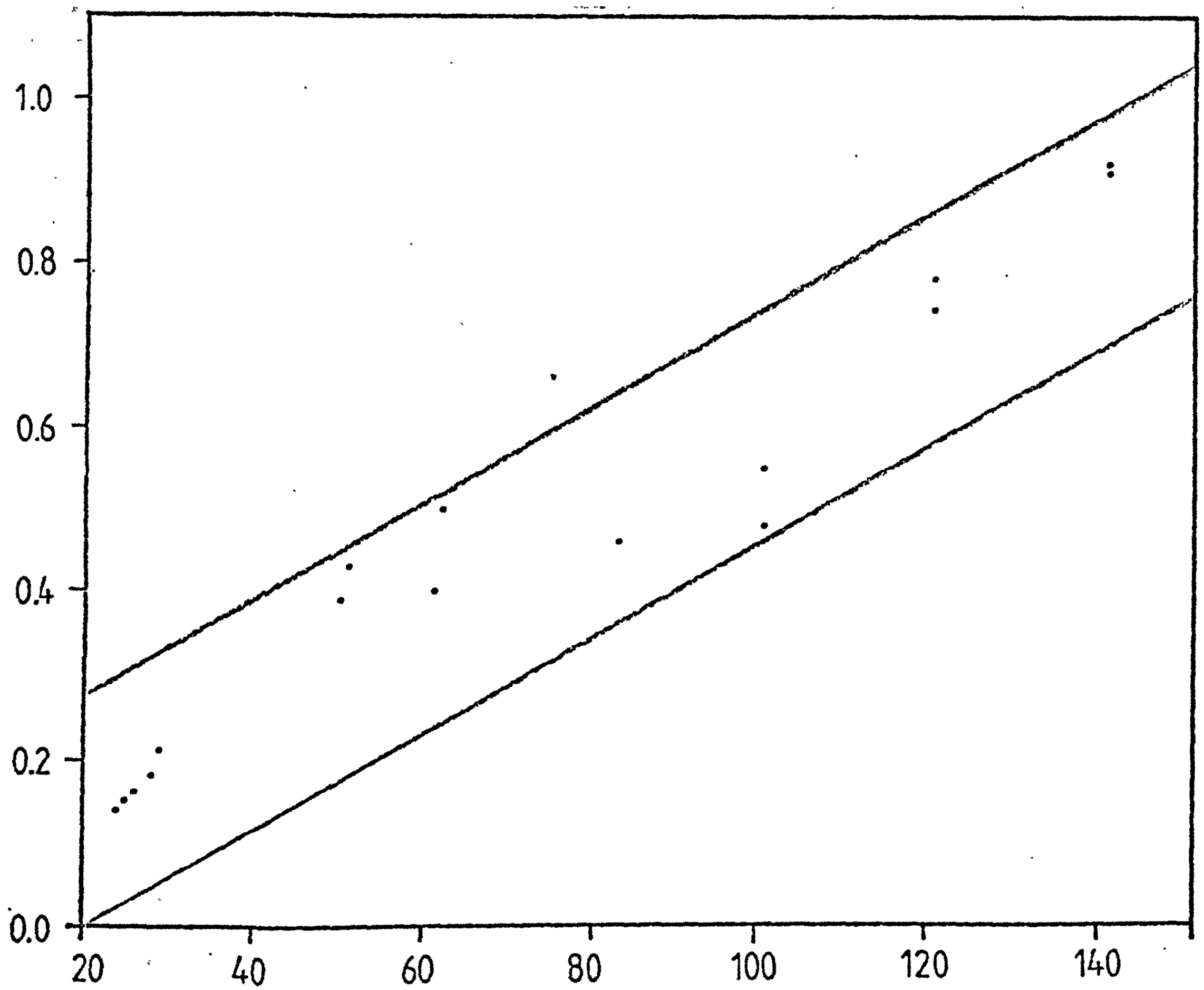

FIG 71C. δ_i DEPENDENCE ON (W - a)

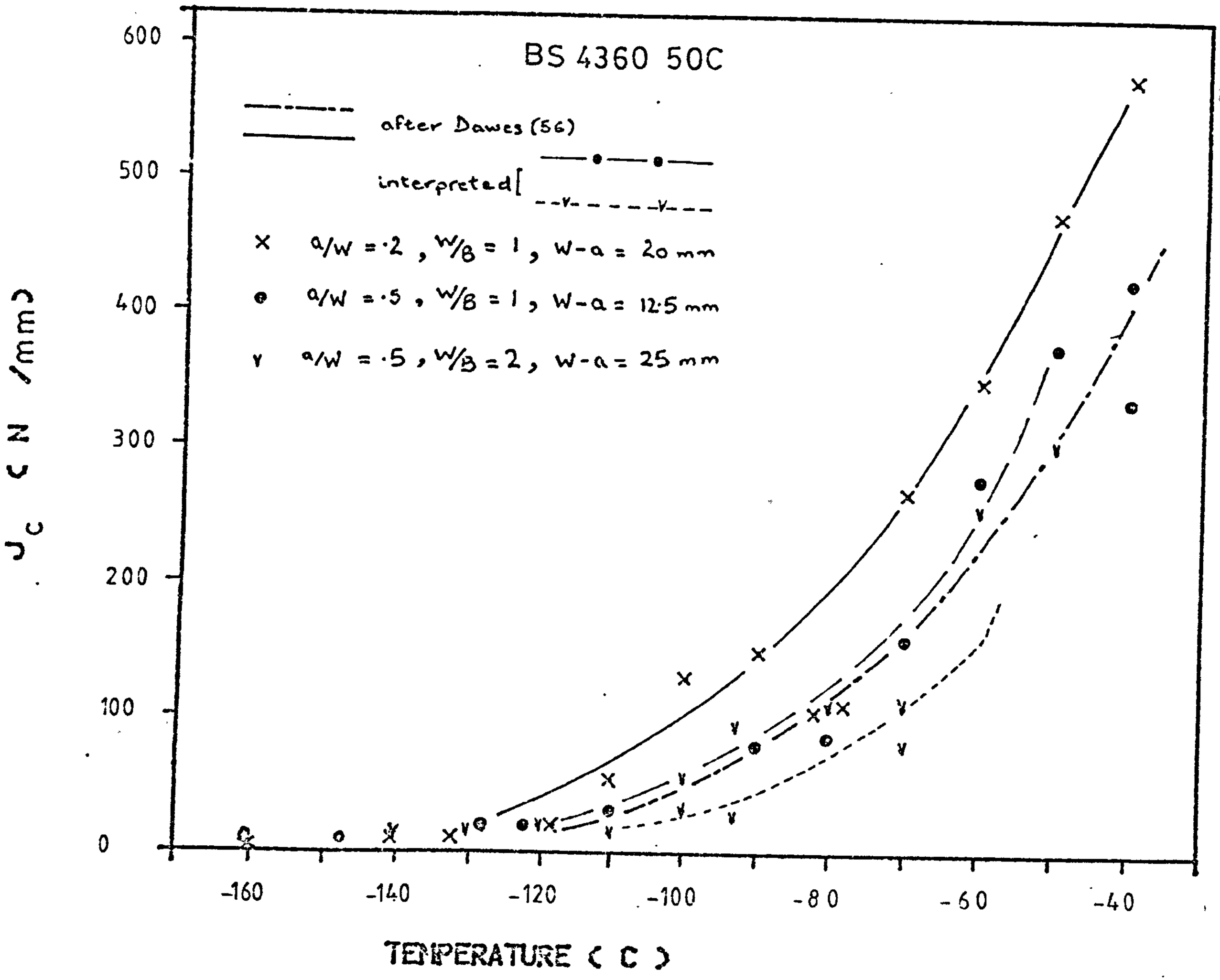

FIG 72. J_c TEMP. TRANSFORMATION CURVES FOR VARIOUS GEOMETRIES

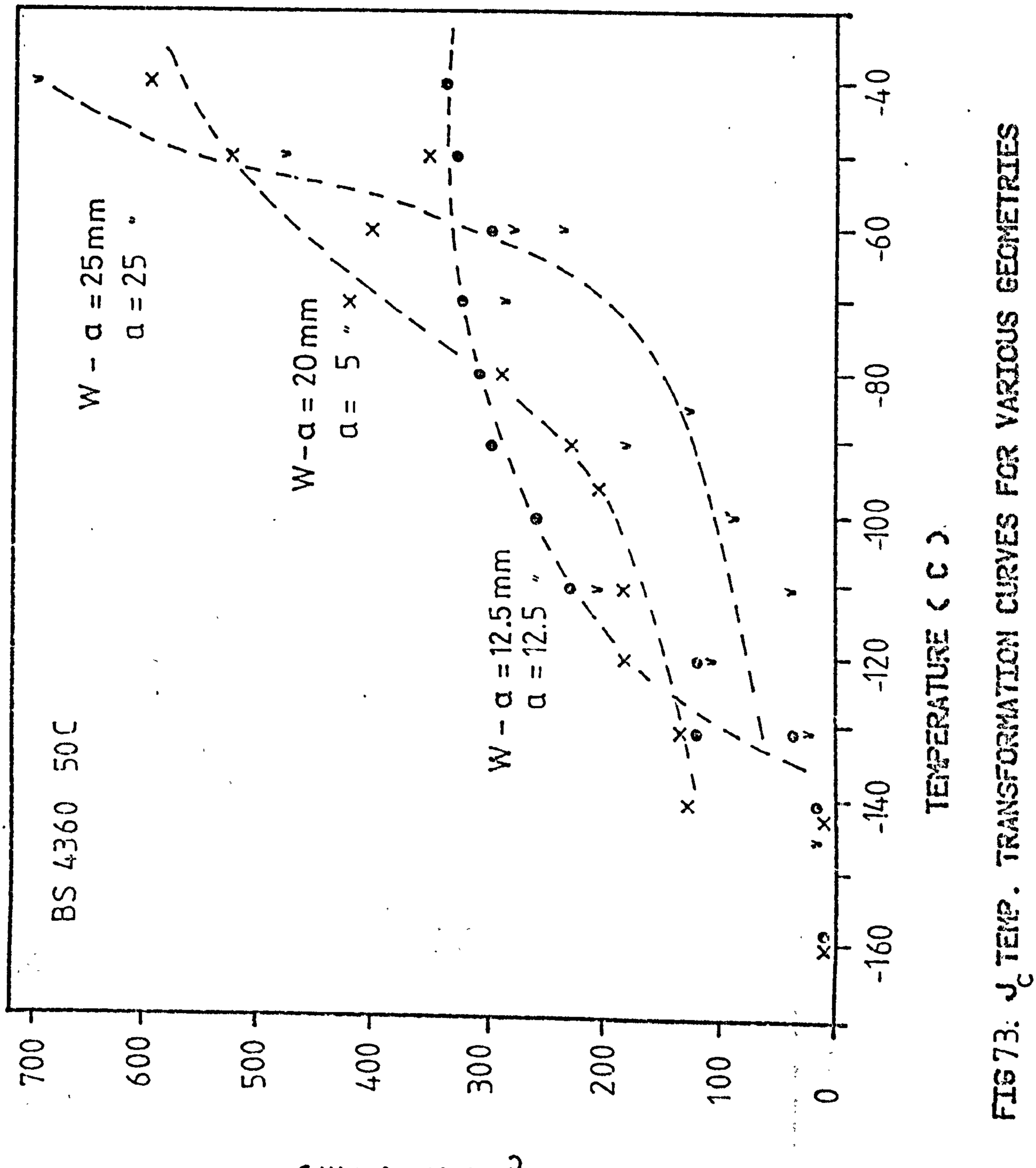

FIG 73: J_c TEMP. TRANSFORMATION CURVES FOR VARIOUS GEOMETRIES

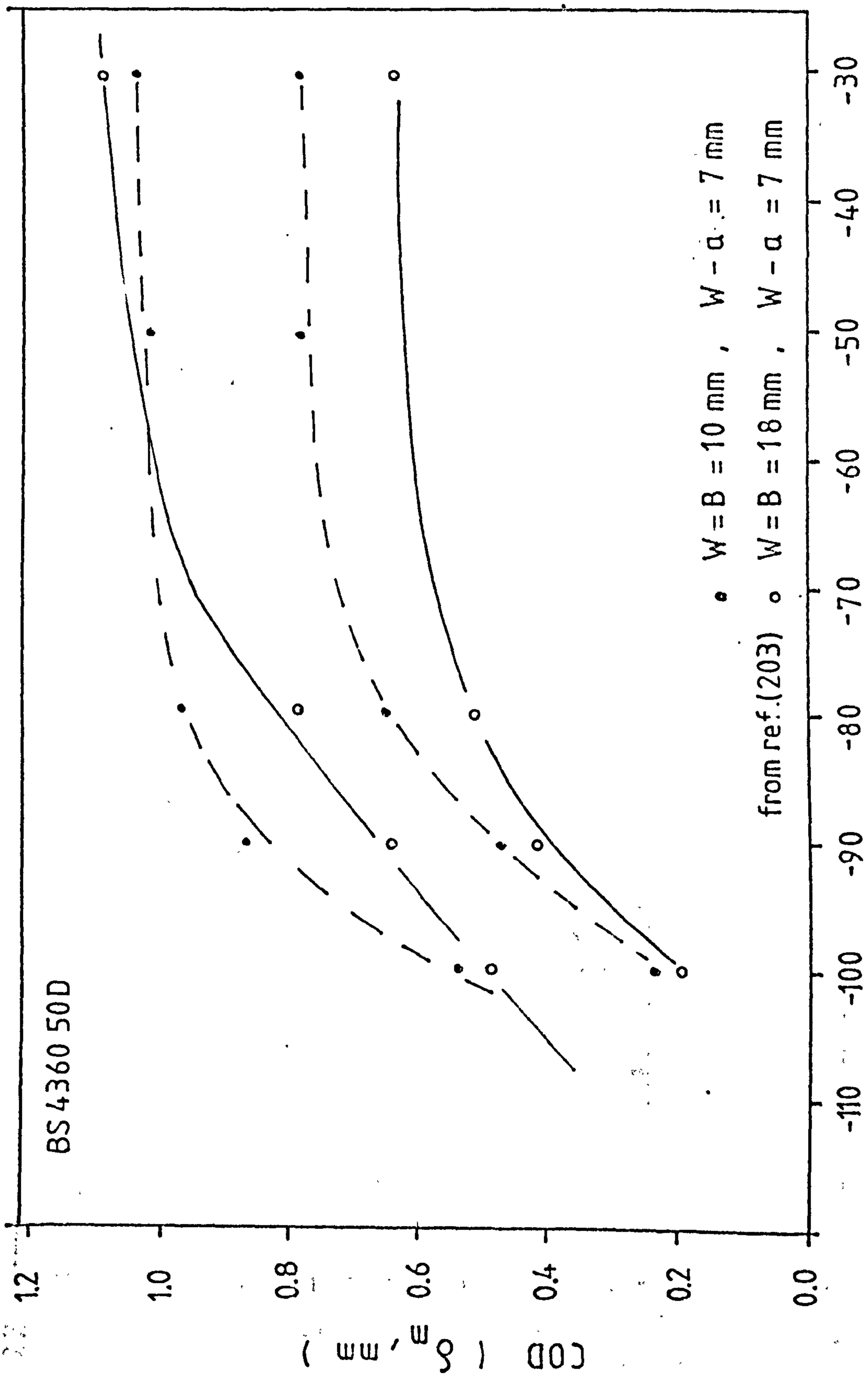

FIG 74. EFFECT O

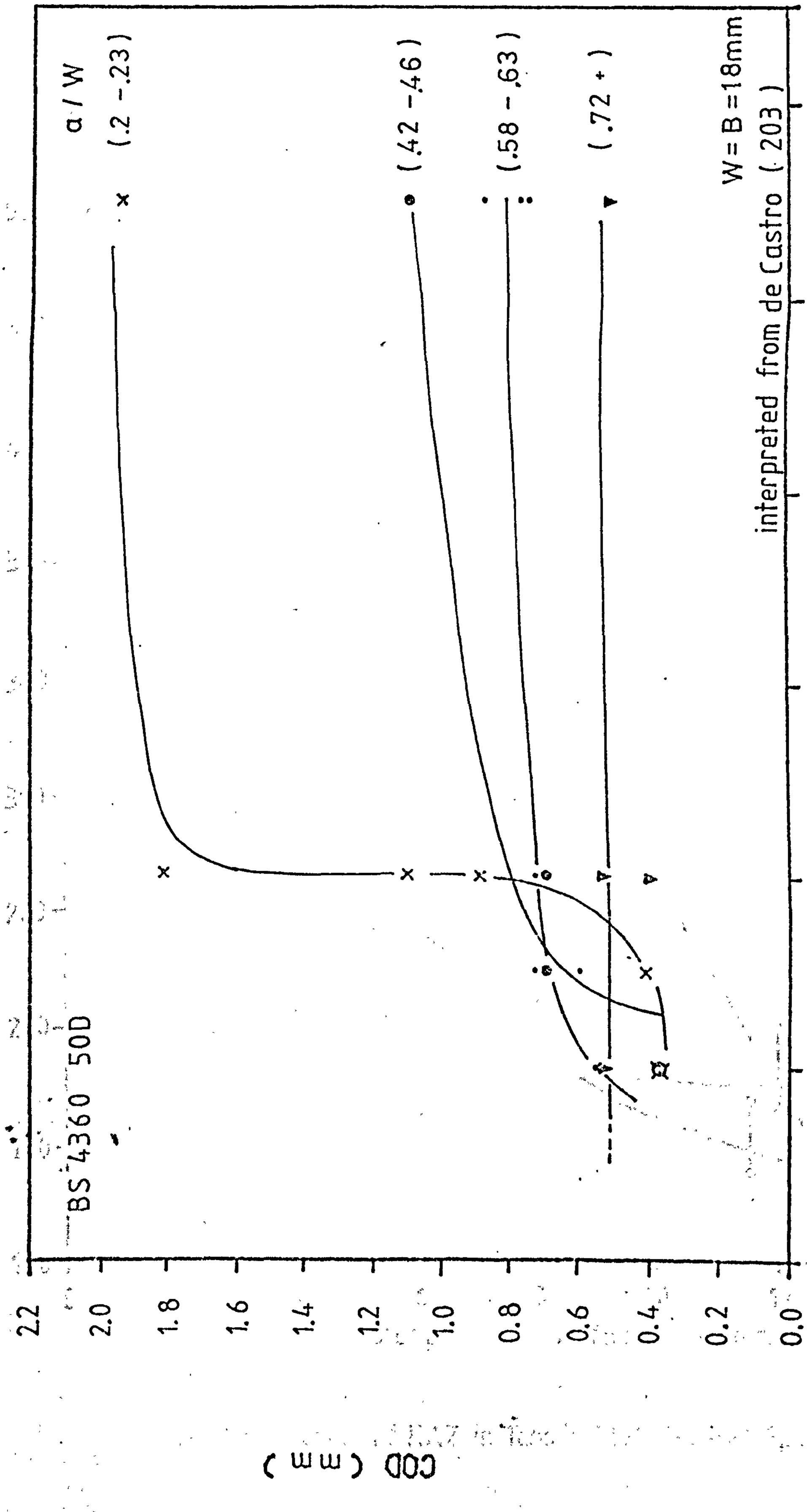

FIG 75 . COD - TEMP. TRANSFORMATION CURVES FOR VARIOUS a / W RATIOS

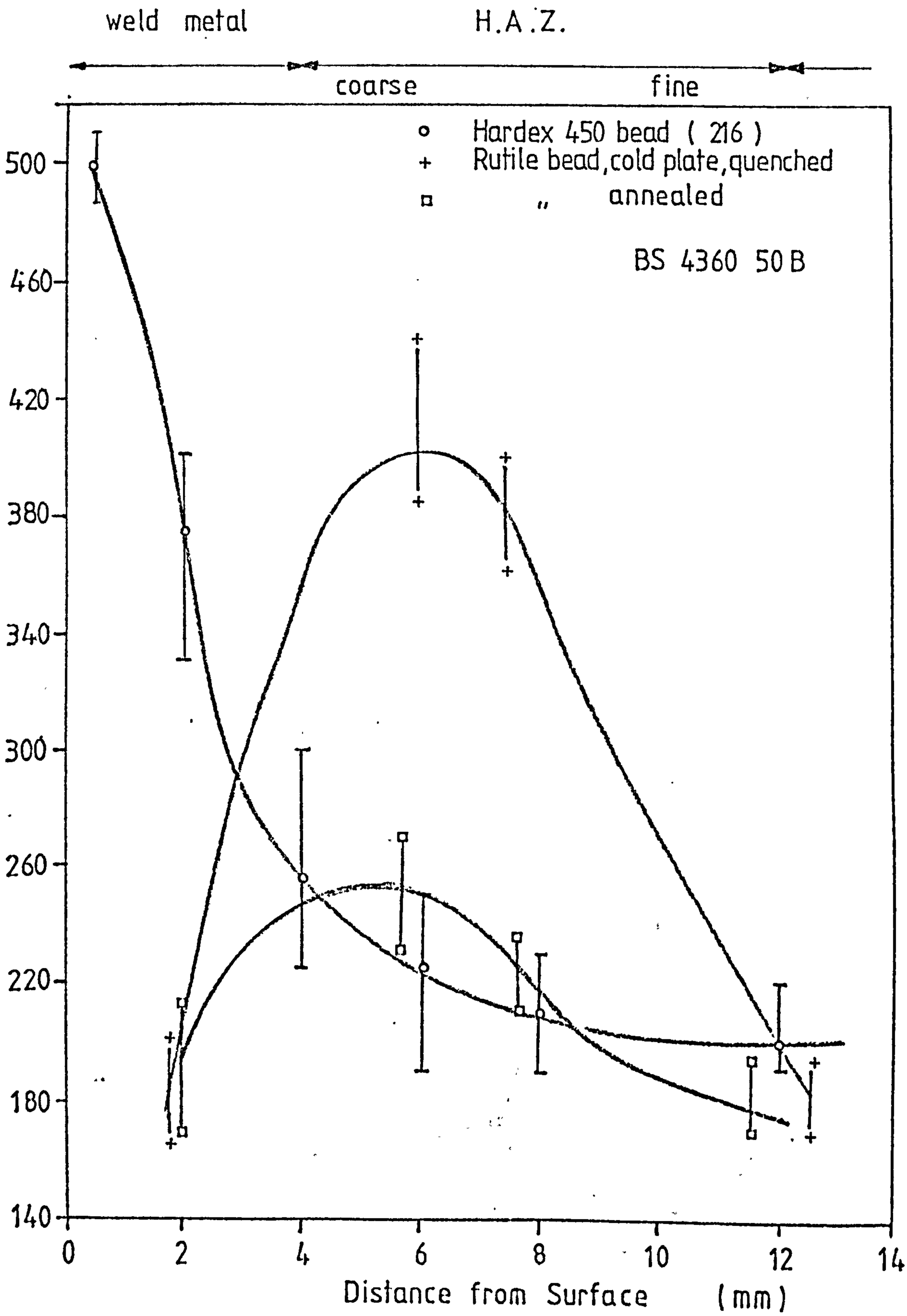

FIG. 76. Extent of HAZ in Tensile Plate Welded Specimens

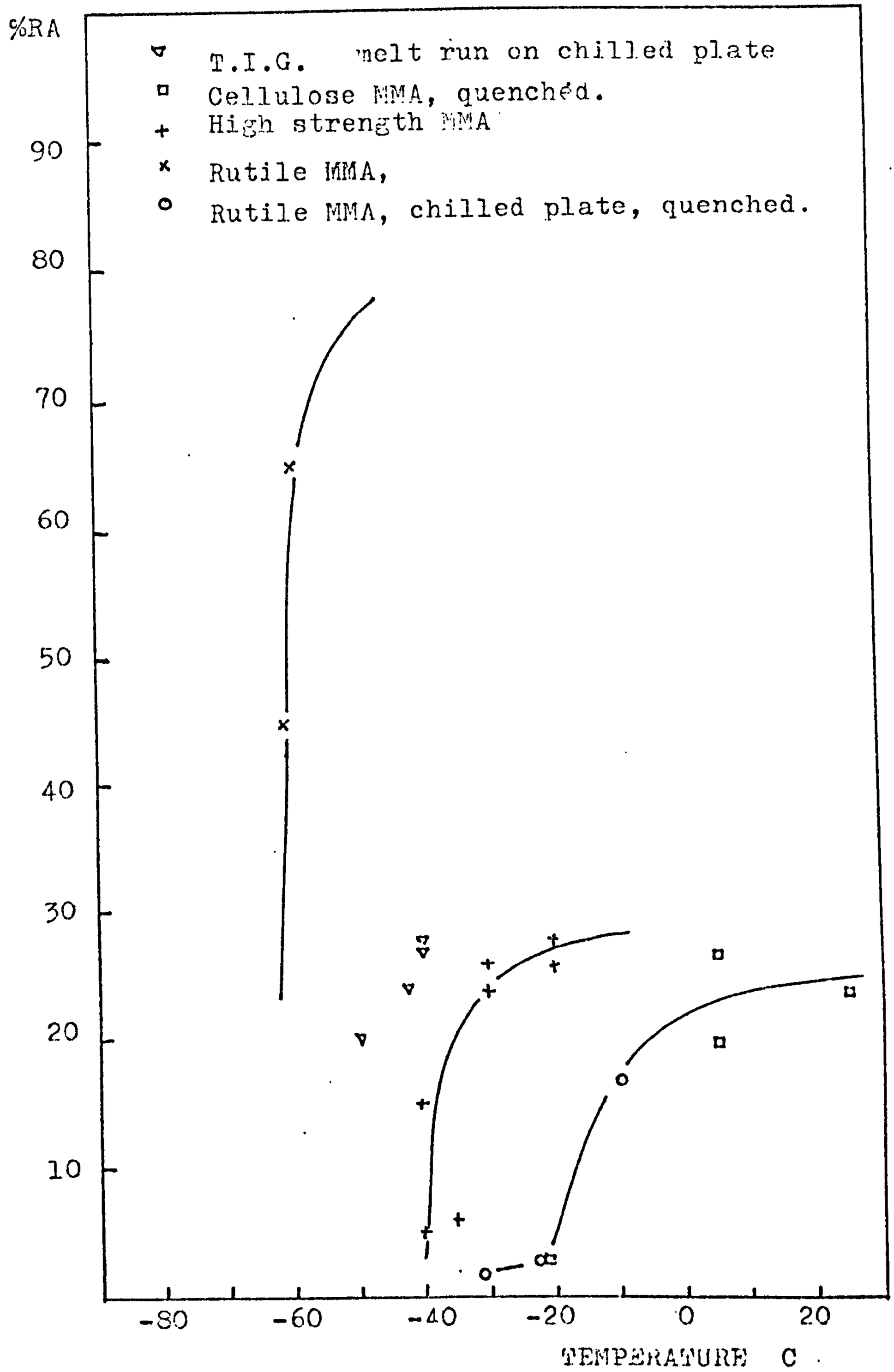

Fig 77 - Effects of Brittle Welds on the Toughness Transition Temperatures of BS 4360 50B Plate

PLATES

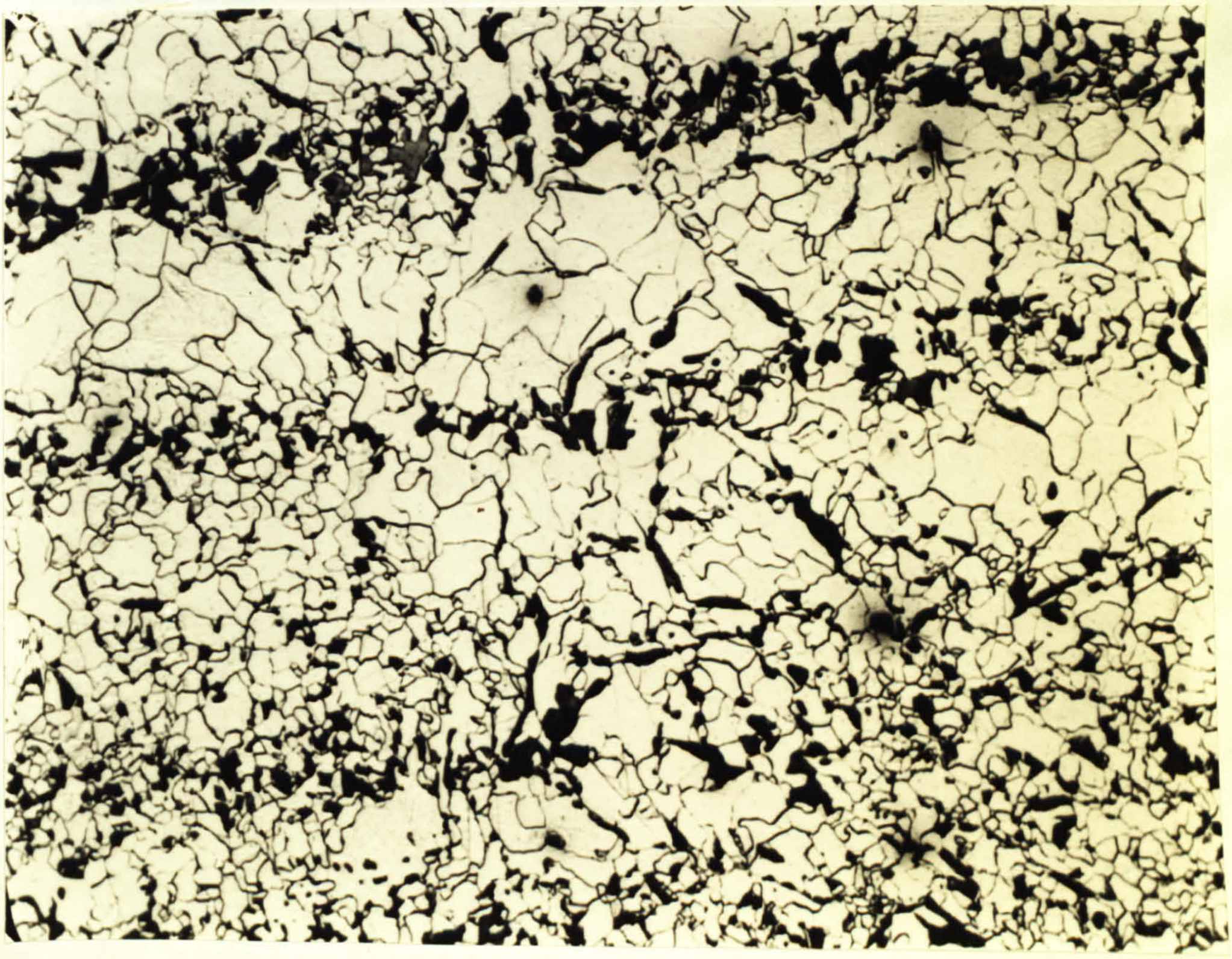

x 250

PLATE 1 Optical Micrograph of BS4360 50D Steel, D Variety, in the Through Thickness Direction

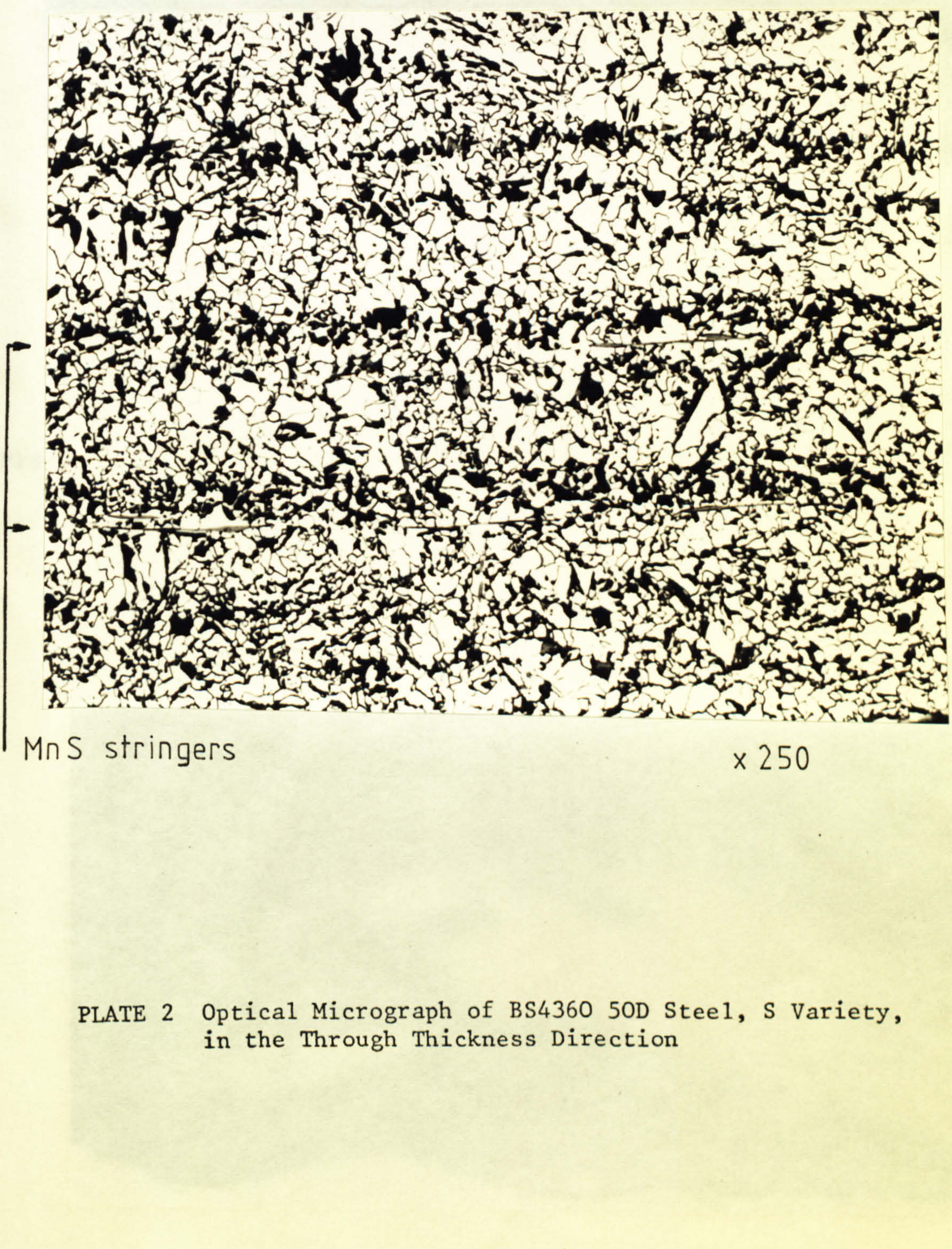

PLATE 2 Optical Micrograph of BS4360 50D Steel, S Variety, in the Through Thickness Direction

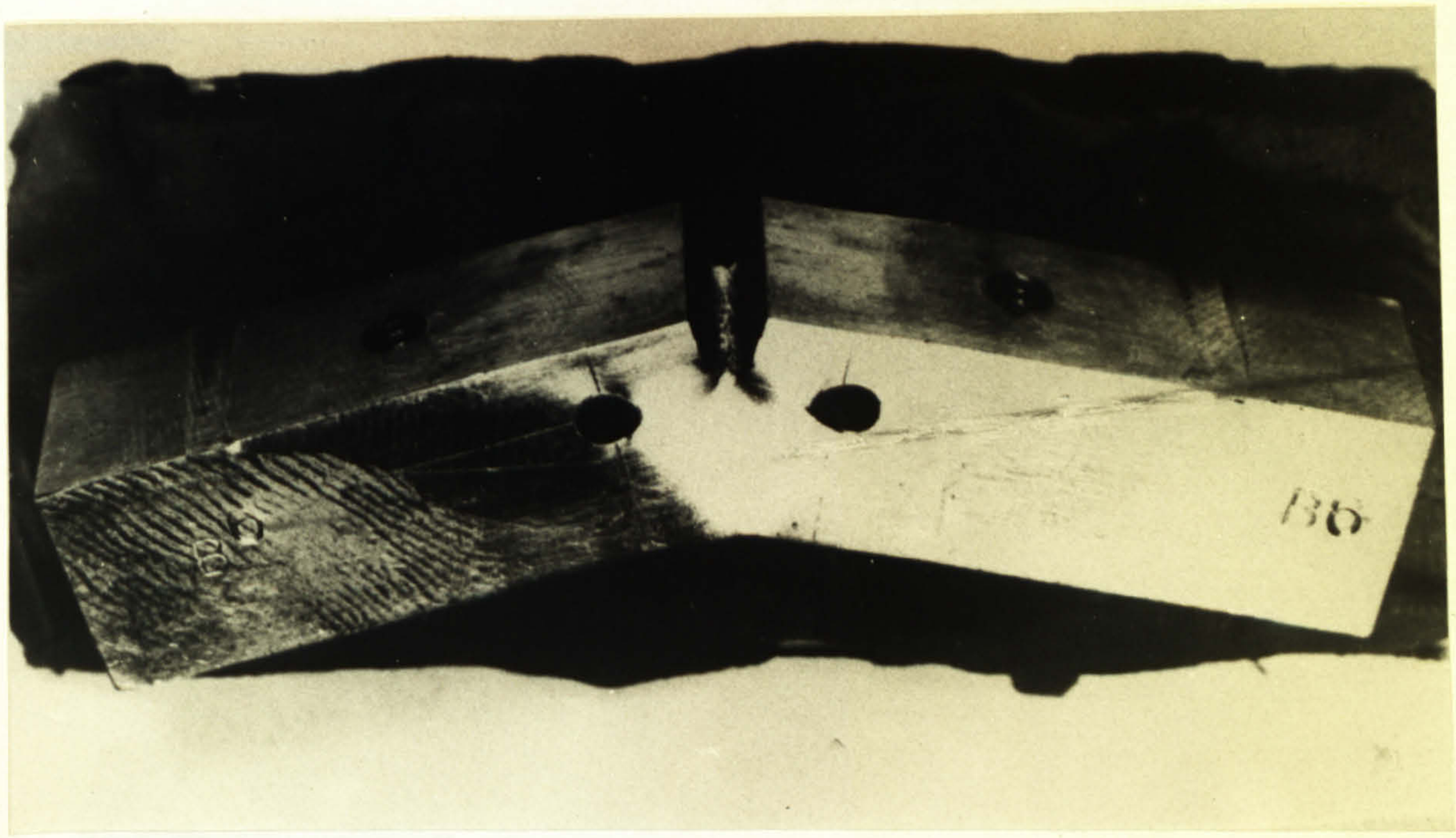

Plate 3 - Specimens with Drilled Holes in the y-Direction Showing Large Crack Tip Openings and Extensive Straining of the Holes

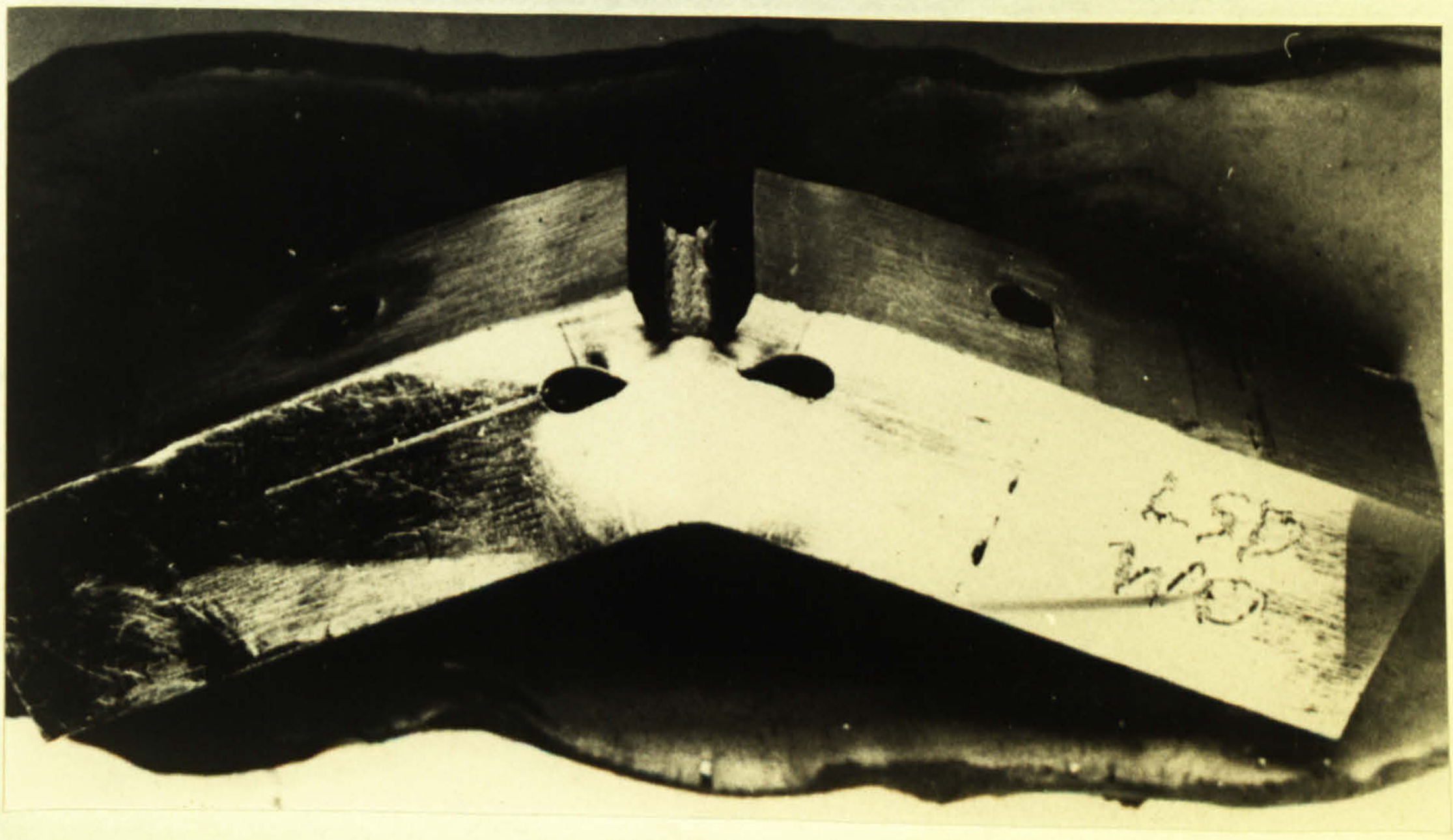

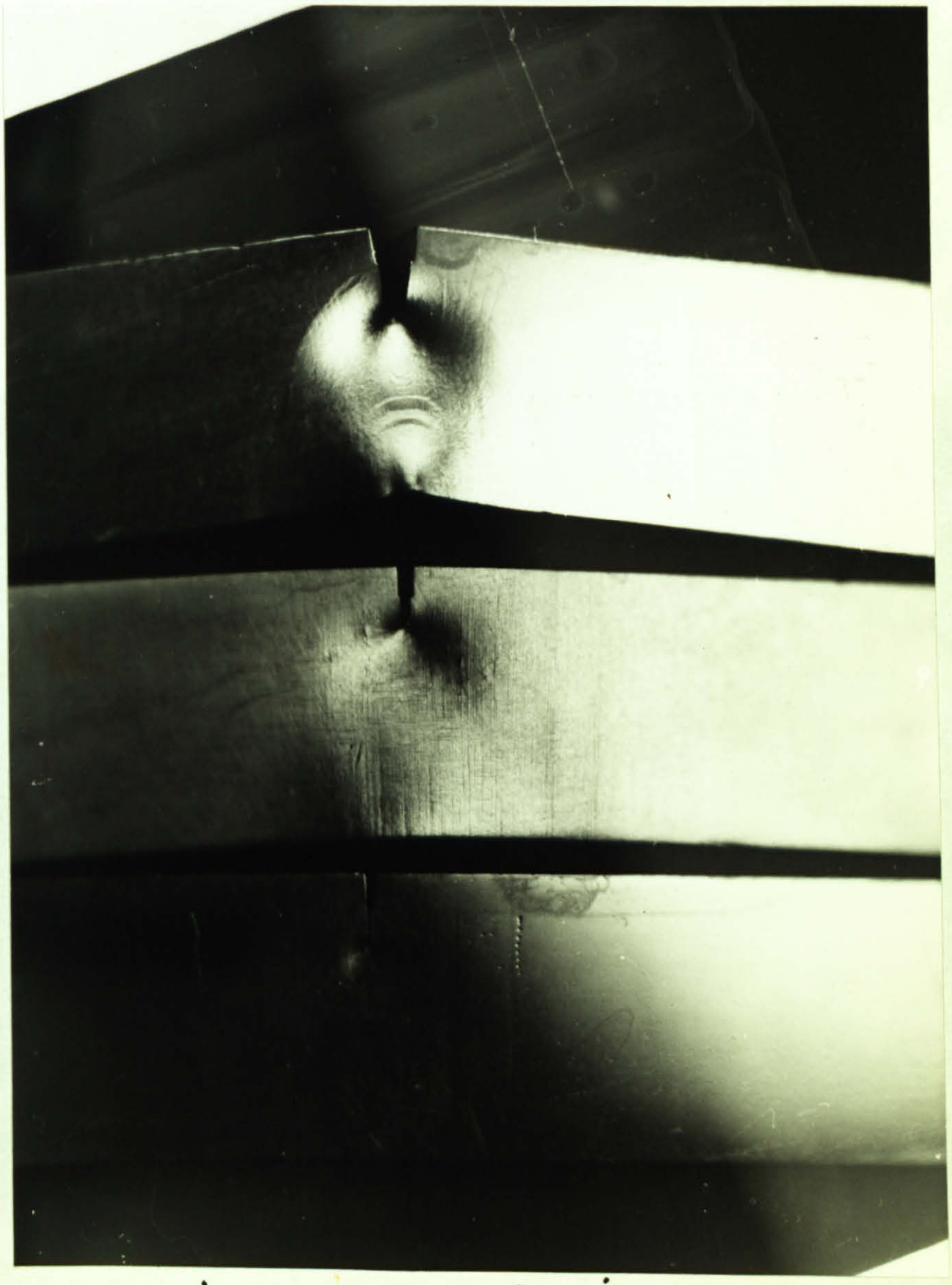

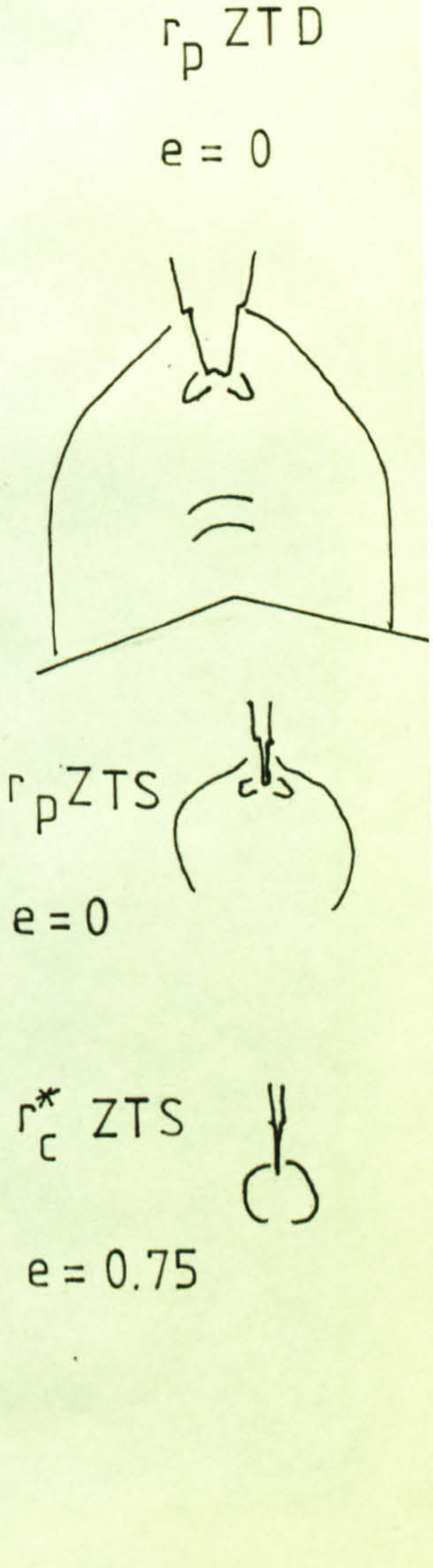

PLATE 4 Variation of Through Thickness Surface Plastic Zone Size as a Function of Inclusion Content for BS4360 50D Steel. Specimen Size 10 x 10 mm.

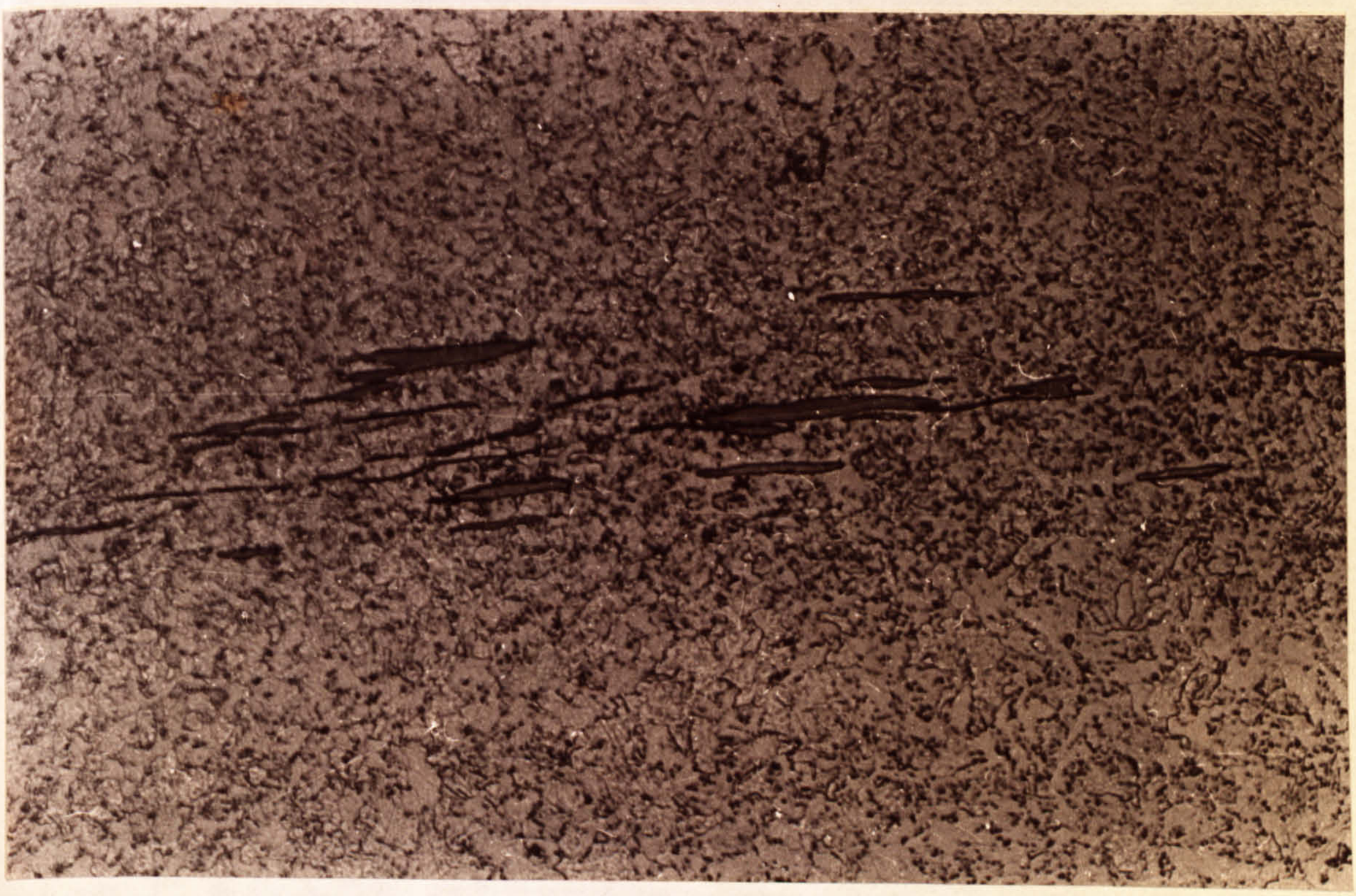

x475

Plate 5 - Optical Micrograph of Banded MnS Inclusions, Elongated by a Hot Rolling Strain of 0.75

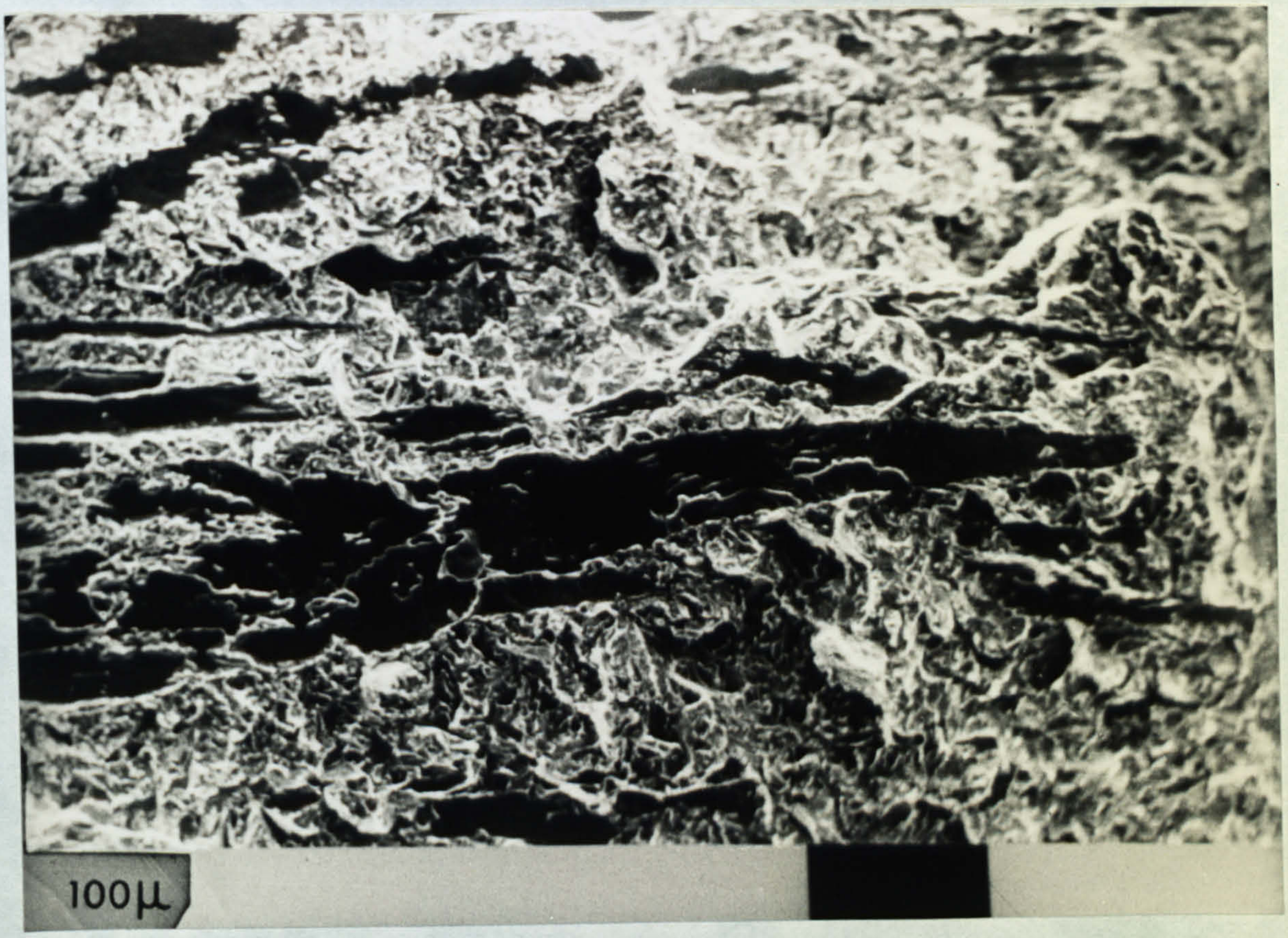

x 210

Plate 6 - Electron Micrograph of Uneven, Through-Thickness Crack Front, Showing Ribbon-Like Extensions into Inclusions

ZRS ZTD ZTS

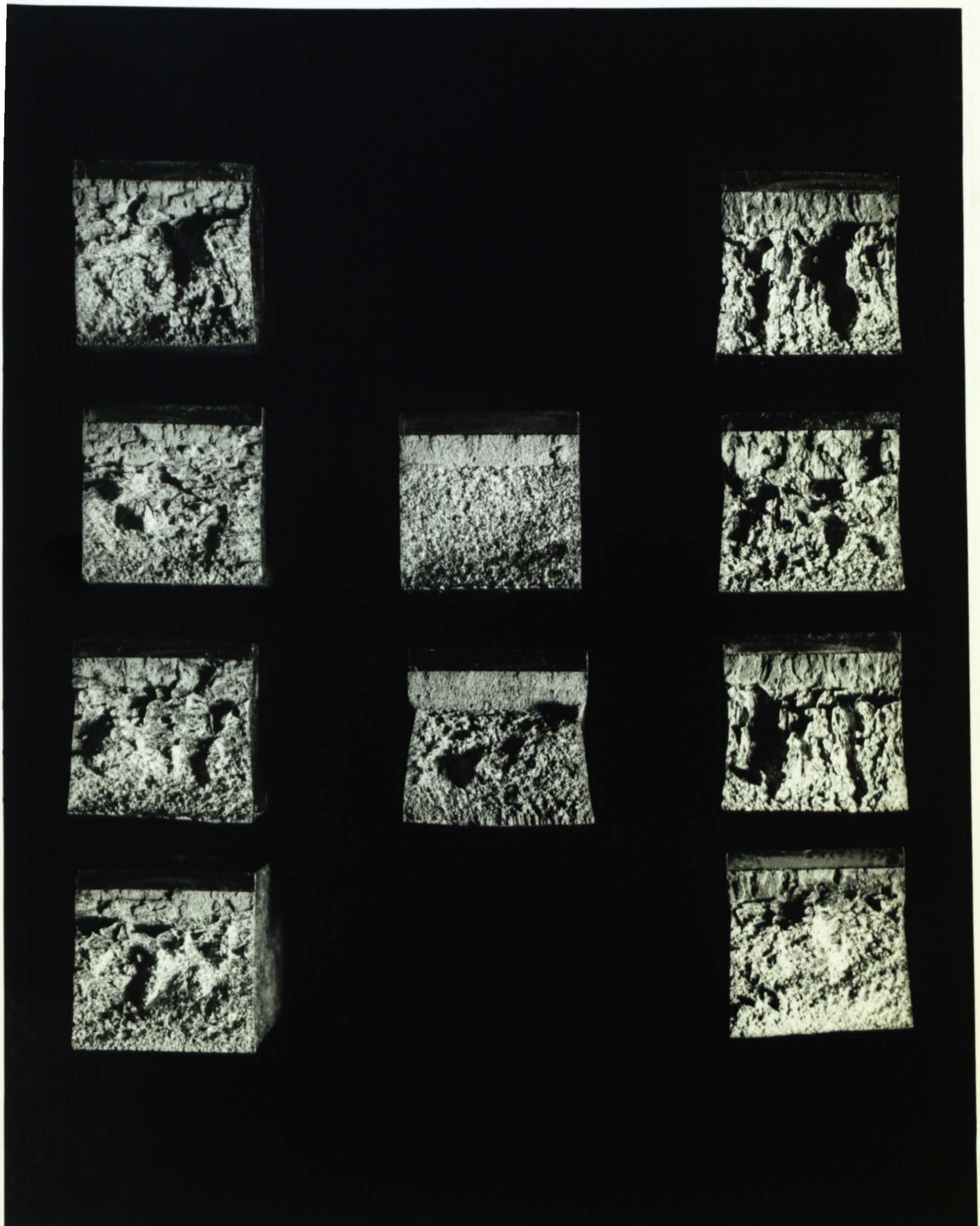

Plate 7 - The Effect of Inclusions on the Shape of the Fatigue Crack Front and Fracture Surface

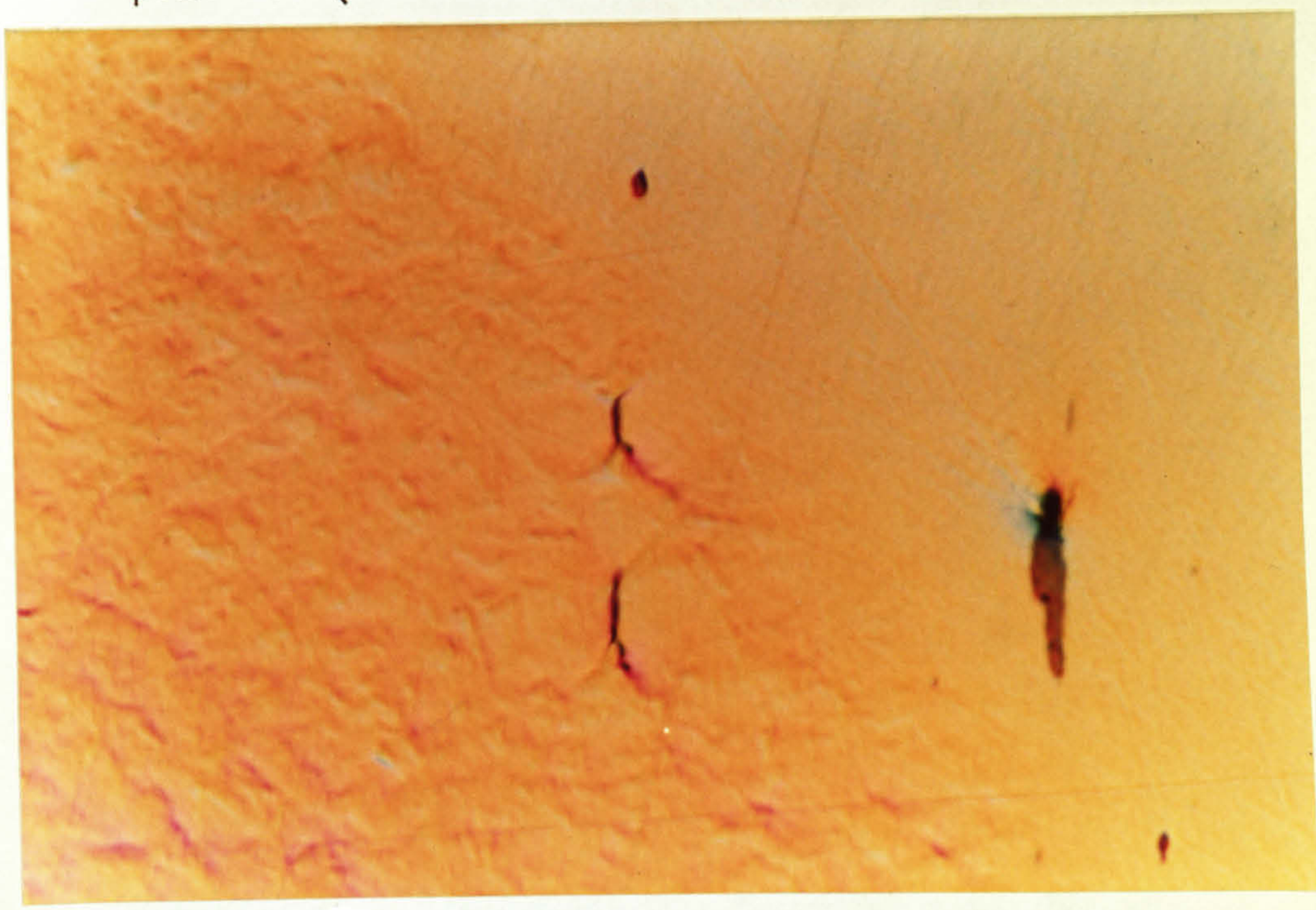

Plate 8 - Polarised Light Optical Micrograph of the Interaction of Inclusions Lying Immediately Beyond Plastic Zone

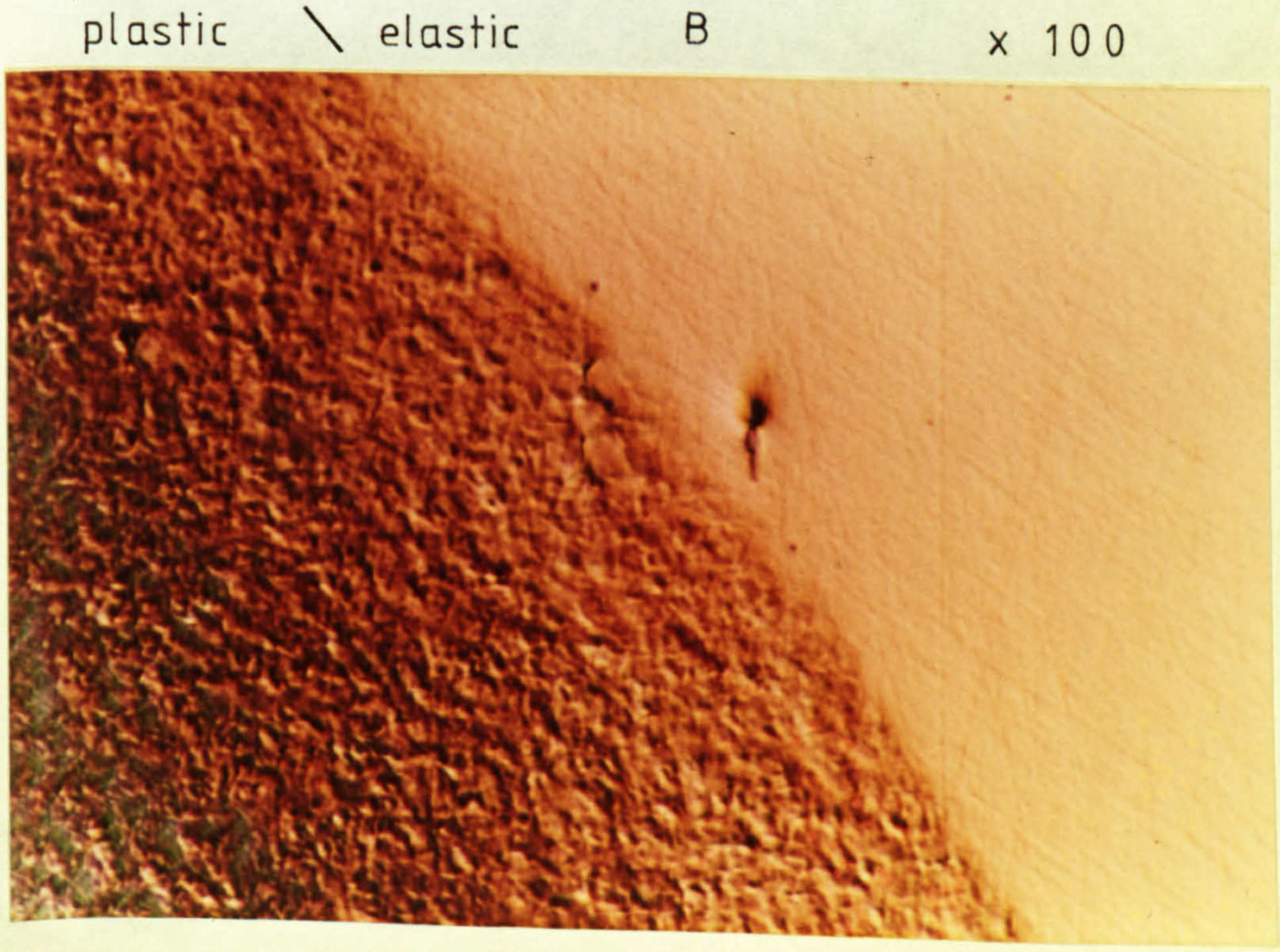

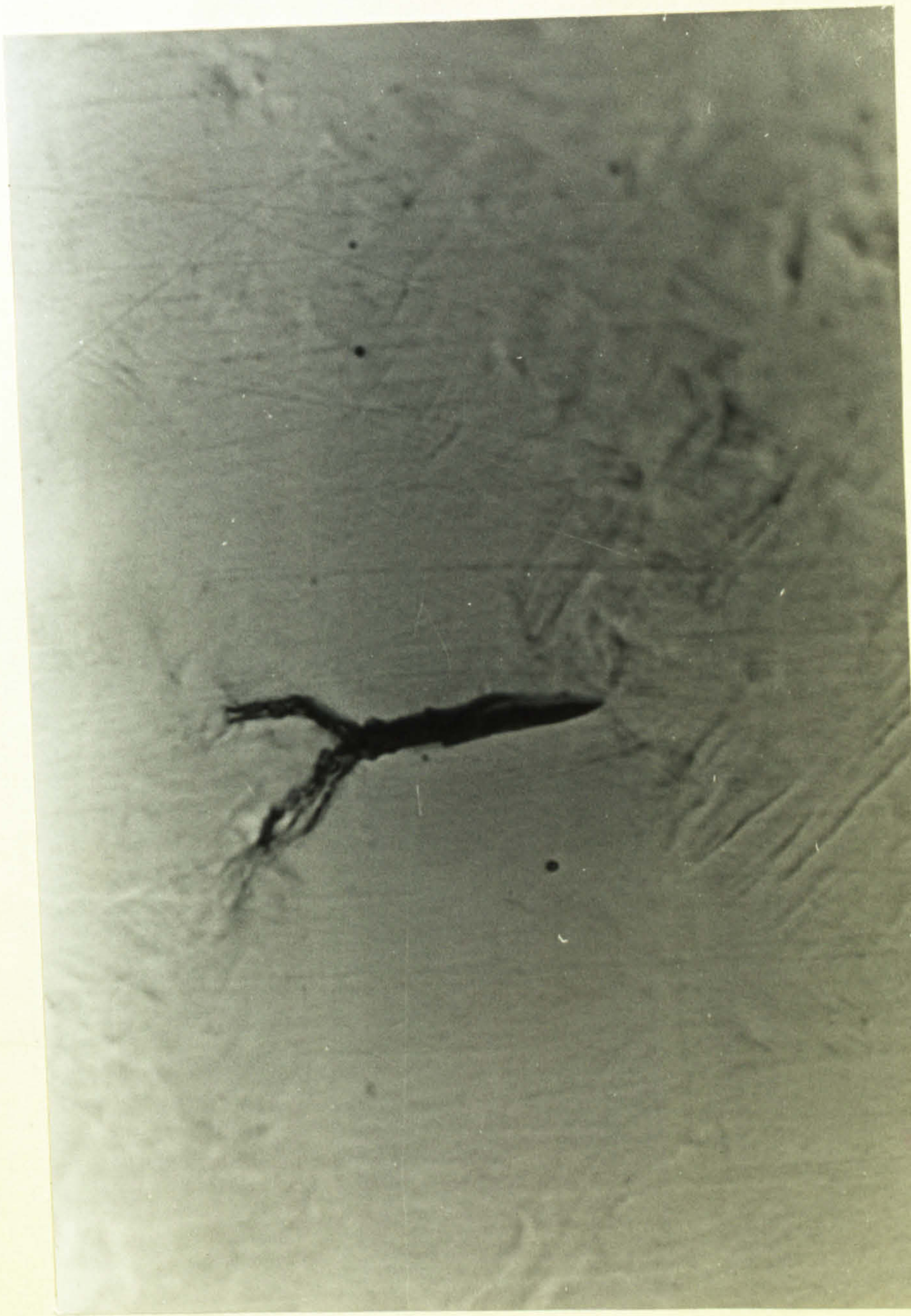

x 650

Plate 9 - Polarised Light Optical Micrograph of Inclusion within Plastic Zone Showing Shearing and Crack Extension at the Apices and Stress Relief at Inclusion Sides

x 400

Plate 10 - Polarised Light Optical Micrograph Showing the Increased Strain at Inclusion Apices after Inclusion - Matrix Debonding

x 900

Plate 11 - Polarised Light Optical Micrograph Showing the Increased Strain at Inclusion Apices Prior to Inclusion - Matrix Debonding

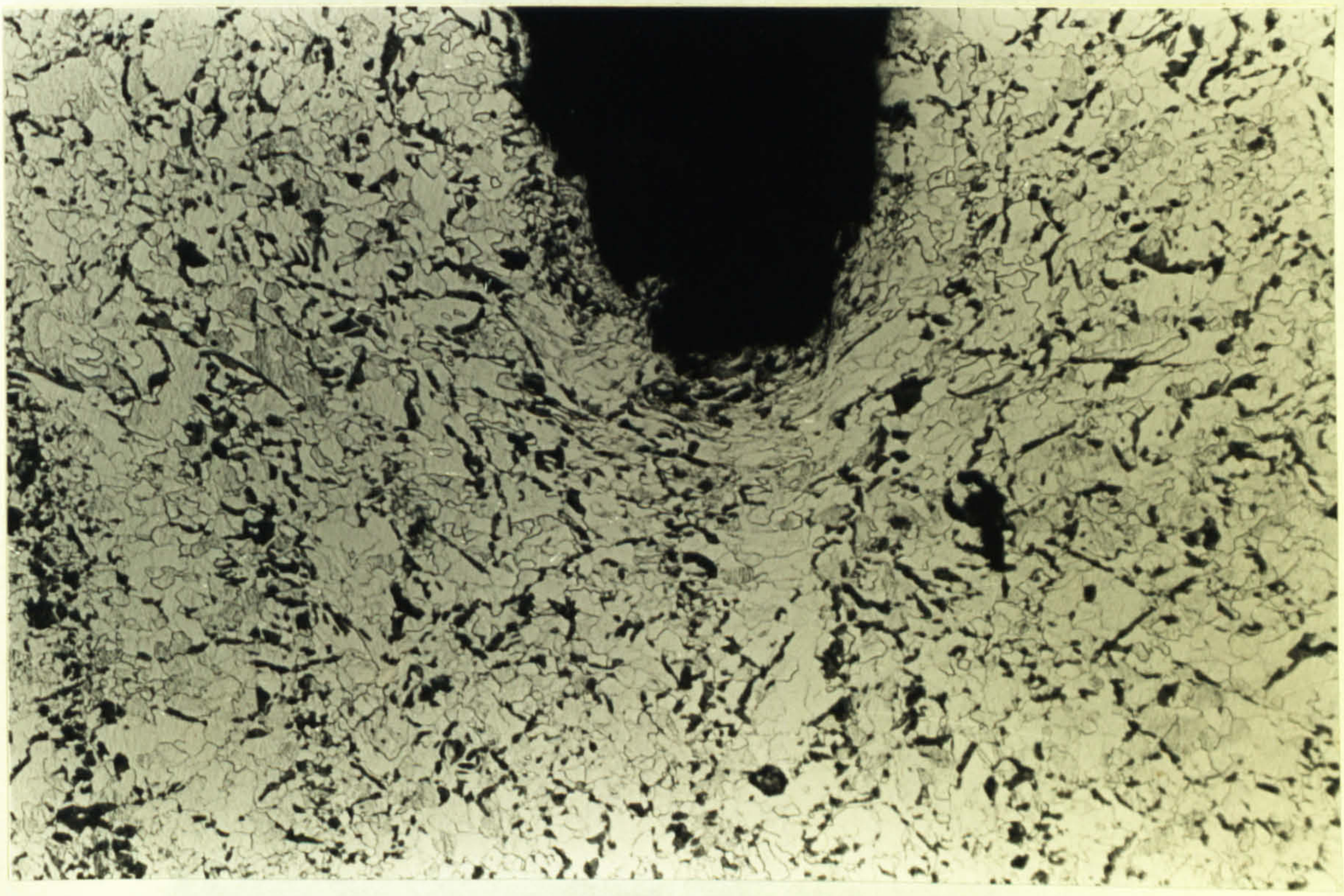

x 175

Plate 12 - Optical Micrograph of Etched ZTD Specimen Showing Large Crack Opening and Extensive Shearing at Crack Tip. Large Void Forming Ahead of Crack Tip

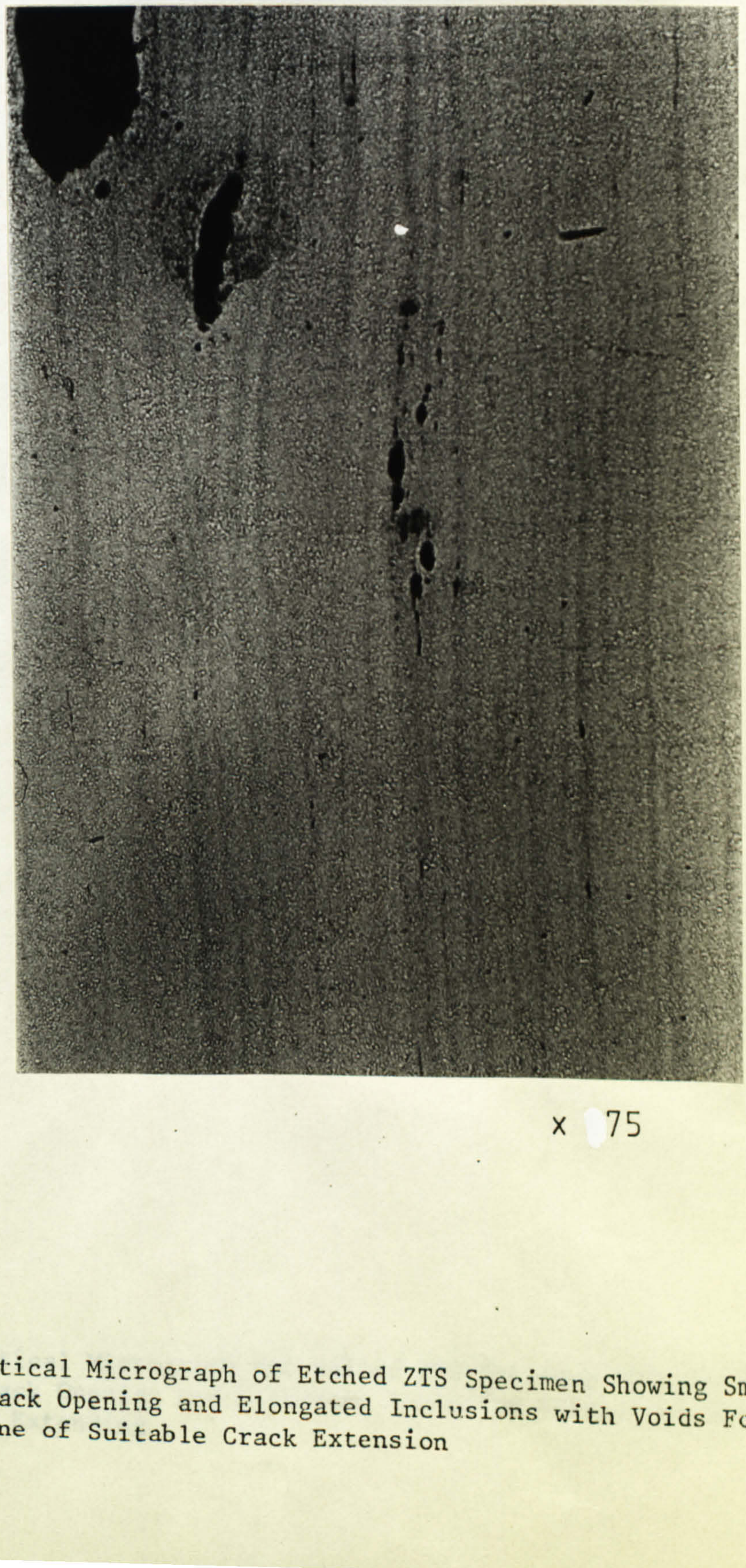

x 75

Plate 13 - Optical Micrograph of Etched ZTS Specimen Showing Small Crack Opening and Elongated Inclusions with Voids Forming Line of Suitable Crack Extension

x 125

Plate 14 - Optical Micrograph Hot Rolled ZTS Specimen Showing Very Small Crack Opening and Elongated Inclusion Band Along Which Crack is Extending .

x 200

Plate 15 - Optical Micrograph of Fracture Surface Showing Large Voids Forming Around Three Inclusions. Note Strain is Concentrated at Inclusion Tips and Relieved on the Inclusion Sides.

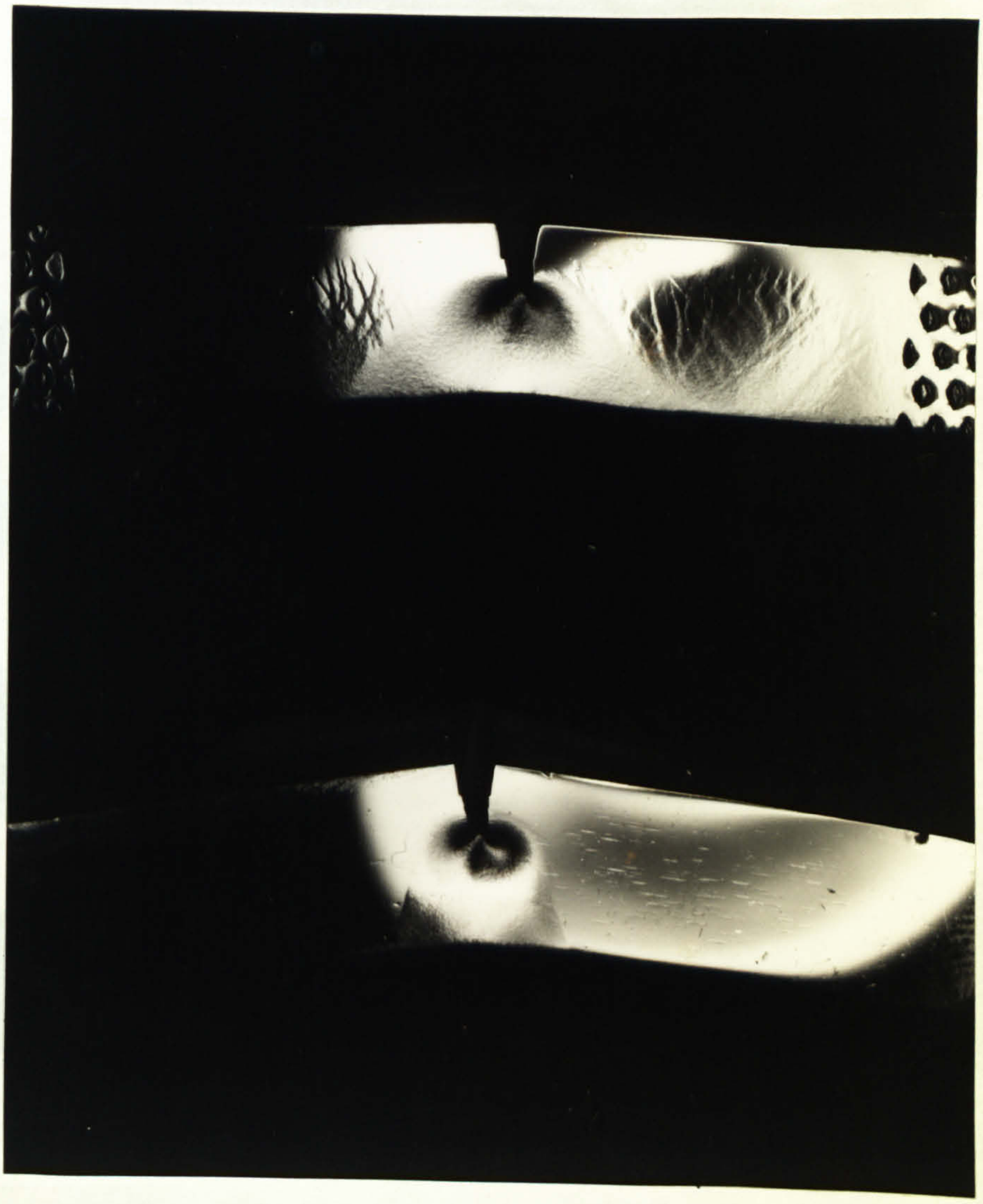

PLATE 16 Plastic Zone Size in 18 x 8.2 mm BS4360 50D Steel, D Variety, in the Longitudinal Direction, as related to the Mode of Loading.

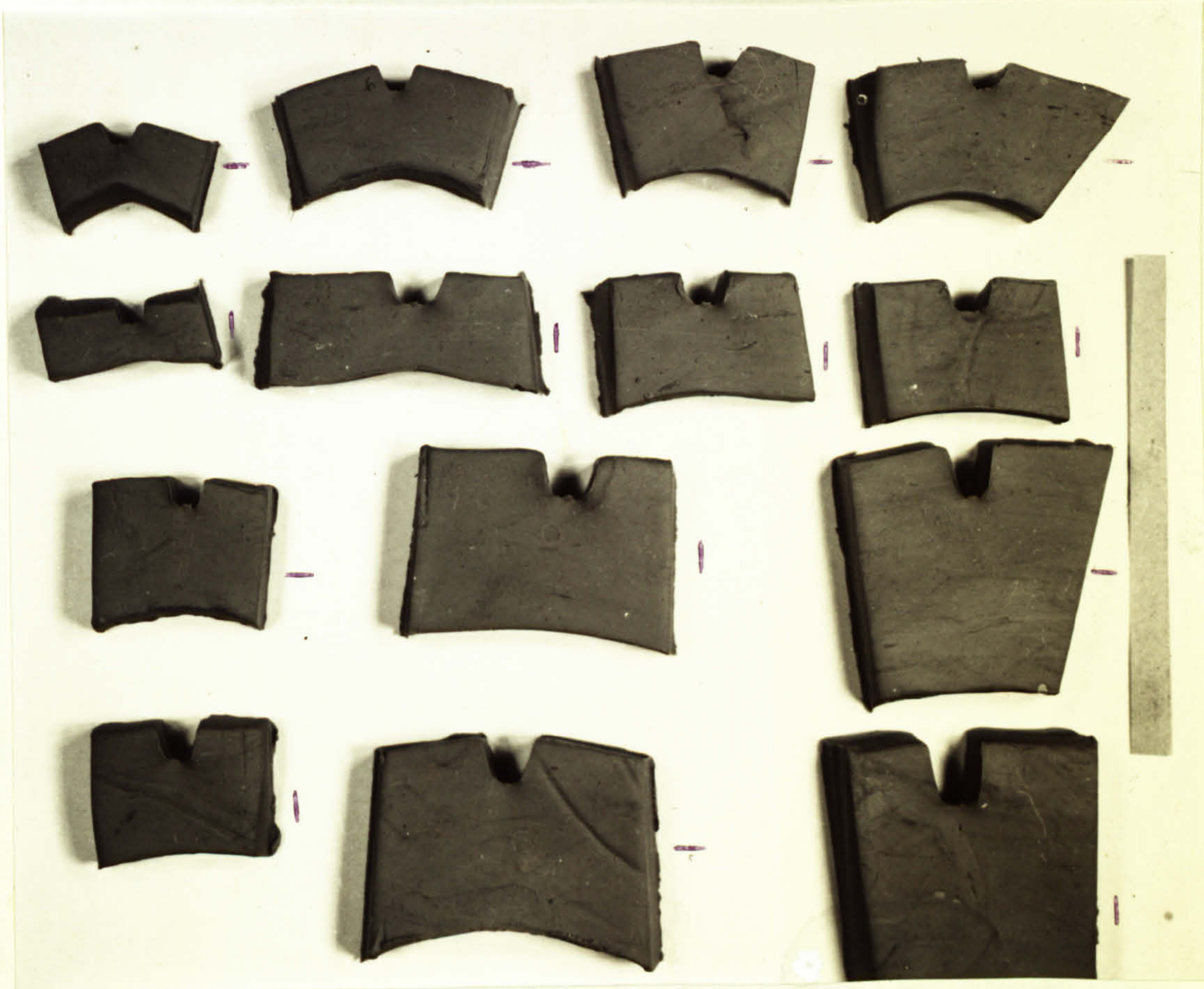

| Tension — Bending

PLATE 17 Plasticine Specimens Loaded in Bending and Tension. Specimen Width and Crack Length Varying, Constant Thickness.

light areas , brittle fracture

Plate 18 - Fracture Surfaces of 50mm Tensile Specimens in BS 4360 50B Steel with Brittle Quenched Weld Bead.

APPENDICES

APPENDIX A

Schematic Defects	Criterion for Interaction	Effective Dimension after Interaction
(i) Ref.(1&2) 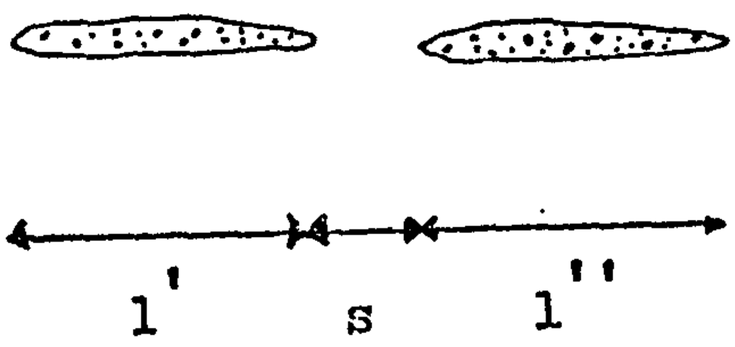	$s \leqslant \frac{l' + l''}{2}$	$l = l' + l'' + s$ $t = t$
(ii) Ref.(1&2) 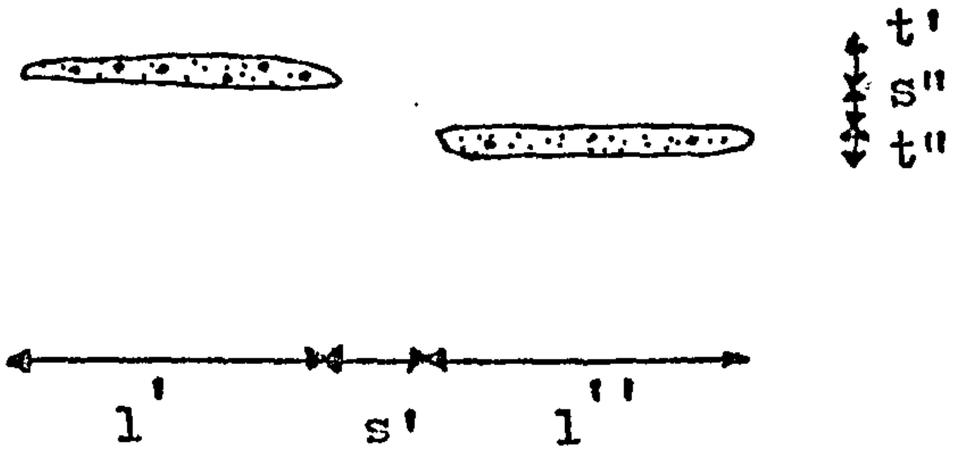	$s' \leqslant \frac{l' + l''}{2}$ $s'' \leqslant \frac{t' + t''}{2}$	$l = l' + l'' + s'$ $t = t' + t'' + s''$
(iii) Proposed interactions 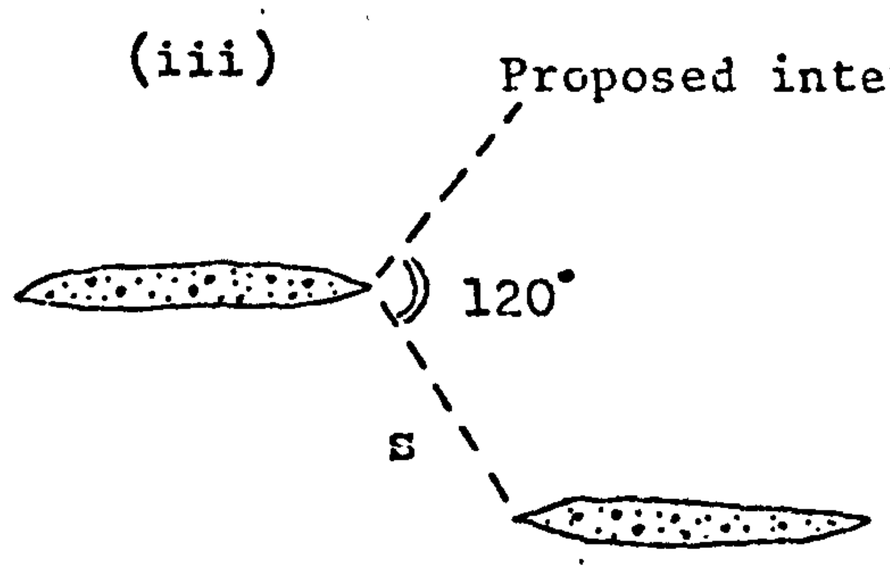	$s \leqslant \frac{l' + l''}{2}$ $\theta \leqslant 120°$	$l = l' + l'' + s$ t not considered
		

(1) BSI 75/77081 , WEE/37 Acceptance Level for Defects

(2) BSI PD 6493:1980 Acceptance Level for Defects

APPENDIX B
COMPUTER MODEL FOR PREDICTING APPROXIMATE THROUGH THICKNESS TOUGHNESS CHARACTERISATIONS

B.1. INTRODUCTION

Given that most engineering structures are constructions of thin plate materials, it is possible to produce fracture toughness specimens in the longitudinal directions, however, the though thickness direction would be too small to produce manageable specimen sizes. Section 4.3 detailed the method for producing through thickness specimens from under-sized plates, by welding of 'dummy' ends. The section outlined the difficulties and drawbacks associated with the welding technique.

A method of predicting through thickness toughness characterisations from thoughness values of longitudinal specimens would be of much benefit to industrial applications.

The work of many authors has shown that the through thickness toughness transition curves are different only in the magnitude of the toughness, not the general shape of the curve. That is, transition temperature, if present in the through thickness direction, does not significantly vary (203, 206).

The present work has shown the effect of inclusion total length per unit area, $\Sigma l/A$, on toughness as in Figure (54). It is, therefore, possible to predict the through thickness toughness from longitudinal specimens, given a value of $\Sigma l/A$ and the relationship of Figure (54). This assumes that the predictions can only apply for:

1. materials of similar inclusion type
2. specimens of similar geometry.

The above limitations are important because it was shown that the inclusion debonding, associated with MnS, was important in facilitating crack growth and hence, affects ductility. It was also shown that maximum load toughness and to a lesser extent the

initiation values that characterise notch tip ductilities were geometry dependent.

Figure (54) applies to BS 4360 50D material in W = B = 10mm specimens. A different material will show different toughness values but it is likely that inclusions will reduce the toughness in the through thickness direction in a similar manner to that shown in Figure (54). This behaviour has been confirmed by other authors (73, 133, 134, 191).

To enable the prediction of through thickness toughnesses, based on the general behaviour shown in this work, one would have to use a scalar relationship. Having obtained longitudinal (LS) toughness data and $\Sigma 1/A$, the following steps would have to be made:

1. the toughness values obtained are to be scaled to a range varying between 0 to 10.

2. five temperatures are to be evaluated and denoted as, T1 > T2 > T3 > T4 > T5, where T5 represents lower transition temperatures or the lower shelf; T4, the upper transition temperatures and T3, T2 and T1 represent the upper shelf values. Three temperatures were used to represent the upper shelf, since, toughness reduction with increasing temperature is now the established upper shelf behaviour.

Having obtained $\Sigma 1/A$ and the scaled toughness values at T1 to T5, one may use the computer program, provided in this Appendix to predict approximate through thickness toughness values. The output from the program would be the toughness values, at the five specified temperatures, in scalar form. These would require conversion into real toughness values.

The program of section B4 is based on polynomial fitting to the curves obtained in Figure (54) at the temperatures T1 to T5. The actual curve represented in Figure (54) is, therefore, characteristic of T1.

B.2. THE FORMULATIONS

The general polynomial equation is of the form:

$$f(y) = a_0 + a_1 x + a_2 x^2 + ... + a_n x^n + ... \qquad ....B.1.$$

For each of the temperatures T1 to T5, eight co-ordinates of toughness against total inclusion length (H,z), are supplied from the set of figures in the general form of Figure (54).

At T1, the following polynomials are produced by substituting the eight co-ordinates in equation [B.1].

$$H_1 = a_0 + a_1 z_1 + ... + a_7 z_1^7$$

$$H_2 = a_0 + a_1 z_2 + ... + a_7 z_2^7$$

. . . . .

. . . . .

. . . . .

$$H_8 = a_0 + a_z z_8 + ... + a_7 z_8^7 \qquad ....B.2$$

Equations [B.2] can be represented in matrix form as:

$$z \quad A = H \qquad ....B.3$$

where:

$$z = \begin{bmatrix} 1 & z_1 & z_1^2 & .... & z_1^7 \\ 1 & z_2 & z_2^2 & .... & z_2^7 \\ . & . & . & . & \\ . & . & . & . & \\ 1 & z_7 & z_7^2 & .... & z_7^7 \end{bmatrix}$$

$$A = \begin{bmatrix} a_0 \\ a_1 \\ . \\ . \\ a_7 \end{bmatrix}$$

$$H = \begin{bmatrix} H_1 \\ H_2 \\ . \\ . \\ H_8 \end{bmatrix}$$

The polynomial coefficient matrix, A, is evaluated for T1, from equation [B.3]. This process is repeated for temperatures T2 to T5. The resulting coefficients are stored in a matrix, termed TA, see below. Matrix TA is arranged such that, row i represents the polynomial coefficients at temperature Ti.

Matrix TA will then have the following format:

$$TA = \begin{bmatrix} ta_{1,1} & ta_{1,2} & .... & ta_{1,8} \\ ta_{2,1} & ta_{2,2} & .... & ta_{2,8} \\ . & . & . & . \\ . & . & . & . \\ ta_{5,1} & ta_{5,2} & .... & ta_{5,8} \end{bmatrix}$$

By substituting the resulting coefficients in equation [B.1], the resulting set of equations are produced:

$$H_{T1} = ta_{1,1} + ta_{1,2}\, z + \ldots + ta_{1,8}\, z^7$$

$$H_{T2} = ta_{2,1} + ta_{2,2}\, z + \ldots + ta_{2,8}\, z^7$$

$$\vdots \qquad\qquad \vdots$$

$$H_{T5} = ta_{5,1} + ta_{5,2}\, z + \ldots + ta_{5,8}\, z^7 \qquad \ldots.B.4$$

Where the user enters a value of z (that is, $\Sigma l/A$), the program will substitute it into equations [B.4], thereby producing toughness values, H at T1, T2, T3, T4 and T5.

B.3. WORKED EXAMPLE

Given longitudinal toughness values for a steel, as:

	T1	T2	T3	T4	T5
Temperature oC	20	-130	-150	-160	-170
δ_i =	0.45	0.50	0.50	0.30	0.15

Having measured the total inclusion length per area as:

$\Sigma l/A = 1.65 mm/mm^2$.

The scalar function of the δ_i values is, in this example, 20. That is:

δ_i = 9.00, 10.00, 10.00, 6.00, and 3.00.

The output from the program reads:

```
Z VALUE = ? 1.65

TOUGHNESS (H) AT TEMPERATURE 1 = 2.25062
TOUGHNESS (H) AT TEMPERATURE 2 = 2.65225
TOUGHNESS (H) AT TEMPERATURE 3 = 2.31517
```

TOUGHNESS (H) AT TEMPERATURE 4 = 1.81402

TOUGHNESS (H) AT TEMPERATURE 5 = 1.09589

Scaling back, by dividing by 20.00, one obtains the transition curve as follows:

	Temperature ^{o}C	Through thickness δ_i mm
Upper Shelf T1	20	0.113
Upper Shelf T2	-130	0.133
Upper Shelf T3	-150	0.116
Transition T4	-160	0.091
Lower transition T5	-170	0.055

Thus, it is observed that an inclusion content of 1.65mm/mm^2 results in the reduction of through thickness δ_i values to one quarter of the longitudinal values at upper shelf temperatures for an inclusion content equivalent to 1.65mm/mm^2.

```
10      REM
20      REM  PROGRAM TO APPROXIMATE THROUGH-THICKNESS COD
30      REM  VALUES FROM LONGITUDINAL COD AND TOTAL
40      REM  INCLUSION LENGTH/UNIT AREA.
50      REM
60      REM  POLYNOMIAL OF ORDER  O% - 1
70      REM
100     O%=8
200     DIM H(O%),Z(O%,O%),ZZ(O%),TA(5,O%),A(O%),PZ(O%)
300     REM
400     REM  COMPILING  Z & H   FOR   Z A = H   AT   T1
500     REM
600     H(1)=6.5: H(2)=6.0: H(3)=4.7: H(4)=2.0: H(5)=1.6: H(6)=1.25: H(7)=1.1
650     H(8)=0.8
700     PZ(1)=0.001: PZ(2)=0.15: PZ(3)=0.6: PZ(4)=1.84: PZ(5)=2.38
750     PZ(6)=3.2:  PZ(7)=4: PZ(8)=5.8
800     S%=0
900     GOSUB 7000
1000    REM
1100    REM  COMPILING  Z & H   FOR   Z A = H   AT   T2
1200    REM
1300    H(1)=8.5: H(2)=7.4: H(3)=5.3: H(4)=2.4: H(5)=2: H(6)=1.6: H(7)=1.4
1350    H(8)=0.8
1400    GOSUB 7000
1500    REM
1600    REM  COMPILING  Z & H   FOR   Z A = H   AT   T3
1700    REM
1800    H(1)=10: H(2)=7.8: H(3)=5.6: H(4)=1.9: H(5)=1.6: H(6)=1.3: H(7)=1.1
1850    H(8)=0.6
1900    GOSUB 7000
2000    REM
2100    REM  COMPILING  Z & H   FOR   Z A = H   AT   T4
2200    REM
2300    H(1)=5: H(2)=3.9: H(3)=2.8: H(4)=1.6: H(5)=1.2: H(6)=0.95: H(7)=0.8
2350    H(8)=0.5
```

```
2400    GOSUB 7000
2500    REM
2600    REM  COMPILING  Z & H   FOR   Z A = H    AT   T5
2700    REM
2800    H(1)=2.8: H(2)=2.5: H(3)=1.9: H(4)=1: H(5)=0.8: H(6)=0.6: H(7)=0.5
2850    H(8)=0.4
2900    GOSUB 7000
3000    PRINT "Z VALUE = ";: INPUT Z1
3100    IF Z1 < 0.0 GOTO 4000
3200    FOR I%=1 TO 5
3300    H1=0.0
3400    FOR J%=1 TO O%
3500    H1=H1+TA(I%,J%)*Z1↑(J%-1)
3600    NEXT J%
3700    PRINT "TOUGHNESS (H) AT TEMPERATURE";I%;" = ";H1
3800    NEXT I%
3900    GOTO 3000
4000    PRINT "END OF RUN"
4100    END
7000    REM
7100    REM  SETTING UP AND CALCULATING THE POLYNOMIAL
7150    REM  COEFFICIENTS MATRIX  TA, EQUATION [7.4]
7200    REM
7300    FOR I%=1 TO O%
7400    ZZ(I%)=PZ(I%)
7500    NEXT I%
7600    FOR I%=1 TO O%
7700    FOR K%=1 TO O%
7800    Z(I%,K%)=ZZ(I%)↑(K%-1)
7900    NEXT K%
8000    NEXT I%
8100    REM
8200    REM  SOLVING  Z A = H   BY  FORMING AND SOLVING
8300    REM  THE UPPER TRIANGULAR MATRIX
8400    REM
8500    FOR K%=1 TO O%-1
```

```
8600    FOR I%=K%+1 TO O%
8700    IF ABS(Z(K%,K%))< 0.00001 GOTO 11400
8800    P=Z(I%,K%)/Z(K%,K%)
8900    H(I%)=H(I%)-H(K%)*P
9000    FOR J%=K% TO O%
9100    Z(I%,J%)=Z(I%,J%)-Z(K%,J%)*P
9200    NEXT J%
9300    NEXT I%
9400    NEXT K%
9500    REM
9600    REM   CALCULATING Z VALUES FOR A
9700    REM
9800    FOR I%=1 TO O%
9900    K%=O%+1-I%
10000   IF ABS(Z(K%,K%)) < 0.00001 GOTO 11400
10100   A(K%)=H(K%)/Z(K%,K%)
10200   IF K% = O% GOTO 10800
10300   SU=0.0
10400   FOR J%=K% TO O%-1
10500   SU =.SU + Z(K%,J%+1)*A(J%+1)
10600   NEXT J%
10700   A(K%)=A(K%)-SU/Z(K%,K%)
10800   NEXT I%
10900   S%=S%+1
11000   FOR I%=1 TO O%
11100   TA(S%,I%)=A(I%)
11200   NEXT I%
11300   RETURN
11400   PRINT "SINGULAR MATRIX"
11500   STOP
```